

Design Analysis of a Narrow Body Medium Range Commercial Aircraft

a project presented to
The Faculty of the Department of Aerospace Engineering San José State University

in partial fulfillment of the requirements for the degree
Master of Science in Aerospace Engineering

by

Veera Venkatesh Vadaparthy

December 2017

approved by

Dr. Nikos Mourtos
Faculty Advisor



by

Veera Venkatesh Vadapartha

December 2017

© 2017

Veera Venkatesh Vadapartha

ALL RIGHTS RESERVED

DESIGN ANALYSIS OF A NARROW BODY MEDIUM RANGE COMMERCIAL
AIRCRAFT

by

Veera Venkatesh Vadaparathi

APPROVED FOR THE DEPARTMENT OF AEROSPACE ENGINEERING
SAN JOSÉ STATE UNIVERSITY

December 2017

Dr. Nikos Mourtos Department of Aerospace Engineering Advisor

ABSTRACT

DESIGN ANALYSIS OF A NARROW BODY MEDIUM RANGE COMMERCIAL AIRCRAFT

by Veera Venkatesh Vadaparthi

Narrow Body aircraft have been gaining importance in the recent years which really proved to be efficient for both medium and short haul travels. These variants emerged from lowest to the highest efficiency both in aerodynamics and propulsion. Previously, there were many narrow body aircraft but they have been limited to short haul and mediocre payload, cargo capabilities. Boeing and Airbus are the key players especially in the narrow body aircraft market whose variants, now, offer increased range, improved handling capabilities, payload and efficient aerodynamics. This aircraft design is targeted towards emerging airline markets like India, China, Africa whose primary aviation is based on a Low-Cost Carrier Business Model. In this project, a new aircraft configuration is proposed with extended payload carrying capacity, increased range (for both medium/short haul travels), improved cabin configurations (e.g. increased seat width, pitch and leg room), increased use of composites (typically aimed at 50% usage) and improved aerodynamics (use of shark lets, increased dihedral angle).

ACKNOWLEDGEMENTS

I would like to sincerely thank **Dr. Nikos Mourtos** for giving his valuable suggestions and support for completing the project.

TABLE OF SYMBOLS
=====

<u>Symbol</u>	<u>Definition</u>	<u>Dimension</u>
A	Aspect ratio	-----
a,b	Regression line constants defined by Eqn. (3.21)	-----
A, B	Regression line constants defined by Eqn. (2.16)	-----
c,d	Regression line constants defined by Eqn. (3.22)	-----
C	Fuel fraction parameter defined by Eqn. (2.31)	-----
c_f	Equivalent skin friction coefficient	-----
c_j	Specific fuel consumption	lbs/lbs/hr
c_p	Specific fuel consumption	lbs/hp/hr
C_D	Drag coefficient	-----
C_{D_0}	Zero lift drag coefficient	-----
CGR	Climb gradient, defined by Eqn. (3.28)	rad
CGRP	Climb gradient parameter, defined by Eqn. (3.30)	rad
C_L	Lift coefficient	-----
D	Drag	lbs
D (Alternate meaning)	$W_{PL} + W_{crew}$	lbs
D_p	Propeller diameter	ft
e	Oswald's efficiency factor	-----
E	Endurance	hours
\bar{E}	$\ln(W_i/W_{i+1})$, Eqns. (2.37 and 2.39)	-----
f	equivalent parasite area	ft ²
F	Weight sensitivity parameter, Eqn. (2.44)	lbs
FAR	Federal Air Regulation	-----
g	acceleration of gravity	ft/sec ²
h	altitude	ft

I_p	Power index, Eqn.(3.51)	$(\text{hp}/\text{ft}^2)^{1/3}$
k	number between 0 and 1	-----
k_1	constant in Eqn.(3.9)	sec^2/ft
k_2	constant in Eqn.(3.9)	-----
l_p	factor in k_2 , see p.102	
L	Lift	lbs
L/D	Lift-to-drag ratio	-----
M_{ff}	Mission fuel fraction (M_{ff} = End weight/Begin weight)	none
n	Load factor	-----
nm	Nautical mile(6,076 ft)	nm
N	Number of engines	-----
P	Power, Horse-power (1hp = 550 ft.lbs/sec)	hp
P_{dl}	Parameter in $\sin\gamma$, Eqns.(3.38) and (3.39)	-----
P_s	Specific excess power	ft/sec
\bar{q}	dynamic pressure	psf
R	Range	nm or m
\bar{R}	$\ln(W_i/W_{i+1})$, Eqns.(2.36 and 2.38)	-----
RC	Rate of climb	fpm or fps
RCP	Rate-of-climb parameter, Eqns.(3.24) and (3.25)	hp/lbs
s	distance, used in take- off and landing equations with subscripts	ft
sm	Statute mile(5,280 ft)	sm
S	Wing area	ft^2
SHP	Shaft horsepower	hp ₂
S_{wet}	Wetted area	ft^2
t	time	sec, min, hr
T	Thrust	lbs
TOP ₂₃	FAR 23 Take-off parameter	$\text{lbs}^2/\text{ft}^2\text{hp}$
TOP ₂₅	FAR 25 Take-off parameter	lbs/ft^2

V	True airspeed	mph, fps, kts
wod, WOD	Wind over the deck	kts
W	Weight	lbs
X	T(hrust) or P(ower)	lbs or hp
Greek Symbols		
=====		
η_p	propeller efficiency	-----
π	product, or 3.142	-----
ρ	air density	slugs/ft ³
σ	air density ratio	-----
μ_G	ground friction coefficient	-----
δ	pressure ratio	-----
γ	flight path angle	deg or rad
$\dot{\psi}$	turn rate	rad/sec
θ	temperature ratio	-----
λ	bypass ratio	-----

LIST OF FIGURES

Figure 1: Mission Profile	16
Figure 2: Global Aviation Market Requirements	16
Figure 3: Trends in Wide, Medium and Narrow Body Aircraft chosen by the Airlines over the years	17
Figure 4: Air travel Growth	17
Figure 5: World Air-Traffic Growth (per region)	18
Figure 6: Trends in Passenger Traffic - India	18
Figure 7: Conventional/Unconventional Wing Structures	20
Figure 8: Boeing 737MAX CAD Drawings	26
Figure 9: Boeing 737-700 CAD Drawings	27
Figure 10: Airbus 320 NEO CAD Drawings	28
Figure 11: Airbus 321 NEO CAD Drawings	29
Figure 12: Bombardier CRJ 1000 CAD Drawings	30
Figure 13: High Wing Configuration - Cessna 172	32
Figure 14: Low Wing Configuration -CRJ1000	33
Figure 15: Mid Wing Configuration -NASA Research Plane	34
Figure 16: Super Critical Air Foil Section	34
Figure 17: Coefficient of lift versus drag, Coefficient of lift versus angle of attack	35
Figure 18: Coefficient of Moments versus drag, Coefficient of Drag versus angle of attack	35
Figure 19: Vertical and Horizontal Tail Configurations	36
Figure 20: Top and front view of the fuselage – CATIAV5	38
Figure 21: Empty Weight vs Take-off Weight	40
Figure 22: Roskam Similar Aircraft results on comparison with current similar aircraft for VER-12XX	42
Figure 23: VER-12XX Mission Profile	46
Figure 24: Design Point Obtained using AAA	56
Figure 25: Mission Profile Outputs for given fuel-fractions, regression coefficients, payload weight and take-off, empty weight estimates	56
Figure 26: Sensitivities Input Parameters	62
Figure 27: Sensitivities (Take-off with respect to Payload, Crew and Empty Weight) Outputs)	62
Figure 28: Trade Studies - Specific Fuel Consumption vs Take-off Weight	62
Figure 29: Weight of Payload(lbs) vs Cruise Range(nm)	63
Figure 30: MAX Coefficient of Lift for Different Flight Scenarios	66
Figure 31: FAR-25 Take-off Run Way Definitions	67
Figure 32: Manual Calculations of FAR-25 Landing Distance	71
Figure 33: FAR-25 Climb Sizing Manual Calculations-I	72
Figure 34: FAR-25 Climb Sizing Manual Calculations-II (Skin Friction Drag Coefficient and Wetted Area)	73
Figure 35: FAR-25 Climb Sizing Manual Calculations-III (Drag Coefficient)	74
Figure 36: Climb Sizing Procedure	75
Figure 37: Climb Gradient Specifications for Take-off and Landing (FAR-25)	76
Figure 38: FAR-25 Climb Sizing Manual Calculations-IV	77
Figure 39: FAR-25 Climb Sizing Manual Calculations-V	78
Figure 40: FAR-25 Climb Sizing Manual Calculations-VI	79
Figure 41: FAR-25 Climb Sizing Manual Calculations-VII (One Engine Operating Condition)	80
Figure 42: Sizing to Manoeuvring Requirement	81
Figure 43: Sizing to Maximum Speed	82

Figure 44:Stall Speed Sizing Plot - AAA	83
Figure 45:Take-off Distance Sizing - AAA.....	83
Figure 46:Sizing to Climb Requirements - Inputs	84
Figure 47:Sizing to Landing Distance -AAA	84
Figure 48:Sizing to Max Speed Requirements -AAA.....	85
Figure 49:Sizing to Manoeuvring Speed - AAA.....	85
Figure 50: Performance Sizing Graph	86
Figure 51: Seating Configurations, Cargo Space for VER-12XX using PRESTO.....	90
Figure 52: Fuselage Cross Section Dimensions - Economy Class	90
Figure 53: Proposed Seat Pitch for Economy and Business Class.....	91
Figure 54: Passenger Dimensions	91
Figure 55: Fuselage- Side View.....	91
Figure 56: Proposed 2-Aisle Configuration for VER-12XX	92
Figure 57: Different Types of Wing Configurations.....	94
Figure 58: Wing Positions	94
Figure 59: GD Wing Weight Calculation from 'Roskam'	96
Figure 60: Cruise Coefficient of Lift Calculations	97
Figure 61:Cruise Coefficient of Lift Calculations-II	98
Figure 62:Sweep Angle and Thickness Ratio Calculations-I	99
Figure 63:Sweep Angle and Thickness Ratio Calculations-II	100
Figure 64:Sweep Angle and Thickness Ratio - Practical Data	100
Figure 65:Pressure, Temperature and Density calculations	103
Figure 66:Reynolds Number calculations.....	104
Figure 67:Coefficient of lift for Wing Calculations.....	105
Figure 68:High-lift devices coefficient of lift calculations	106
Figure 69:High-lift devices calculations - I	107
Figure 70:High-lift device calculations -II.....	108
Figure 71:High-lift device calculations -III	109
Figure 72:Wing Planform for VER-12XX using AAA program.....	111
Figure 73:Wing Planform for VER-12XX showing Spoilers using AAA program	111
Figure 74:Wing Planform for VER-12XX showing Ailerons using AAA program.....	112
Figure 75:Empennage Disposition Calculations-I	114
Figure 76:Empennage Disposition Calculations-II.....	115
Figure 77:CL versus Angle of Attack at Reynolds Number.....	116
Figure 78:Vertical Stabilizer Planform -AAA	117
Figure 79: Vertical Stabilizer with Ridder Tabs -AAA	117
Figure 80:Horizontal Stabilizer Planform -AAA.....	118
Figure 81:Horizontal Stabilizer Trim Tabs -AAA.....	118
Figure 82:Class-I: Component wise weight and centre of gravity breakdown structure	122
Figure 83:Tip over criteria Definition.....	123
Figure 84: Aircraft Landing Gear Definitions - 'Roskam: Airplane Design Part VIII'	124
Figure 85: Components Weight Table -AAA	126
Figure 86: C.G. using Empty Weight from AAA	127
Figure 87: X-C.G. Excursion Table Inputs -AAA	127
Figure 88: C.G. Excursion Outputs.....	128
Figure 89:Y-C.G. Excursion Table Inputs -AAA	128
Figure 90:Z-C.G. Excursion Table Inputs -AAA	129
Figure 91:Z-C.G. Excursion Table Outputs -AAA.....	129

Figure 92:Side View of VER-12XX.....	130
Figure 93:Top View of VER-12XX.....	130
Figure 94:Front View of VER-12XX	131
Figure 95:Longitudinal Stability Calculations-I	134
Figure 96:Longitudinal Stability Calculations-II.....	135
Figure 97:Longitudinal Stability Calculations-III.....	136
Figure 98:Longitudinal Stability Calculations-IV	137
Figure 99:Longitudinal Stability Calculations-V.....	138
Figure 100:Longitudinal Stability Calculations-VI	139
Figure 101:Longitudinal Stability Calculations-VII.....	140
Figure 102:Longitudinal Stability Calculations-VIII.....	141
Figure 103:Longitudinal Stability Calculations-IX	142
Figure 104:Longitudinal Stability Calculations-X.....	143
Figure 105:Longitudinal Stability Calculations-XI	144
Figure 106:Longitudinal Stability Calculations-XII.....	145
Figure 107: Static Margin - Longitudinal Stability.....	146
Figure 108: Inherent Stability Inputs – Directional	146
Figure 109: Horizontal Tail - XPlot.....	146
Figure 110: Lateral X-Plot.....	147
Figure 111:Directional Stability Calculations-I.....	148
Figure 112:Directional Stability Calculations-II.....	149
Figure 113:AAA Directional Stability Inputs and Outputs.....	149
Figure 114:AAA Directional Stability Derivative Outputs	150
Figure 115:One engine out Calculations-I.....	150
Figure 116:One Engine Out Calculations-II	151
Figure 117:AAA One Engine Out Inputs/Outputs.....	151
Figure 118:Drag Polar Calculations - I.....	154
Figure 119:DragPolar Calculations - II.....	155
Figure 120:Drag Polar Calculations – III.....	156
Figure 121:Drag Polar Calculations -IV	157
Figure 122:Drag Polar Calculations – V.....	158
Figure 123:Drag Polar Calculations - VI.....	159
Figure 124:Drag Polar Calculation-VII	160
Figure 125:Drag Polar Calculation -VIII.....	161
Figure 126:Equivalent Parasite Area	162
Figure 127:Landing Gear Definitions with C.G.	163
Figure 128:Total Drag and Drag increments due to flaps and Landing gear.....	164
Figure 129:Landing Gear Drag Calculations -I	165
Figure 130:Landing Gear Drag Calculations-II	166
Figure 131:Critical Mach Number	167
Figure 132:Drag Coefficient versus Mach Number.....	167
Figure 133:Take-off Gear Up Drag Polar	168
Figure 134:Take-off Gear Down Drag Polar	169
Figure 135: Drag Polar during Landing Gear ‘UP’	169
Figure 136:Drag Polar-One Engine Inoperative	170
Figure 137:Clean Configuration Polar	170
Figure 138:All Flight Conditions Drag Polar	171

Figure 139: Take-off field Length for a given Wing loading at respective Maximum Lift Coefficient	176
Figure 140: Landing field Length for a given Wing loading at respective Maximum Lift Coefficient	177
Figure 141: Wing Loading versus L/D max	178
Figure 142: Ride Quality versus Wing loading	178
Figure 143: High Wing Configuration - Cessna 172	179
Figure 144: Low Wing Configuration - CRJ1000	179
Figure 145: Mid Wing Configuration - NASA Research Plane	180
Figure 146: Symmetrical Aerofoil in Stability terms.....	181
Figure 147: Symmetrical, Cambered Aerofoils in stability terms	182
Figure 148: Conventional and Supercritical Aerofoils Shock Wave separation and Pressure Distributions.....	182
Figure 149: (Conventional, Supercritical) Aerofoil Drag Rise data as the Mach number Increases..	183
Figure 150: Super Critical Air Foil Section	183
Figure 151: Coefficient of lift versus drag, Coefficient of lift versus angle of attack	184
Figure 152: Coefficient of Moments versus drag, Coefficient of Drag versus angle of attack.....	184
Figure 153: Sweep Angle Definition	185
Figure 154: Airflow over a Swept Wing.....	186
Figure 155: Variation of Max Lift Coefficient with Sweep Angle	186
Figure 156: Straight and Swept Wing Lift-Curve Slope.....	187
Figure 157: United Airlines Boeing 737 Winglets located at Wing tips	189
Figure 158: Wing Tips with and Without Winglets.....	190
Figure 159: Incidence Angle of Wing Profile showing the Root, Mid-wing and Tip	191
Figure 160: Wing Drag Coefficient versus Mach Number	192
Figure 161: VER-12X with sweep.....	193
Figure 162: Waix v-tail	197
Figure 163: T-tail and Low Horizontal T-tail Configurations	198
Figure 164: Aircraft Three Axes	199
Figure 165: Pitching Moment versus Coefficient of Lift.....	201
Figure 166: FAR-23 Stable Pitch Break Behaviour.....	202
Figure 167: Unstable Pitch Breaks - FAR25	202
Figure 168: Empennage Configurations as related to Stall and Spin Characteristic's.....	203
Figure 169: C_L vs C_d and C_L vs Alpha and C_m vs Alpha	206
Figure 170: V-n diagram for VER-12X using AAA.....	211
Figure 171: Drag breakdown due to physical causes.....	214
Figure 172: Typical Drag breakdown for Transport Jet.....	215
Figure 173: Fuselage Definitions.....	218
Figure 174: Aircraft angle of attack vs Fuselage Total Drag – MATLAB	220
Figure 175: Drag produced by various fuselage cross-section	220
Figure 176: Fuselage fineness ratio vs fuselage drag coefficient.....	221
Figure 177: Angle of attack vs fuselage transonic drag.....	222
Figure 178: Drag parameters of wing - Output.....	225
Figure 179: Drag parameters fuselage - output.....	225
Figure 180: Drag parameters for horizontal tail - Output	225
Figure 181: Drag parameters for vertical tail - output	225
Figure 182: Coefficient of drag versus lift – Class II AAA.....	226
Figure 183: Overall VER-12X drag - Class II AAA.....	226

Figure 184: Jet-engine working principle	228
Figure 185: RAM Drag effects on turbo-jet.....	229
Figure 186:Power extraction calculations - MATLAB.....	230
Figure 187: GE-9X Engine	232
Figure 188:Side View of VER-12XX.....	233
Figure 189:Top View of VER-12XX.....	233
Figure 190:Front View of VER-12XX	234
Figure 191:Global Aircraft Fuel Burn	234
Figure 192:Fatalities by Phase of Flight	235

LIST OF TABLES

Table 1: Mission Specifications.....	15
Table 2: Comparison of Different Aircraft Mission Capabilities	21
Table 3: Comparison of Important Design Parameters.....	22
Table 4: Performance Analysis for different Aircraft.....	25
Table 5: Take-off Weight and Empty Weights of Similar Airplanes	40
Table 6:Weight Sensitivities Summary.....	61
Table 7:Determined Power Loading for specified Wing Loading values at $CL_{max}=1.2$	68
Table 8:Determined Power Loading for specified Wing Loading values at $CL_{max}=1.4$	68
Table 9:Determined Power Loading for specified Wing Loading values at $CL_{max}=1.6$	68
Table 10:Determined Power Loading for specified Wing Loading values at $CL_{max}=1.8$	69
Table 11: C_{Lmax} obtained for different Wing-Loading at Landing.....	70
Table 12: Estimated Wing Parameters.....	110
Table 13: Centre of Gravity Assumptions from Roskam.....	121
Table 14: VER-12XX Landing Gear Parameters.....	124
Table 15: Centre of Gravity Manual Calculations in X-Direction.....	125
Table 16:Centre of gravity calculation in Y-direction	125
Table 17:Centre of gravity calculation in Z-direction.....	126
Table 18:Take-off field Length for a given Wing loading at respective Maximum Lift Coefficient .	175
Table 19:Landing field Length for a given Wing loading at respective Maximum Lift Coefficient..	176
Table 20: Determining the Coefficient of Drag using the parameters specified in Equation 1.5 for variable Wing loading.....	177
Table 21:Wing Weight comparison with and without Sweep using GD Method from 'Roskam' part V	188
Table 22: Horizontal Tail Geometry	205
Table 23: Vertical Tail Geometry	205
Table 24: Parameters required to construct V-n diagram for VER-12X.....	211
Table 25 : GE-9X Engine characteristics.....	231

CHAPTER-1

MISSION SPECIFICATIONS AND CONFIGURATION DESIGN

The proposed VER-12XX aircraft is a twin-engine turbo jet designed mainly to serve the purpose of short to medium range travel with distinctive range and endurance. This aircraft has a typical seating capacity of 150-200 passengers with two crew piloting the aircraft. The VER-12XX is a next generation aircraft that is carefully designed with reduced noise and emissions from the engines. Composite materials replaced traditional aluminium metal and their alloys in this aircraft construction, increasing the strength of the aircraft structures with reduced weight which ultimately results in significant changes in the overall efficiency. VER-12XX uses the glass cockpit technology; replacing all the interface systems with touch enabled screens which is user-friendly and does not require additional training. VER-12XX features computer mediated controls i.e. fly-by wire systems which reduces the pilot work load and improved redundancy.

VER-12XX can be a good a competitor for the Boeing-737 MAX and Airbus-321,320 NEO aircraft in terms of range, fuel consumption, reduced maintenance costs and total cost per seat(miles). In this preliminary design chapter, the mission specifications for the proposed configuration will be laid down where the key aircraft parameters such as range, endurance, take-off and landing field distance will be estimated. It is important to precisely understand the global aviation market needs while introducing a new aircraft which will also be thoroughly studied in the market analysis section.

1.1 MISSION SPECIFICATION

1.1.1 MISSION SPECIFICATION

Table1, clearly explains the preliminary estimated parameters for the proposed aircraft configuration(VER-12XX). It is to be noted that all the parameters that have been listed are estimated based on technical data of current aircraft from Boeing, Airbus and Bombardier.

Table 1: Mission Specifications

Pay Load Capacity	Passengers: 150-200 Cargo Capacity: 30 Pallets (518.2 m ³)
Crew	2 pilots
Range	7400 nmi (13705 kms)
Cruise Speed	526 knots (975.5 km/hr)
Mach Number	0.79
Cruise Altitude	35000 feet
Take-off Field Length	9300 feet
Landing Field Length	10000 feet
Approach Speed	149 knots (275.95 km/hr)
Engines	GE 9X – 1,00,000 lbs (Thrust) (each)

1.1.2 MISSION PROFILE

Since, VER-12XX is a commercial jet, the mission profile shown in figure1, is like most of the current transport jet's. The mission profile includes taxi, take-off, climb, cruise, descent, loiter, approach, land and taxi. As per FAR-25 guidelines, it is required, an aircraft should carry additional fuel for reserves apart from the mission just in the case of missed approach or long wait times to land.

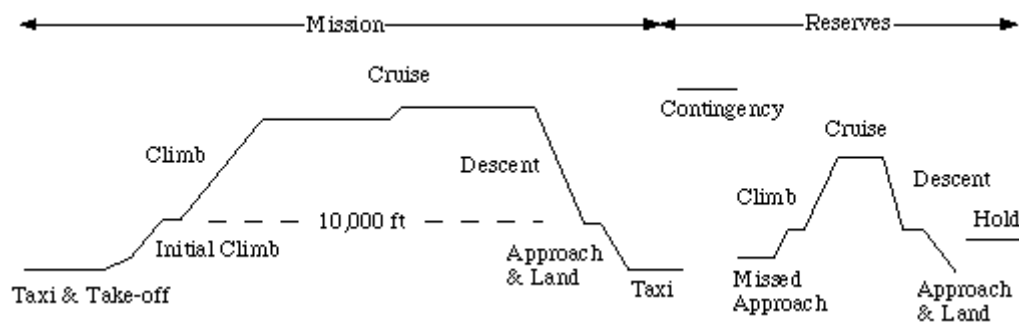


Figure 1: Mission Profile

1.1.3 MARKET ANALYSIS

With the increasing passenger traffic around the world and the increased demand for long haul travel; almost all the airlines in the world are looking forward to expanding their markets into global frontiers. The major factors that an airline consider meeting these demands are an aircraft with:

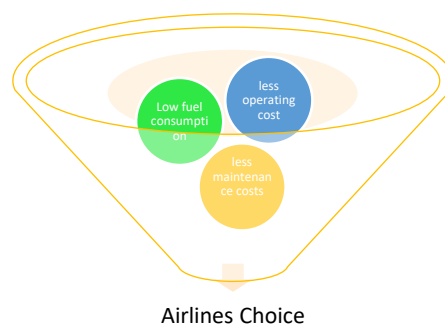


Figure 2: Global Aviation Market Requirements

Below is a graphical representation that shows a shift in demand from larger airplanes to medium and narrow body aircraft.

Airlines moving from large airplanes to small and medium widebodies

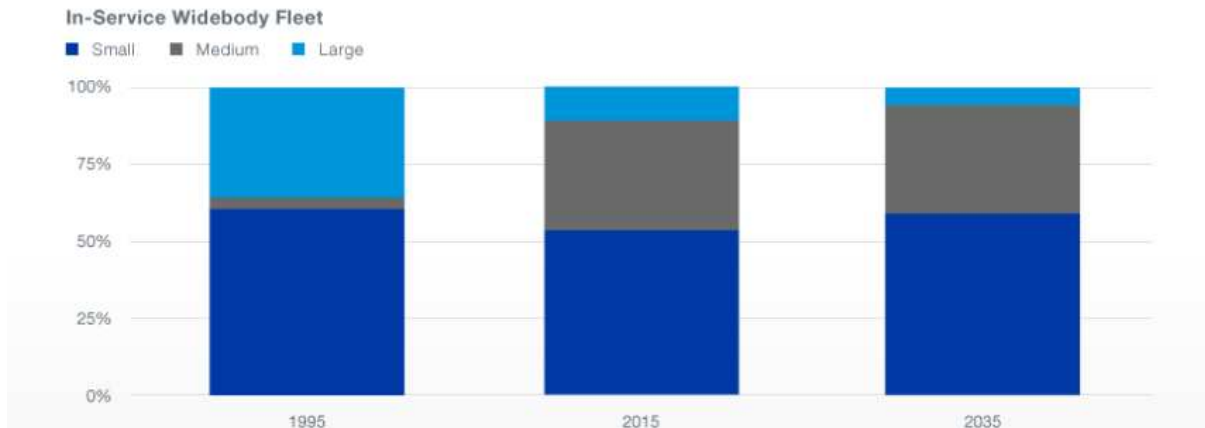


Figure 3: Trends in Wide, Medium and Narrow Body Aircraft chosen by the Airlines over the years

The statistical data below shows the percentage increase/decrease in the passenger air travel from the year 2005 – 2016* all over the world. Despite the challenges being faced by the Airlines (e.g. Fuel, operating costs); the demand for air travel which is a favourable factor for airlines; is forcing them to make significant changes to their fleet to meet the demands.

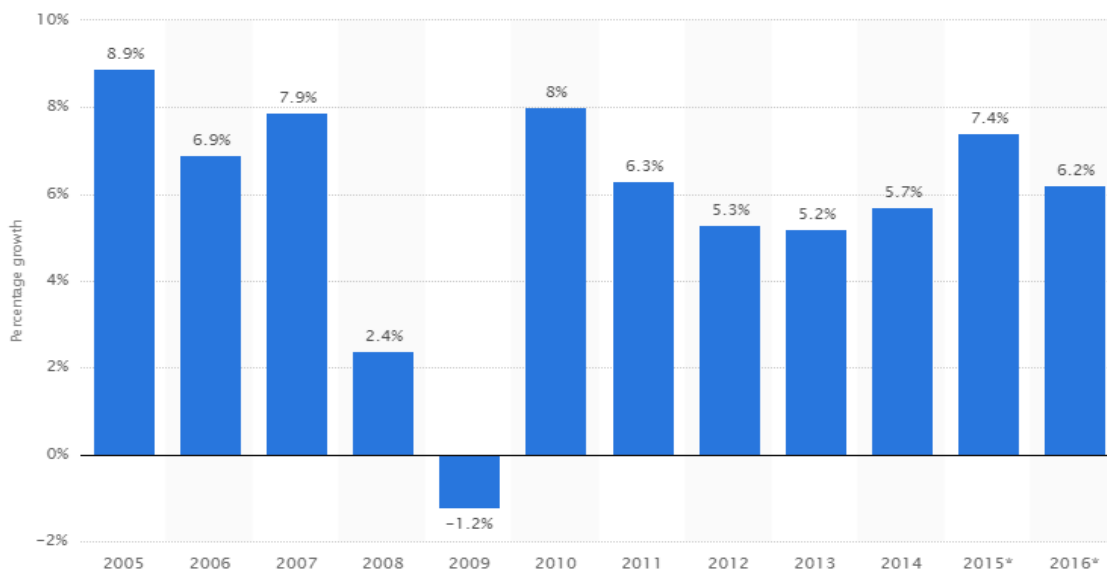


Figure 4: Air travel Growth

With new destinations being added, global airline markets are emerging at rapid rates, proved a point in the increased revenues and GDP. Figure5 shows the percentage increase in air traffic with an estimate (i.e. between years 2016*-2035)

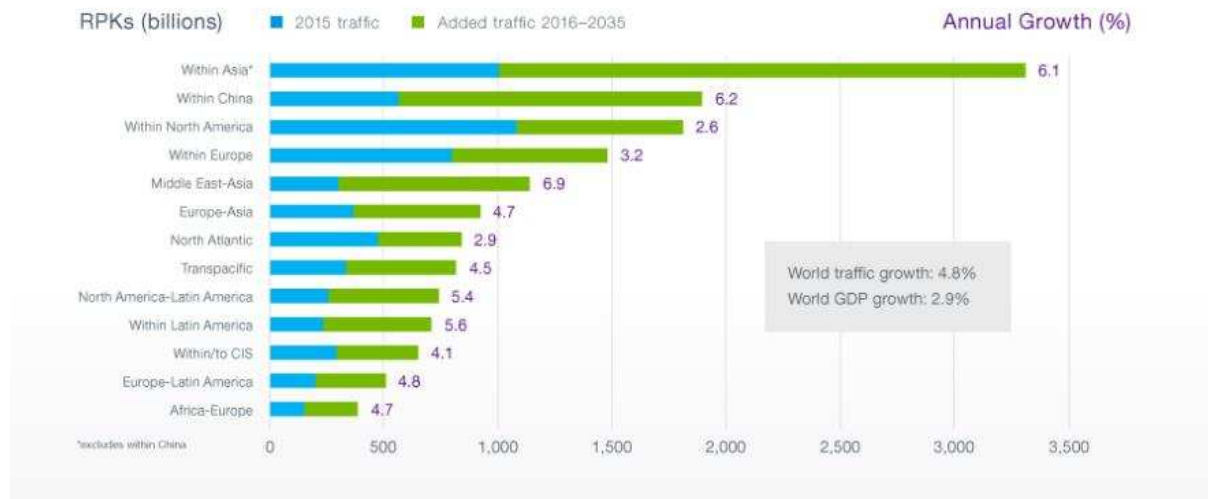


Figure 5: World Air-Traffic Growth (per region)

VER-12XX is going to be a key player especially in the emerging airline markets countries like India, who are considering major changeover in their present civil aviation fleet and for the LCC (Low Cost Carrier) business models. It is clear from their increasing domestic passenger traffic (i.e. to almost 21.63 percent) and total aircraft movements of 160830; that they are one of the fastest growing aviation sectors in the world. Low cost carriers play a vital role in Indian Civil Aviation; as their Business is mainly targeted towards the lower middle-class people with affordable costs apart from the Business Class passengers. Figure6 shows the trends in the air traffic passenger in India.



Figure 6: Trends in Passenger Traffic - India

1.1.4 TECHNICAL AND ECONOMIC FEASIBILITY:

VER-12XX is a narrow body aircraft with all new wing design which has foldable blended winglets making it compatible to land at any airport. Winglets helps in improving the overall efficiency of the aircraft by reducing the drag and by weakening the wing tip vortices. This configuration directly results in reduced fuel consumption with an approximation of 4 to 5 percent efficiency. 45% of the airframe structures are manufactured using composite materials; which resulted in improved structural strength of materials. The GE9X engines are lot quieter than its predecessors which are the first engines to lay the basis for **greener** aviation. The cross section of the aircraft fuselage is an **ellipse** which allows us to accommodate seats in an aimed 2-2 configuration with extra legroom increasing the comfort for passengers and more cargo carrying capacity*.

The estimated operating cost per hour of VER-12XX is \$8905 which is a lot cheaper when compared with Boeing-777(\$9138.19/hour) and Airbus-350(\$8383.15/hour). The estimated cycle of maintenance apart from regular checks for VER-12XX is once every year; which shows the aircraft efficiency for continuous flights (i.e. to fly continuously with minimal maintenance). VER-12XX uses fuel efficient GE9X engines to combat the impacts of increased fuel costs.

1.1.5 CRITICAL MISSION REQUIREMENTS

VER-12XX is medium range aircraft with an estimated continuous flight of 9 hours. The critical mission requirements for this proposed configuration are the payload, range and cruising altitude. As per 'General Electric', the use of GE-9X Engines requires the aircraft to cruise nominally at 38000 ft. to produce the required thrust for any range specification. Apart from the above specified critical requirements, Aerodynamics also play a vital role to achieve the 7400 nmi range. Recently, Boeing and Airbus claims that the use of winglets have greatly improved the fuel efficiency of their variants (e.g. B-777,727; A-320,321) and reduced tip

vortices with significant reductions in drag. Figure7 includes different types of wing structure both conventional/un-conventional design with different wing-tips. Figure7 is included in this section to present the reader with an idea of the possible wing structures which will be critical while estimating the overall range and these wing structures design can be considered during the latter sections of the project.



Figure 7: Conventional/Unconventional Wing Structures

1.2 COMPARATIVE STUDY OF SIMILAR AIRPLANES

1.2.1 MISSION CAPABILITIES AND CONFIGURATION SELECTION

In this section, the mission capabilities of 5 different aircraft will be studied. Table2 includes different parameters related to those aircraft and are essential for estimating the take-off, empty weights for VER-12X.

Table 2: Comparison of Different Aircraft Mission Capabilities

Aircraft Model	Boeing 737-MAX	Boeing 737-700	Airbus 320 NEO	Airbus 321 NEO	Bombardier CRJ 1000
Range	7080nmi. (13600 km)	7370 nmi. (13600 km)	7370 nmi. (13600 km)	7370 nmi. (13600 km)	1622 nmi. (3004 km)
Passengers (max seating)	178	128	440	277	104
Fuel per Seat – km(/100km)	3.08 litres*	3.90 litres*	3.66 litres*	2.98* litres	3.50 litres*
Maximum Take-off distance (meters)	3300	3100	2200	2500	2120
Landing Field Length (meters)	1900	1519	1966	1750	1750

Note: The * indicates that the values are estimated and may differ from the exact values.

1.2.2 COMPARISON OF IMPORTANT DESIGN PARAMETERS

Table 3: Comparison of Important Design Parameters

Aircraft Model	Boeing 737-MAX	Boeing 737-700	Airbus 320 NEO	Airbus 321 NEO	Bombardier CRJ 1000
Weight at Take-off (W_{TO})	775000 lb (351534 kg)	154500 lb (70100 kg)	172000 lbs (78018 kg)	206000 lb (93440 kg)	91800 lb (41640 kg)
Empty Weight(W_E)	80200 lbs (36379 kg)	83000lbs (37649 kg)	93900 lbs (42593 kg)	107000 lbs (48535 kg)	51120 lbs (23188 kg)
Engine Weight(E_{weight})	CFM LEAP-1B	CFM 56-7 Series	CFM 56-5B	CFM 56-5B	GE CF-34-8C5A1
Weight of Fuel(WF)	47890 US gal (181283 litres)	33340 US gal (126206 litres) / 101323 kg	37200 US gal (140817.32 litres)	36744 US gal (109185 kg)	36650 US gal (138720 litres)
Thrust (T)	Thrust _{take-off} = 366.1 kN (x2)	Thrust _{take-off} = 284.7 kN (x2)	Thrust _{take-off} = 120 kN (x2)	Thrust _{take-off} = 147 kN (x2)	Thrust _{take-off} = 64.5 kN (x3)
Cruising Speed (V_{cr})	482 knots; Mach 0.84	488 knots; Mach 0.85	448 knots; Mach 0.78	470 knots; Mach 0.82	470 knots; Mach 0.78
Range (R)	7370 nmi. (13600 km)	7355 nmi (13621 km)	3300 nmi (6100 km)	3700 nmi (6850 km)	1622 nmi (3004 km)
Cruising Altitude (h_{cr})	35000 ft.	40000 ft.	39000-4100 ft.	39000-4100 ft.	37000 ft.
Wing Area (S)	436.8 m ²	325 m ²	122.4 m ²	122.4 m ²	77.4 m ²
Wing Span (b)	64.8 m	58.8 m	34.10 m	34.10 m	26.2 m
Wing Aspect Ratio (AR)	9.613	10.638	9.5	9.5	8.87
Payload Type	Passengers and cargo	Passengers and cargo	Passengers and cargo	Passengers and cargo	Passengers and cargo

1.3 DISCUSSION:

For any new entry, commercial aircraft, it is very important that its purpose is well defined and meeting the current requirements of Airlines Business. Though the inclusion of winglets is a key factor but the additional attachment increases maintenance costs. From the table in the previous page we can see different aircraft with different capabilities; some operate at high speeds with higher efficiency while some offer less weight. In the design trade off it is important to consider present available technology, the need for the introduction of new aircraft and scalability. For a commercial aircraft, to accommodate passenger's in the range of 150-200, the design considerations must be based on current airline needs, production and manufacturability besides integration of newer technologies. VER-12XX has a wider range which allows the airlines to use this aircraft for inter-continental flight also. VER-12XX can be a good replacement for Boeing737, further increasing the range of narrow body aircraft with comparatively less operating costs. To sum up with; an aircraft with improved aerodynamics and high structural integrity with reduced weight can be a good addition to the family of narrow body commercial aircraft.

CHAPTER 2

CONFIGURATION DESIGN

Configuration design for this aircraft is based on the current and previous designs which only includes current gasoline aircraft. Almost every aircraft today has an integrated gasoline engine with traditional configuration. The very fact that current aircraft follow certain traditions in terms of wing, engine, tail and fuselage placements. For commercial aviation; low/high wing configuration, engines dangling down the wings and sometimes integrated into the vertical tail can be vividly seen where these types of configurations are aerodynamically efficient which the aircraft have both the current/past technologies integrated into them. The proposed aircraft is typically made to be efficient, stable and easily controllable. The mission specifications of documented similar aircraft will be compared again to check whether the integration of a light weight engines, 50% composites used for structures along with the blended winglets made any difference while proving a point.

A comprehensive list of similar aircraft design with similar mission specifications will be discussed in the later sections where the key configuration parameters are tabulated. This is important as it helps in understanding a key aspect i.e. a relation between available technology versus integration of advanced technologies. Unlike Electric Aircraft, there are numerous resources available on the internet today, which enables us to make precise evaluations in terms of weights and other parameters for gasoline aircraft. Propulsion system location is integrated based on the safety, reliability and efficiency. Though the mission requirements cannot be met due to certain limitations; the configuration design helps us to accomplish them.

Once the propulsion selection is made then the aircraft configuration is designed as per the trade-offs based on the aircraft data presented. Overall aircraft configuration will be made as simple and predictable that which matches the behaviour and performance of regular aircraft. These predictions which help us to evaluate the critical mission requirements at the end are viable because they save time and money which is crucial in aviation industry.

2.1 COMPARATIVE STUDY OF AIRPLANES WITH SIMILAR MISSION PERFORMANCE

2.1.1 COMPARISON OF WEIGHTS, PERFORMANCE AND GEOMETRY OF SIMILAR AIRPLANES.

Table 4: Performance Analysis for different Aircraft

Aircraft Model	Boeing 737-MAX	Boeing 737-700	Airbus 320 NEO	Airbus 321 NEO	Bombardier CRJ 1000
Weight at Take-off (W_{TO})	775000 lb (351534 kg)	154500 lb (70100 kg)	172000 lbs (78018 kg)	206000 lb (93440 kg)	91800 lb (41640 kg)
Empty Weight(W_E)	80200 lbs (36379 kg)	83000lbs (37649 kg)	93900 lbs (42593 kg)	107000 lbs (48535 kg)	51120 lbs (23188 kg)
Engine Weight(E_{weight})	CFM LEAP-1B	CFM 56-7 Series	CFM 56-5B	CFM 56-5B	GE CF-34-8C5A1
Weight of Fuel(WF)	47890 US gal (181283 litres)	33340 US gal (126206 litres) / 101323 kg	37200 US gal (140817.32 litres)	36744 US gal (109185 kg)	36650 US gal (138720 litres)
Thrust (T)	Thrust _{take-off} = 366.1 kN (x2) T_cruise = 72.2 kN	Thrust _{take-off} = 284.7 kN (x2)	Thrust _{take-off} = 120 kN (x2)	Thrust _{take-off} = 147 kN (x2)	Thrust _{take-off} = 64.5 kN (x3)
Cruising Speed (V_{cr})	482 knots; Mach 0.84	488 knots; Mach 0.85	448 knots; Mach 0.78	470 knots; Mach 0.82	470 knots; Mach 0.78
Range (R)	7370 nmi. (13600 km)	7355 nmi (13621 km)	3300 nmi (6100 km)	3700 nmi (6850 km)	1622 nmi (3004 km)
Cruising Altitude (h_{cr})	35000 ft.	40000 ft.	39000-4100 ft.	39000-4100 ft.	37000 ft.
Wing Area (S)	436.8 m ²	325 m ²	122.4 m ²	122.4 m ²	77.4 m ²
Wing Span (b)	64.8 m	58.8 m	34.10 m	34.10 m	26.2 m
Wing Aspect Ratio (AR)	9.613	10.638	9.5	9.5	8.87
Payload Type	Passengers and cargo	Passengers and cargo	Passengers and cargo	Passengers and cargo	Passengers and cargo

2.1.2 CONFIGURATION COMPARISON OF SIMILAR AIRPLANES

a) Boeing 737-MAX:

* Static ground line condition, all gears approximately 80% compressed

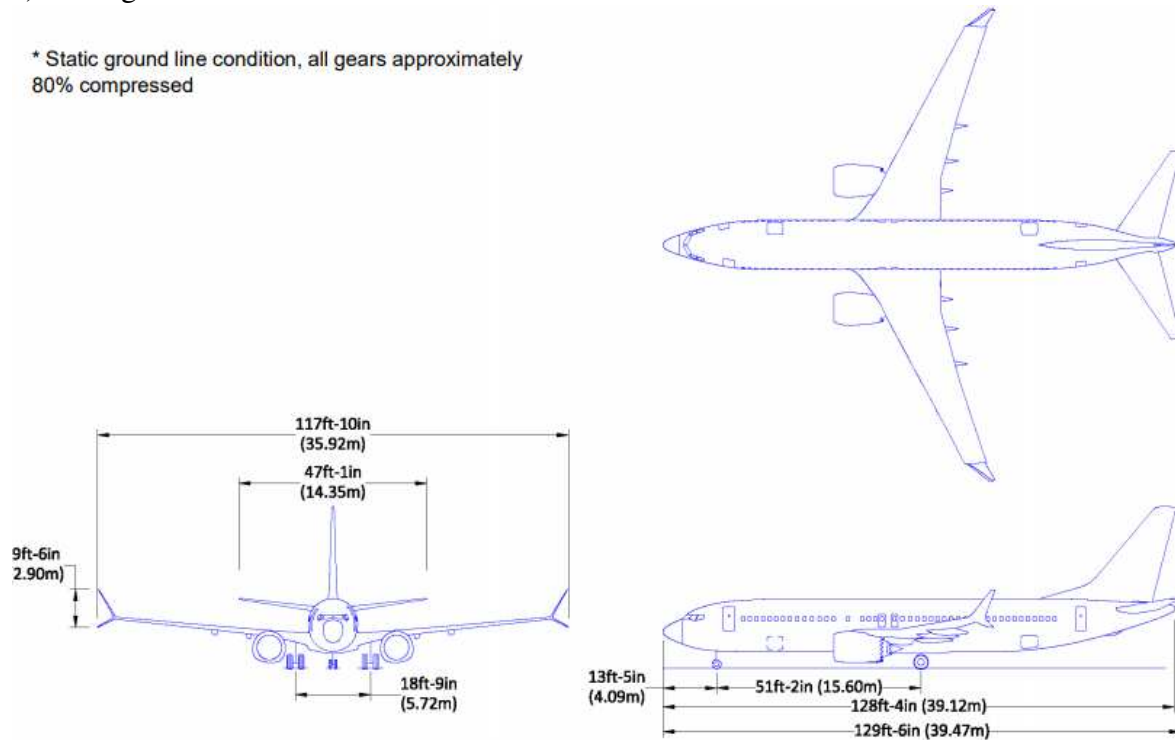


Figure 8: Boeing 737MAX CAD Drawings

b) Boeing 737-700:

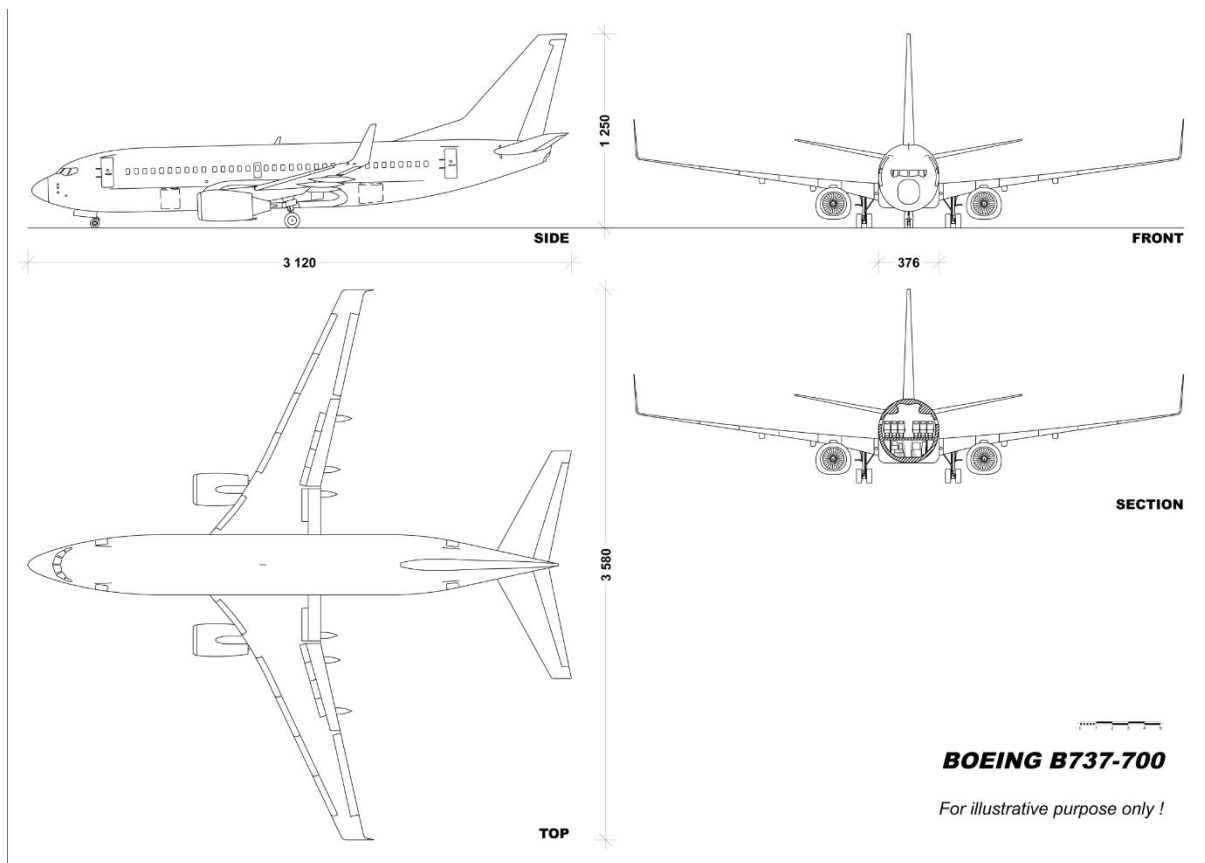


Figure 9: Boeing 737-700 CAD Drawings

c) Airbus 320NEO:



Wing span 35.80 m



Overall length 37.57 m



Height 11.76 m

Figure 10:Airbus 320 NEO CAD Drawings

d) Airbus 321 NEO:



Figure 11: Airbus 321 NEO CAD Drawings

e) Bombardier CRJ 1000:

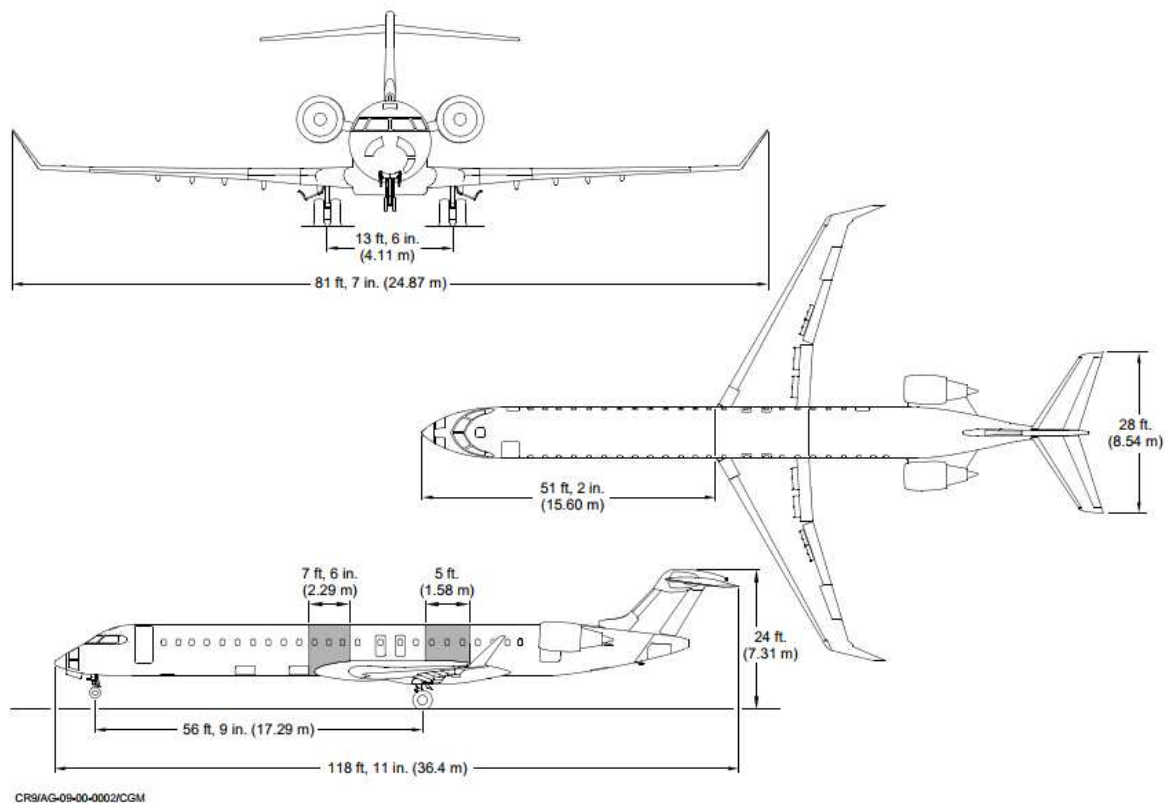


Figure 12: Bombardier CRJ 1000 CAD Drawings

2.2 DISCUSSION

From section 2.1, comparing all the important mission capabilities, CAD-drawings of the listed aircraft; it can be inferred that for four out of five aircraft, the propulsion system are attached to the wing; except for CRJ-1000 the propulsion system is located at the aft of the fuselage. There are several advantages when the engines are attached to the wing especially in a low wing configuration. It enhances maintenance activities without the need to reach out things for and making it easy for visual inspections. Boeing, while considering the Rolls Royce Engines for their 737's there has been quite a bit of debating about the ground clearance because their landing gear length is less compared to Airbus 320's which forced them to flatten the engine outer cowl. Since, engines location play a vital role in Drag, Centre of Gravity, Wing Bending Relief, Stall Speeds and so on it is key to thoroughly understand its location impact before proposing an ideal engine design for the proposed aircraft. Practically, when engines are mounted in the wing root they are nominally closer to the C.G. which requires less downward force from the tail and this reduces the drag especially during an engine failure. But, when they are mounted in pods under the wings; reduced controllability during a cross wind landing, wing

bending relief which could be favourable for thin wings integration, at high incidence angles there can be reduced span wise flow. Engines which are located on the pods near the rear end of the fuselage result in low asymmetric yaw during an engine failure and remove the necessity of using larger rudder movements which ultimately results in reduced drag and better aircraft handling capabilities. It is required that for engines located at the rear of the fuselage the vertical stabilizer needs to be relatively big as the wings should move further aft.

Wing configuration is one of the key design parameters. The tabulated aircraft data in the previous sections gives us a glimpse of their respective wing configurations. We can see that all the five aircraft have low wing configurations. The low wing offers excellent weight reductions, while the high wing offers longitudinal stability. The longitudinal stability in the low wing configuration is achieved/compensated by means of 'dihedral'. The landing gear can be retracted into the low wing configuration only which is lighter and shorter. Whilst the high wing configuration requires room to accommodate retractable landing gear into the fuselage or the gear must be heavier. Conventional winglets on their wing tips result in increased wing span which means reduced drag and adding up for the increase of the overall lift to drag ratio. For a transport aircraft like this there would not be an adverse impact on its performance if the landing gear sticks outside as it helps increase the drag during landing which reduces the aircraft speed.

As we can see the tails of the above documented aircraft, all five aircraft have conventional tail configurations. All the aircraft horizontal stabilizers are in relation with the line of thrust. A major disadvantage with this type of configuration is that in the event of a spin the aircraft's airflow should help the pilot to recover but instead it is being blocked by the horizontal stabilizer and making the pilot incapable of operating the rudder. The lower positioned horizontal stabilizer is affected by the downwash from the wings. The CRJ1000 aircraft has a T-tail with horizontal stabilizer on the top of the tail which experiences less downwash. Since CRJ-1000 is a recent entry into the aviation market it is believed that the aircraft structure is much stronger as their manuals read that 25% of composites are used in its construction. This is a preferred configuration especially when the aircraft spins but, the conventional configuration will be equally considered as this design has been serving passenger jet needs since many years.

2.3 CONFIGURATION SELECTION

2.3.1 FUSELAGE:

Aircraft fuselage is the first part to encounter the effects of air and it accounts for 20-30% of total drag. Fuselage exterior surface roughness and the nose shape determine the laminar flow around the aircraft at various Mach speeds and Reynolds number. The amount of drag generated by an aircraft is directly proportional to the wetted area which is responsible for different types of drag. Usually for long/medium range commercial aircraft, the fuselage lengths are more and to accommodate more number of passengers the designers have no option but to improvise the material fineness ratio to minimise drag effects and to change the cabin configurations. For VER-12XX; the nose is cambered, fuselage boundary layer control is not used as this significantly reduces drag.

2.3.2 WING CONFIGURATION

Wing configuration play an important role in the overall lift for the aircraft. This is a section where the key aspects of the wing will be thoroughly analysed. Conventional aircraft has three wing placement options i.e. high, low and mid wing. Each wing configuration has its own advantage and disadvantages. In general aviation, most aircraft have high wing configuration. Few examples for high wing aircraft are Cessna 172,310.



Figure 13:High Wing Configuration - Cessna 172

High wing configuration offers effective ground clearance and better view for the pilot especially while searching for landmarks and runways. It can also be the best configuration especially for the trainers and does not become a barrier for airport equipment. In this configuration, a pilot can have a visibility of 270 degrees. An aircraft with high wing configuration will have high stability. Since the centre of gravity is below the wing and when the aircraft banks the natural tendency will make the wings level reducing the pilot' effort.

On the other hand, Low wing configuration is also the most commonly used in general aviation aircraft. Compared to the high wing the low wing configuration are not inherently stable as the centre of gravity is above the wing. For this a dihedral angle, must be used for the wings to compensate for stability. This configuration is also used for aircraft cruising at high subsonic speeds. Few examples for high wing configuration are Cessna 400 Corvails, Mooney M20.



Figure 14: Low Wing Configuration -CRJ1000

The low wing with retractable landing gear into the fuselage means a shorter gear. The result is gear easily being fitted into the wing with minimum weight of the gear structure. Since, the proposed aircraft is used for passenger travel this wing configuration will keep the aircraft afloat during an event of ‘ditching’.

Mid wing configuration is the least commonly used for the aircraft. The major problem for its rarity is that this wing configuration requires spars which run through the fuselage. This removes the necessary space for payload and interferes with passenger seating. To avoid spars running through the fuselage additional structures must be integrated; which adds extra weight to the aircraft. Also, the landing gear must be longer and retracted into the fuselage instead of the wing. The mid-wing configuration is better than low-wing in terms of stability as it produces less interference drag which increase the lift to drag ratio and hence the range. Few examples of mid-wing aircraft are Piper Aerostar, FJ 100.



Figure 15: Mid Wing Configuration -NASA Research Plane

Air foil Selection:

Wing configurations are responsible for the aircraft total lift and they vary as per the mission requirements. For VER-12XX a super critical aerofoil is being for the wing configuration. A supercritical aerofoil reduces the wave drag with highly cambered surface towards the aft. Figure16 shows us the supercritical aerofoil section with its important graphical representation of aerodynamics forces in Figure 17,18.

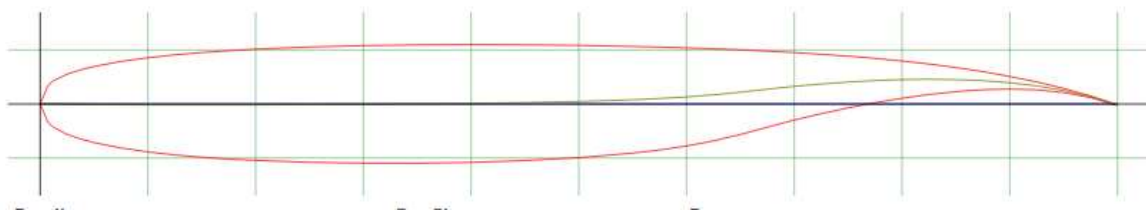


Figure 16: Super Critical Air Foil Section

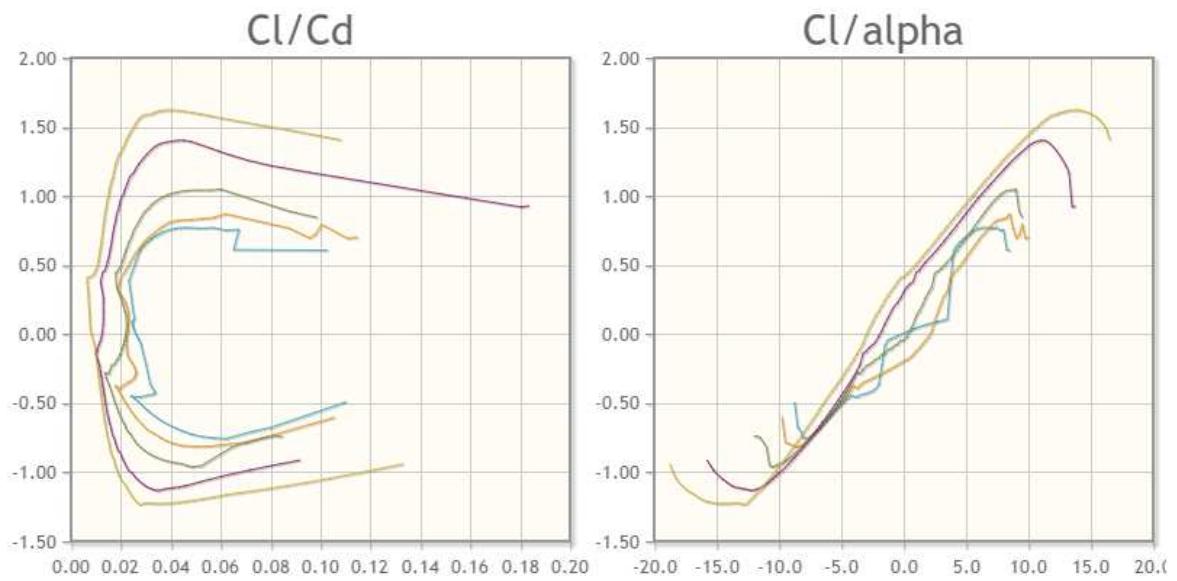


Figure 17: Coefficient of lift versus drag, Coefficient of lift versus angle of attack

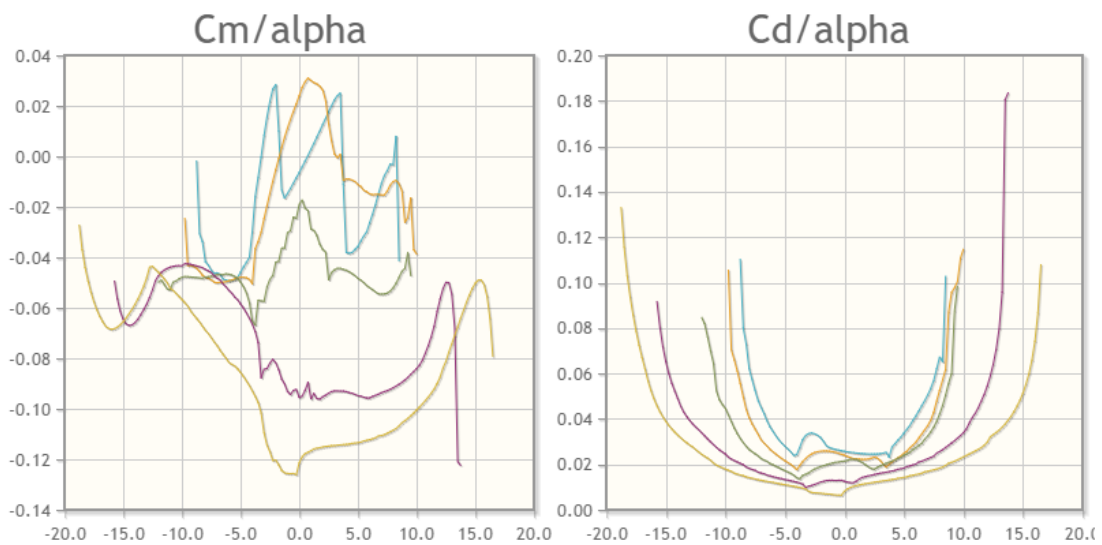


Figure 18: Coefficient of Moments versus drag, Coefficient of Drag versus angle of attack

A supercritical aerofoil cross section could be advantageous for a commercial aircraft which are nearing speeds of Mach 1. It is a known fact that, when an aircraft is approach Mach1 with conventional wing; airflow on the top of the wing is increased reducing laminar flow which results in shock wave generation. But, when a supercritical air foil is used, there is a delay in the shock wave which greatly enhances the fuel efficiency with significant drag reductions.

2.3.3 EMPENNAGE CONFIGURATION

VER-12XX share the same fuselage and wing characteristics alongside the present medium narrow body commercial aircraft. To reduce the drag, the aircraft uses supercritical blended wing structures which reduces drag and improves the aircraft efficiency by 20% without the need for a large vertical stabilizer. Usually to compensate the amount of drag produced by the fuselage, vertical stabilizer length is increased to gain more directional and longitudinal stability. VER-12XX uses conventional aft tail and one aft vertical tail. This basic conventional design is used to increase the longitudinal and directional trim stabilities.

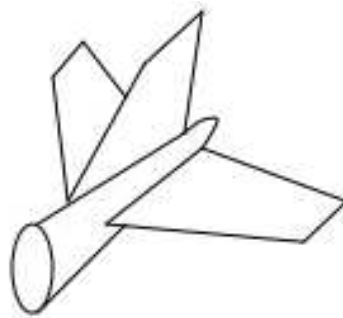


Figure 19: Vertical and Horizontal Tail Configurations

2.3.4 INTEGRATION OF THE PROPULSION SYSTEM:

The propulsion system integration depends usually on the specified mission requirements. It is a good idea to use combination of engines (i.e. turbojet plus piston engine) but this increases the maintenance cost. For VER-12XX mission requirements an existing turbo-jet engine GE-9X will be studied as it has few favourable factors that stand out from other turbo jet engines such as improved fuel efficiency, reduced noise, CO₂ and NOX emissions and lighter. In the preliminary design, as per the take-off weight requirements and range, the possibility of using GE-9X engines will be analysed in further sections of the project.

Engines integration with respect to the position is very important as they determine the structural integrity of the wing and is also responsible for impacting the boundary layer. Conventionally the engines are placed at the leading edge of the aircraft wing and they are podded structures which are useful in energising the boundary layer. It is aimed that for VER-12XX to use the same design in terms of the engine location.

2.3.5 LANDING GEAR DISPOSITION:

Landing gear design play an important role in the aircraft design as these are the structures through which aircraft is balanced when on ground and during landing. There are different types of landing gear configurations like tail dragger, single landing gear, bicycle gear, tricycle gear and bogie type. Depending on the aircraft type and weight landing gear specifications should be adjusted. Usually for medium/short range aircraft, a conventional tricycle or bogie type landing gear serves the purpose. Since it is a passenger aircraft the landing gear struts should have the capability to dampen the vibrations and provide a cushioning effect. The landing gear will be stowed into the fuselage and not into the wings because of the joined wing configuration. Also, tricycle gear configuration will be used. Some of the advantages of a tricycle configuration are:

- Good Visibility
- Directionally stable on ground and during taxi
- Large Crab Angle during cross wind landing
- Increased number of Wheels will increase the aircraft performance
- Better protection for Propellers

2.5.6 PROPOSED CONFIGURATION

Fuselage cross sectional view:

The CAD drawings are drawn using CATIA-V5 software. Below are the sectional views of the fuselage.

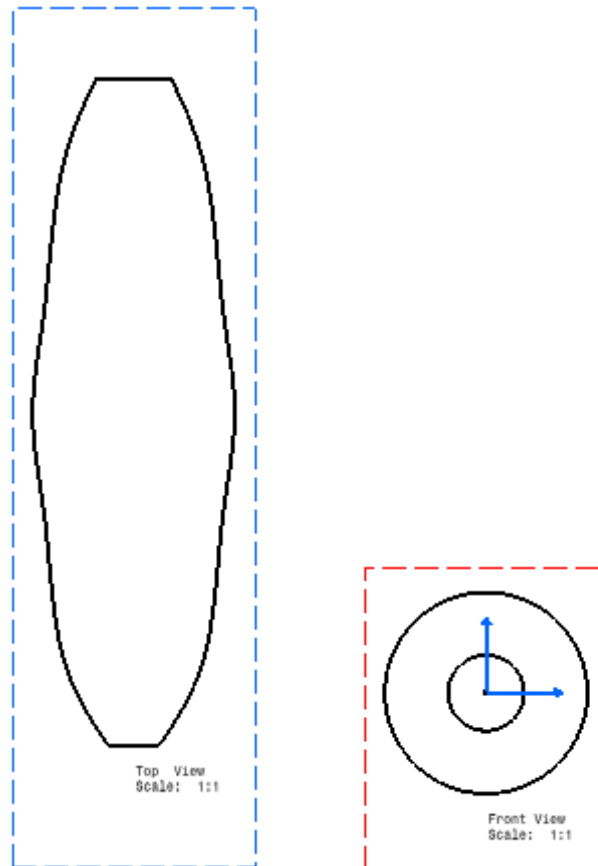


Figure 20: Top and front view of the fuselage – CATIAV5

CHAPTER 3

WEIGHT SIZING AND WEIGHT SENSITIVITIES

Weight estimation is one of the key areas in the aircraft design. A conventional gasoline weight sizing is a standard process with many different approaches. But for an electric aircraft, the procedures have not been put in place which requires a standard as the conventional aircraft. Growing concerns over environment is one of the sole requirements for the increased demand of non-polluting environment friendly aircraft.

Previously, the urge for developing gasoline aircraft became the basis for standard procedures and now it is important to have robust design practises for an unconventionally propelled aircraft (i.e. by means of batteries, fuel cells and bio-fuels). Since these design practises are for developing full-scale future aircraft; the weight estimation process also includes few suppositions which may reduce the over-all reliability on this process. The Range equation is a powerful estimation tool for the preliminary analysis which gives us a clear estimate as to how much the calculated aircraft range matches the proposed value.

After checking for the range attainability, the empty, payload and cargo weights can be decided. There are three categories that contribute to the over-all aircraft weight:

- Cargo Weight
- Empty weight – Includes structural, fixed-equipment and power-plant weights
- Payload – Weight of Passengers and Luggage.

The mission weights play a vital role in an aircraft performance as it helps us to determine the important parameters those, which directly contribute to the final design. In the initial weight sizing calculations, firstly, take-off weights of similar aircraft are determined and then the aircraft database from table4 and table6 are used for estimating the entire mission weights for VER-12XX. The previous design chapters have laid down the basis for weight sizing as the basic specifications for VER-12XX and in this chapter mission weights will be fixed.

3.1. MISSION WEIGHT ESTIMATES

3.1.1 Data Base for Take-off Weights and Empty Weights of Similar Airplanes

Table 5: Take-off Weight and Empty Weights of Similar Airplanes

Aircraft	Take-off (lbs)	Empty Weight(lbs)	Wing Span(m)	Range(km)	Mach
B737-MAX	159500	80200	35.9	7080	0.785
B737-700	154500	83000	34.32	8149	0.785
B737-800	174200	91300	35.79	7408	0.785
B737-900 ER	187700	93680	35.79	5926	0.785
A320 NEO	162040	142198	35.8	6850	0.82
A321 NEO	196211	104720	35.8	6850	0.82
CRJ100	91800	51120			
VER-12XX	160850	99183	36	7400	0.8

3.1.2 Determination of Regression Coefficients A and B

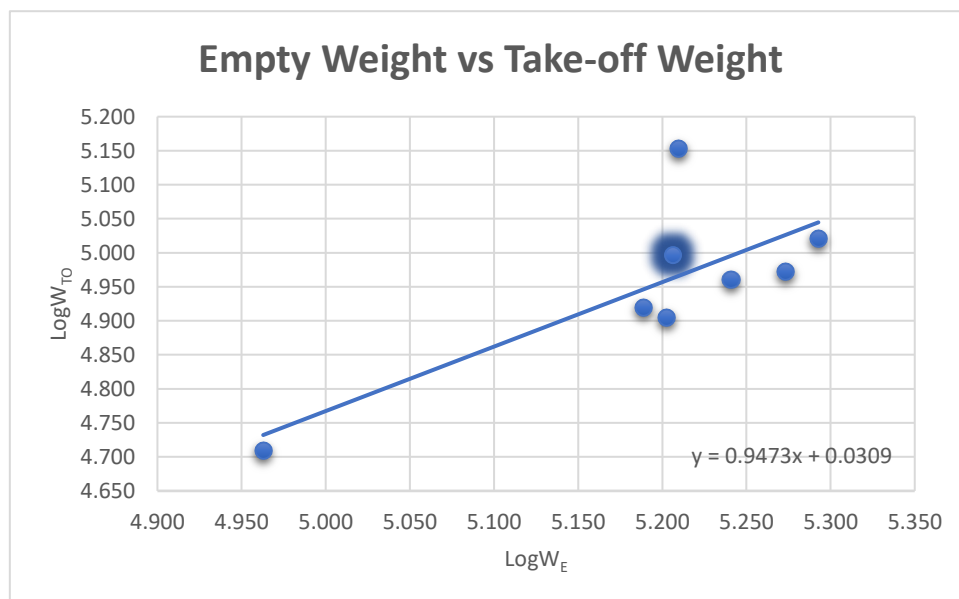


Figure 21: Empty Weight vs Take-off Weight

The above log-log plot of the similar aircraft allows us to calculate the regression coefficients for VER-12XX. The dark blue diamond represents VER-12XX position in the graph and the trend line gives us an equation through which the regression coefficients can be determined.

$$y = 0.9473x + 0.0274 \quad (3.1)$$

E.q.3.2 shows us the relation between the take-off weight and empty weight with the regression coefficients. If we observe closely, regression coefficients play a vital role in estimating the empty weight of the aircraft and they can be determined with the similar aircraft data specified in section 2.1. Since, the data had been logged in a spread sheet a graphical illustration along with the trend line, trend line equation are presented above which is compared with e.q.3.2 for obtaining regression coefficients A and B.

$$\log W_E = \frac{\log W_{TO} - A}{B} \quad (3.2)$$

By comparing the equation 3.2 with 3.1

$$y = \log W_E$$

$$x = \log W_{TO}$$

$$\Rightarrow \frac{1}{B} = 0.9473$$

$$\Rightarrow B = \frac{1}{0.9473}$$

$$\Rightarrow B = 1.0556$$

$$\therefore B = 1.0556 \quad (3.3)$$

$$\therefore A = 0.03 \quad (3.4)$$

3.1.3 Comparison of results with Roskam:

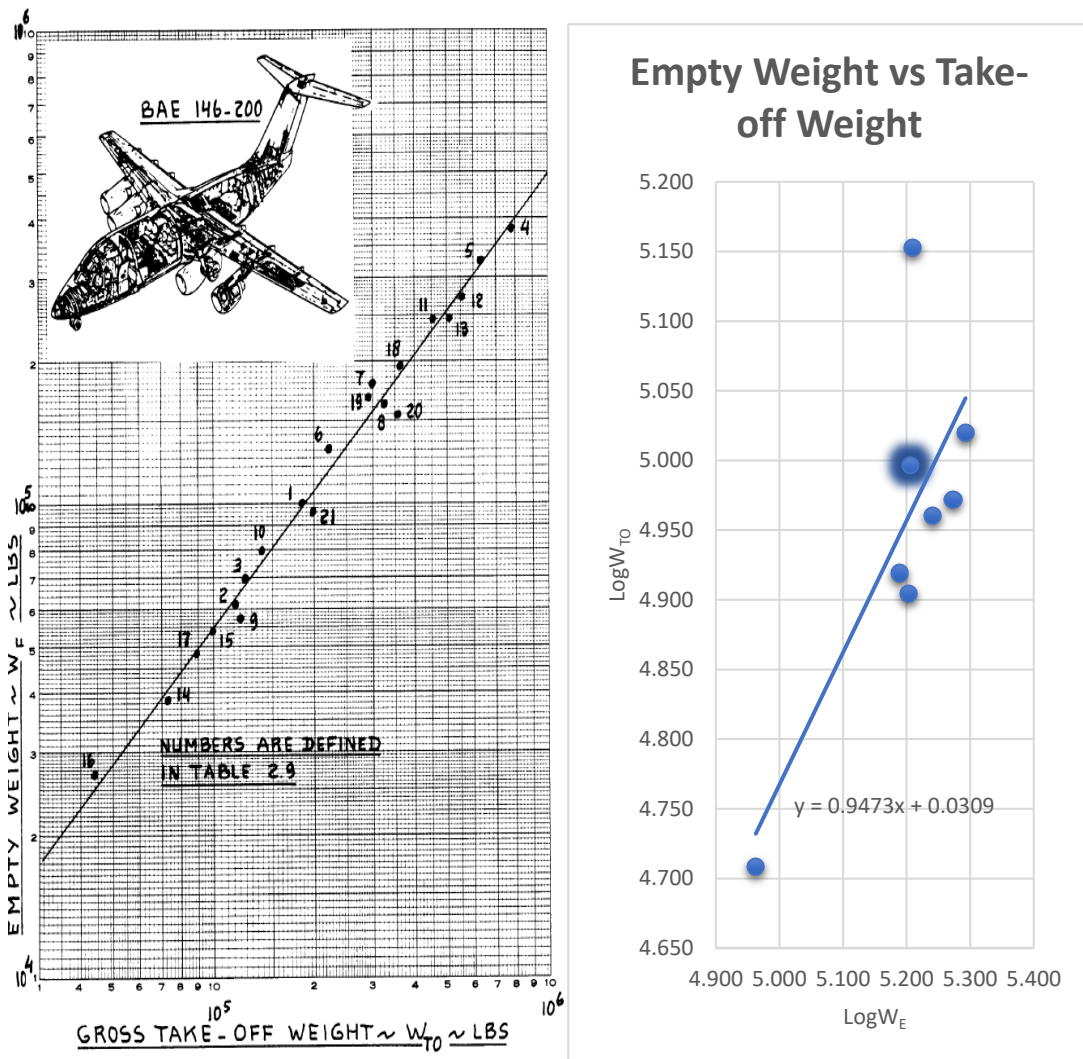


Figure 22: Roskam Similar Aircraft results on comparison with current similar aircraft for VER-12XX

The comparison results of similar aircraft database with Roskam are almost similar apart from the fact that ‘Roskam’ used around 21 similar aircraft. The referenced comparative analysis considers the technology incorporated into aircraft are of 1970’s but today, modern aircrafts improved L/D values and with the development of composites, graphene, morphine materials; the right-hand side graphical representation is more current and can be used in the next sections to determine key aircraft characteristics.

3.2 DETERMINATION OF MISSION WEIGHTS – HAND CALCULATIONS

In this section, the mission weights are manually determined. This gives us a chance to understand the mission weights calculation procedure; comprehensively iteration process and

key assumptions made in terms of mission weights can be precisely understood. For consistency, Advanced Aircraft Analysis Software program is used and is a powerful tool that allow designers to perform initial sizing, performance and aerodynamics analysis, structures, certification and to approximately calculate the overall aircraft cost.

3.2.1 Manual Calculation of Mission Weights:

Formulae used for calculating mission weights:

Take-off weights break down - (Roskam part1 section2)

$$W_{TO} = W_{OE} + W_F + W_{PL} \quad (3.5)$$

- W_{TO} – *Takeoff weight*
- W_{OE} – *Airplane operating empty weight*
 - W_F – *Payload weight*

$$W_{EO} = W_E + W_{tfo} + W_{crew} \quad (3.6)$$

- W_E – *Empty weight*
- W_{tfo} – *Weight of all trapped oil and fuel*
 - W_{crew} – *Weight of the crew*

W_E can further be written as manufacturer's empty weight and FEQ (fixed equipment weight).

$$W_E = W_{ME} + W_{FEQ} \quad (3.6)$$

- W_{ME} – *Manufacturers empty weight*
- W_{FEQ} – *Fixed equipment weight*

(Step1) Payload Weight (W_{PL}):

- Number of passengers = 200
- Number of Pilots = 2
- Number of crew = 3
- The weight of each passenger is assumed to be 185 lb (As per ICAO regulations)
- Baggage Weight – 30 lb (Short haul travel)
- Baggage Weight – 40 lb (Long haul travel)

For Short- haul Travel:

$$\begin{aligned} W_{PL} &= \text{number of passengers} \\ &\quad * (\text{weight of each passenger} + \text{each bag weight}) \\ &\quad + \text{number of crew} * (\text{weight of each crew} \\ &\quad + \text{each bag weight}) \quad (3.7) \end{aligned}$$

$$\Rightarrow W_{PL} = 200 * (185 + 30) + 5 * (185 + 30) \quad (lbs)$$

$$\Rightarrow W_{PL} = 205 * (215) \quad (lbs)$$

$$\Rightarrow W_{PL} = 44075 \quad lbs$$

$$\therefore W_{PL} = 44075 \quad lbs \quad (3.8)$$

For Long-haul Travel:

$$\begin{aligned} W_{PL} &= \text{number of passengers} \\ &\quad * (\text{weight of each passenger} + \text{each bag weight}) \\ &\quad + \text{number of crew} * (\text{weight of each crew} \\ &\quad + \text{each bag weight}) \end{aligned}$$

$$\Rightarrow W_{PL} = 200 * (185 + 40) + 5 * (185 + 40) \quad (lbs)$$

$$\Rightarrow W_{PL} = 200 * (225) \quad (lbs)$$

$$\Rightarrow W_{PL} = 45000 \quad lbs$$

$$\therefore W_{PL} = 45000 \text{ lbs} \quad (3.9)$$

Determining the Cargo Capacity for VER-12XX

To calculate the cargo capacity of an aircraft we need the operating empty weight and zero fuel weight of the aircraft. Therefore, from VER-12XX specifications its cargo capacity is determined using the payload capacity equation below.

$$\text{Payload capacity}_{VER-12X} = \text{Zero fuel weight} - \text{Operating empty weight} \quad (3.10)$$

$$\Rightarrow \text{Payload capacity}_{VER-12X} = 160850 - 99183 \text{ (lbs)}$$

$$\Rightarrow \text{Payload capacity}_{VER-12X} = 61667 \text{ lbs}$$

$$\therefore \text{Payload capacity}_{VER-12X} = 61667 \text{ lbs} \quad (3.11)$$

With the above value, we can understand the maximum the payload that an aircraft can be loaded is 61667 lbs. Payload can further be broken down to get the cargo capacity of the aircraft.

$$\text{Cargo capacity}_{VER-12X} = \text{Payload capacity}_{VER-12X} - W_{PL} \quad (3.12)$$

$$\Rightarrow \text{Cargo capacity}_{VER-12X} = 61667 - 45000 \text{ (lbs)}$$

$$\Rightarrow \text{Cargo capacity}_{VER-12X} = 16667 \text{ lbs}$$

$$\therefore \text{Cargo capacity}_{VER-12X} = 16667 \text{ lbs} \quad (3.13)$$

Payload of an aircraft determines several mission aspects like range, cruise duration, fuel consumption and manoeuvrability. As the payload increases, there will be significant changes to the performance of the aircraft, which sometimes results in a shift of optimum performance to minimum performance, which is entirely dependent on the aircraft mission requirements.

(Step2) Guessing the likely values of take-off weight:

The take-off weight for VER-12XX is a guess value initially to check if it satisfies the condition of for the allowable aircraft weight.

- $W_{TO} = 160850 \text{ lbs}$ – *Initial guess takeoff weight for VER – 12X*
- W_{E-TENT} when compared to $W_{E-allowable}$ should be within 0.5% limits

(Step3) Determination of Mission Fuel Weights:

Fuel Fraction: Fuel fraction is the ratio of the mission end weight to the mission begin weight. Fuel fractions tabulated in Roskam 2.1; assumed a close match for the proposed aircraft mission profile.

3.2.2 VER-12XX Mission Profile:

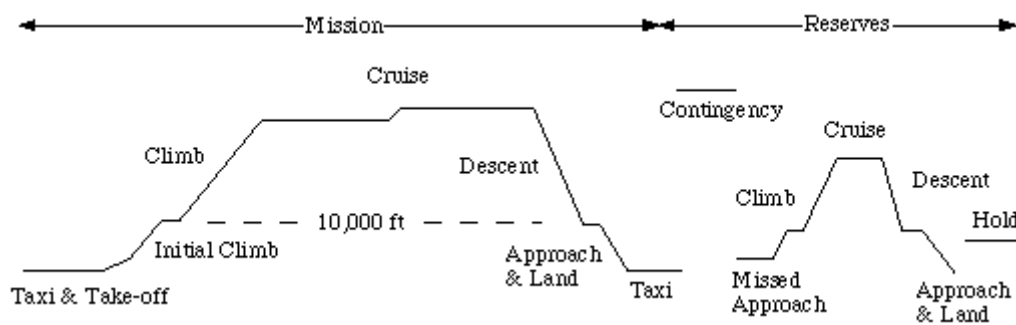


Figure 23: VER-12XX Mission Profile

Flight Phase I – Engine start and Warmup:

For this mission phase end weight is W_1 and the begin weight is W_{TO} . The fuel fraction for this phase is 0.990.

$$\frac{W_1}{W_{TO}} = 0.990$$

$$\Rightarrow \frac{W_1}{160850 \text{ lbs}} = 0.990$$

$$\Rightarrow W_1 = 0.990 * 650000 \text{ lbs}$$

$$\Rightarrow W_1 = 159241.5 \text{ lbs}$$

$$\therefore W_1 = \mathbf{159241.5 \text{ (3.14)}}$$

Flight Phase II – Taxi:

For this mission phase end weight is W_2 and the begin weight is W_1 . The fuel fraction for this phase is 0.990.

$$\frac{W_2}{W_1} = 0.990$$

$$\Rightarrow \frac{W_2}{159241.5 \text{ lbs}} = 0.990$$

$$\Rightarrow W_2 = 0.990 * 159241.5 \text{ lbs}$$

$$\Rightarrow W_2 = 157649 \text{ lbs}$$

$$\therefore W_2 = \mathbf{157649 \text{ lbs (3.15)}}$$

Flight Phase III – Take-off:

For this mission phase end weight is W_3 and the begin weight is W_2 . The fuel fraction for this phase is 0.995.

$$\frac{W_3}{W_2} = 0.995$$

$$\Rightarrow \frac{W_3}{157649 \text{ lbs}} = 0.995$$

$$\Rightarrow W_3 = 0.995 * 157649 \text{ lbs}$$

$$\Rightarrow W_3 = 156860 \text{ lbs}$$

$$\therefore W_3 = 156860 \text{ lbs (3.16)}$$

Flight Phase IV – Climb to Cruise Altitude and accelerate to cruise speed:

For this mission phase end weight is W_4 and the begin weight is W_3 . The fuel fraction for this phase is 0.995.

$$\frac{W_4}{W_3} = 0.980$$

$$\Rightarrow \frac{W_4}{156860 \text{ lbs}} = 0.980$$

$$\Rightarrow W_4 = 0.980 * 156860 \text{ lbs}$$

$$\Rightarrow W_4 = 153723 \text{ lbs}$$

$$\therefore W_4 = 153723 \text{ lbs (3.17)}$$

Using the endurance equation, we can back calculate the fuel fraction to check if the conventional value matches with calculated value.

Endurance equation:

$$E_{cl} = \left(\frac{1}{c_j}\right)_{cl} * \left(\frac{L}{D}\right)_{cl} * \ln\left(\frac{W_3}{W_4}\right) \text{ (3.18)}$$

During climb phase:

- **Lift to drag ratio is 15**
- **c_j is 0.9**
- **Climb rate is estimated 2500 fpm and total climb time is 10 minutes.**

- Average speed during climb to cruise is 526 knots.

$$\Rightarrow \ln \left(W_3 / W_4 \right) = \frac{\left(E_{cl} * (c_j)_{cl} \right)}{\left(L/D \right)_{cl}} \quad (3.19)$$

$$\Rightarrow \frac{W_3}{W_4} = e^{\frac{\left(E_{cl} * (c_j)_{cl} \right)}{\left(L/D \right)_{cl}}}$$

$$\Rightarrow W_4 = \frac{W_3}{e^{\frac{\left(E_{cl} * (c_j)_{cl} \right)}{\left(L/D \right)_{cl}}}}$$

$$\Rightarrow W_4 = \frac{153723}{e^{\frac{\left(10/60 * 0.9 \right)}{15}}}$$

$$\Rightarrow W_4 = 139094 \text{ lbs}$$

$$\therefore W_{4 \text{ corrected}} = \mathbf{139094 \text{ lbs}} \quad (3.20)$$

Now that we have the corrected end weight, (W_4) ; we can calculate the actual fuel fraction for this mission phase.

$$\Rightarrow W_4 / W_3 = \text{Fuelfraction}_{\text{phase IV}}$$

$$\Rightarrow \frac{139094 \text{ lbs}}{156860 \text{ lbs}} = \text{Fuelfraction}_{\text{phase IV}}$$

$$\Rightarrow \text{Fuelfraction}_{\text{phase IV}} = 0.88$$

$$\therefore \text{Fuelfraction}_{\text{phase IV}} = \mathbf{0.88}$$

Flight Phase V – Cruise

For this mission phase end weight is W_5 and the begin weight is W_4 . The fuel fraction and missions end weight for this phase is determined using Breguet range equation.

$$R_{cr} = \left(\frac{V}{c_j}\right)_{cr} * \left(\frac{L}{D}\right)_{cr} * \ln\left(\frac{W_4}{W_5}\right) \quad (3.21)$$

To calculate the range for VER-12XX we can use the following inputs:

- Cruise speed = 482 knots
- Cruising time = 2 hours

Cruising range = cruise speed * cruising time

$$\Rightarrow \text{Cruising range} = 482 * 2 \text{ (knots * hours)}$$

$$\therefore \text{Cruising range} = 964 \text{ nmi}$$

$$\Rightarrow \ln\left(\frac{W_4}{W_5}\right) = \frac{\left(R_{cr} * (c_j)_{cr}\right)}{\left(\frac{L}{D}\right)_{cl} * V}$$

$$\Rightarrow \frac{W_4}{W_5} = e^{\frac{\left(R_{cr} * (c_j)_{cr}\right)}{\left(\frac{L}{D}\right)_{cr} * V}}$$

$$\Rightarrow W_5 = \frac{W_4}{e^{\frac{\left(R_{cr} * (c_j)_{cr}\right)}{\left(\frac{L}{D}\right)_{cr} * V}}}$$

$$\Rightarrow W_5 = \frac{139094}{e^{\frac{(964 * 0.9)}{15 * 482}}}$$

$$\Rightarrow W_5 = 123365 \text{ lbs}$$

$$\therefore W_5 = 123365 \text{ lbs} \quad (3.22)$$

Therefore, the fuel fraction for phase V is:

$$\frac{W_5}{W_4} = \text{Fuel fraction}_{\text{phase V}}$$

$$\Rightarrow \frac{123365 \text{ lbs}}{139094 \text{ lbs}} = \text{Fuel fraction}_{\text{phase V}}$$

$$\Rightarrow \text{Fuel fraction}_{\text{phase V}} = 0.887$$

$$\therefore \text{Fuel fraction}_{\text{phase V}} = 0.887 \quad (3.23)$$

Flight Phase VI – Loiter

For this mission phase; end weight is W_6 and the begin weight is W_5 . The fuel fraction and mission weight for this phase can be determined using below Breguet equation.

$$E_{ltr} = \left(1/c_j\right)_{ltr} * (L/D)_{ltr} * \ln\left(W_5/W_6\right) \quad (3.24)$$

- **Lift to drag ratio = 18 (for loiter phase)**
- **$c_j = 0.6$ (during loiter)**
- **Endurance for loiter phase is estimated as an hour**

$$\Rightarrow \ln\left(W_5/W_6\right) = \frac{E_{ltr} * (c)_j}{(L/D)_{ltr}}$$

$$\Rightarrow \frac{W_5}{W_6} = e^{\frac{E_{ltr} * (c)_j}{(L/D)_{ltr}}}$$

$$\Rightarrow W_6 = \frac{W_5}{e^{\frac{E_{ltr} * (c)_j}{(L/D)_{ltr}}}}$$

$$\Rightarrow W_6 = \frac{139094}{e^{\frac{1 * 0.6}{18}}}$$

$$\Rightarrow W_6 = 134533 \text{ lbs}$$

$$\therefore W_6 = 134533 \text{ lbs} \quad (3.25)$$

Therefore, the fuel fraction for phase VI is:

$$W_6/W_5 = \text{Fuel fraction}_{\text{phase VI}}$$

$$\Rightarrow \frac{134533 \text{ lbs}}{139094 \text{ lbs}} = \text{Fuelfraction}_{\text{phase V}}$$

$$\Rightarrow \text{Fuelfraction}_{\text{phase VI}} = 0.967$$

$$\therefore \text{Fuelfraction}_{\text{phase VI}} = \mathbf{0.967} \quad (3.26)$$

Flight Phase VII – Descent:

For this mission phase end weight is W_7 and the begin weight is W_6 . The fuel fraction for this phase is 0.99.

$$\frac{W_7}{W_6} = 0.99$$

$$\Rightarrow \frac{W_7}{134533 \text{ lbs}} = 0.99$$

$$\Rightarrow W_7 = 0.99 * 134533 \text{ lbs}$$

$$\Rightarrow W_7 = 133188 \text{ lbs}$$

$$\therefore W_7 = \mathbf{133188 \text{ lbs}} \quad (3.27)$$

Flight Phase VIII – Landing, Taxi and Shutdown:

For this mission phase end weight is W_8 and the begin weight is W_7 . The fuel fraction for this phase is 0.99.

$$\frac{W_8}{W_7} = 0.992$$

$$\Rightarrow \frac{W_8}{133188 \text{ lbs}} = 0.992$$

$$\Rightarrow W_8 = 0.992 * 133188 \text{ lbs}$$

$$\Rightarrow W_8 = 132123 \text{ lbs}$$

$$\therefore W_8 = 132123 \text{ lbs (3.28)}$$

Mission Fuel Fraction:

The total mission fuel fraction determined using:

$$M_{ff} = \frac{W_1}{W_{TO}} * \prod_{i=1}^{i=7} \left(\frac{W_{i+1}}{W_i} \right) \text{ (3.29)}$$

$$\Rightarrow M_{ff} = \left(\frac{W_1}{W_{TO}} * \frac{W_2}{W_1} * \frac{W_3}{W_2} * \frac{W_4}{W_3} * \frac{W_5}{W_4} * \frac{W_6}{W_5} * \frac{W_7}{W_6} * \frac{W_8}{W_7} \right)$$

$$\Rightarrow M_{ff} = \frac{W_8}{W_{TO}}$$

$$\Rightarrow M_{ff} = \frac{132123 \text{ lbs}}{160850 \text{ lbs}}$$

$$\Rightarrow M_{ff} = 0.82$$

Fuel Used:

$$W_{F-used} = (1 - M_{ff}) * W_{TO} \text{ (3.30)}$$

$$\Rightarrow W_{F-used} = (1 - 0.82) * 160850 \text{ (lbs)}$$

$$\Rightarrow W_{F-used} = 28953 \text{ lbs (3.31)}$$

Fuel Weight:

$$W_{Fuel} = (1 - M_{ff}) * W_{TO} + W_{F-res} \text{ (3.32)}$$

- Reserve fuel accounts to 5% of total fuel weight.

Therefore, the above equation changes as:

$$\Rightarrow W_{Fuel} = (1 - M_{ff}) * W_{TO} + 0.05 * W_F$$

$$\Rightarrow W_{Fuel} - 0.05 * W_{Fuel} = (1 - M_{ff}) * W_{TO}$$

$$\Rightarrow W_{Fuel}(1 - 0.05) = 28953 \text{ lbs}$$

$$\Rightarrow W_{Fuel} = \frac{28953}{0.95}$$

$$\Rightarrow W_{Fuel} = 30477 \text{ lbs}$$

$$\therefore W_{Fuel} = 30477 \text{ lbs}$$

Tentative Operating Empty weight:

$$W_{OE-TENT} = W_{TO} - W_{Fuel} - W_{Payload} \quad (3.33)$$

$$\Rightarrow W_{OE-TENT} = 160850 - 30477 - 45000$$

$$\Rightarrow W_{OE-TENT} = 85373 \text{ lbs}$$

$$\therefore W_{OE-TENT} = 85373 \text{ lbs}$$

Tentative Empty Weight:

The Tentative empty weight is determined using the equation below. The trapped fuel and oil weight is an estimate and is considered as 0.5% of the take-off weight

$$W_{E-TENT} = W_{OE-TENT} + W_{TFO} - W_{Crew} \quad (3.34)$$

$$\Rightarrow W_{E-TENT} = 85373 + 0.005 * W_{TO} - 925 \text{ (lbs)}$$

$$\Rightarrow W_{E-TENT} = 85252 \text{ lbs}$$

$$\therefore W_{E-TENT} = 85252 \text{ lbs}$$

The allowable empty weight is determined using the equation:

$$\begin{aligned}\log W_{E-allowable} &= \frac{\log W_{TO} - A}{B} \\ \Rightarrow \log W_{E-allowable} &= \frac{\log 160850 - 0.03}{1.0556} \\ &\Rightarrow \log W_E = 4.90 \\ &\Rightarrow W_{E-allowable} = 79433 \text{ lbs} \\ \therefore W_{E-allowable} &= 79433 \text{ lbs}\end{aligned}$$

When take-off weight compared to allowable weight a difference of 81417 lbs is obtained which is barely falls within the specified design limit. This iteration is repeated until allowable weight is within the design limits. A MATLAB code in the appendix section calculates the allowable weights.

3.3 CALCULATION OF MISSION WEIGHTS USING THE AAA PROGRAM:

Below graph from AAA shows the allowable weight for VER-12XX

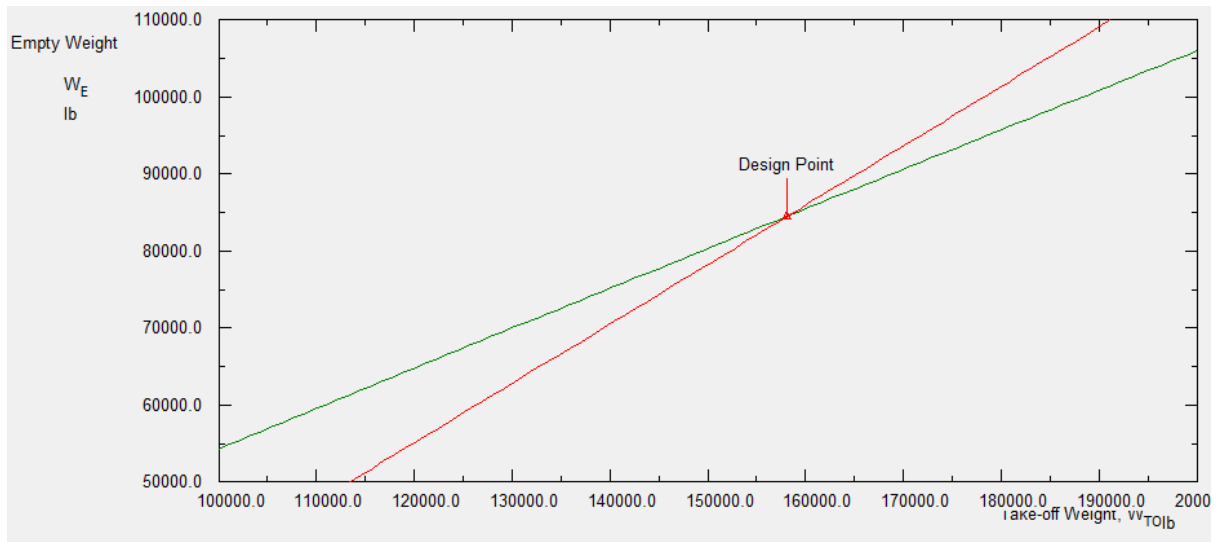


Figure 24: Design Point Obtained using AAA

Mission Profile Table: Output				
	Mission Profile	W_{begin} lb	$\Delta W_{F_{used}}$ lb	$W_{F_{begin}}$ lb
1	Warmup	158162.0	1581.6	35424.9
2	Taxi	156580.4	1565.8	33843.3
3	Take-off	155014.6	775.1	32277.5
4	Climb	154239.5	415.0	31502.4
5	Cruise	153824.5	27130.1	31087.4
6	Descent	126694.4	1266.9	3957.3
7	Land/Taxi	125427.4	1003.4	2690.3

Figure 25: Mission Profile Outputs for given fuel-fractions, regression coefficients, payload weight and take-off, empty weight estimates

Figure 23, 24 are from Advanced Aircraft Analysis Software. After manual calculations, the similar aircraft database and determined variables from the previous sections are fed into the software for most robust design practises. From Figure 23 the design point for VER-12XX is determined I.e. for an empty weight of 85000 lbs an obtained take-off weight of

158162 lbs*. Based on the determined mission fuel fractions the mission weights have also been calculated which are shown in Figure24.

3.4. Manual Calculation of Take-off Weight Sensitivities

After the initial sizing of the aircraft, it is important to understand the parameters that are responsible for the design. In addition, the sensitivity study helps us to understand the variation of some key parameters with respect to take-off weight.

The manual calculations for sensitivity analysis are as follows:

$$W_E = W_{TO} - W_F - W_{PL} - W_{Tfo} - W_{crew} \quad (3.35)$$

$$W_E = CW_{TO} - D \quad (3.36)$$

Where

$$C = \{1 - (1 + M_{res})(1 - M_{ff}) - M_{tfo}\} \quad (3.37)$$

$$\Rightarrow C = 0.885$$

$$D = W_{PAYLOAD} + W_{CREW} \quad (3.38)$$

$$\Rightarrow D = 45000 + 1125 \text{ lbs}$$

$$\Rightarrow D = 46125 \text{ lbs} \quad (3.39) \quad ;$$

Simplifying equations 3.35 and 3.36, we can determine the take-off weight in terms of regression coefficients A, B, C and D.

$$\log W_{TO} = A + B \log(CW_{TO} - D) \quad (3.40)$$

3.3.1) SENSITIVITY OF TAKE-OFF WEIGHT WITH RESPECT TO PAYLOAD:

From Roskam; sensitivity of Take-off weight to payload is determined using the equation:

$$\frac{\partial W_{TO}}{\partial W_{PAYLOAD}} = BW_{TO}\{D - C(1 - B)W_{TO}\}^{-1} \quad (3.41)$$

$$\Rightarrow \frac{\partial W_{TO}}{\partial W_{PAYLOAD}} = 1.056 * 160850 * [46125 - 0.885(1 - 1.0056) * 160850]^{-1}$$

$$\therefore \frac{\partial W_{TO}}{\partial W_{PAYLOAD}} = 3.13$$

3.3.2) SENSITIVITY OF TAKE-OFF WEIGHT WITH RESPECT TO EMPTY WEIGHT:

Sensitivity of take-off weight with respect to empty weight is determined using the equation:

$$\frac{\partial W_{TO}}{\partial W_E} = B * W_{TO} * \left[\text{inv log}_{10} \left\{ \frac{(\log_{10} W_{TO} - A)}{B} \right\} \right]^{-1} \quad (3.42)$$

$$\Rightarrow \frac{\partial W_{TO}}{\partial W_E} = 1.056 * 160850 * \left[\text{inv log}_{10} \left\{ \frac{(\log_{10} 160850 - 0.03)}{1.0556} \right\} \right]^{-1}$$

$$\therefore \frac{\partial W_{TO}}{\partial W_E} = 2.12$$

3.3.3) SENSITIVITY OF TAKE-OFF WEIGHT WITH RESPECT TO RANGE:

Sensitivity of take-off weight with respect to range is determined using the equation:

$$\frac{\partial W_{TO}}{\partial R} = F * c_j * \left(V * L/D \right)^{-1} \quad (3.43)$$

$$\Rightarrow \frac{\partial W_{TO}}{\partial R} = \frac{437843 * 0.9}{482 * 16}$$

$$\therefore \frac{\partial W_{TO}}{\partial R} = 52 \text{ lbs / nm}$$

The calculation procedure for quantity F is shown in detail in Appendix D. Typically, c_j is assumed as 0.9 and an L/D of 16 is reasonable for Commercial Jet's.

3.3.4) SENSITIVITY OF TAKE-OFF WITH RESPECT TO ENDURANCE:

The sensitivity of take-off with respect to endurance is determined using the equation:

$$\begin{aligned}\frac{\partial W_{TO}}{\partial R} &= F * c_j * \left(\frac{L}{D}\right)^{-1} \quad (3.44) \\ \Rightarrow \frac{\partial W_{TO}}{\partial R} &= \frac{437843 * 0.9}{16} \\ \therefore \frac{\partial W_{TO}}{\partial R} &= 24629 \text{ lbs / hr}\end{aligned}$$

3.3.5) SENSITIVITY OF TAKE-OFF WEIGHT WITH RESPECT TO CRUISE SPEED:

The sensitivity of take-off weight with respect to cruise speed is determined using the equation:

$$\begin{aligned}\frac{\partial W_{TO}}{\partial V} &= F * R * c_j * \left(V^2 * \frac{L}{D}\right)^{-1} \quad (3.45) \\ \Rightarrow \frac{\partial W_{TO}}{\partial V} &= \frac{437843 * 0.9 * 7400}{482^2 * 16} \\ \therefore \frac{\partial W_{TO}}{\partial V} &= -78.4 \text{ lbs / kt}\end{aligned}$$

3.3.6) Sensitivity of Take-off Weight with respect to Specific Fuel Consumption and Lift to Drag Ratio:

These sensitivities must be addressed as the aircraft mission specification includes loiter and range which would be a key parameter to evaluate whether the proposed configuration requires higher wing loading. The sensitivities of take-off weight with respect to specific fuel consumption and L/D are determined using the equations:

With respect to Range Requirement:

$$\frac{\partial W_{TO}}{\partial c_j} = \frac{F * R}{V L/D} \quad (3.46)$$

$$\Rightarrow \frac{\partial W_{TO}}{\partial c_j} = \frac{437483 * 7400}{482 * 16}$$

$$\therefore \frac{\partial W_{TO}}{\partial c_j} = 40200 \text{ lbs / lbs / lbs / hr}$$

$$\frac{\partial W_{TO}}{\partial (L/D)} = -F * R * c_j * (V * L/D)^{-1} \quad (3.47)$$

$$\Rightarrow \frac{\partial W_{TO}}{\partial (L/D)} = \frac{-437483 * 7400 * 0.9}{482 * 16^2}$$

$$\therefore \frac{\partial W_{TO}}{\partial (L/D)} = -2363 \text{ lbs}$$

With respect to Loiter Requirement:

$$\frac{\partial W_{TO}}{\partial c_j} = \frac{F * E}{L/D} \quad (3.48)$$

$$\Rightarrow \frac{\partial W_{TO}}{\partial c_j} = \frac{437483 * 1}{16}$$

$$\therefore \frac{\partial W_{TO}}{\partial c_j} = 27342 \text{ lbs / lbs / lbs / hr}$$

$$\frac{\partial W_{TO}}{\partial (L/D)} = -F * E * c_j * (L/D)^{-2} \quad (3.49)$$

$$\Rightarrow \frac{\partial W_{TO}}{\partial (L/D)} = \frac{-437483 * 7400 * 0.9}{16^2}$$

$$\therefore \frac{\partial W_{TO}}{\partial (L/D)} = -1140 \text{ lb}$$

Table 6: Weight Sensitivities Summary

$\frac{\partial W_{TO}}{\partial W_{PAYLOAD}}$	3.13
$\frac{\partial W_{TO}}{\partial W_E}$	2.12
$\frac{\partial W_{TO}}{\partial R}$	52lbs / nm
$\frac{\partial W_{TO}}{\partial R}$	24629lbs / hr
$\frac{\partial W_{TO}}{\partial V}$	-78.4lbs / kt
$\frac{\partial W_{TO}}{\partial c_j}$	40200lbs / lbs / lbs / hr
$\frac{\partial W_{TO}}{\partial (L/D)}$	-2363lbs

3.4 CALCULATION OF TAKE-OFF WEIGHT SENSITIVITIES USING THE AAA PROGRAM

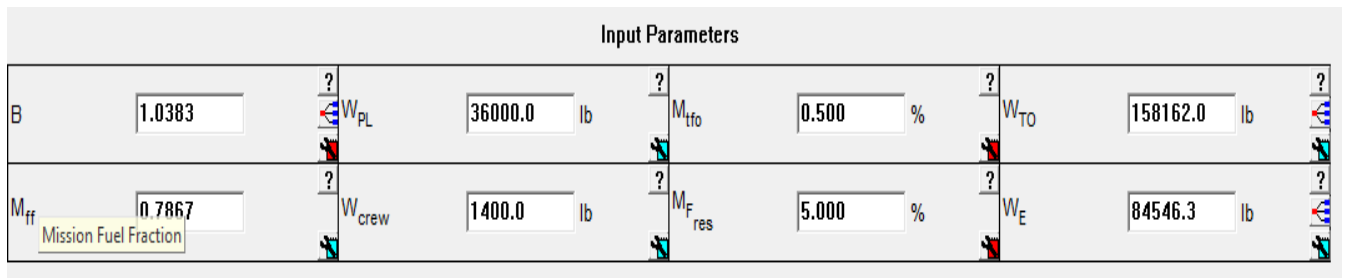


Figure 26: Sensitivities Input Parameters

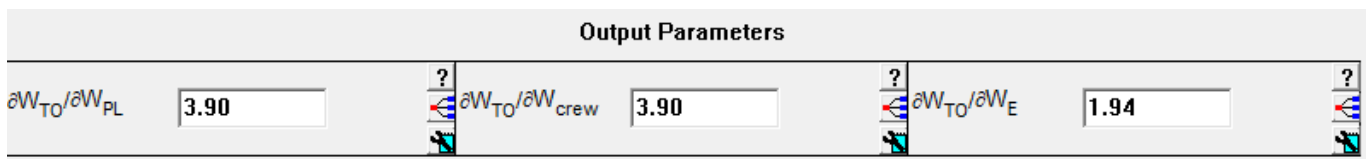


Figure 27: Sensitivities (Take-off with respect to Payload, Crew and Empty Weight) Outputs)

3.5 TRADE STUDIES

It is an important part of conceptual design approach as this is the point where the refinement in design as per the customer requirements. In this study, first the range of aircraft for example let's say 1000 nmi; to get the desired design point, we must take the range from 900 nmi to 2000 nmi. Below is the iterated graph. The same procedure applies for L/D trade study as well

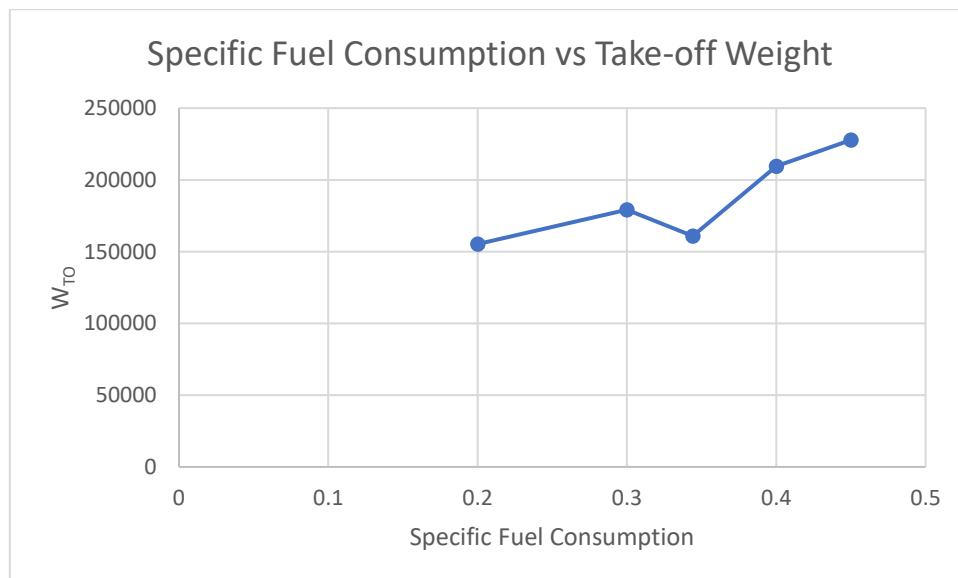


Figure 28: Trade Studies - Specific Fuel Consumption vs Take-off Weight

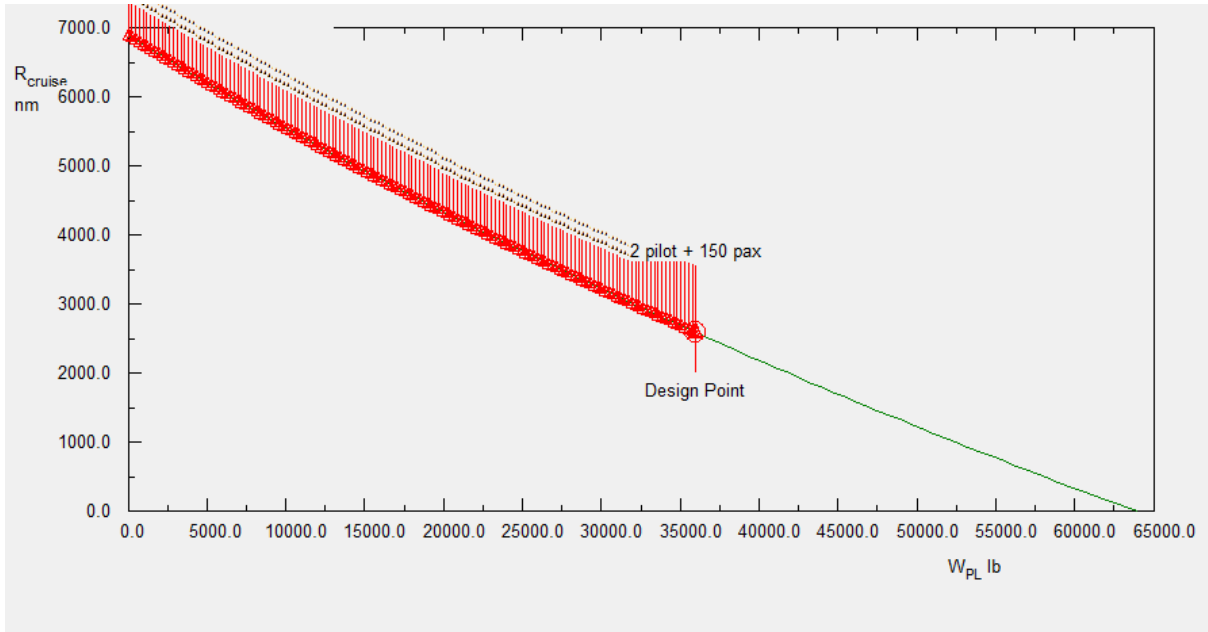


Figure 29: Weight of Payload (lbs) vs Cruise Range (nm)

3.6 DISCUSSION:

Weight sizing is an important phase of aircraft design as it involves key elements like take-off weight and allowable weight. The importance of take-off weight in the calculation of the empty weight of the aircraft proves us inter relation in aircraft design. The regression coefficient is an important factor in determining the aircraft allowable weight and is directly proportional to the used fuel of the aircraft. The iteration process involved in the mission calculations allows to clearly find an exact design value. The sensitivity studies determine key parameters with respect to the take-off weight which essentially gives an idea about VER-12XX sensitivities with specific fuel consumption, L/D ratio, range, payload and endurance. The limitations of AAA program especially with the aircraft database posed few problems in calculating precise values for regression coefficients. In addition, the weight of passengers is determined not using the current limits, which may add up to the payload weight if the present airline weight limits are used.

3.7 RECOMMENDATIONS

VER-12XX mission weights calculations show that they are like the modern-day aircraft. These calculations help in optimising the performance of the VER-12XX by choosing the best power plant for the intended mission. In addition, the design point for VER-12XX is an important factor as the sensitivity analysis is determined based on the allowable empty weight. The fuel fractions values should be precisely calculated as they directly affect the mission fuel weights and the range. ‘Roskam’ came up with some key graphical representations that have become the basis for similar aircraft comparison in this chapter. The sensitivity values obtained are quite reasonable and they are close to the design values. To sum up with; the weights obtained for VER-12XX are further used in performance sizing and aerodynamics analysis.

CHAPTER 4

PERFORMANCE AND CONSTRAINT ANALYSIS

Performance sizing is an integral part of Aircraft Design where key performance constraints will be determined. It is important to understand the stall speed, take-off, landing distance, preliminary drag polar analysis, climb, manoeuvring, and speed constraints for the aircraft as they play a vital role in comprehending the required power loading for a specified wing loading. In this report, the procedures related to those constraints will be presented for rapid estimation of the proposed aircraft configuration. Since, VERHY-12 is a turbo-jet powered aircraft and with a take-off weight of greater than 6000 lbs, this aircraft falls into FAR-25 Certification. It is to be noted that all the performance constraint calculations will be determined based on FAR-25 guidelines. For consistency, VER-12XX propulsion will be revisited while discussing any changes made when compared to previous design reports. In addition to that a matching plot is presented for the proposed configuration with all the performance constraints showing exactly the critical mission requirements.

4.1. Manual Calculations of Performance Constraints:

4.1.1) Stall Speed:

Few aircraft have their pre-determined limit for the stall speed specified in the mission configuration which there will be a requirement for minimum stall. From ‘Airplane Design; Part-I Chapter 3’ by ‘Roskam’ an aircraft whose weight at take-off is below 6000 lbs must have a stall speed limit of less than 61 kts and should fall into FAR-23 certification, unless for certain climb gradient values. Since VER-12XX is above this weight limit and is a jet transport aircraft, there aren’t any specified limits imposed on their stall speed. It should also be noted that VER-12XX falls into the category of FAR-25 certification. To determine the ‘**power-off**’ stall speed for VER-12XX, ‘Roskam’ specifies the following equation.

$$V_{stall} = \sqrt{\left[\frac{(2 * W/S)}{\rho C_{L_{max}}} \right]} \quad (4.1)$$

Note: The $C_{L_{max}}$ being considered is the Clean Aircraft Configuration, W/S is the wing-loading, and ρ is the density at sea-level.

Let us consider that VERHY-12 has a stall speed requirement during landing with full flaps of no more than 120kts and with flaps up not more than 150 kts. Now, we can determine the wing loading value at take-off.

Airplane Type	$C_{L_{max}}$	$C_{L_{max_{TO}}}$	$C_{L_{max_L}}$
1. Homebuilts	1.2 - 1.8	1.2 - 1.8	1.2 - 2.0
2. Single Engine Propeller Driven	1.3 - 1.9	1.3 - 1.9	1.6 - 2.3
3. Twin Engine Propeller Driven	1.2 - 1.8	1.4 - 2.0	1.6 - 2.5
4. Agricultural	1.3 - 1.9	1.3 - 1.9	1.3 - 1.9
5. Business Jets	1.4 - 1.8	1.6 - 2.2	1.6 - 2.6
6. Regional TBP	1.5 - 1.9	1.7 - 2.1	1.9 - 3.3
7. Transport Jets	1.2 - 1.8	1.6 - 2.2	1.8 - 2.8
8. Military Trainers	1.2 - 1.8	1.4 - 2.0	1.6 - 2.2
9. Fighters	1.2 - 1.8	1.4 - 2.0	1.6 - 2.6
10. Mil. Patrol, Bomb and Transports	1.2 - 1.8	1.6 - 2.2	1.8 - 3.0
11. Flying Boats, Amphibious and Float Airplanes	1.2 - 1.8	1.6 - 2.2	1.8 - 3.4
12. Supersonic Cruise Airplanes	1.2 - 1.8	1.6 - 2.0	1.8 - 2.2

Figure 30: MAX Coefficient of Lift for Different Flight Scenarios

$$\Rightarrow V_{stall} = \sqrt{\left[\frac{(2 * W/S)}{\rho C_{L_{max}}} \right]}$$

$$\Rightarrow \frac{V_{stall}^2 * \rho C_{L_{max}}}{2} > (W/S)_{wingloading}$$

$$\Rightarrow \frac{120^2 * 0.033 * 1.8}{2} > (W/S)_{wingloading} \quad (C_{L_{maf}} = 1.8)$$

$$\therefore (W/S)_{wingloading} < 428 \text{ psf}$$

$$\Rightarrow \frac{V_{stall}^2 * \rho C_{L_{max}}}{2} > (W/S)_{wingloading} \quad (C_{L_{max-landing}} = 2.6)$$

$$\Rightarrow \frac{120^2 * 0.033 * 2.6}{2} > (W/S)_{wingloading} \quad (C_{L_{maf}} = 2.6)$$

$$\therefore (W/S)_{wingloading} < 428 \text{ psf}$$

Therefore, to meet both the requirements, a wing-loading a value of 428 psf is considered reasonable during take-off.

4.1.2) Sizing to Take-off Distance:

The definition of take-off distance as specified by FAR-25 requirements is shown below:

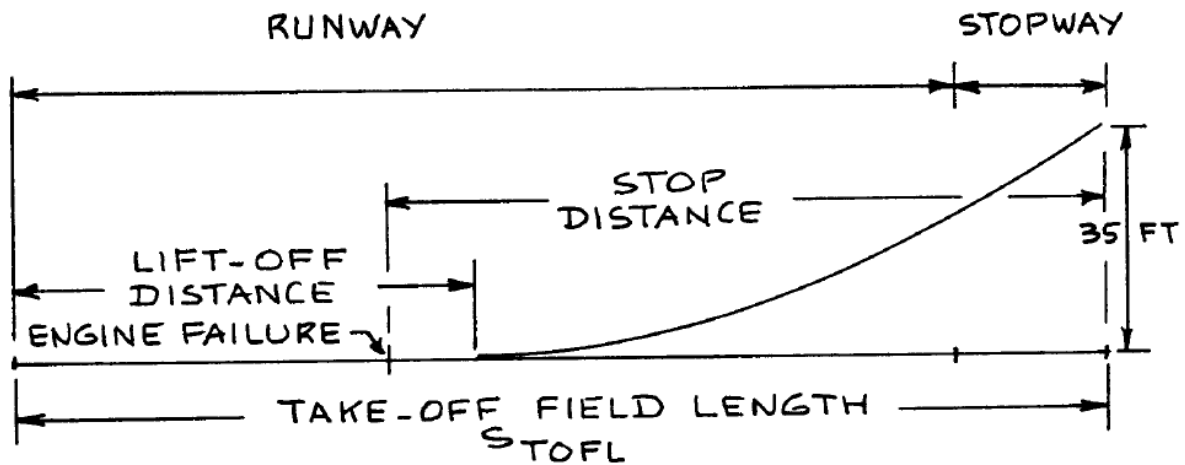


Figure 31: FAR-25 Take-off Run Way Definitions

$$s_{TOFL} \propto \frac{(W/S)_{TO}}{\left\{ \sigma * C_{L_{MAX_{to}}} * (T/W)_{TO} \right\}} = TOP_{25} \quad (4.2)$$

$$\Rightarrow s_{TOFL} = 37.5 \frac{(W/S)_{TO}}{\left\{ \sigma * C_{L_{MAX_{to}}} * (T/W)_{TO} \right\}} = TOP_{25} \quad (4.3)$$

$$\Rightarrow s_{TOFL} = 37.5 * TOP_{25}$$

$$\Rightarrow TOP_{25} = \frac{9300}{37.5}$$

$$\therefore TOP_{25} = 248 \text{ lbs} / \text{ft}^2$$

Now, we can relate wing to power loading by simplifying the equation:

$$\Rightarrow \left(\frac{W}{S} \right)_{TO} = 248 * (C_{L_{to}} * 0.786) * \left(\frac{T}{W} \right) \quad (4.4)$$

For different values of take-off lift coefficient, we can vary the wing and power loading required during take-off.

Table 7: Determined Power Loading for specified Wing Loading values at $CL_{max}=1.2$

Wing Loading (psf)		σ (kg/m ³)	TOP25 (Take-off Parameter)	$(W/S)_{TO} = 248 * (C_{L_{TO}} * 0.786) * (T/W)$	T/W
100	1.2	0.786	248	195	0.43
200	1.2	0.786	248	195	0.85
300	1.2	0.786	248	195	1.28
400	1.2	0.786	248	195	1.71
500	1.2	0.786	248	195	2.14

Table 8: Determined Power Loading for specified Wing Loading values at $CL_{max}=1.4$

Wing Loading (psf)	$C_{L_{MAX_{to}}}$	σ (kg/m ³)	TOP25 (Take-off Parameter)	$(W/S)_{TO} = 248 * (C_{L_{TO}} * 0.786) * (T/W)$	T/W
100	1.4	0.033	248	195	0.37
200	1.4	0.033	248	195	0.73
300	1.4	0.033	248	195	1.10
400	1.4	0.033	248	195	1.47
500	1.4	0.033	248	195	1.83

Table 9: Determined Power Loading for specified Wing Loading values at $CL_{max}=1.6$

Wing Loading (psf)	$C_{L_{MAX_{to}}}$	σ (kg/m ³)	TOP25 (Take-off Parameter)	$(W/S)_{TO} = 248 * (C_{L_{TO}} * 0.786) * (T/W)$	T/W
100	1.6	0.033	248	195	0.32
200	1.6	0.033	248	195	0.64
300	1.6	0.033	248	195	0.96
400	1.6	0.033	248	195	1.28
500	1.6	0.033	248	195	1.60

Table 10: Determined Power Loading for specified Wing Loading values at $CL_{max}=1.8$

Wing Loading (psf)	$C_{L_{MAX_{to}}}$	σ (kg/m ³)	TOP25 (Take-off Parameter)	$\left(\frac{W}{S}\right)_{TO} = 248 * (C_{L_{TO}} * 0.786) * \left(\frac{T}{W}\right)$	T/W
100	1.8	0.033	248	195	0.28
200	1.8	0.033	248	195	0.57
300	1.8	0.033	248	195	0.85
400	1.8	0.033	248	195	1.14
500	1.8	0.033	248	195	1.42

4.1.3) Landing Distance:

The landing field length for a jet transport must be sized and this value had earlier been specified in the mission specifications. It is again possible to define a relation between wing loading and $C_{L_{MAX_{LANDING}}}$ using e.q.4.9.

The landing to take-off weight ratio is assumed to be 0.84

$$V_A = 1.3 * V_{S_L} \quad (4.5)$$

$$s_{FL} = 0.3 * V_A^2 \quad (4.6)$$

$$\therefore V_A^2 = \frac{s_{FL}}{0.3} \quad (4.7)$$

$$\Rightarrow V_A = \sqrt{\frac{10000 \text{ ft}}{0.3}}$$

$$\therefore V_A = 183 \text{ kts}$$

$$\Rightarrow V_{S_L} = \frac{183}{1.3}$$

$$\therefore V_{S_L} = 141 \text{ kts}$$

$$\Rightarrow V_{S_L} = \sqrt{\left[\frac{(2 * W/S)}{\rho C_{L_{max-landing}}} \right]} \quad (4.8)$$

$$\Rightarrow \frac{V_{S_L}^2 * \rho C_{L_{max-landing}}}{2} = \left(\frac{W}{S}\right)_{wingloading-landing} \quad (4.9)$$

$$\Rightarrow \frac{(141 * 1.688)^2 * 0.036 * C_{L_{max-landing}}}{2} = \left(\frac{W}{S}\right)_{wingloading}$$

$$\therefore \left(\frac{W}{S}\right)_{wingloading} = 67.12 C_{L_{max-landing}}$$

Using the above correlation between wing loading and max- landing coefficient we can determine the required $C_{L_{\max-landing}}$ for a specified wing-loading while considering the landing field length.

Table 11: $C_{L_{\max}}$ obtained for different Wing-Loading at Landing

Wing Loading (psf)	$C_{L_{\max-landing}}$
40	0.6
50	0.7
60	0.9
70	1.0
80	1.2
90	1.3
100	1.5
200	3.0
300	4.5
400	6.0

② Sizing to FAR25 Landing Distance Requirements

$$\text{Approach speed} = 1.3 V_{S_L}$$

$$V_A = (1.3) \times (103.83) \text{ kts}$$

$$\therefore V_A = 134.98 \text{ kts}$$

Landing ground run is related to stall speed as:

$$S_{L_G} = 0.265 \cdot V_{S_L}^2$$

$$= (0.265) (103.83)^2$$

$$S_{L_G} = 2856.87 \text{ feet}$$

The Relation b/w S_L & S_{L_G}

$$S_L = 1.938 \times S_{L_G}$$

$$= (1.938) \times (2856.87)$$

$$S_L = 5536.61 \text{ feet}$$

Figure 32: Manual Calculations of FAR-25 Landing Distance

4.1.4) Sizing to Climb Requirements:

⊕ Sizing to Climb Requirements.

Aircraft have to meet climb & climb gradient requirements. An important factor that helps us to determine these factors is by evaluating drag polar.

⊕ The drag polar coefficient of an airplane

$$C_D = C_{D0} + k C_L^2 \Rightarrow k = \frac{1}{\pi A e}$$

where $C_{D0} = f/S = \frac{\text{Equivalent Parasite Area}}{\text{Wing Area}}$

we can relate wetted Area to Equivalent Parasite drag as

$$\log_{10} f = a + b \log_{10} S_{wet}$$

We can also evaluate S_{wet} using the following equation:

$$\log_{10} S_{wet} = c + d \log_{10} W_{T0}$$

⊕ For take-off & landing the effect of flaps & landing gear are to be considered.

Figure 33: FAR-25 Climb Sizing Manual Calculations-1

From the previous weight sizing report we know the regressionline coefficients

$$A = 0.2368, B = 1.0096 ; C = 0.885, D = 72225$$

$$W_{10} = 207379.2 \text{ lbs}$$

$$\begin{aligned} \log_{10} S_{wet} &= C + d \log_{10} W_{10} \\ &= (0.885) + (0.199) \log_{10}(207379.2) \end{aligned}$$

$$\log_{10} S_{wet} = 1.943$$

$$\boxed{S_{wet} = 87.70} \Rightarrow \boxed{S_{wet} = 87.70 \text{ feet}}$$

From table 3.5 Postkam		
jet	c	d
Frangjet	0.079	0.753
Jet3		

Estimating a skinfriction coefficient (C_f) to be $\boxed{0.0090}$ from Postkam table 3.4

$$a = -2.0458, b = 1$$

$$\begin{aligned} \log_{10} f &= a + b \log_{10} S_{wet} \\ &= -2.0458 + (1) (\log_{10} 87.252) \end{aligned}$$

$$\log_{10} f = -0.1050$$

$$\boxed{f = 1.2735 \text{ feet}}$$

Figure 34: FAR-25 Climb Sizing Manual Calculations-II (Skin Friction Drag Coefficient and Wetted Area)

so for a wingspan of 64.8m & wing Area of 4701.67 feet the

aspect ratio is

$$AR = \frac{b^2}{S} = \frac{(212.6)^2}{4701.67}$$

$$AR = 9.613$$

$$q \quad C_{D0} = f/S$$

$$= \frac{1.2735}{4701.67}$$

$$C_{D0} = 0.002708$$

& assuming an e value of 0.80

$$e = 0.80, C_{D0} = 0.002708, AR = 9.613$$

$$C_D = C_{D0} + kC_L^2$$

$$\therefore C_D = 0.002708 + 0.044C_L^2$$

From Roskam Table 3.6		
configuration	ΔC_{D0}	e
clean	0	0.80
T/O flaps	0.010	0.75
landing flaps	0.055	0.7
landing gear	0.015	-

Therefore the airplane drag polar is as follows:

$$\text{Low speed, clean; } C_D = 0.002708 + 0.0414C_L^2$$

$$\text{Takeoff, gear up; } C_D = 0.012708 + 0.04415C_L^2$$

$$\text{Takeoff gear down; } C_D = 0.027708 + 0.04730C_L^2$$

Figure 35: FAR-25 Climb Sizing Manual Calculations-III (Drag Coefficient)

$$\text{Landing, gear up } C_D = 0.062708 + 0.0473 C_L^2$$

$$\text{Landing gear down; } C_D = 0.079 + 0.03311 C_L^2$$

② Sizing Method for FAR-25 Climb Requirements:

The following are the requirements:

→ for Jet powered airplanes

with one engine inoperative

$$(T/w) = \left\{ N/(N-1) \right\} \left\{ (L/D)^{-1} + CGR \right\}$$

with all engines operating (AEO):

$$(T/w) = \left\{ (L/D)^{-1} + CGR \right\}$$

CGR → required climb gradient & it is similar to flight path angle (γ)

L/D & T/w are those for take-off & landing

The process of sizing for climb requirements amounts to finding relations b/w , $(w/s)_{T0}$, $(T/w)_{T0}$ & $(w/p)_{T0}$

Figure 36: Climb Sizing Procedure

For Take-off climb:

FAR 25.111 (OEI)

$$CGR > 0.012 \cdot (1.2 V_{SO})$$

[Grossup, T/O thrust, ground effect]

FAR 25.121 (OEI) $CGR > 0$

FAR 25.121 (OEI) $CGR > 0.024$

FAR 25.121 (OEI) $CGR > 0.012$

→ These values are completely dependant on the flaps setting, landing gear, engine operation

For landing climb:

FAR 25.119 (AEO) $CGR > 0.032$

FAR 25.121 (OEI) $CGR > 0.021$

For VER-12x

$$f = 31 \text{ ft}^2 \rightarrow \text{from the figure 3.21}$$

$$C_f = 0.0030 \rightarrow \text{" " " "}$$

$$W_{T0} = 207379.2 \text{ lbs}$$

Assuming wetted area to be = 9000 ft^2

Assuming an average wing loading of 150 psf

$$\frac{W}{S} = 150$$

$$\Rightarrow \frac{207379.2}{150} = S$$

Figure 37: Climb Gradient Specifications for Take-off and Landing (FAR-25)

$$S = 1382 \text{ feet}^2$$

Drag polar below is now assumed:-

<u>Configuration</u>	C_{D0}	A	e	C_{Di}	C_{Lmax}
clean	0.0184	10	0.85	$C_L^2/26.7$	1.8
Take-off flaps	0.0334	10	0.80	$C_L^2/25.1$	2.0
Landing flaps	0.0784	10	0.7	$C_L^2/23.6$	2.8
Gear down	0.050	10	-	-	no effect

climb sizing calculations -

with one engine operative

$$(T/w) = \left\{ \frac{2}{(2-1)} \right\} \left\{ \frac{1}{(L/D)} + \frac{CGIR}{L} \right\}$$

↳ at $1.2 V_{STO}$

Since we assumed $C_{Lmax} = 2.0$

The actual lift coefficient in this flight condition is $\frac{2.0}{(1.2)^2}$

$$C_L = 1.4$$

Figure 38: FAR-25 Climb Sizing Manual Calculations-IV

The drag polar is $C_D = 0.0334 + \frac{C_L^2}{25.1}$

$$\Rightarrow C_D = 0.0334 + \frac{(1.4)^2}{25.1}$$

$$C_D = 0.111$$

$$\boxed{L/D = \frac{1.4}{0.11} = \frac{C_L}{C_D}}$$

$$\boxed{L/D = 12.72}$$

$$(T/w)_{10} = 2 \times \left\{ \frac{1}{12.72} + \frac{0.012}{1} \right\}$$

As per FAR 25.111 (OEI)
 $\hookrightarrow X_{GR} > 0.012$

$$\boxed{(T/w)_{10} = 0.1832}$$

↓

This value does not account for 50°F temperature effect
 & together max thrust at 50°F

So for the purpose of sizing, $(T/w)_{10(50)} = 0.80$

$$(T/w)_{10 \text{ without } 50^\circ\text{F}} = 0.1832$$

$$\Rightarrow (T/w)_{10(50)} = \frac{0.1832}{0.80}$$

$$(T/w)_{10(50)} = 0.23$$

Figure 39: FAR-25 Climb Sizing Manual Calculations-V

AR 25-121 (OFA) grossed, to flaps \rightarrow 70

$$(T/w)_{T0} = 2 \left\{ N/(W-1) \right\} \left\{ \frac{1}{L/D} + \frac{C_{Gr}}{2} \right\}$$

$$= 2 \left\{ \frac{1}{L/D} + 0.5 \right\}$$

D/w V_{Lof} & V_2 we assume $V_{Lof} = 1.1 V_{STO}$

$$C_{L_{maxT0}} = 2.0; \quad C_{L_{Lof}} = \frac{2.0}{(1.1)^2} = 1.65$$

$$C_D = 0.0484 + \frac{C_L^2}{25.1}$$

$$= 0.0484 + \frac{1.65^2}{25.1}$$

$$C_D = 0.1141$$

$$L/D = \frac{1.65}{0.1141}$$

$$L/D = 14.46$$

$$(T/w)_{T0} = 2 \left\{ \frac{1}{14.46} + 0.5 \right\}$$

$$(T/w)_{T0} = 1.138$$

correcting the temperature requirement

$$(T/w)_{T0} = \frac{1.138}{0.8} = 1.4225$$

$$(T/w)_{T0} = 1.4225$$

Figure 40: FAR-25 Climb Sizing Manual Calculations-VI

FAR25121 (OE+) (gear up, + 0 slope) at $1.2 V_{STO}$

$$(T/w)_{TO} = 2 \left\{ \frac{1}{L/D} + 0.026 \right\}$$

Lift coefficient $\frac{2.0}{(1.2)^2} = 1.4$

Drag polar $C_D = 0.0334 + \frac{C_L^2}{25.1}$

$L/D = 12.72$

$$(T/w)_{TO} = 2 \left\{ \frac{1}{12.72} + 0.026 \right\}$$

$$(T/w)_{TO} = 0.209$$

The correction is $(T/w)_{TO} / 0.8 = 0.209 / 0.8 = 0.26125$

Figure 41: FAR-25 Climb Sizing Manual Calculations-VII (One Engine Operating Condition)

4.1.5) Sizing to Maneuvering Requirements:

B) Sizing to Maneuvering Requirement.

for equilibrium flight it is necessary that

$$nW = C_L \bar{q} S = 1.482 \rho M^2 C_L S$$

$$n_{max} = (1.482 C_{L_{max}} S M^2) / (W/S)$$

$$T = C_D \bar{q} S + (C_L^2 / \pi A e) \bar{q} S$$

for Ver 12-X Max speed = 482 kts

$$M = \frac{482 \text{ kts}}{661.47} = \left[\frac{\text{object speed}}{\text{speed of sound.}} \right] \cdot \frac{\text{knots}}{\text{knots}}$$

$$M = 0.728$$

$$(T/W)_{req} = \frac{6.6}{(W/S)} + 0.01591 \times (W/S)$$

for (W/S) = 150 lbs $(T/W)_{req} = 2.4305$

Figure 42: Sizing to Manoeuvring Requirement

4.1.6) Sizing to Maximum Speed for Jet Aircraft :

1) Sizing to Maximum speed for a Jet:

$$W_{TO} = 207379.21 \text{ lbs}$$

$$S_{wet} = 9000 \text{ ft}^2$$

$$f = 31 \text{ ft}^2$$

$$w/s = 150 \text{ psf}$$

$$C_{D0} = 0.0184$$

$$C_f = 0.0030$$

$$A = 10$$

$$e = 0.8$$

$$g_{jet}(w/s) = 150$$

$$T/w = \frac{267}{(w/s)} + \frac{(w/s)}{(30159.28)}$$

$$= \frac{267}{150} + \frac{150}{(30159.28)}$$

$$\boxed{T/w = 1.785}$$

$$g_{jet}(w/s) = 200 ; \boxed{T/w = 1.341}$$

$$g_{jet}(w/s) = 250 ; \boxed{T/w = 1.076}$$

$$V = 77.3 \left[\frac{\eta_p (w/s)}{\sigma C_D (w/p)} \right]^{1/2}$$

$$C_D = \eta_p \cdot 77.3^3 \left(\frac{T/w}{V} \right)^3$$

Assuming $\eta_p = 0.85$, $C_{D0} = 0.9 C_D$

$$\left(\frac{T/w}{w} \right)_{req} = C_{D0} \bar{q} S / w + \frac{w}{\bar{q} S \pi A}$$

Figure 43: Sizing to Maximum Speed

4.2 CALCULATION OF PERFORMANCE CONSTRAINTS WITH THE AAA

PROGRAM:

4.2.1 STALL SPEED:

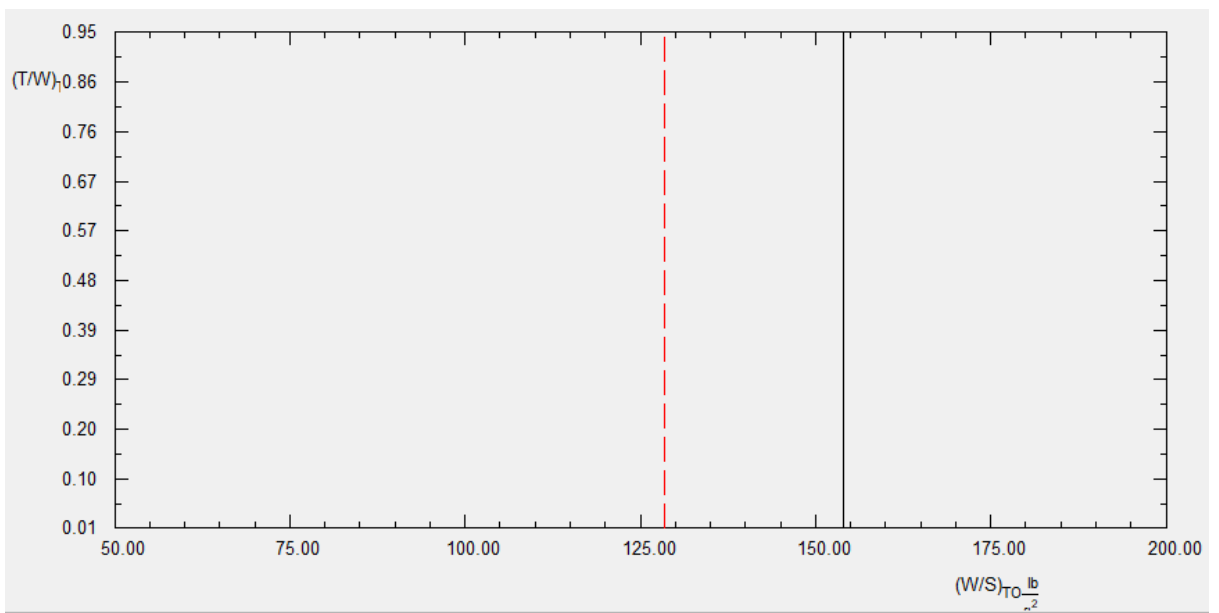
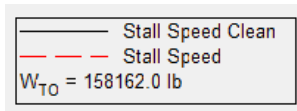


Figure 44: Stall Speed Sizing Plot - AAA

4.2.2 TAKE-OFF DISTANCE REQUIREMENTS FROM AAA:

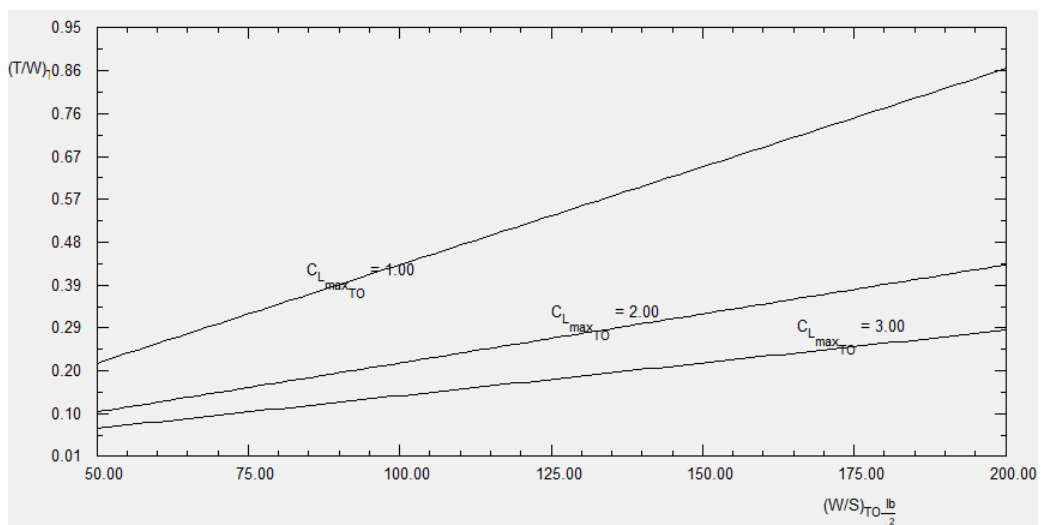


Figure 45: Take-off Distance Sizing - AAA

4.2.3 SIZING TO CLIMB REQUIREMENTS:

Input Parameters									
$F_{MaxCont}$	0.950	$C_{L_{maxL}}$	2.880	e_{TO}	0.9000	$\Delta C_{D_{oA}}$	0.0260	$CGR_{25.121_{SS}}$	0.024
F_{8sec}	0.970	W_L / W_{TO}	0.850	$C_{D_{TO_up}}$	0.0070	$C_{D_{wm}}$	0.0030	$CGR_{25.121_{ER}}$	0.012
$C_{L_{max_{clean}}}$	1.560	AR_w	10.60	$C_{D_{TO_down}}$	0.0150	CGR	User Defined	$CGR_{25.121_L}$	0.021
$C_{L_{max_{TO}}}$	2.000	e_{clean}	0.8500	e_L	0.6000	$CGR_{25.111}$	0.012	$CGR_{25.119}$	0.032
$C_{L_{max_A}}$		$C_{D_{clean,M}}$	0.0300	$C_{D_{L_down}}$	0.0530	$CGR_{25.121_T}$	0.002		

Figure 46: Sizing to Climb Requirements - Inputs

4.2.4 SIZING TO LANDING DISTANCE:

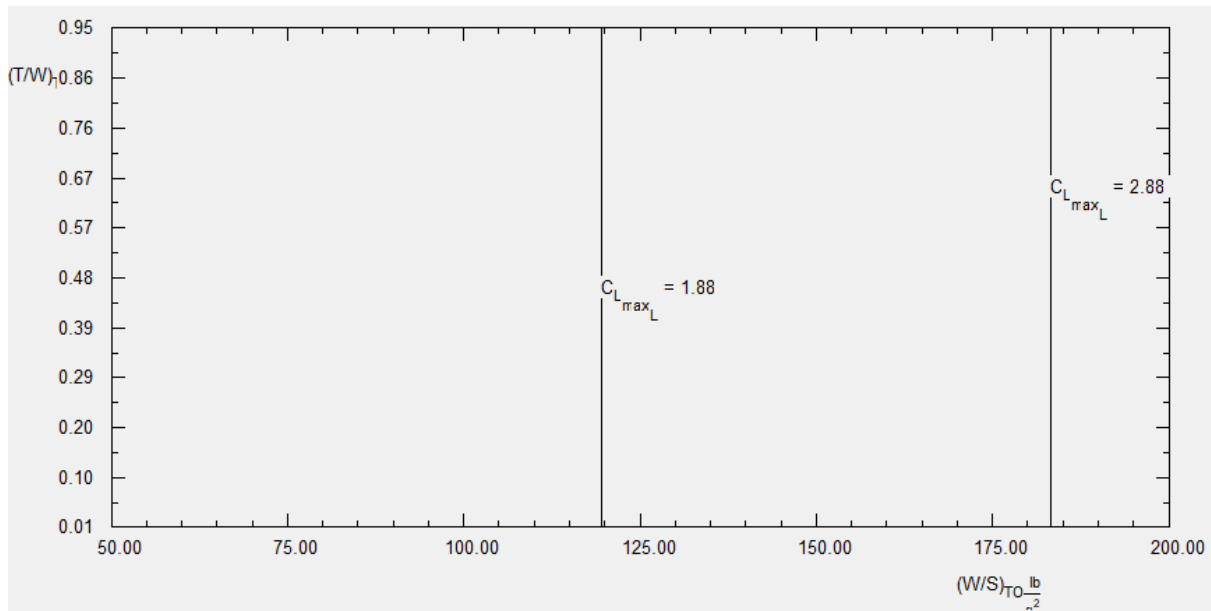


Figure 47: Sizing to Landing Distance -AAA

4.2.5 SIZING TO MAXIMUM SPEED:

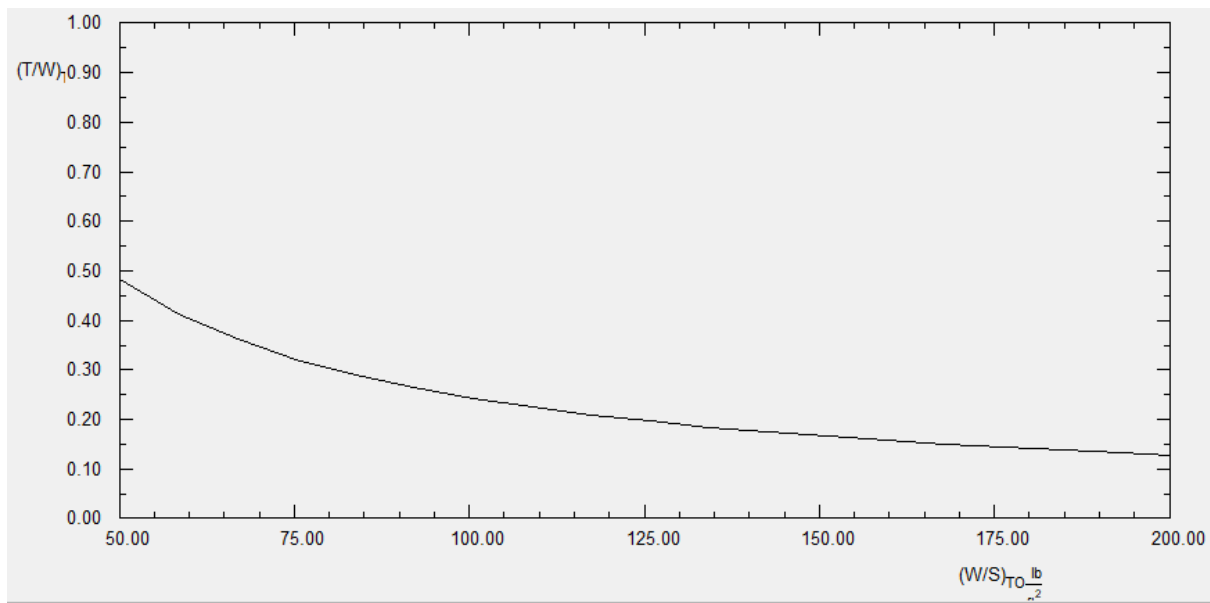


Figure 48: Sizing to Max Speed Requirements -AAA

4.2.6 SIZING TO MANOEUVRINGS SPEEDS:

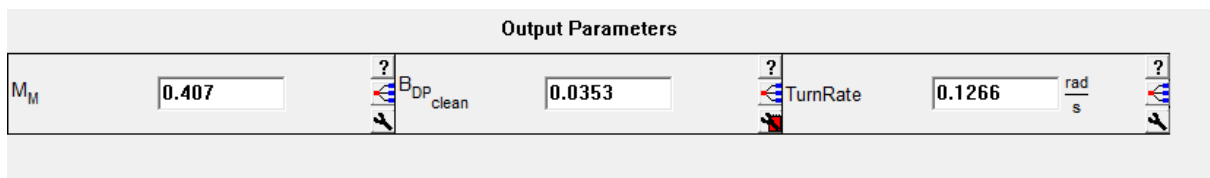


Figure 49: Sizing to Manoeuvring Speed - AAA

4.2.7 MATCHING GRAPH:

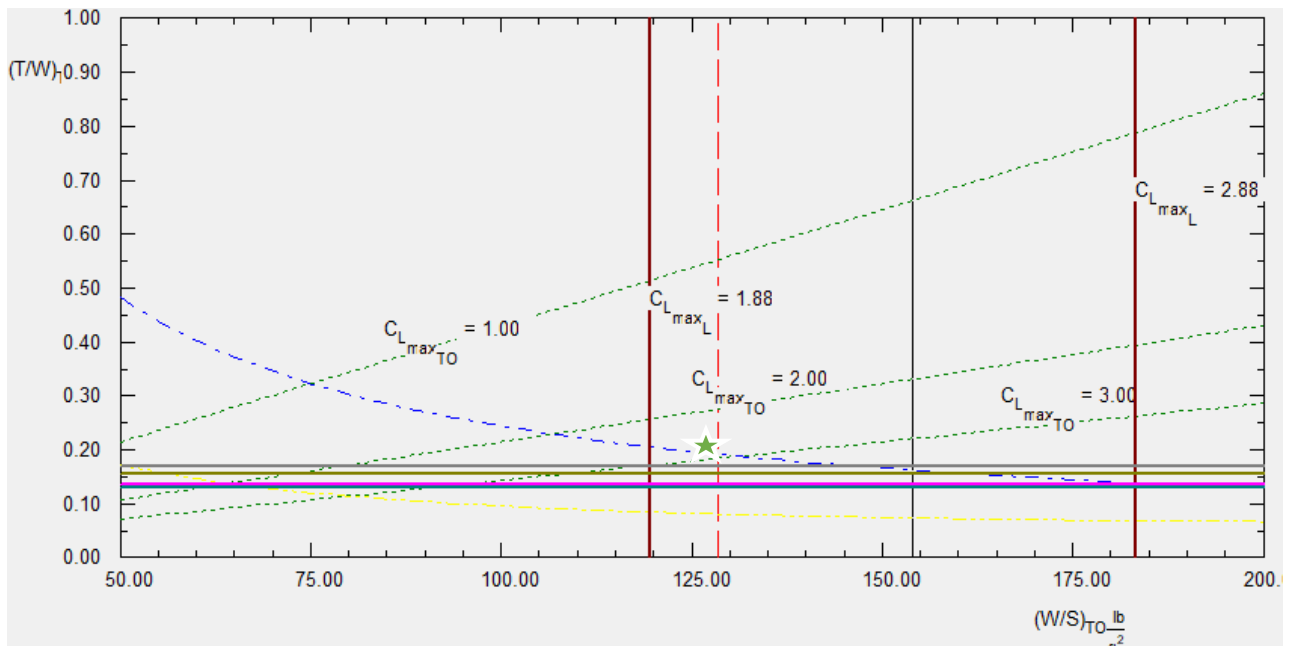


Figure 50: Performance Sizing Graph

In this section, all the computed performance constraints are plotted on a single graph against wing loading and thrust loading. Since the critical parameters being take-off and stall speed, the favourable thrust loading for a for a stall speed of 125 kts is 0.25* and this gives us a wing loading of 127 lbs/ft^2

4.3 SELECTION OF PROPULSION SYSTEM:

The propulsion system integration depends usually on the specified mission requirements. It is a good idea to use combination of engines (i.e. turbojet plus piston engine) but this increases maintenance costs. For VER-12XX mission requirements an existing turbo-jet engine will be studied as it has few favourable factors that stand out from other turbo jet engines such as improved fuel efficiency, reduced noise, Co₂ and NO_X emissions and lighter. In the preliminary design, as per the take-off weight requirements and range, the possibility of using GE-9X engines will be analysed in further sections of the project. Engines integration with respect to the position is very important as they determine the structural integrity of the wing and is also responsible for impacting the boundary layer. Conventionally the engines are placed at the leading edge of the aircraft and they are podded structures which are useful in energising the boundary layer. It is aimed that for VER-12XX to use the same design in term of engine location.

4.4 Discussion:

From the performance constraint analysis, some of the crucial parameters for VER-12XX are determined. The values for take-off parameters in Roskam have been determined using old aircraft database and they change when compared to existing aircraft which directly results to change the landing and take-off distance values. Therefore, a correction factor of 10% percent is considered while determining take-off weight for VER-12XX. By comparing the power and wing loading there is an actual design trade off which helps us to find the optimum value and thereby improving the performance of the aircraft. While calculating the manoeuvring speeds for VER-12XX there are many estimated values, which can be useful in iteration process and could finally lead us to choosing an optimum value. Performance constraint analysis is an important tool especially for understanding the performance constraints for VER-12XX. Through the above calculations and the iterations process, we can understand the variations in power loading for VER-12XX. The sizing to climb requirements is challenging. This is an important phase for any aircraft and notable design point where designers should be very careful in using precise coefficient of lift values. FAR25 aircraft have various flight settings i.e. Flaps up, flaps down, landing gear up and landing gear down and they have direct effects on the drag polar of the aircraft, which are responsible for increase or decrease of drag coefficients of the aircraft. To sum

up with it is important that basic lift and drag data collected should be precise or calculated precisely to determine the near to exact values for the performance of the aircraft and to understand the performance constraint's that are associated with them.

CHAPTER 5

FUSELAGE DESIGN

Fuselage design is an integral part of aircraft design and at this point the total length of the fuselage, cabin configurations, cabin layout and Cargo will all be thoroughly studied using the proposed aircraft CAD Drawings of the aircraft in the later section of this design chapter. It is known that, length of Fuselage accounts to the total wetted area and this parameter in turn can be considered as an estimate to determine the overall drag of the aircraft. Area ruling is an important concept as it determines the airflow over the fuselage especially at the point of integration of wings to the fuselage. Since, the payload for VER-12XX are passengers, a study is included on the dimensions of a person that matches the 2-aisle configuration with 3 seats on each aisle. The cabin seats recline angle, seat width and leg room will also be discussed.

5.1 LAYOUT DESIGN OF COCKPIT:

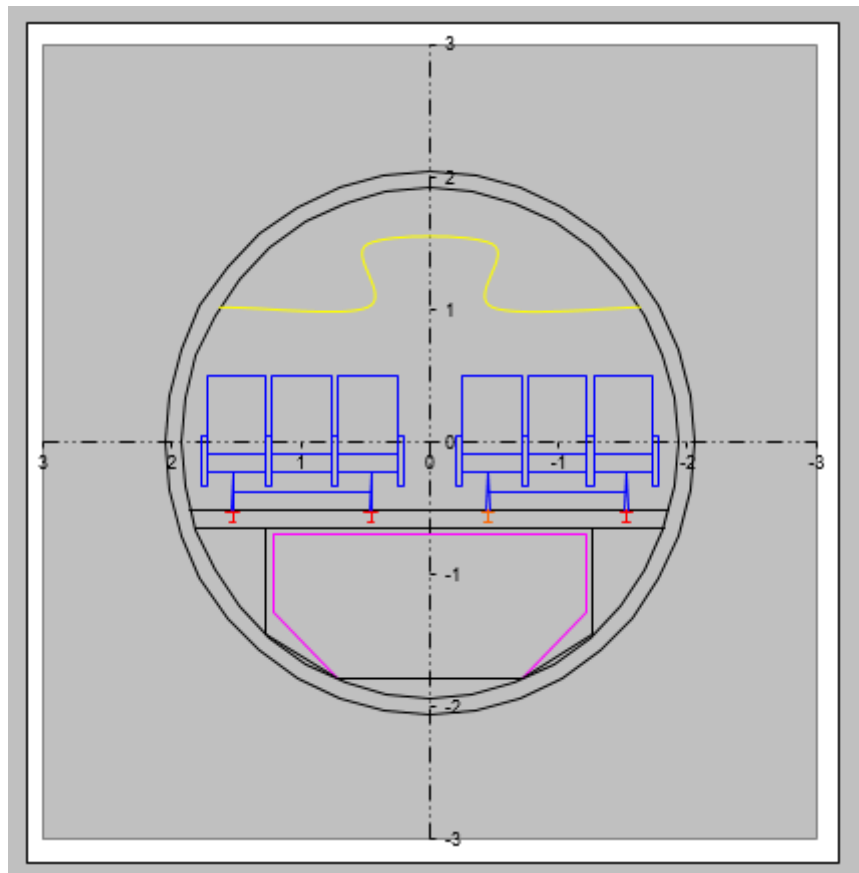


Figure 51: Seating Configurations, Cargo Space for VER-12XX using PRESTO

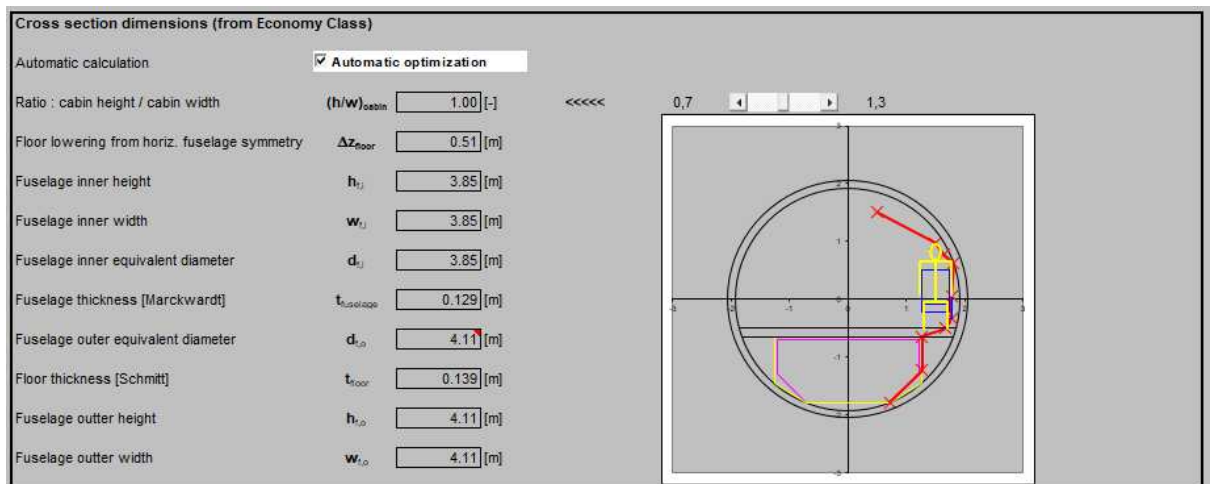


Figure 52: Fuselage Cross Section Dimensions - Economy Class

Seat pitch	
Seat pitch, first class	$pitch_{FC}$ <input type="text" value="36"/> [inch]
Seat pitch, economy class	$pitch_{VC}$ <input type="text" value="32"/> [inch]

Figure 53: Proposed Seat Pitch for Economy and Business Class

Passenger dimensions	
Midshoulder height, sitting	$\Delta y_{midshoulder}$ <input type="text" value="0.70"/> [m]
Shoulder breadth	$w_{shoulder}$ <input type="text" value="0.53"/> [m]
Eye height, sitting	Δy_{eye} <input type="text" value="0.87"/> [m]
Head to wall clearance	d_{hw} <input type="text" value="0.06"/> [m]
Shoulder to wall clearance	d_{sw} <input type="text" value="0.04"/> [m]

Figure 54: Passenger Dimensions

5.2 LAYOUT DESIGN OF THE FUSELAGE:

For the preliminary CAD drawings of the fuselage CATIA V-5 software is used.

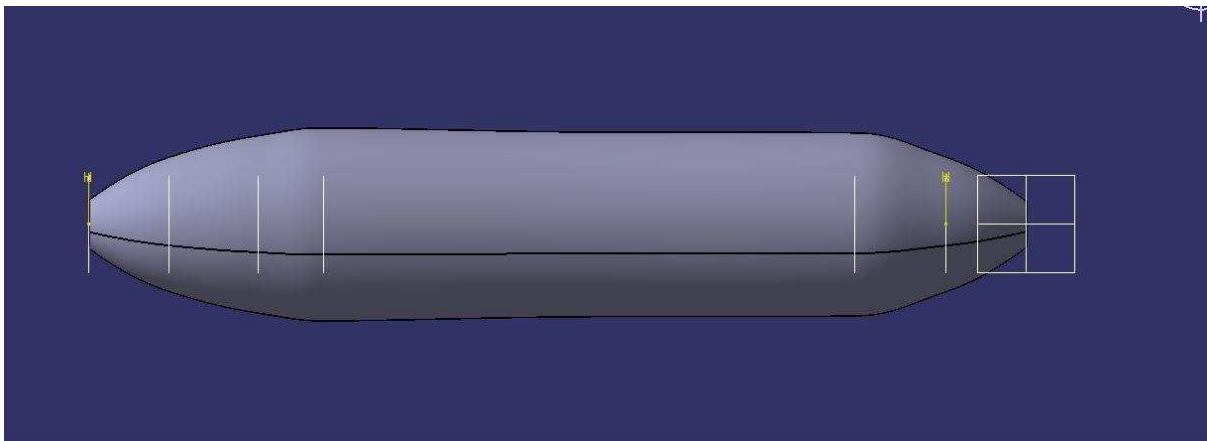


Figure 55: Fuselage- Side View

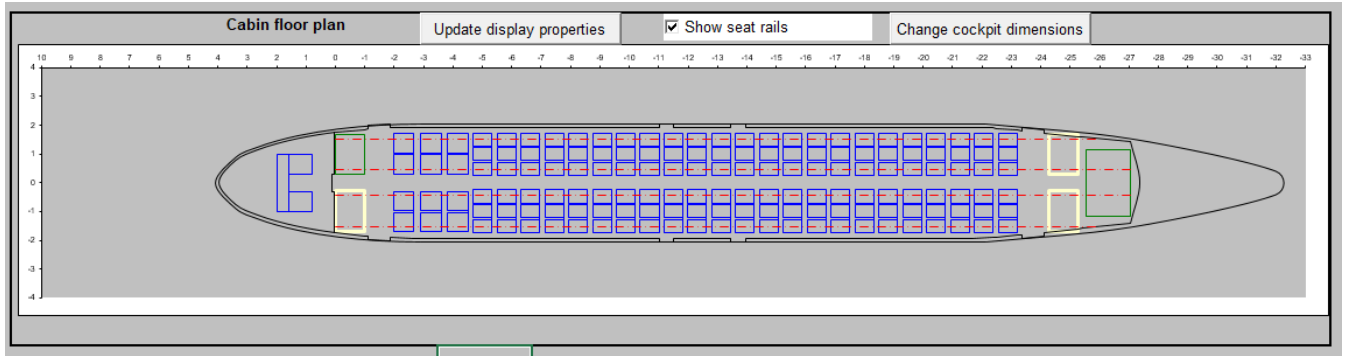


Figure 56: Proposed 2-Aisle Configuration for VER-12XX

CHAPTER 6

WING, HIGH-LIFT SYSTEM AND LATERAL CONTROL DESIGN

Aircraft wing play a prominent role in aircraft lift generation and contributes to the overall stability of the aircraft. In this chapter, for VER-12XX the wing design analysis will be extensively studied. Firstly, wing parameters such as taper ratio, thickness ratio, sweep angle are determined and then overall weight contribution of wing will be calculated. A trade off study will be carried between the thickness ratio and sweep angle to select the optimum sweep angle of the wing. In the AAA program, all the determined values will be used as inputs to determine the wing planform schematic.

6.1 WING PLANFORM DESIGN:

A cantilever wing is the most common type amongst the high subsonic travel aircraft. Its structural configuration is a standpoint and makes it most favourable for choosing them. There is another type of wing which is a braced configuration and is suitable for low speed flight (e.g. below 200 knots). In the design of aircraft, it is important to keep its weight minimum whereas the braced structures add up weight because of their structural arrangement. Figure 56 shows the variations in different types of cantilevered wing structures.

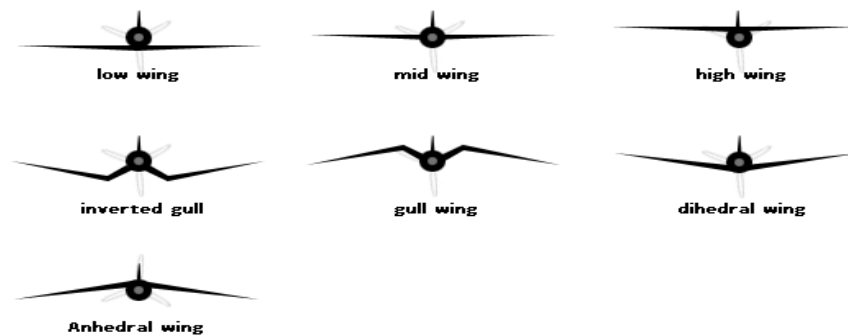


Figure 57: Different Types of Wing Configurations

Wing /Fuselage Arrangement:

Wing disposition is an important aspect that effect the overall aerodynamics and efficiency of the aircraft. There are different types of wing configurations like high, medium and low and their selection is completely dependent on the aircraft mission requirements.

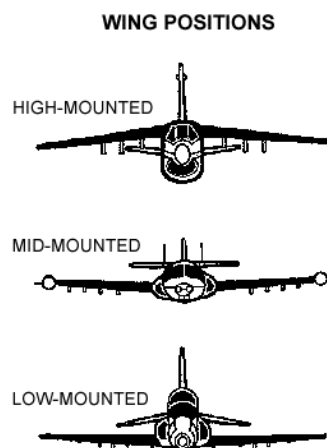


Figure 58: Wing Positions

Now-a-days low wing configuration can be profoundly seen in subsonic transport jets. This configuration allows better visibility for the pilots, eases aircraft maintenance, removes the need for special equipment while refuelling and keeps the fuselage afloat during ditching. Safety in passenger jets is very important and the low wing configuration facilitates with that feature.

Weight of the wing or wing loading is an important factor as it determines some of the flight characteristics of the aircraft. It is a known fact that if the aircraft has low wing loading the aircraft has relatively larger wing area and the amount of lift produced per every square foot of the wing is also higher but reverse is the case when the wing loading is higher which is especially the case of modern airlines. This factor also determines the take-off, landing distances and manoeuvrability of the aircraft. For VER-12XX; initial calculations of the wing loading are determined and are shown below. The method used for determining the wing loading is a GD method and is an excerpt Roskam Textbook.

⊕ Wing Weight Estimation

for transport jet cruising at Mach 0.84 we can use

G-D Method :

$$W_w = \frac{(0.00428 \cdot S^{0.48}) \times (A \times M_{cr}^{0.43}) \left\{ W_{to} n_{ult} \right\}^{0.84} (1)^{0.14}}{\left[\left\{ 100 \left(\frac{t}{cm} \right) \right\}^{0.76} (\cos \Lambda_{1/2})^{1.54} \right]}$$

$$= \frac{(0.00428 \cdot (4700)^{0.48}) \times (9.61 \times (0.84)^{0.43}) \left\{ (528962 \times 4.44)^{0.84} \cdot (0.149)^{0.14} \right\}}{\left[\left\{ (100) (0.15) \right\}^{0.76} (56.8)^{1.54} \right]}$$

$$= \frac{(0.247) (8.91) \times (172077.6)}{(7.831) (503.14)}$$

Figure 59: GD Wing Weight Calculation from 'Roskam'

Manual Calculations

→ The cruise lift coefficient can be estimated using

$$C_{L_{CR}} = \frac{(W_{TO} - 0.4W_F)}{\bar{q}_S} \quad \text{--- ①}$$

we know during cruise lift \approx weight

$$\therefore L = W = \frac{1}{2} \rho V^2 S C_L$$

$$\therefore C_L = \frac{2W}{\rho V^2 S}$$

so from Roskam eq. (3.42) we can substitute ① as

$$C_{L_{CR}} = \frac{(W_{TO} - 0.4W_F)}{1482 \times S \times M^2 \times S \times \rho_{H(\text{ftam})}}$$

⊙ from the previous design reports we have determined $W_{TO} = 5,28,961.811$

⊙ $W_F = 1,57,414 \text{ lbs}$ & we also estimated the grosswing Area

& aircraft maximum mach number

$$\therefore \begin{cases} S = 1433 \text{ ft}^2 \\ M = 0.84 \end{cases}$$

Now we can calculate $C_{L_{CR}}$

Figure 60: Cruise Coefficient of Lift Calculations

$$C_{L_{CR}} = \frac{(528961.8 - (0.4 \times 157414))}{1482 \times (0.84)^2 \times 1433 \times 0.2353}$$

$$= \frac{528961.8 - 62965.6}{1498486.95 \times 0.2353}$$

$$C_{L_{CR}} = \frac{1.321}{\cancel{0.94}}$$

Figure 61: Cruise Coefficient of Lift Calculations-II

- Sweep Angle: 31.6 degrees
- Thickness ratio: 0.139 (estimated using the supercritical air foil used for the wing section).

The hand calculations for selectin the optimum sweep angle is detailed below

Assuming $M_{cruise} = M_{div}$ & $M_{div} = 1.02 M_{cc}$

$$\frac{M_{cc}^2 \cos^2 \lambda}{\sqrt{1 - M_{cc}^2 \cos^2 \lambda}} \cdot \left[\left(\frac{\gamma+1}{2} \right) \cdot \frac{2.64 \times t/c}{\cos \lambda} + \left(\frac{\gamma+1}{2} \right) \cdot \frac{2.64 \times (t/c) \times (0.34 C_L)}{\cos^3 \lambda} \right] +$$

$$\frac{M_{cc}^2 \cos^2 \lambda}{1 - M_{cc}^2 \cos^2 \lambda} \cdot \left[\left(\frac{\gamma+1}{2} \right) \left[\frac{1.32 \cdot (t/c)^2}{\cos \lambda} \right] \right] +$$

$$M_{cc}^2 \cos^2 \lambda \left[1 + \left(\frac{\gamma+1}{2} \right) \cdot \frac{(0.68 C_L)}{\cos^2 \lambda} + \left(\frac{\gamma+1}{2} \right) \cdot \left(\frac{(0.34 C_L)^2}{\cos^4 \lambda} \right) \right] = 1$$

$\therefore M_{cruise} = 0.84$ FOR VER-12X

$\therefore M_{cruise} = M_{div} = 0.84$

$\therefore M_{div} = 1.02 M_{cc}$

$\rightarrow M_{cc} = \frac{M_{div}}{1.02}$

$M_{cc} = 0.82$

$$\frac{(0.82)^2 \cos^2 \lambda}{\sqrt{1 - (0.82)^2 \cos^2 \lambda}} \cdot \left[\frac{2.4}{2} \cdot \frac{2.64 \times t/c}{\cos \lambda} + \frac{2.4}{2} \cdot \frac{2.64 \times t/c \times 0.34 \times 1.32}{\cos^3 \lambda} \right] +$$

$$\frac{(0.82)^2 \cos^2 \lambda}{1 - (0.82)^2 \cos^2 \lambda} \cdot \left[\left(\frac{2.4}{2} \right) \left[\frac{1.32 \cdot (t/c)^2}{\cos \lambda} \right] \right] +$$

$$(0.82)^2 \cos^2 \lambda \left[1 + \left(\frac{2.4}{2} \right) \cdot \frac{0.68 \times 1.32}{\cos^2 \lambda} + \left(\frac{2.4}{2} \right) \cdot \frac{(0.34)^2 \times (1.32)}{\cos^4 \lambda} \right] = 1$$

Figure 62: Sweep Angle and Thickness Ratio Calculations-I

$$\left[\frac{0.67}{\sqrt{1-0.67\cos^2\lambda}} \left[\frac{3.168}{\cos\lambda} + \frac{1.42 t/c}{\cos^2\lambda} \right] + \frac{0.67\cos^2\lambda}{1-0.67\cos^2\lambda} \times \frac{1.584(t/c)^2}{\cos\lambda} \right] +$$

$$(0.67)\cos^2\lambda \left[1 + \frac{1.077}{\cos^2\lambda} \right] + \frac{0.24}{\cos^4\lambda} = 1$$

$$\frac{2.122}{\cos\lambda \sqrt{1-0.67\cos^2\lambda}} + \frac{0.9514 t/c}{\cos^2\lambda \cdot \sqrt{1-0.67\cos^2\lambda}} + \frac{1.061\cos^2\lambda \cdot (t/c)^2}{\cos\lambda(1-0.67\cos^2\lambda)}$$

$$+ 0.67\cos^2\lambda + 0.722 + \frac{0.24}{\cos^4\lambda} = 1$$

$$= 0.278$$

$$\frac{7.633}{\cos\lambda \cdot \sqrt{1-0.67\cos^2\lambda}} + \frac{3.42 t/c}{\cos^2\lambda \sqrt{1-0.67\cos^2\lambda}} + \frac{3.81\cos\lambda (t/c)^2}{(1-0.67\cos^2\lambda)} + \frac{2.41}{\cos^2\lambda} + \frac{0.863}{\cos^4\lambda} = 1$$

$$\frac{1}{\cos\lambda \sqrt{1-0.67\cos^2\lambda}} \left[7.633 + \frac{3.42 t/c}{\cos^2\lambda} \right] + \frac{3.81\cos\lambda \cdot (t/c)^2}{1-0.67\cos^2\lambda} + \frac{2.41}{\cos^2\lambda} + \frac{0.863}{\cos^4\lambda} = 1$$

Figure 63: Sweep Angle and Thickness Ratio Calculations-II

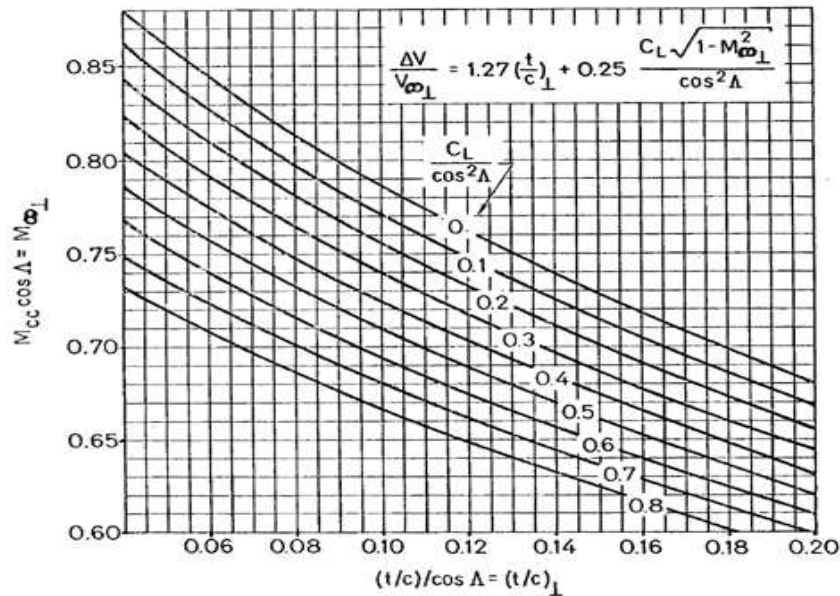
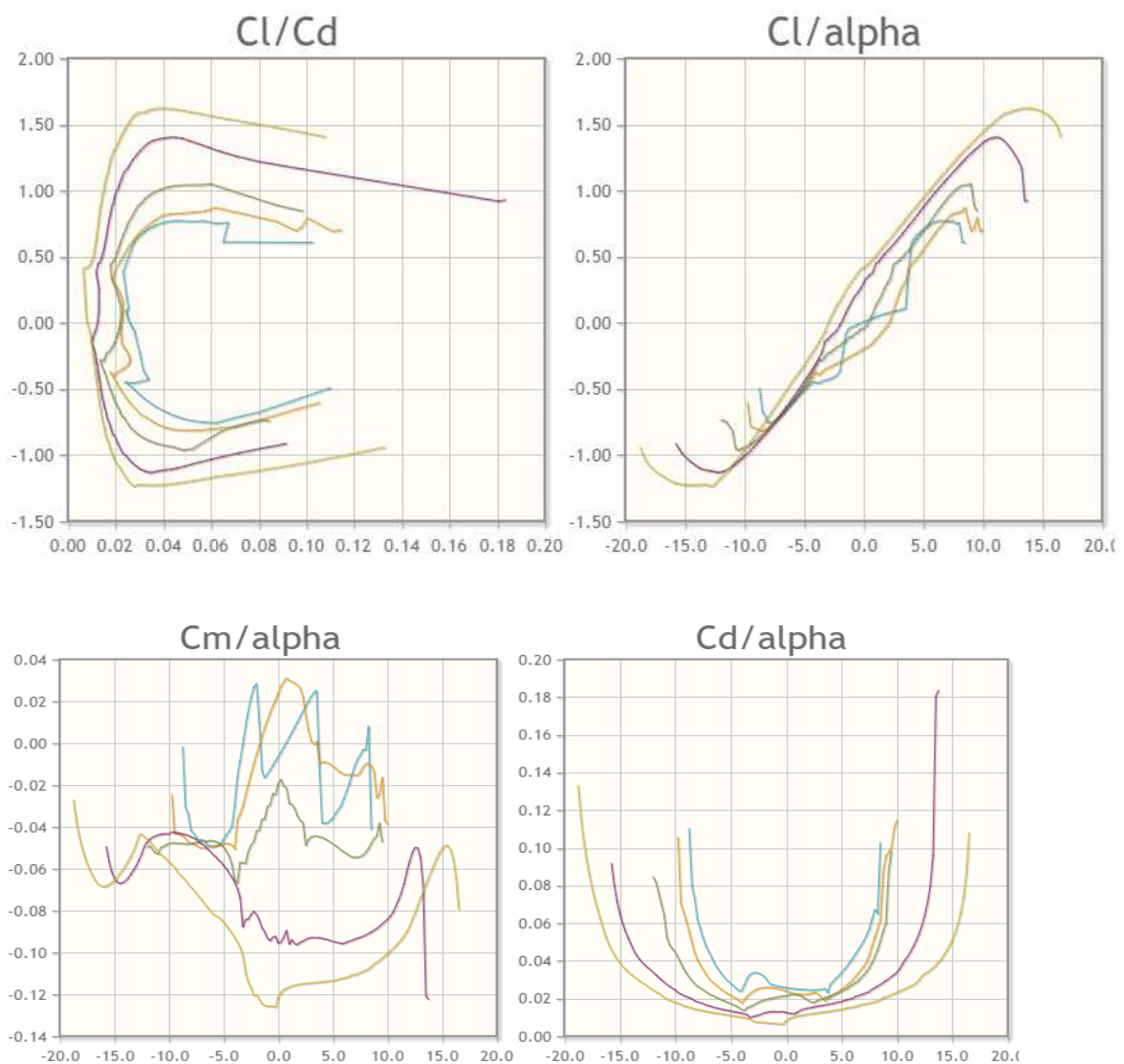
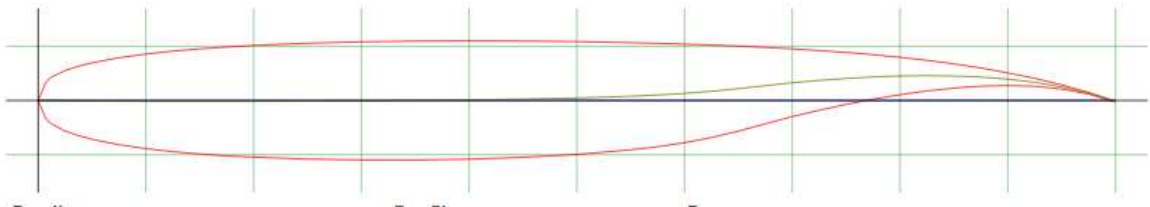


Figure 64: Sweep Angle and Thickness Ratio - Practical Data

6.2 AIR FOIL SELECTION:

For VER-12XX a super critical air foil section will used for the wings. The air foil below is from Raymer and it belongs to SC (2)-0714 series.



The above graphical representation of C_l versus α (angle of attack) we can see this air foil can produce a C_l of 1.50 and the lift drops off abruptly when it reaches a critical angle

of attack. These air foils are effective in increasing the critical angle of attack which means the stall speed of aircraft is relatively less when compared with conventional aircraft. In the above graph, a representation between coefficient of moments and angle of attack is also given.

Selection of an air foil is a critical point in aircraft design process as it determines the flow properties over the aircraft especially the wings. The evolution of air foils has been an advantage for designing subsonic aircraft closer to Mach 1. Some of the key aspects of wing like thickness ratio and taper ratio are very useful because if these parameters vary the overall aerodynamic characteristics of the wing significantly changes. Supercritical air foils are effective in reducing the wave drag produced by the wings especially in the transonic range because of their flattened upper surface. It is most widely in Airbus-350, Boeing-777X aircraft which contributed in increasing the overall lift resulting in the increased overall range for these aircraft.

6.2 WING DESIGN EVALUATION AND DESIGN OF HIGH-LIFT DEVICES:

The wing section is evaluated using the AAA program and the evaluated values are used while calculating the high lift devices.

Manual calculation is shown below and the procedure used is from Roskam

⊗ Pressure at particular height is calculated from the below formula:

$$\frac{P}{P_0} = (1 - 2.2558 \times 10^{-5} h)^{5.25864}$$

P_0 at 11000 feet meters

$$\Rightarrow \frac{P}{P_0} = (1 - 2.2558 \times 10^{-5} \cdot 11000)^{5.25864}$$

$$\Rightarrow \boxed{P = 22613 \text{ Pascals}}_{11000 \text{ meters}}$$

$$\boxed{T = T_0 - 0.0065 \times h}$$

$$= 288.15 - 0.0065 \times 11000$$

$$\therefore \boxed{T = 216.65 \text{ Kelvin}}$$

→ Density at 11000 meters

we know $P = \rho R T$

$$\Rightarrow \frac{P}{R T} = \rho$$

$$\Rightarrow \rho = \frac{22613}{(287.05) \times (216.65)}$$

$$\boxed{\rho_{11000 \text{ meters}} = 0.3636 \text{ kg/m}^3}$$

at 11000 meters the dynamic viscosity of air = $0.03455 \text{ lbm/ft} \cdot \text{s}$
 Density of air = 0.10189 lbm/ft^3

★ ★

Figure 65: Pressure, Temperature and Density calculations

$$\therefore \text{Reynolds number at wing root } R_{n_{gr}} = \frac{\rho_{11000} V_{11000} C_{gr}}{\mu}$$

$$= \frac{0.10189 \times 482 \text{ knots} \times 38.99 \text{ ft}}{0.034551 \text{ lbm/ft}\cdot\text{h}}$$

$$= \frac{0.10189 \times 813.524 \text{ ft/sec} \times 38.99 \text{ ft} \times 60 \times 60 \text{ sec}}{0.034551 \text{ lbm/ft}}$$

$$\therefore R_{n_{gr}} = 332423503.4$$

$$\boxed{R_{n_{gr}} = 33.24 \times 10^8}$$

$$\therefore \text{Reynolds number at wing tip } R_{n_t} = \frac{\rho_{11000} \times V_{11000} \times C_t}{\mu}$$

$$= \frac{0.10189 \frac{\text{lbm}}{\text{ft}^3} \times 813.524 \frac{\text{ft}}{\text{sec}} \times 5.74 \text{ ft} \times 60 \times 60 \text{ sec}}{0.034551 \text{ lbm/ft}}$$

$$R_{n_t} = 49574198.75$$

$$\therefore \boxed{R_{n_t} = 49.5 \times 10^8}$$

Since Rockam provides data only for lower Reynolds numbers & for the purpose of calculating C_{wing} we are estimating

Figure 66: Reynolds Number calculations

$C_{L_{max_{root}}}$ & $C_{L_{max_{tip}}}$

$$\therefore C_{L_{max_{root}}} \rightarrow 2.0$$

$$\therefore C_{L_{max_{tip}}} \rightarrow 1.8$$

$$\begin{aligned} \therefore C_{L_{max_{wing}}} &= K_1 \left[\frac{C_{L_{max_{root}}} + C_{L_{max_{tip}}}}{2} \right] \\ &= 0.98 \left[\frac{2.0 + 1.8}{2} \right] \end{aligned}$$

$$\boxed{\therefore C_{L_{max_{wing}}} = 1.862}$$

\therefore since this aircraft uses a sweep angle of 28.4° therefore for the correction of the sweep angle we will be using \cos -rule

$$C_{L_{max_{unswept}}} = \frac{C_{L_{max_{wing}}}}{\cos A_{sweep}}$$

$$\Rightarrow \cos A_{sweep} \times C_{L_{max_{unswept}}} = C_{L_{max_{wing_{swept}}}}$$

$$\Rightarrow (1.862) \times \cos(28.4) = C_{L_{max_{wing_{swept}}}}$$

$$\Rightarrow \boxed{C_{L_{max_{wing_{swept}}} = 1.638}$$

Figure 67: Coefficient of lift for Wing Calculations

Since VER-12X is a relatively long coupled aircraft

$$\therefore C_{L_{max_{wing}}} = 1.1 C_{L_{max}}$$

$$\Rightarrow C_{L_{max}} = \frac{C_{L_{max_{wing}}}}{1.1}$$

$$= \frac{1.638}{1.1}$$

$$\boxed{C_{L_{max}} = 1.49}$$

⊕ Incremental values of maximum lift coefficient needed to be produced by the high lift devices

Takeoff: $\Delta C_{L_{max_{TD}}} = 1.05 (C_{L_{max_{TD}}} - C_{L_{max}})$
 $= (1.05) [2.42 - 1.49]$

$$\boxed{\Delta C_{L_{max_{TD}}} = 0.9765}$$

Landing: $\Delta C_{L_{max_L}} = 1.05 (C_{L_{max_L}} - C_{L_{max}})$
 $= 1.05 [2.8 - 1.49]$

$$\boxed{\Delta C_{L_L} = 1.3755}$$

Figure 68: High-lift devices coefficient of lift calculations

for landing

$$\eta \frac{S}{S_w} = 0.6$$

$$\begin{aligned} \Delta C_{l_{max}} &= \Delta C_{l_{max_L}} \times \left(\frac{S}{S_w}\right) \times k_L \\ &= 1.3755 \times (0.6) \times 0.852 \end{aligned}$$

$$\Delta C_{l_{max}} = 0.703$$

for landing

$$\eta \frac{S}{S_w} = 0.8$$

$$\begin{aligned} \Delta C_{l_{max}} &= \Delta C_{l_{max_L}} \times \left(\frac{S}{S_w}\right) \times k_L \\ \Delta C_{l_{max}} &= 1.3755 \times (0.8) \times 0.852 \end{aligned}$$

$$\therefore \Delta C_{l_{max}} = 0.9375$$

Consider the case of take-off:

$$\Delta C_l = \left(\frac{1}{k}\right) \Delta C_{l_{max}}$$

$$\eta \frac{S}{S_w} = 0.6$$

$$\Delta C_l = \frac{1}{k} \times \Delta C_{l_{max_{to}}}$$

$$\Delta C_l = \frac{1}{k} \times 0.5$$

assuming $k = 0.94$

$$\Delta C_l = 0.532$$

for take-off

$$\eta \frac{S}{S_w} = 0.8$$

$$\Delta C_l = \frac{1}{k} \times \Delta C_{l_{max_{to}}}$$

$$\Delta C_l = \frac{1}{k} \times 0.66$$

$$\Delta C_l = \frac{0.66}{k}$$

assuming $k = 0.94$

$$\Delta C_l = 0.702$$

considering the case of landing

$$\Delta C_l = \left(\frac{1}{k}\right) \Delta C_{l_{max}}$$

$$\eta \frac{S}{S_w} = 0.6$$

$$\Delta C_l = \left(\frac{1}{0.94}\right) \times 0.703$$

$$\Delta C_l = 0.747$$

considering the case of

landing

$$\eta \frac{S}{S_w} = 0.8$$

$$\Delta C_l = \left(\frac{1}{0.94}\right) \times 0.9375$$

$$\Delta C_l = 0.997$$

Figure 70: High-lift device calculations -II

⊙ Fowler flap will be used for this aircraft.

An estimated guess of max 30° is taken for flaps deflection angle

$$\delta_{f_{T0}}^p = 5-20^\circ \text{ degrees}; \quad \delta_{f_L}^p = 30^\circ \text{ degrees} \quad \text{and } c_{f/c} = 0.39$$

Take off:

$$C_{d_{f}} = \frac{C_{l_{\alpha}}}{\alpha} (1 + c_{f/c}) \quad \begin{array}{l} \text{unflapped section lift curve slope} \\ \text{approximated to } 2\pi \end{array}$$

$$= (2\pi) (1 + 0.39)$$

$$\boxed{C_{d_{f}} = 8.733}$$

⊙ Assuming that the flaps own from the fuselage we estimate

$$\eta_f = 0.11, \quad \eta_o = 1.0$$

$$S_w/S = \frac{(\eta_o - \eta_f) \{ 2 - (1-\lambda)(\eta_f + \eta_o) \}}{1+\lambda}$$

$$= \frac{(1.0 - 0.11) \{ 2 - (1-0.149)(1.1) \}}{(1 + 0.149)}$$

$$= (0.774) (1.0554)$$

$$\boxed{S_w/S = 0.816}$$

Figure 71: High-lift device calculations -III

6.3 DESIGN OF THE LATERAL CONTROL SURFACES:

The design of the lateral control surfaces is a vital step in the design process as they are responsible for the lateral stability of the aircraft. For this VER-12XX wing will be accommodated with the leading-edge devices and for additional landing control spoilers will also be fitted. The compliance of these devices must be cross checked so that they perform the intended requirement. Ailerons are the primary flight control devices that provide lateral control for the aircraft and to some extent spoilers. The design of lateral control surfaces is shown in figure 73, 74. For VER-12X, hydraulic power mechanism that actuates the ailerons will be studied in further chapters rather than conventional push-pull pulley system.

6.4 WING PARAMETERS AND AAA DRAWINGS:

Table 12: Estimated Wing Parameters

Wing Parameters	
Wing Area	3982 ft²
Wing Span	646 ft²
Taper Ratio	0.149 (value is estimated from 737-MAX Aircraft)
Aspect Ratio	9.61
Dihedral Angle	6° (estimated from Boeing 737-MAX Aircraft Technical Data)
Sweep Angle	35 degrees (average of all the supercritical air foils with a cruise Mach between 0.79-0.84)
Thickness Ratio	0.139 (value is from the data of supercritical air foil SC (2)-0714 series)
Wing Type/ Wing Fuselage attachment	Cantilever Low wing
Root Chord	350 in
Tip Chord	110 in

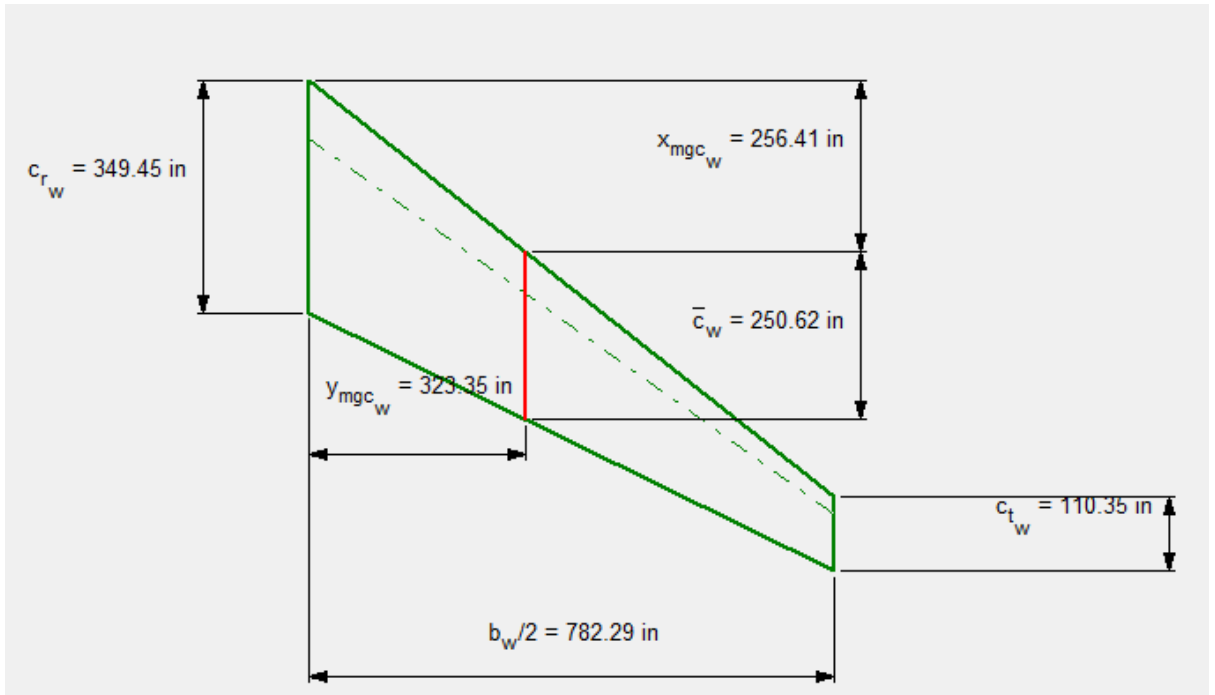


Figure 72: Wing Planform for VER-12XX using AAA program

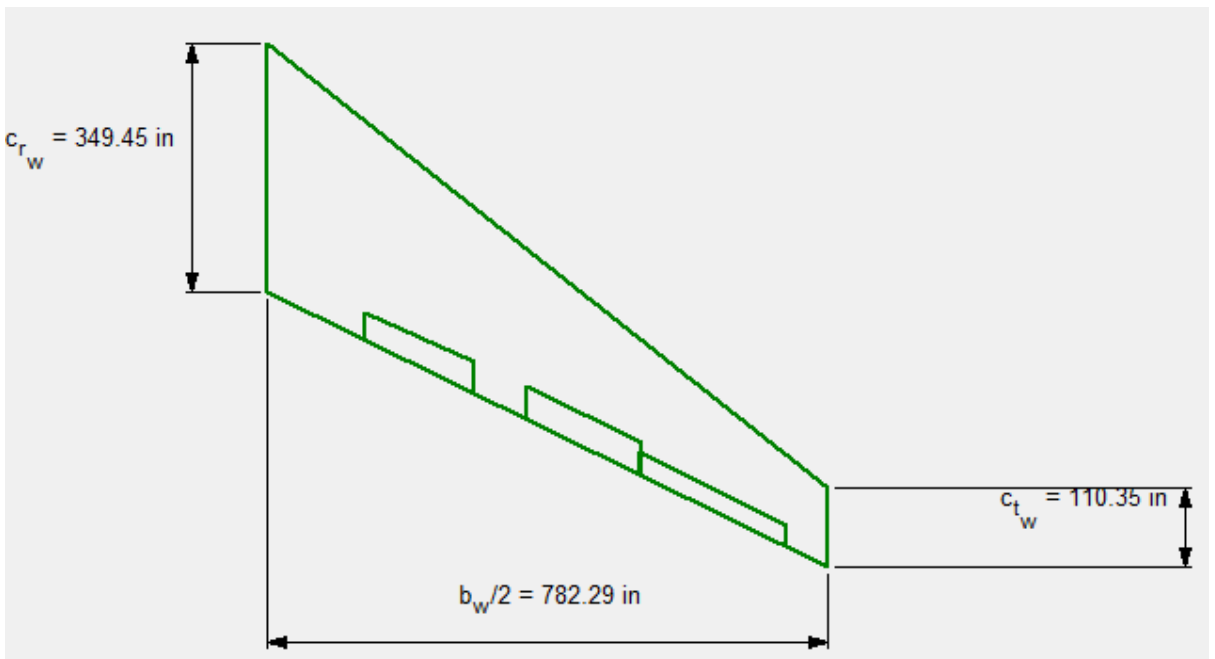


Figure 73: Wing Planform for VER-12XX showing Spoilers using AAA program

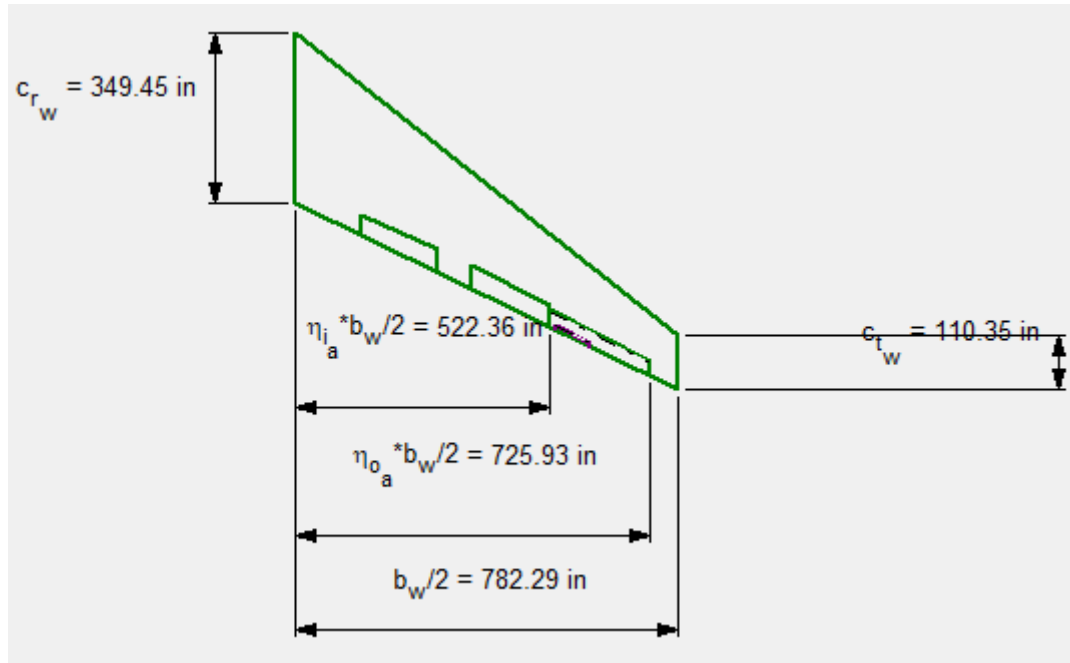


Figure 74: Wing Planform for VER-12XX showing Ailerons using AAA program

6.5 DISCUSSION:

Aircraft wing depends on many parameters and they directly affect their geometry and effecting the overall lift. In the above calculations, the procedure used for calculating weight of aircraft wing is not precise as the methods provided in Roskam are limited and are not updated to meet the standards of the current subsonic wing structures. A trade off study between sweep angle and thickness ratio is provided to select the optimum sweep angle which in this is case is an important factor. Coefficient of lift calculations for the high lift devices are determined based on guess values of S_w / S which may result in the appropriate positioning of these devices.

CHAPTER 7

Design of the Empennage and the Longitudinal and Directional Controls

The vertical stabilizer along with the horizontal together are responsible for the lateral and longitudinal stability of the aircraft. Aircraft wings can generate lift and any destabilizing moments produced by these configurations or by any other configurations must be nullified so that the aircraft attains its equilibrium. The position of the empennage on the fuselage is important as it decides the overall size and stability of the aircraft. In this chapter, a brief description on the selected empennage configuration, evaluation of certain design parameters of the horizontal and vertical stabilizer will be analysed. Finally, an analysis on the selected overall empennage configuration will be provided by cross checking the design with the AAA program.

7.1. OVERALL EMPENNAGE DESIGN

VER-12XX share the same fuselage and wing characteristics alongside the present long-range commercial aircraft. To reduce the drag, the aircraft uses supercritical wing structures and blended wing which reduces drag and therefore improving the aircraft efficiency by 20% without the need to go for a relatively large vertical stabilizer. Usually to compensate the amount of drag produced by the fuselage; vertical stabilizer length is increased which also enhances directional and longitudinal stability. VER-12XX uses conventional aft tail and one aft vertical tail. This basic conventional design is used to increase the longitudinal and directional trim stabilities.

7.1.1 EMPENNAGE DISPOSITION CALCULATIONS:

The determination of empennage disposition is a key factor as it gives the designer a complete picture on their location and to an extent their aerodynamics. In this section, manual calculations related to empennage location, volume coefficients and surface areas of respective empennage components (i.e. horizontal and vertical tail) will be presented using the procedure from Roskam text book.

→ To keep the airplane weight & drag down as much as possible it is obviously desirable to keep the empennage area as small as possible.

a) Conventional Configuration :



The tail Volume coefficients are given as:
(using the V method)

$$\bar{V}_h = X_h S_h / S C \quad , \quad \bar{V}_v = \frac{X_v S_v}{S b}$$

⊕ Vertical tail sizes are often dictated by the engine-out condition (ie V_{mc})

$$V_{mc} = 1.2 V_S$$

where V_S = lowest stall speed usually taken as landing stall speed.

⊕ from the drawing of Boeing 777-300ER, Airbus 350-900 & now estimating

⊕ Moment arm for the vertical stabilizer (X_v) = 33.3 m = 109.25 ft

⊕ Moment arm for the horizontal stabilizer (X_h) = 32.63 m = 107 feet

Figure 75: Empennage Disposition Calculations-I

for the horizontal stabilizer let us assume the Volume Coefficients & Area

$$\bar{V}_h = 0.8$$

$$\bar{S}_h = 1600 \text{ feet}^2$$

for the vertical stabilizer let us assume the Volume Coefficients to be & Area

$$\bar{V}_v = 0.083$$

$$\bar{S}_v = 1000 \text{ feet}^2$$

or now we can estimate ^{compare the} of the wing area by calculation & determine the correct values for the wing area.

from eq's (8.1) & (8.2) for S_w

$$\bar{V}_h = X_h S_h / S_w$$

$$\Rightarrow S_h = \frac{\bar{V}_h \times S_w \bar{C}}{X_h \times}$$

$$= \frac{(0.8) \times (4700) \times 0.8 \times (b/c)}{107.25}$$

$$= \frac{4700 \times 0.8 \times \left(\frac{212.6}{9.61}\right)}{107}$$

$$S_h = 777.4 \text{ feet}^2$$

for vertical stabilizer

$$S_v = \frac{\bar{V}_v \cdot S_w}{X_v}$$

$$= \frac{(0.083) \times (4700) (212.6)}{109.25}$$

$$S_v = 760 \text{ feet}^2$$

Figure 76: Empennage Disposition Calculations-II

7.2. DESIGN OF THE HORIZONTAL STABILIZER

The following parameters of the horizontal stabilizer are estimated from Roskam tables 8.13 and 8.14. For purpose of initial sizing of horizontal stabilizer all the highest values in the range specified are considered.

- Aspect ratio – 6.1
- Taper ratio – 0.63
- Sweep angle – 28.4 degrees
- Thickness ratio – 0.3 (estimated from Roskam Table 8.7)
- Air foil(s) – NACA 009 (Symmetric)
- Incidence angle - Variable
- Dihedral angle – 11 degrees

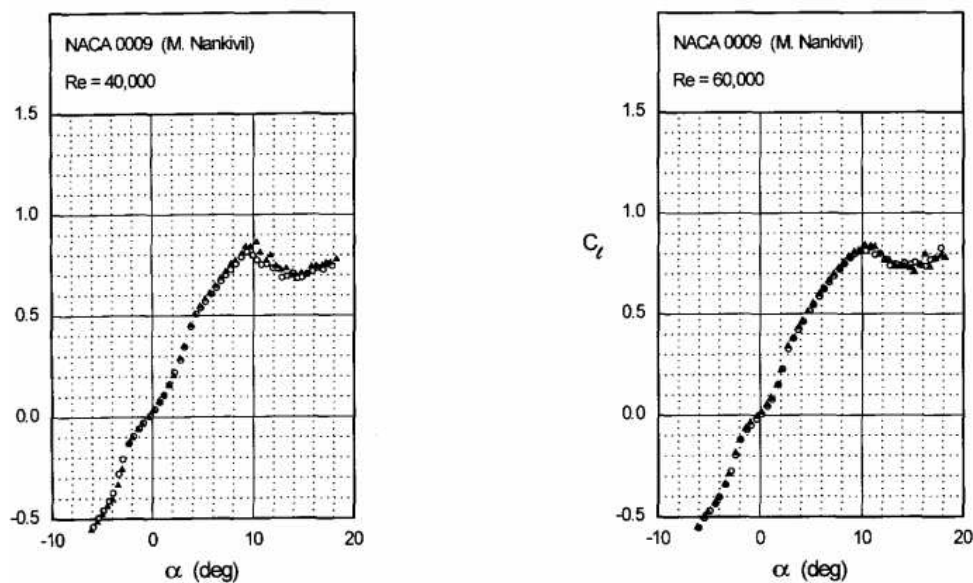


Figure 77: C_L versus Angle of Attack at Reynolds Number

The above graphical representation details NACA 009 air foils at different Reynolds numbers.

7.3. DESIGN OF THE VERTICAL STABILIZER

The following parameters of the horizontal stabilizer are estimated from Roskam tables 8.13 and 8.14. For purpose of initial sizing of horizontal stabilizer all the highest values corresponding to the parameters are considered.

- Aspect ratio – 2.0
- Taper ratio – 0.73
- Sweep angle – 53 degrees
- Thickness ratio – 0.33(estimated from Roskam Table 8.7)

- Air foil – NACA 009 (Symmetric)
- Incidence angle – 0 degrees
- Dihedral angle – 90 degrees

7.4 EMPENNAGE DESIGN EVALUATION

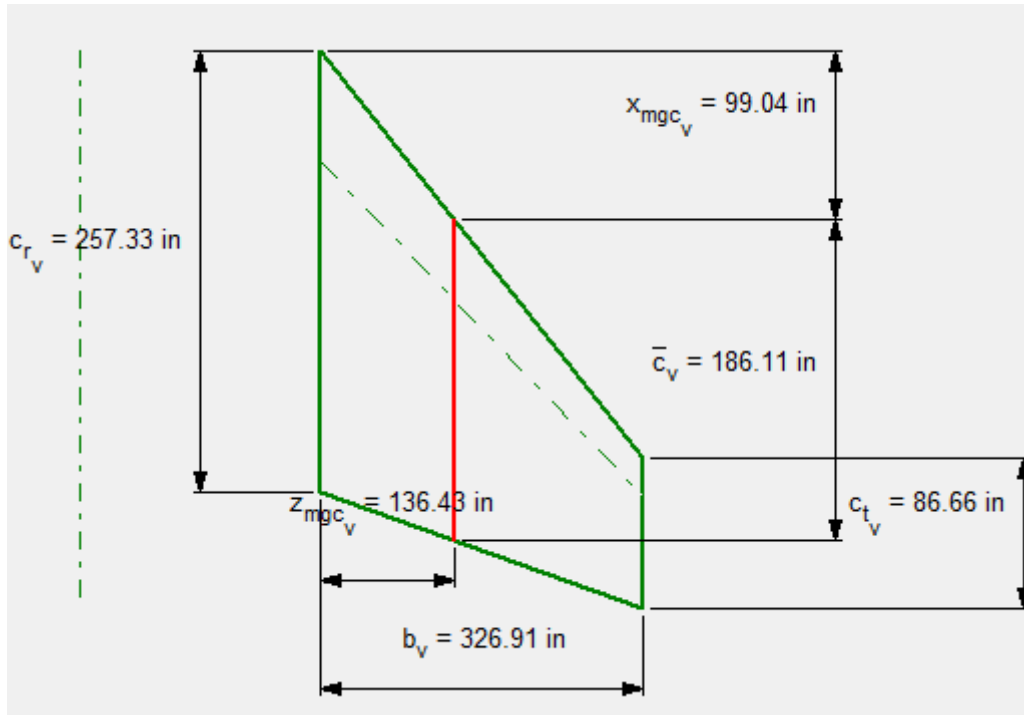


Figure 78: Vertical Stabilizer Planform -AAA

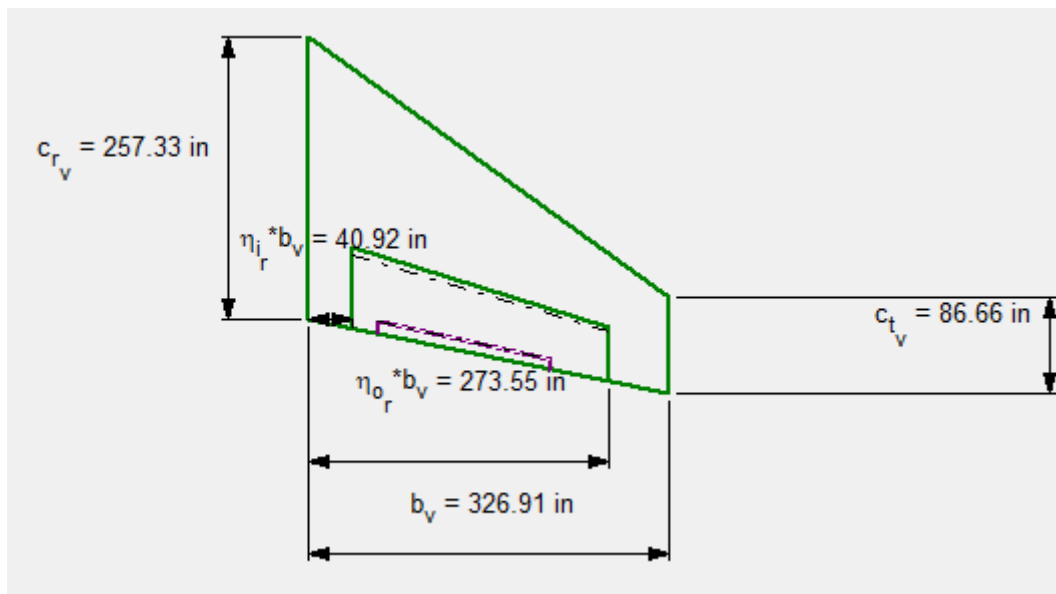


Figure 79: Vertical Stabilizer with Ridder Tabs -AAA

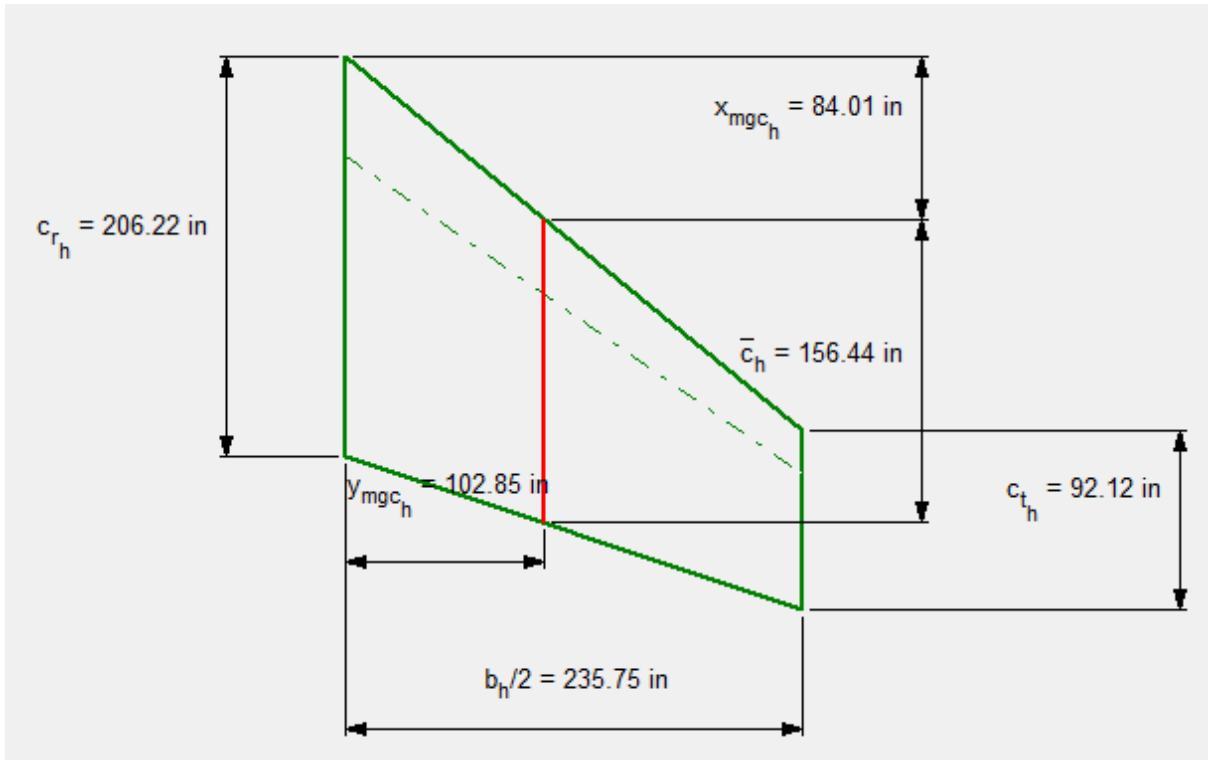


Figure 80: Horizontal Stabilizer Planform -AAA

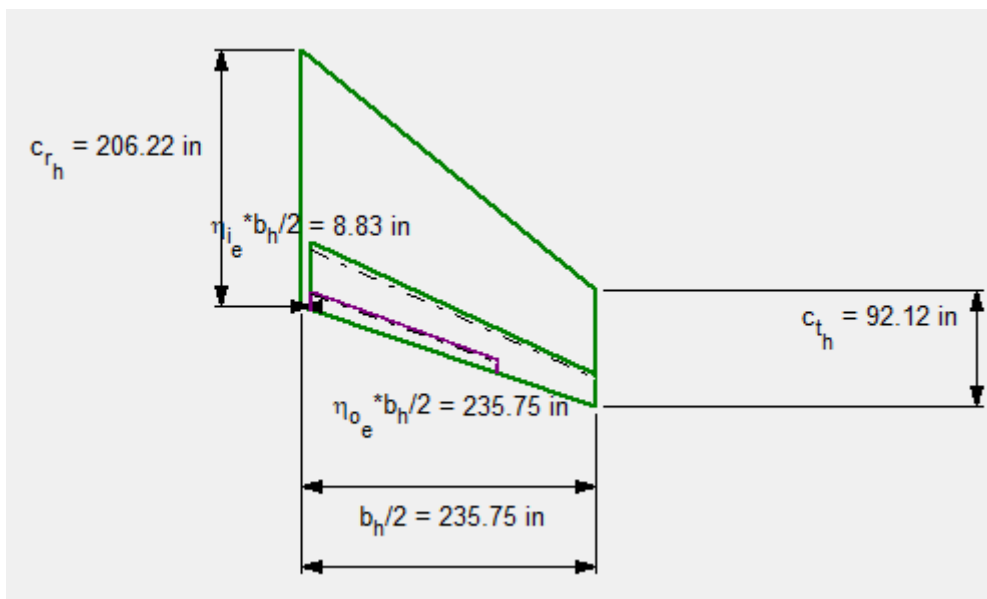


Figure 81: Horizontal Stabilizer Trim Tabs -AAA

7.5 DESIGN OF THE LONGITUDINAL AND DIRECTIONAL CONTROLS

Outboard Aileron Span – 0.736

Outboard Aileron Chord – 0.647

Inboard Spoiler Span – 0.68

Inboard Spoiler Chord – 0.75

Inboard Spoiler Hinge Loc in/out – 0.71

Outboard Spoiler Span Loc in/out – none

Outboard Spoiler Chord in/out – none

Outboard Spoiler Hinge Loc in/out – none

7.6 DISCUSSION:

The empennage for an aircraft is vital for the lateral stability and their positioning determines the manoeuvrability. From the above calculations and analysis, the surface areas of horizontal and vertical are determined basing on the approximations of their respective volume coefficients which are close to VER-12XX. Roskam text book provides an in-depth analysis for the empennage selection and their database is completely based on 20th century technology forcing the author to use the values higher than those suggested in the book. Though the analysis on the empennage structure is made few difficulties have been faced to determine their location with respect to the fuselage interims of their exact position and on root and tip air foil selection.

CHAPTER 8

LANDING GEAR DESIGN, WEIGHT AND BALANCE ANALYSIS

From the previous design reports a clear idea on the empennage configurations, wing and the preliminary aircraft sizing has been obtained. They are the vital aspects of the aircraft design analysis through which most of the key design parameters are locked. There has been a considerable issue related to stability of the aircraft especially for a jet transport whose primary payload is passengers. It is important that apart from the aerodynamics; passenger comfort do play a pivotal role. Since aircraft is a highly coupled stable system it is the nature of a stable system to even out any disturbances (i.e. gusts, manoeuvring). Landing gear absorbs all the landing loads during and the pneumatic struts assembly provides a cushioning effect. Landing disposition effects the manoeuvrability of the aircraft while steering on the ground or while taxiing. In this report, a detailed analysis on the VER-12XX landing gear configuration, number of tires and a complete weight and balance including the centre of gravity calculations will be determined.

8.1 ESTIMATION OF THE CENTER OF GRAVITY LOCATION FOR THE AIRPLANE

Before proceeding into the landing gear disposition analysis, it is important to have a rough idea on the overall centre of gravity of the proposed aircraft. At this point in this section an estimate of the location of centre of gravities of aircraft major components are first defined. Furthermore, in the next sections a detailed analysis on the COG calculations are discussed.

Table 13: Centre of Gravity Assumptions from Roskam

Component	Centre of gravity Assumptions
Wings	Estimated to be 0.42* wing chord length
Empennage	Horizontal Stabilizer: estimated to be 0.30* horizontal stabilizer chord length Vertical Stabilizer: estimated to be 0.30* vertical stabilizer chord length
Nacelles	Estimated to be 0.40 * overall length of the engines
Fuselage	Estimated to be 0.39* overall approximated length of the fuselage

Below is a break down structure on the respective component weights, x, y, z axis locations and the format is from 'Roskam chapter 10 part-II.

Table 10.1b Class I Weight and Balance Calculation
 =====

No.	Type of Component	W_i	x_i	$W_i x_i$	Y_i	$W_i Y_i$	z_i	$W_i z_i$
		lbs	in.	inlbs	in.	inlbs	in.	inlbs
1.	Fuselage group	W_1	x_1	$W_1 x_1$	Y_1	$W_1 Y_1$	z_1	$W_1 z_1$
2.	Wing group							
3.	Empennage group							
4.	Engine group							
5.	Landing gear group							
6.	Fixed equipm't group							
Empty weight: $W_E = \sum_{i=1}^{i=6} W_i$						$x_{cg_{W_E}} = (\sum_{i=1}^{i=6} W_i x_i) / W_E$		
7.	Trapped fuel and oil							
8.	Crew							
Operating weight empty: $W_{OE} = \sum_{i=1}^{i=8} W_i$						$x_{cg_{W_{OE}}} = (\sum_{i=1}^{i=8} W_i x_i) / W_{OE}$		
9.	Fuel							
10.	Passengers							
11.	Baggage							
12.	Cargo							
13.	Military load							
Take-off weight: $W_{TO} = \sum_{i=1}^{i=13} W_i$						$x_{cg_{W_{TO}}} = (\sum_{i=1}^{i=13} W_i x_i) / W_{TO}$		

Note: Locations for y_{cg} and for z_{cg} are found from similar equations.

Figure 82: Class-I: Component wise weight and centre of gravity breakdown structure

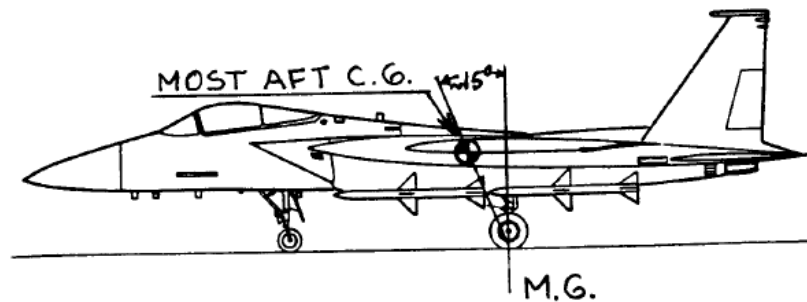
8.2 LANDING GEAR DESIGN

Since VER-12XX is transport jet; the landing gear for this aircraft cannot be of fixed configuration because of the enormous drag penalties they incur during the flight. The conventional retractable tricycle landing gear configuration will be used for VER-12XX to maximise on the lift produced by wing during its flight. Positioning of nose and the main wheels decided the balance and manoeuvrability of the aircraft especially when on ground. Placing the landing gear beyond the designed limits can make the entire aircraft design invalid.

After making the necessary estimations from the weight and balance data we must next proceed towards the most important parameter that is associated with the landing gear disposition i.e. the geometric criteria. There are two factors included in the geometric criteria which helps in finding the length of the **struts** and they are

- **Tip over criteria:** It is noted that in the case of tricycle landing gear and for the aircraft to maintain its longitudinal stability it is necessary that the main landing

gear must be behind the aft c.g. and maintain 15-degree angle from c.g. to the main gear.



Longitudinal Tip-over Criterion for Tricycle Gears

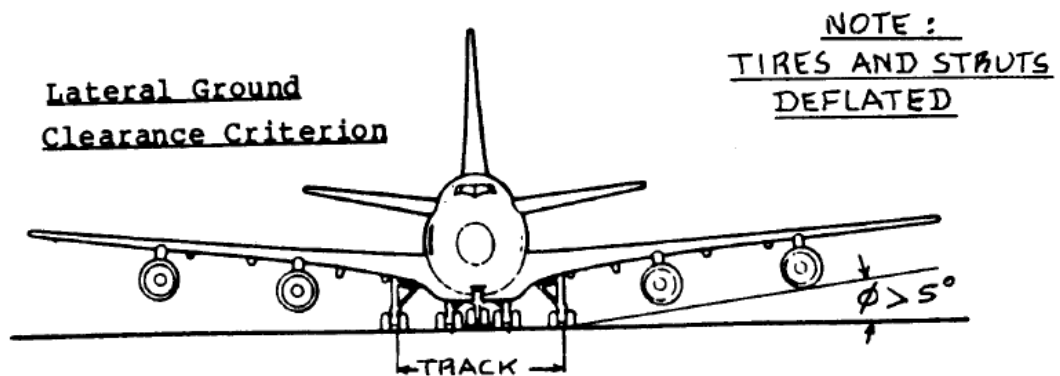


Figure 83: Tip over criteria Definition

- **Ground Clearance criteria:** The lateral ground clearance angle applies to both tricycle and tail dragger but the longitudinal ground clearance can only be applied to tricycle landing gear.

Having mentioned all the important design considerations, we can now decide on the following; bearing in mind the geometric criterion.

- ✓ Number, type and size of tires.
- ✓ Length and diameter of the struts.
- ✓ Preliminary arrangement.

The maximum static loading on each strut of the landing gear are determined below. For this purpose, the following Class-I equations will be used and these are the best match for tricycle landing gear.

Nose wheel strut: $P_n = (W_{TO} l_m) / (l_m + l_n)$

Main gear strut: $P_m = (W_{TO} l_n) / n_s (l_m + l_n)$

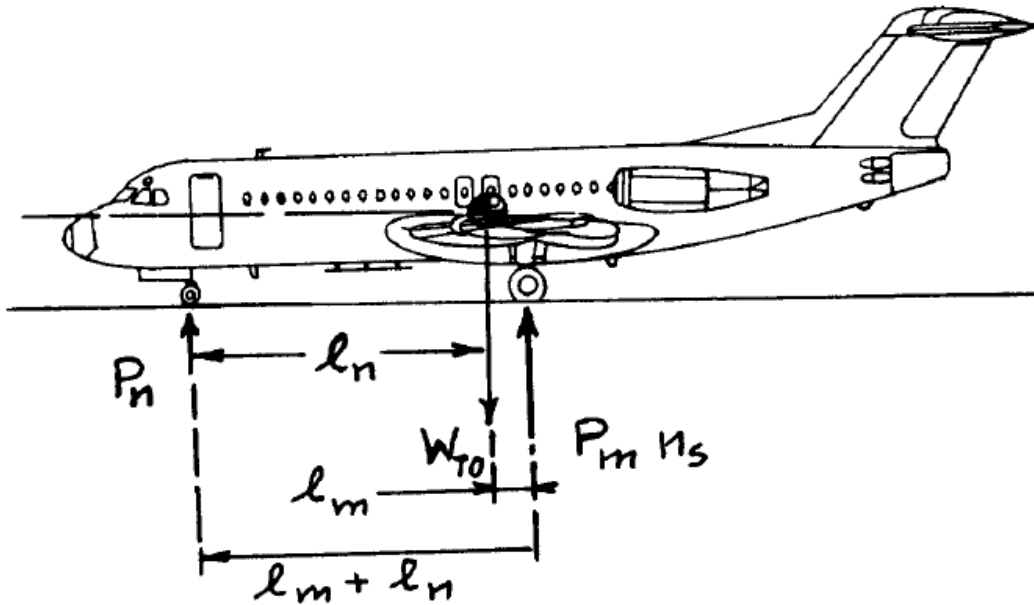


Figure 84: Aircraft Landing Gear Definitions - 'Roskam: Airplane Design Part VIII'

Table 14: VER-12XX Landing Gear Parameters

Landing Gear Configuration	Tricycle
Number of Tires	Nose Wheel – 2 Main Gear – 4 in Tandem
L_m (Distance to the main gear from AC C.G.)	-13 m (511 in)
L_n (Distance to the AC C.G. from nose gear)	21 m (827 in)
Static Loading on Nose wheel	71952 Psi
Static Loading on Main wheel	116447 Psi
Location of the Landing Gear	Nose Wheel – on the fuselage Main Gear – attached under the wing
Tip over angle	82° (Estimated by comparing all the Narrow-Body Aircraft)
Turning Radius	20° (An estimate from Boeing Technical Manuals)

8.3 WEIGHT AND BALANCE

For the weight and balance analysis firstly manual calculations have been performed using the procedure from Roskam and the determined values are carefully documented in Microsoft Excel. In the previous sections the class1 weight and balance table is already detailed which is now used for determining the respective component x, y, z locations and their centre of gravities in the x, y, z directions.

The following table details the location, enter of gravity of major aircraft components in the x-direction.

Table 15: Centre of Gravity Manual Calculations in X-Direction

Component	X_cg (operating take-off weight) (lbs)	X_cg (operating empty weight) (lbs)
Fuselage	217	33
Wing	4	1
Empennage	6	1
Landing Gear	48	7
Nacelle	90	14
Structure	1228	187
Power plant	749	114
Fixed Equipment	20285	3083
Empty Weight	2119	322

The following table details the location, enter of gravity of major aircraft components in the y-direction

Table 16: Centre of gravity calculation in Y-direction

Component	Op Component Weight	y	Wy	Y_cg (operating take-off weight)	Y_cg (operating empty weight)
Fuselage	16664	0	0	0	0
Wing	18743	0	0	0	0
Empennage	3938	0	0	0	0
Landing Gear	6973	0	0	0	0
Nacelle	2666	0	0	0	0
Structure	48983	0	0	0	0
Power plant	13478	0	0	0	0
Fixed Equipment	22085	0	0	0	0
Empty Weight	84546	0	0	0	0

The following table details the location, center of gravity of major aircraft components in the z-direction

Table 17: Centre of gravity calculation in Z-direction

Component	Op Component Weight	z	Wz	Z_cg (operating take-off weight)
Fuselage	16664	1025	17080600	31
Wing	18743	1000	18742600	34
Empennage	3938	1157	4556266	8
Landing Gear	6973	860	5996436	11
Nacelle	2666	910	2426242	4
Structure	48983	996	48787466.4	88
Power plant	13478	910	12265162	22
Fixed Equipment	22085	900	19876230	36
Empty Weight	84546	958	80995355.4	146

- Component weight breakdown:

In this section, the AAA program is used for determining the centre of gravity in x, y, z directions using pre-determined empty weight fractions.

AAA Program:

Component Weight Table				
Component	F_w	$W_{estimate}$ lb	ΔW lb	Weight lb
Fuselage	0.094	15115.2	-303.1	14812.1
Wing	0.113	18170.4	-364.3	17806.1
Empennage	0.026	4180.8	-83.8	4097.0
Landing Gear	0.040	6432.0	-129.0	6303.0
Nacelle	0.022	3537.6	-70.9	3466.7
Structure	0.294	47436.0	-951.2	46484.8
Powerplant	0.078	12542.4	-251.5	12290.9
Fixed Equipment	0.122	19617.6	-393.4	19224.2
Empty Weight	0.494	79596.0	-1596.0	78000.0

Figure 85: Components Weight Table -AAA

VER-12XX Loading Table:

Empty Weight Table				
Component	Weight lb	X _{cg} in	Y _{cg} in	Z _{cg} in
Fuselage Group	14812.1	872.00	0.00	213.00
Wing Group	17806.1	995.00	0.00	199.00
Empennage Group	4097.0	1655.00	0.00	310.00
Landing Gear Group	6303.0	935.00	0.00	150.00
Nacelle Group	3466.7	913.00	0.00	158.00
Powerplant Group	12290.9	880.00	0.00	150.00
Fixed Equipment Group	19224.2	990.00	0.00	193.00

Figure 86: C.G. using Empty Weight from AAA

X-CG Excursion Table:

C.G. Excursion Table				
Component	Weight lb	X _{cg} in	Load (1-13)	Unload (1-13)
Empty Weight	78000.0	978.46	1	13
Crew	720.0	335.00	3	10
Trapped Fuel and Oil	1125.2	885.00	2	11
Mission Fuel Group 1	75053.9	1060.00	4	7
Mission Fuel Group 2	0.0	0.00		
Passenger Group 1	25200.0	1014.00	5	8
Passenger Group 2	0.0	0.00		
Passenger Group 3	0.0	0.00		
Passenger Group 4	0.0	0.00		
Baggage	4200.0	688.00	6	9

Figure 87: X-C.G. Excursion Table Inputs -AAA

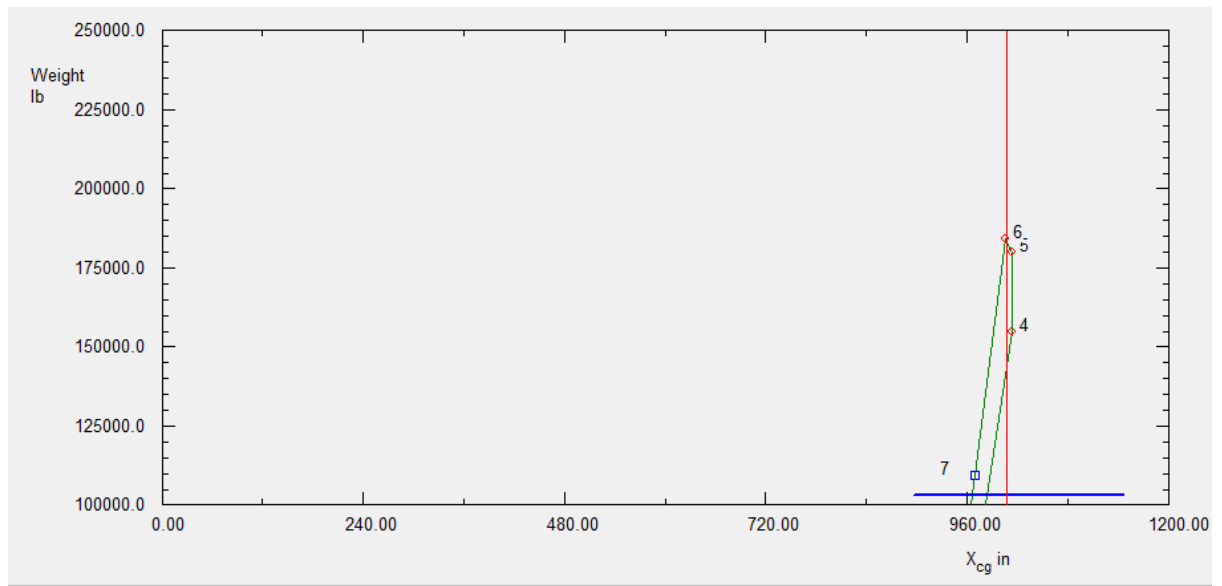


Figure 88: C.G. Excursion Outputs

Y-CG Excursion Table:

C.G. Excursion Table				
Component	Weight lb	Y _{cg} in	Load (1-13)	Unload (1-13)
Empty Weight	78000.0	0.00	1	13
Crew	720.0	0.00	3	10
Trapped Fuel and Oil	1125.2	0.00	2	11
Mission Fuel Group 1	75053.9	0.00	4	7
Mission Fuel Group 2	0.0	0.00		
Passenger Group 1	25200.0	0.00	5	8
Passenger Group 2	0.0	0.00		
Passenger Group 3	0.0	0.00		
Passenger Group 4	0.0	0.00		
Baggage	4200.0	0.00	6	9

Figure 89: Y-C.G. Excursion Table Inputs -AAA

Z-CG Excursion Table:

C.G. Excursion Table				
Component	Weight lb	Z _{cg} in	Load (1-13)	Unload (1-13)
Empty Weight	78000.0	192.51	1	13
Crew	720.0	230.00	3	10
Trapped Fuel and Oil	1125.2	155.00	2	11
Mission Fuel Group 1	75053.9	181.00	4	7
Mission Fuel Group 2	0.0	0.00		
Passenger Group 1	25200.0	230.00	5	8
Passenger Group 2	0.0	0.00		
Passenger Group 3	0.0	0.00		
Passenger Group 4	0.0	0.00		
Baggage	4200.0	166.00	6	9

Figure 90:Z-C.G. Excursion Table Inputs -AAA

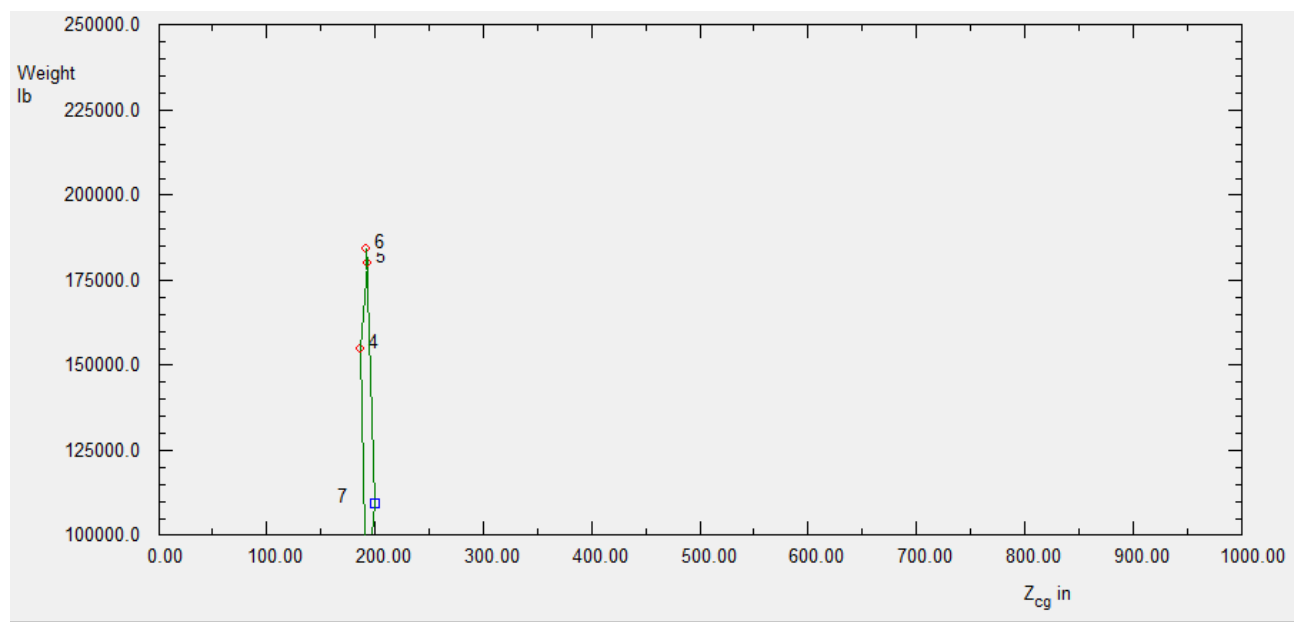


Figure 91:Z-C.G. Excursion Table Outputs -AAA

Aircraft Total C.G.

Output Parameters											
W _{current}	184299.2	lb	X _{cg}	1006.82	in	Y _{cg}	0.00	in	Z _{cg}	192.26	in

8.4 DISCUSSION

The landing gear disposition is a very key parameter which the entire aircraft design depends. In the above sections a brief analysis on the weight and balance and the centre of gravity excursion in the x, y, z directions. The potato plot was drawn but they haven't matched to those documented in Roskam. The aircraft landing gear tip over criteria is an important factor as it determines the maximum limits of loading the aircraft. Also, the parts that were related to the landing gear stick diagram and potato plot in the Roskam text book are not clear and this one reason why the plots are not close to those in the textbook.

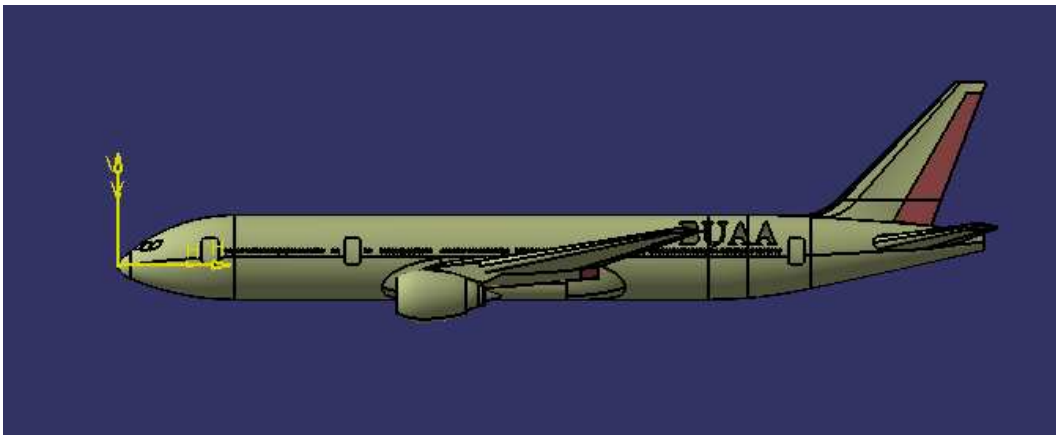


Figure 92:Side View of VER-12XX

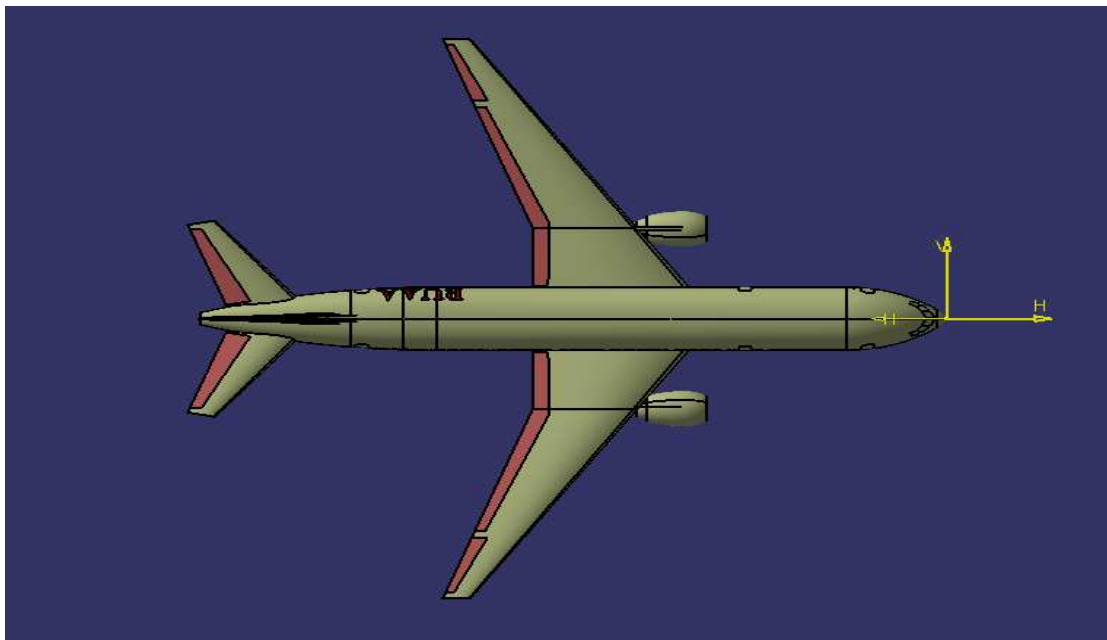


Figure 93:Top View of VER-12XX



Figure 94: Front View of VER-12XX

The landing gear is an integral part of aircraft besides a deciding factor of safety when the aircraft is on ground. The tip over criteria is an essential factor as it is determined by the overall cg travel of the aircraft. This poses few problems and even leads to catastrophic accidents as the vertical tail comes closer to the ground. To avoid this problem VER-12XX is equipped with a horn which alerts the crew when the aircraft is reaching the tip over angle. The weight and balance data detailed in this report helps in understanding the behaviour of the aircraft when it loaded beyond and within its limits.

CHAPTER 9

STABILITY AND CONTROL ANALYSIS / WEIGHT & BALANCE- STABILITY & CONTROL CHECK

In the previous design report on the landing gear disposition a detailed analysis on the tip over criteria, the centre of gravity excursions and their locations have been carried out. In this report, a brief analysis is carried on the proposed aircraft stability and control i.e. the aircraft stability in terms of both longitudinal and directional will be determined. In support to the analysis the x-plots in both the longitudinal and lateral directions will be documented to check for any deviations from the previous calculated tail areas and necessary corrections are made which is determined through a factor called the static margin. In addition to that the stability of the aircraft is also determined in the case of any engine power outage.

9.1 STATIC LONGITUDINAL STABILITY:

Longitudinal stability defines the stability of the aircraft around the lateral axis. For the aircraft to be statically longitudinal stable the centre of gravity should be ahead of the centre of pressure. This design consideration proves to be handy during engine failure which allows the aircraft to glide normally without losing complete stability of the aircraft. This section details the static longitudinal stability of VER-12XX. Firstly, calculations related to the static margin are performed manually and then the aircraft is determined whether it has the inherent or the defacto stability. VER-12XX considered to have a defacto stability because of the high-performance requirements and closed loop feedback control system. The longitudinal stability is determined by the position of the horizontal tail and position of the centre of gravity.

Defacto Longitudinal stability:

The static margin is estimated from:

$$SM = \bar{x}_{ac} - \bar{x}_{cg}$$

\bar{x}_{cg} for a horizontal tail is given by

$$\bar{x}_{cg} = \bar{x}_{cg_{oh}} + \frac{d\bar{x}_{cg}}{dS_h} \cdot S_h$$

$$\text{or } \frac{d\bar{x}_{cg}}{dS_h} = \frac{dx_{cg}}{dS_h} \cdot \frac{1}{z_w}$$

Aerodynamic center location is given by

$$\bar{x}_{ac} = \bar{x}_{ac_{wf}} + \left\{ \frac{C_{L_{dh}}}{C_{L_{dwf}}} \left(1 - \frac{dE_h}{dd} \right) \frac{S_h}{S_w} \bar{x}_{ac_h} \right\}$$

$$+ \left\{ \frac{C_{L_{dh}}}{C_{L_{dwf}}} \left(1 - \frac{dE_h}{dd} \right) \frac{S_h}{S_w} \right\}$$

Static margin for aerodynamic center is

$$\text{Feedback Gain } (K_d) = \frac{(\Delta S.M) \cdot C_{L_d}}{C_{mp_{\alpha}}}$$

$$\Delta S.M = |(\bar{x}_{ac} - \bar{x}_{cg} - 0.05)|$$

Figure 95: Longitudinal Stability Calculations-I

⊙ Wing fuselage left wing edge including any flap effects
($C_{L_{dwf}}$)

$$C_{L_{dwf}} = K_{wgf} \cdot C_{L_{w2}}$$

$K_{wgf} \rightarrow$ Wing-fuselage Interference factor

$C_{L_{w2}} \rightarrow$ Wing-Lift curve slope including any flap effects

$$\text{⊙ } K_{wgf} = 1 + 0.025 \times \frac{D_{f_{maxw}}}{bw} - 0.25 \left(\frac{D_{f_{maxw}}}{bw} \right)^2$$

$D_{f_{maxw}} \rightarrow$ Maximum fuselage diameter at wing fuselage interaction

$bw \rightarrow$ wing span

⊙ for wings with non-translating flap system (flap, split & nose)

$$C_{L_{w2}} = C_{L_{w2 \text{ clean}}}$$

⊙ for a conventional, straight tapered clean wings (flaps up) with sweep angles $b/w \pm 60^\circ$

$$C_{L_{w2 \text{ clean}}} = \frac{2\pi AR_{l.s.} f_{gapw}}{2\pi \left\{ \frac{AR_w^2 \beta^2}{k^2} \left(1 + \frac{\tan^2 \Lambda c/2 w}{\beta^2} \right) + 4 \right\}^{1/2}}$$

Figure 96: Longitudinal Stability Calculations-II

① Wing gap correction factor:

$$f_{gpw} = f(A_{Rw}, (x_{gp}/c)_a, (gp/c)_a)$$

$(x_{gp}/c)_a \rightarrow$ wing-division gap to chord ratio

$(gp/c)_a \rightarrow$ division gap location aft of leading edge as fraction of chord

② Prandtl-Glauert transformation factor:

$$\beta = \sqrt{1 - M_1^2}$$

③ Ratio of Incompressible section lift coefficient to 2π is solved from

$$k = \frac{C_{L_{2w}} @ M=0}{2\pi}$$

④ Wing Semi-chord sweep Angle

$$\Lambda_{c/2w} = \tan^{-1} \left\{ \tan \Lambda_{c/4w} - \frac{(1 - \lambda_{wing})}{AR_{wing} (1 + \lambda_{wing})} \right\}$$

⑤ Wing Airfoil gap correction factor:

$$f_{gpw_0} = f((x_{gp}/c)_a, (gp/c)_a)$$

Figure 97: Longitudinal Stability Calculations-III

⊙ Left Curve slope - Horizontal Tail:

$$C_{L_{hd}} = C_{L_{hd_{exp}}} \frac{S_{h_{exp}}}{S_h} (K_{h(B)} + K_{B(H)})$$

⊙ Part VI : Section 8-1-1-1 Pg - [215-217]
 8-1-3-2 Pg - 248
 8-1-4-2 Pg - 262
 8-1-5-3 Pg 272
 10-2-4-1 Pg - 386-389

Tanbak : Pg 533-534

⊙ Exposed horizontal tail lift curve slope :

$$C_{L_{hd_{exp}}} = \frac{2\pi AR_{h_{exp}} f_{gap}}{2 + \left\{ \frac{AR_{h_{exp}}^2}{k^2} \beta^2 \left(\frac{1 + \tan^2 \Lambda_{1/2} h}{\beta^2} \right) + 4 \right\}^{1/2}}$$

correction

⊙ horizontal gap factor :

$$f_{gap} = f(AR_h, (x_{gap}/c)_e, (y_{gap}/c)_e)$$

⇒ $(x_{gap}/c)_e$ → Horizontal tail elevator gap to chord

⇒ $(y_{gap}/c)_e$ → elevator gap location aft of leading edge as a fraction of chord

Figure 98: Longitudinal Stability Calculations-IV

⊙ Ratio of the sectional lift curve slope to 2π

$$k = \frac{C_{L\alpha h_0 @ M=0}}{2\pi}$$

⊙ Horizontal tail semi-chord sweep Angle

$$\Lambda_{c/h} = \tan^{-1} \left[\tan \Lambda_{c/h} \cdot \frac{(1 - \lambda_{hexp})}{AR_{hexp} (1 + \lambda_{hexp})} \right]$$

⊙ Exposed horizontal tail aspect ratio

$$AR_{hexp} = \frac{b_{hexp}^2}{S_{hexp}}$$

⊙ Exposed horizontal tail Area

$$S_{hexp} = \frac{b_{hexp}}{2} (c_{\alpha/h} + c_{\alpha/h} \Lambda_{c/h})$$

⊙ Exposed horizontal tail span

$$b_{hexp} = b_h - w_{f/h}$$

⇒ $w_{f/h}$ = width of the fuselage in the region of horizontal tail

⊙

→ is governed by the statement:

$$|Z_{c_{\alpha/h}} - Z_{f_{c/h}}| > \frac{1}{2} h_{f/h} \text{ then } u$$

Figure 99: Longitudinal Stability Calculations-V

⊙ The downwash gradient at the horizontal tail without flap effects ⊙
is found using:

$$\left(\frac{d\epsilon}{dx}\right)_{\text{clean}} = 4.44 \times (K_A K_\lambda K_h \sqrt{\cos \Lambda_{c/4w}})^{1.19} \frac{(C_{l,w \text{ clean}})_{M_1}}{(C_{l,w \text{ clean}})_{M=0}}$$

⊙ $K_A \rightarrow$ correction factor of aspect ratio

$$K_A = \frac{1}{AR_w} = \frac{1}{1 + AR_w^{1.7}}$$

⊙ $K_\lambda \rightarrow$ correction factor of the taper ratio:

$$K_\lambda = \frac{10.3 \lambda_w}{7}$$

⊙ The factor for the distance b/w the wing chord plane & the horizontal tail chord plane is defined from:

$$K_h = \frac{1 - \left|\frac{h_h}{b_w}\right|}{\left(2 \frac{h_h}{b_w}\right)^{1/3}}$$

⊙ The z-distance b/w the wing root chord plane & the horizontal tail aerodynamic center is calculated from:

$$h_h = (Z_{ac_h} - Z_{c/4w}) \cos i_w + (X_{ac_h} - X_{ac_w}) \sin i_w$$

⊙ The z-coordinate of the horizontal tail aerodynamic center measured from reference line is

$$Z_{ac_h} = Z_{c/4w} + y_{\text{magch}} \tan \Gamma_h \rightarrow$$

$\Gamma_h \rightarrow$ horizontal dihedral angle.

Figure 101: Longitudinal Stability Calculations-VII

③ y_{mgc_h} → Y-distance b/w horizontal tail mean geometric chord & the fuselage centerline

$$y_{mgc_h} = \frac{\sqrt{AR_h S_h} \times (1 + 2\lambda_h)}{6(1 + \lambda_h)}$$

④ The X-distance b/w the wing aerodynamic center & horizontal tail aerodynamic center is given by

$$I_h = (x_{ac_h} - x_{ac_w}) \cos i_w - (z_{ac_h} - z_{ac_{t_w}}) \sin i_w$$

i_w → Incidence of the wing

Figure 102: Longitudinal Stability Calculations-VIII

$$C_{L_{\text{clean}}} = \frac{2\pi AR_{LS} \frac{f_{\text{flap}}}{\omega}}{2 + \left\{ \frac{AR_{LS}^2 \omega^2}{k^2} \left(1 + \frac{\tan^2 \alpha_{\frac{1}{2}} \omega}{\beta^2} \right) + 4 \right\}^{1/2}}$$

$$= \frac{(2\pi) (10) (0.039)}{2 + \left\{ \frac{(10)^2 (0.542)^2}{(0.975)^2} \cdot \left(1 + \frac{\tan^2 (28.3^\circ)}{(0.542)^2} \right) + 4 \right\}^{1/2}}$$

$$= \frac{(2\pi) (10) (0.039)}{10.1}$$

$$\therefore C_{L_{\text{clean}}} = 0.301 \text{ @ } 4.076 \text{ rad}^{-1}$$

$$\therefore C_{L_{\text{flap}}} = K_{\text{flap}} \cdot C_{L_{\text{clean}}}$$

$$= (4.076) \times (1.00005)$$

$$\therefore C_{L_{\text{flap}}} = 4.0762 \text{ rad}^{-1}$$

④ Left-Curve Slope - Horizontal Tail =

$$C_{L_{\text{hd}}} = C_{L_{\text{hdeep}}} \cdot \frac{S_{\text{hexp}}}{S_{\text{h}}} (K_{h(B)} + K_{BCH})$$

④ Ratio of the sectional lift curve slope to 2π

$$d = \frac{C_{L_{\text{hd}} @ M=0}}{2\pi} = \frac{6.2510}{2\pi} = 0.9948 \text{ rad}^{-1}$$

Figure 103: Longitudinal Stability Calculations-IX

⊙ Horizontal tail semi-chord sweep Angle:

$$\Lambda_{c/2h} = \tan^{-1} \left[\tan \Lambda_{c/4h} - \frac{(1 - \lambda_{heep})}{AR_{heep} (1 + \lambda_{heep})} \right]$$

⊙ $\Lambda_{c/4h} = 31.5 \text{ deg}$ $AR_h = 4.62$

$\lambda_h = 0.3$

$$\Lambda_{c/2h} = \tan^{-1} \left[\tan(0.549) - \frac{(1 - 0.3)}{(4.62)(1 + 0.3)} \right]$$

$\Lambda_{c/2h} = 30.49^\circ$

⊙ Exposed horizontal tail Area:

$$S_{heep} = \frac{b_{heep}}{2} (C_{ah} + C_{ah} \lambda_h)$$

$$= \frac{577}{2} (194.10 + (194.10)(0.3))$$

$S_{heep} = 72797.2 \text{ in}^2$

$AR_{heep} = 4.16$

$\lambda_{heep} = 0.33$

$f_{gap} = 0.93$

$K_{h(b)} + K_{b(h)} = 1.40$

$b_{heep} = 461.81 \text{ in}$

Horizontal tail gap correction factor = 0.95

Horizontal tail Airfoil gap correction factor

Figure 104: Longitudinal Stability Calculations-X

① The downwash gradient at the horizontal tail

$$\frac{d\epsilon}{dx} = \left(\frac{d\epsilon}{dx}\right)_{\text{p.f.f.}} + 4 \left(\frac{d\epsilon}{dx}\right)_{\text{power}}$$

② Defacto Stability Calculations:

③ Wing-fuselage lift curve slope including any flap effects:

$$C_{L_{\text{w/f}}} = K_{\text{w/f}} \cdot C_{L_{\alpha}}$$

④ Since VER-12X uses non-translating flap system

$$\therefore C_{L_{\alpha}} = C_{L_{\alpha \text{ clean}}}$$

$$\therefore C_{L_{\alpha \text{ clean}}} = \frac{2\pi A \cdot R_{L/S} \cdot f_{\text{flap}}}{2 + \frac{5AR_{\text{w}}\beta^2}{K^2} \left(\frac{1 + \tan^2 \Lambda_{\text{c/2w}}}{\beta^2} \right) + 4} \cdot \frac{1}{2}$$

⇒ Prandtl-Glauert transformation:

$$\beta = \sqrt{1 - M_1^2} \quad \text{q VER-12X cruises at } 0.84$$

$$\therefore \beta = \sqrt{1 - (0.84)^2}$$

$$\therefore \beta = 0.542$$

④ Wing Serrichord Sweep Angle:

$$\Lambda_{\text{c/2w}} = \tan^{-1} \left[\tan \Lambda_{\text{flw}} - \frac{(1 - \lambda_{\text{wing}})}{AR_{\text{wing}}(1 + \lambda_{\text{wing}})} \right]$$

$$= \tan^{-1} \left[\tan(31.5) - \frac{(1 - 0.15)}{(10)(1 + 0.15)} \right]$$

Figure 105: Longitudinal Stability Calculations-XI

$$\therefore \Lambda_{c/2w} = 28.32^\circ = 0.5 \text{ rad}$$

⊕ Ratio of incompressible section lift coefficient to 2π

$$k = \frac{C_{L_{2w}} @ M=0}{2\pi}$$

[∵ $C_{L_{2w}} \rightarrow$ depends on the ^{type of} airfoil used
so for the calculation the reference of
B-777 airfoil is used
which is 6.1806 rad]

$$\rightarrow k = \frac{6.1806 \text{ rad}}{2\pi}$$

$$\therefore k = 0.975 \text{ rad}^{-1}$$

$$D_{fmax} = 250 \text{ inches} \rightarrow \text{reference from B-777 drawings}$$

⊕ Assuming

$$(\xi_{gap/c})_a = 78\%, \quad (\eta_{pp/c})_a = 0.50\%$$

$$\therefore f_{gap} = f(AR_w, (\xi_{gap/c})_a, (\eta_{pp/c})_a)$$

$$= f(10, 78\%, 0.50\%)$$

$$f_{gap} = 0.039$$

$$k_{up} = 1 + 0.025 \times \frac{D_{fmaxw}}{b_w} - (0.25) \left(\frac{D_{fmaxw}}{b_w} \right)^2$$

$$= 1 + 0.025 \times \frac{250}{212.6 \times 2} - (0.25) \times \left(\frac{250}{212.6 \times 2} \right)^2$$

$$= 1 + 0.00245 - 0.0024$$

$$k_{up} = 1.00005 \quad \text{⊕}$$

Figure 106: Longitudinal Stability Calculations-XII

Output Parameters											
$C_{L_{\alpha}}$	4.8445	rad ⁻¹	x_{cg}	0.4589		x_{ac}	0.4698		x_{ac_h}	3.0544	
X_{cg}	1006.82	in	$x_{ac_{wf}}$	0.2378		SM	1.09	%			

Figure 107: Static Margin - Longitudinal Stability

Input Parameters											
S_w	2497.93	ft ²	S_v	390.47	ft ²	X_{cg}	1006.82	in	$C_{n_{\beta_f}}$	-0.0916	rad ⁻¹
AR_w	6.81		$C_{y_{v\beta}}$	-3.0144	rad ⁻¹	x_{ac_v}	1587.48	in			

Figure 108: Inherent Stability Inputs – Directional

X-PLOT:

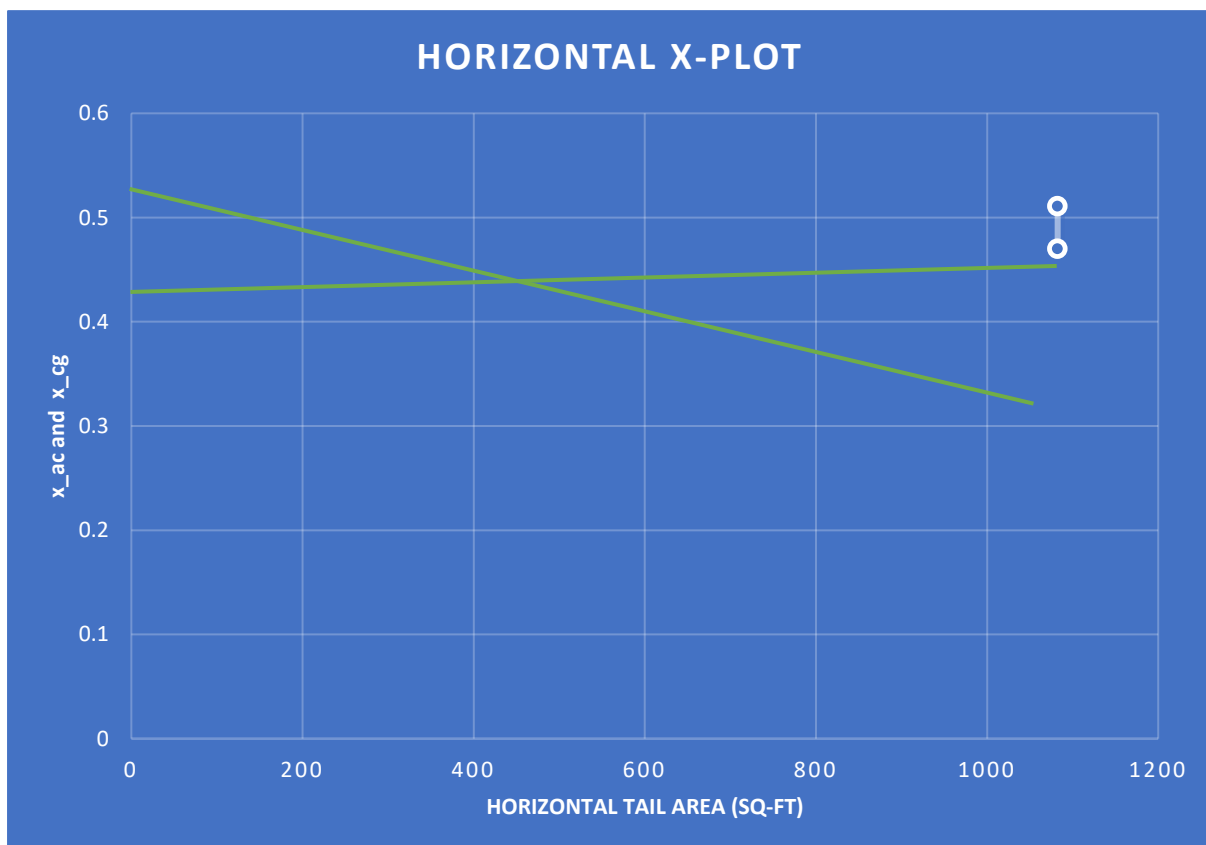


Figure 109: Horizontal Tail - XPlot

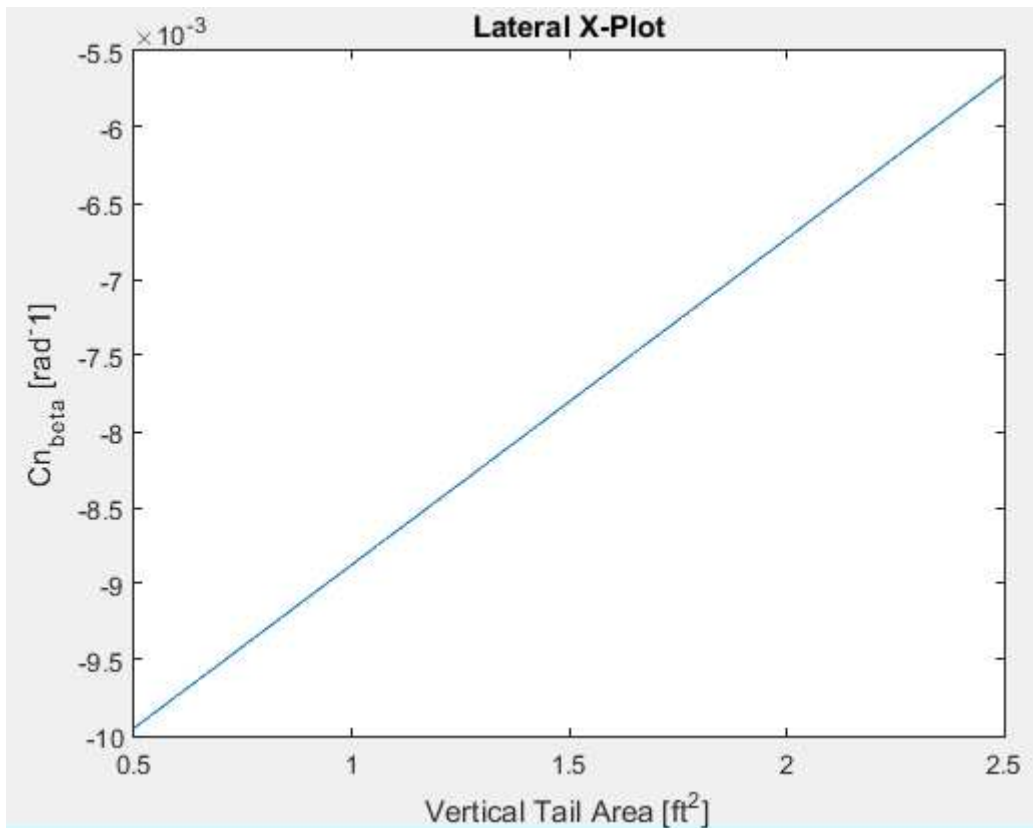


Figure 110: Lateral X-Plot

The X-plot for the horizontal and vertical tail area is shown in the above figure defining the static margin.

9.2 Static Directional Stability:

Lateral stability is defined as the aircraft stability around the vertical or normal axis. Usually this stability is achieved by means of dihedral, wing sweep and appropriate weight distribution. All the assumptions and calculations for determining the static directional stability are documented below:

⊕ Inherent directional stability: Yawing Moment Coefficients due to side slip derivatives

⊕ Normally the overall level of directional stability is given by

$$C_{n\beta} = 0.0010/\text{degree} \\ = 0.0573/\text{radian}$$

⊕ Static directional stability is calculated using:

$$C_{n\beta} = C_{n\beta_{Wf}} - C_{y_{V\beta}} \left(\frac{S_V}{S_W} \right) \left(\frac{x_{acV} - x_{cg}}{b_W} \right)$$

$C_{n\beta_{Wf}}$ → Wing-fuselage contribution to the static directional stability derivative

$C_{y_{V\beta}}$ → Vertical tail lift curve slope

x_{acV} → X-location of the vertical tail aerodynamic center measured from the reference line.

$$C_{n\beta_{Wf}} = \underbrace{C_{n\beta_W}} + \underbrace{C_{n\beta_f}} \rightarrow \text{fuselage contribution to the static directional stability derivative}$$

↳ wing contribution to the static directional stability derivative

⊕ $C_{n\beta_W} = 0$ → assumed to be "0"

Figure 111: Directional Stability Calculations-I

⊙ Also the overall directional stability calculations can also be determined using the yawing moment coefficient due to side slip derivative

$$C_{n\beta_c} = C_{n\beta_w} + C_{n\beta_f} + C_{n\beta_v} + C_{n\beta_{\text{tail}}} + C_{n\beta_{\text{fin}}}$$

Wing contribution to the static directional stability derivative
fuselage contribution to the static directional stability derivative
Vertical tail contribution to static stability derivative

Figure 112: Directional Stability Calculations-II

$\Lambda_{c/4_v}$	40.3	deg	?	$(x_{\text{gap}}/C)_r$	68.86	%	?
$(t/c)_{r_v}$	12.0	%	?	x_{apex_v}	2940.24	in	?
$(t/c)_{t_v}$	12.0	%	?	z_{apex_v}	1060.08	in	?
$(\text{gap}/C)_r$	0.50	%	?	h_{f_v}	205.16	in	?

Altitude	35000	ft	?	$C_{l_{\alpha_{TV}}@M=0}$	6.2504	rad ⁻¹	?	z_{fc_v}	1049.99	in	?
ΔT	0.0	deg F	?	S_h	500.00	ft ²	?	S_v	802.71	ft ²	?
U_1	482.00	kts	?	x_{ac_h}	3319.01	in	?	AR_v	1.81		?
$C_{l_{\alpha_{rv}}@M=0}$	6.2504	rad ⁻¹	?	z_{ac_h}	1073.64	in	?	λ_v	0.29		?

Figure 113: AAA Directional Stability Inputs and Outputs

Output Parameter							
$(d\sigma/d\beta)_v$		-0.1748					
Output Parameters							
M_1	0.836	$C_{l_{\alpha_v}}@M=0$	6.2504 rad ⁻¹	$C_{l_{\alpha_{TV}}}$	11.3898 rad ⁻¹	f_{gap_v}	0.96
x/C_v	0.9525	$C_{l_{\alpha_v}}@M=0.6$	7.8130 rad ⁻¹	$C_{l_{\alpha_v}}$	11.3898 rad ⁻¹	$C_{y_{v_p}}$	-3.1274 rad ⁻¹
AR_{eff}	3.00	$C_{l_{\alpha_{TV}}}$	11.3898 rad ⁻¹	$f_{gap_{v_0}}$	0.93	$C_{y_{v_p}}@M=0.6$	-3.1644 rad ⁻¹

Figure 114:AAA Directional Stability Derivative Outputs

One Engine Out:

⊕ One Engine out condition

→ The critical engine-out yawing moment is found from:

$$N_{\text{out}} = \frac{T_{10}}{N_e} \cdot Y_T$$

T_{10} → Take-off Thrust

N_e → Number of Engines

Y_T → moment arm of the most critical engine

⊕ The induced drag by the Inoperative Engine is determined from

∴ VFR-12X uses high bypass ratio engines

$$\therefore N_D = 0.25 N_{\text{out}}$$

⊕ The minimum controllable speed:

$$V_{mc} = 1.2 V_S$$

⊕ The sudden deflection required to hold the engine out condition at minimum controllable speed is solved from:

$$\delta_{\beta 1} = \frac{N_D + N_{\text{out}}}{\bar{q}_{V_{mc}} S_w b_w C_{n_{\delta_{\beta 1}}}}$$

$C_{n_{\delta_{\beta 1}}}$ → yawing moment coefficient due to sudden deflections derivative

$\bar{q}_{V_{mc}}$ → dynamic pressure at the minimum controllable speed

Figure 115:One engine out Calculations-I

② The dynamic pressure at the minimum controllable speed

$$\bar{q}_{mc} = \frac{1}{2} \rho V_{mc}^2$$

③ The induced drag due to the inoperating engine

$$D_{OEI} = \frac{N_{out} (F_{OEI} - 1)}{Y_T}$$

$F_{OEI} \rightarrow 1.25$ for high B.P. engines

Figure 116: One Engine Out Calculations-II

Output Parameters														
N_{OEI}	15515500.00	ft-lb	D_{OEI}	19250.00	lb	$N_{b_{OEI}}$	3878875.00	ft-lb	V_{mc}	373.61	kts	δ_r	-88.50	deg
Input Parameters														
Altitude	35000	ft	S_w	4833.43	ft ²	T_{TO}	154000	lb	Y_T	2418.00	in	F_{OEI}	1.25	
ΔT	0.0	deg F	AR_w	8.27		V_S	311.34	kts	$C_{n_{\delta_r}}$	-0.0885	rad ⁻¹			

Figure 117: AAA One Engine Out Inputs/Outputs

It is important to determine the aircraft engine out condition as it directly effects the overall stability of the aircraft. For VER-12XXX the safe altitude at which the aircraft can fly with minimum stability is 16000 feet and at Mach 0.4 and the descent rate to this safe altitude from the original altitude must be 2500 ft./min.

9.3 EMPENNAGE DESIGN – WEIGHT & BALANCE – LANDING GEAR DESIGN – LONGITUDINAL STATIC STABILITY & CONTROL CHECK:

(a) A tip-over problem

The tip over criteria is an essential factor as it is determined by the overall cg travel of the aircraft. This poses few problems and even leads to catastrophic accidents as the vertical tail comes closer to the ground. To avoid this problem VER-12XX is equipped with a horn which alerts the crew when the aircraft is reaching the tip over angle. In addition to the tip over problem there is a tip forward problem which occurs during the case too much cg travel forward. In the tip forward condition, the rotation speed of the aircraft play a prominent role. The tip forward problem is not commonly seen in tricycle landing gear configurations and is mostly seen in the tail dragger. VER-12XX is designed to meet the tip over criteria by having relatively small landing gear strut length which increase the empennage angle from the ground and therefore removing the scope for catastrophes.

(b) Too much or too little longitudinal and/or directional stability

VER-12XX is well within the limits of the determined centre of gravity and static margins which proves the aircraft is stable both in longitudinal and directional. Too much directional or longitudinal stability is required for the aircraft which requires high manoeuvrability and since the entire design scope is based on transport jet the calculations prove that they are within the limits.

(c) A V_{mc} problem

Whenever there is a single engine out condition it is a known fact that the engines cannot produce the required lift at the operating altitude and it effects the stability too. If the aircraft engine is buried into the vertical tail, then the effected engine may cause adverse yaw which results in stability problems. VER-12XX have conventional tail configuration which does minimum effect during the engine loss but this can be averted by descending to the safest operating altitude.

9.4 DISCUSSION

The stability and control analysis in this section is the Class-1 analysis which defines the basic aircraft stability. The X plots presented in the above sections are very important especially when the determined co-ordinates of C.G. and aerodynamic centre does not fall into the required static margin limits. Also, the x plots help in determining the optimal values of control for both longitudinal and directional stability. The engine out condition is also very basic whereas the class II calculations provide detailed analysis on the aircraft safe operating condition when there is power loss. Stability and control play a vital role in the aircraft flight right from the ground to flight this factor has an impact on each aspect of the flight conditions. It is essential that the design analysis comply with the statistical data as it enhances the vertical and horizontal control and to improve handling capabilities. In the preliminary design analysis, it is important to have a clear idea on the aircraft stability and control which this data can further be refined and used for class II calculations.

CHAPTER 10

DRAG POLAR ESTIMATION

In the previous design chapters, the design analysis of landing gear, empennage and wing have been detailed. We knew that the aircraft design is locked 90% in the preliminary design analysis. Drag is an important factor in addition to lift as it is a factor which helps in improving the aerodynamics of the aircraft so that the aircraft performance is not limited. Aircraft drag is determined in terms of the wetted area of the aircraft components. In this design report the drag polar calculations are documented by determining the wetted area of the aircraft. Finally, the drag due to remaining components of the aircraft are also analysed and determined.

10.1 AIRPLANE ZERO LIFT DRAG:

⊙ class-1 Drag Polar Determination ⊙

⊙ The convenient way to find the drag polar is to find the wetted areas of the airplane (by determining its major components)

- fuselage
- wings
- empennage
- Nozzles
- other components

⊙ for straight-tapered planforms (wings) the wetted areas found from

$$S_{wet\,plf} = 2 \cdot S_{plan} \left(1 + 0.25 \left(\frac{t}{c} \right)_m (1 + \lambda) / (1 + \lambda) \right)$$

where $\lambda = (t/c)_m / (t/c)_t$ & $\lambda = C_L / C_D$

→ If the planform has broken or curved leading or trailing edges the wetted area must be obtained from a spanwise integration of the planform at each planform stations

$$P_{plf} = 2c (1 + 0.25 t/c)$$

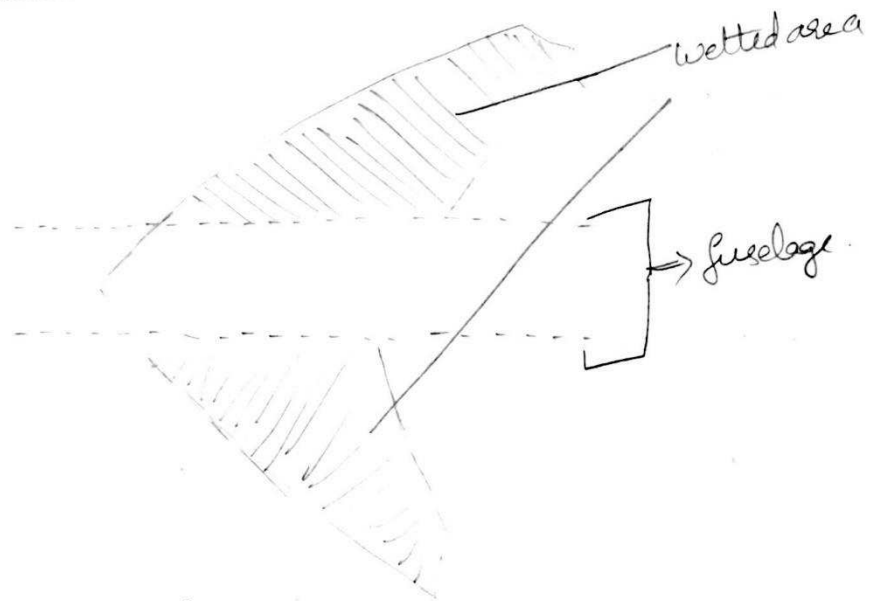
for V62-12X

$C_{Lw} = 81.60 \text{ in}$	$(t/c)_m = 15\%$		
$C_{Dw} = 498.65 \text{ in}$	$(t/c)_{tw} = 12\%$		$S_{w\,sweep} = 4053.76 \text{ ft}^2$

Figure 118: Drag Polar Calculations - I

$$\therefore S_{wet_{wing}} = 2 \times (4053.76) \times \left(1 + (0.25)(15)\% \left(1 + \frac{15}{13}\right)^{0.15} / (1 + 0.15)\right)$$

$$\therefore S_{wet_{wing}} = 7363.96 \text{ feet}^2$$



→ This planform perimeter is

$$P_{P/F} = 2 \cdot c (1 + 0.25 t/c)$$

$$= (2)(340.09) + (1 + (0.25)(0.14/340.09))$$

$$wing \leftarrow P_{P/F} = 680.25 \text{ in}$$

Figure 119: Drag Polar Calculations - II

⊕ Wetted Area for fuselage:

⇒ for fuselage with cylindrical mid-sections

$$S_{wet\ fus} = \pi D_f l_f \left(1 - \frac{2}{\lambda_f}\right)^{2/3} \left(1 + \frac{1}{\lambda_f^2}\right)$$

where $\lambda_f = l_f / D_f \rightarrow$ fuselage fineness ratio

⊕ from the previous design report (fuselage design)

the fuselage length = 2506.58 in

Maximum fuselage diameter = 242 in

$$\therefore \lambda_f = l_f / D_f = \frac{2506.5}{242} = 10.357$$

$$\therefore S_{wet\ fus} = (\pi) (242) (2506.58) \left(1 - \frac{2}{10.357}\right)^{2/3} \left(1 + \frac{1}{10.357^2}\right)$$

$$S_{wet\ fus} = 11576.9 \text{ ft}^2$$

Figure 120: Drag Polar Calculations – III

② Wetted Area for externally mounted nacelles: ③

$$S_{wet_{fan}} = L_n D_n \left\{ 2 + 0.35 L_1 / L_n + 0.81 L_1 D_{hL} / L_n D_n + 1.15 (1 - L_L / L_n) D_e \right.$$

$$S_{wet_{gas_{gen}}} = \pi L_g D_g \left[1 - (V_3) (1 - D_{eg} / D_g) \left\{ 1 - 0.18 (D_g / L_g)^{5/3} \right\} \right]$$

$$S_{wet_{plug}} = 0.7 \pi L_p D_p$$

$$\rightarrow L_n = 263.83 \text{ in}$$

$$\rightarrow L_1 = 131.91 \text{ in}$$

$$\rightarrow D_{hL} = 116 \text{ in}$$

$$\rightarrow D_{ef} = 150 \text{ in}$$

$$\rightarrow D_h = 130 \text{ in}$$

$$\rightarrow D_n = 200 \text{ in}$$

$$\therefore S_{wet_{fan}} = (131.11) \times (200) \left\{ 2 + \left(0.35 \times \frac{131.91}{263.83} \right) + 0.81 \times \frac{131.91 \times 116}{263.83 \times 200} + 1.15 \left(1 - \frac{263.83}{131.91} \right) \times \frac{150}{200} \right\}$$

$$\therefore S_{wet_{fan}} = 407.65 \text{ Feet}^2$$

Figure 121: Drag Polar Calculations -IV

$$\textcircled{*} S_{\text{wet gas}} = \pi L_g D_g \left[1 - \left(\frac{1}{3}\right) \left(1 - \frac{D_{\text{eg}}}{D_g}\right) \left\{ 1 - 0.18 \left(\frac{D_g}{L_g}\right)^{5/3} \right\} \right]$$

$$\left. \begin{array}{l} L_g = 100 \text{ in} \\ D_g = 120 \text{ in} \\ D_{\text{eg}} = 90 \text{ in} \end{array} \right\} \rightarrow \text{These values are assumed from the Trent-900 engine.}$$

$$= \pi \times 100 \times 120 \left[1 - \left(\frac{1}{3}\right) \left(1 - \frac{90}{120}\right) \left\{ 1 - 0.18 \left(\frac{120}{100}\right)^{5/3} \right\} \right]$$

$$\therefore S_{\text{wet gas}} = 35150 \text{ in}^2 = 244 \text{ feet}^2$$

$$\textcircled{*} S_{\text{wet plug}} = 0.7 \pi L_p D_p$$

$$L_p = 60 \text{ in}$$

$$D_p = 30 \text{ in}$$

$$\therefore S_{\text{wet plug}} = (0.7) \times \pi \times (60)(30)$$

$$= 27.48 \text{ feet}^2$$

$$\therefore \boxed{S_{\text{wet plug}} = 27.48 \text{ feet}^2}$$

Figure 122: Drag Polar Calculations – V

$$\therefore S_{wet_{engines}} = S_{wet_{nacelles}} + S_{wet_{gas}} + S_{wet_{plug}}$$

$$= 407.65 \text{ feet}^2 + 244 \text{ feet}^2 + 27.48 \text{ feet}^2$$

$$S_{wet} = 678.85 \text{ feet}^2$$

Wetted Area Calculations for the Horizontal & Vertical tail :

→ Horizontal tail :

⇒ from the formula

$$S_{wet_{planform}} = 2 \times S_{exp_{planform}} \left\{ (1 + 0.25(t/c)_{a_h}) (1 + z) / (1 + z) \right\}$$

$$C_{a_h} = 285.06 \text{ in} ; C_{t_h} = 81.60 \text{ in}$$

$$(t/c)_{a_h} = 12\%$$

$$(t/c)_{t_h} = 11.0\%$$

$$S_{exp} = 865.07 \text{ ft}^2$$

$$\therefore S_{wet} = 2 \times 865.07 \times 144 \text{ in}^2 \left\{ (1 + 0.25)(12\%) \left(1 + \frac{81.60}{285.06} \right)^{0.16} / (1 + 0.16) \right\}$$

$$S_{wet_h} = 1538.3 \text{ feet}^2$$

Figure 123: Drag Polar Calculations - VI

→ for Vertical tail :

$$S_{wet\,vertical\,tail} = 2 \cdot S_{eap\,tail} \left(1 + 0.25 \left(\frac{t/c}{c_{91}} \right) \right) \frac{(1 + \tau)}{(1 + \lambda)}$$

where $\tau = \frac{(t/c)_{91}}{(t/c)_t}$ $\lambda = \frac{c_t}{c_{91}}$

for VFR-12x the vertical tail parameters are as follows:

→ $(t/c)_{91} = 12\%$

→ $(t/c)_t = 12\%$

→ $c_{91} = 391.68 \text{ in}$

→ $c_t = 114.24 \text{ in}$

→ $S_{eap} = 569.18 \text{ ft}^2$

→ $S_{wet\,v} = 2 \times 569.18 \left[\frac{1 + \left(0.25 \times \frac{12}{100} \right) \left(1 + \frac{12}{12} \times \frac{114.24}{391.68} \right)}{\left(1 + \frac{114.24}{391.68} \right)} \right]$

∴ $S_{wet\,v} = 915.46 \text{ ft}^2$

Figure 124: Drag Polar Calculation-VII

Wetted Area Configurations :			⑤
	Calculated wetted Area (feet ²)	Fuselage Interaction subtraction (feet ²)	Actual wetted Area (feet ²)
Fuselage	11576.9	-	11576.9
Horizontal tail Area	1538.3	- 150 feet ²	1388.3
Vertical tail Area	915.46	- 750 feet ²	795.46
Wing	7363.96	- 200 feet ²	7163.96
Nacelles	678.65	- 50 feet ²	628.65
			<u>21553.27 feet²</u>

We know initially the wetted area is calculated using (Chap 2 Eq. 3.22)

$$\log_{10} S_{wet} = c + d \log_{10} W_{F0}$$

$$c = 0.0199, \quad d = 0.7531$$

$$\rightarrow \log_{10} S_{wet} = 0.0199 + (0.7531) \log_{10} (546912.2)$$

$$\log_{10} S_{wet} = 3.2704 + 4.3411$$

$$\therefore S_{wet} = 10^{7.6115} = 21934.4$$

Figure 125: Drag Polar Calculation -VIII

10.2 EQUIVALENT PARASITE AREA:

The value of the determined wetted area & the statistical data show that for the take off value of 549912.2 lbs the calculations remain below 1% of the required limits.

⇒ Calculating the Equivalent Parasite drag :

$$\log_{10} f = a + b \log_{10} S_{wet}$$

from Rostam table 3.4

$$a = -2.0458; b = 1$$

$$\Rightarrow \log_{10} f = -2.0458 + \log_{10} (21553.27)$$

$$= -2.0458 + 4.33$$

$$\log_{10} f = 2.2877$$

$$\therefore f = 2.2877 \text{ feet}^2$$

⊗ Clean zero lift drag coefficient (C_{D0})

$$C_{D0} = \frac{\text{Equivalent Parasite area}}{\text{Wing Area}}$$

$$= \frac{2.2877}{4700}$$

$$C_{D0} = 0.000486 = 0.018 \%$$

Figure 126: Equivalent Parasite Area

10.3 LOW SPEED DRAG INCREMENTS

10.3.1) HIGH-LIFT DEVICE/LANDING GEAR DRAG INCREMENTS FOR TAKE-OFF AND LANDING:

In this section, the drag due to the flaps and landing gear are determined. VER-12XX uses plain flap and tricycle landing gear configuration.

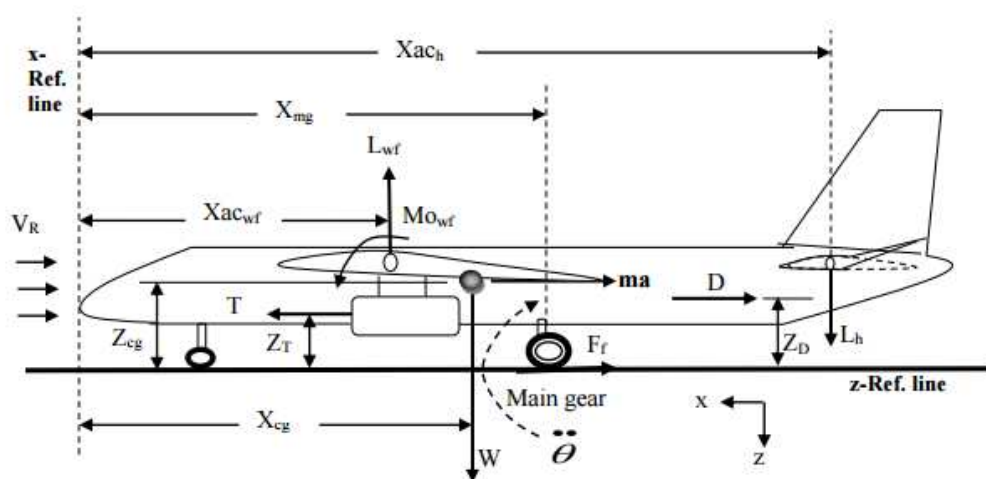


Figure 127: Landing Gear Definitions with C.G.

from the graph (12.7) the incompressibility drag at Mach 0.8 is approximately 2.6

if we knew

$$k = \frac{1}{\pi A R}$$

$$= \frac{1}{\pi \times 9.613 \times 0.8}$$

$$= 0.0414$$

$$\therefore C_D = C_{D0} + kC^2$$

$$C_D = 0.0118 + 0.0414C^2$$

②) Flap drag increments

→ For the calculation ease only the plain flap drag increments are determined:

$$C_{D0 \text{ flap}} = \left(\frac{C_f}{C} \right) \cdot A \cdot (\delta_f)^2$$

$\delta_f \rightarrow$ flap deflection angle

$\frac{C_f}{C} =$ Average flap chord to Average wing chord

Figure 128: Total Drag and Drag increments due to flaps and Landing gear

$$\rightarrow A = 0.2368$$

$$B = 1.0096$$

$$\delta_f = 20^\circ$$

$$\rightarrow C_w = 340.09 \text{ in}$$

$$\rightarrow C_f = 270 \text{ in}$$

$C_w \rightarrow$ the geometric mean of chord wing root & wing tip

$$\therefore C_{D_{\text{flap}}} = \left(\frac{270}{340.09} \right) \cdot (0.2368) \cdot (20)^{1.0096}$$

$$C_{D_{\text{flap}}} = 3.87$$

⊕ Drag due to landing gear:

$$C_{D_{Lg}} = \sum_{i=1}^n C_{D_{Lg}} \left(\frac{S_{Lg}}{S} \right)$$

S_{Lg} = Area of the landing gear

S = wing area

$C_{D_{Lg}}$ = Drag coefficient on each wheel

for ~~Main~~ ^{Nose} wheel

$$D_t = 40 \text{ in}$$

$$b_t = 15.5 \text{ in}$$

$$S_{Lg_{\text{nose}}} = 620 \text{ in}^2 = 4.3 \text{ feet}^2$$

for Main Gear

$$D_t = 52 \text{ in}$$

$$b_t = 20.5 \text{ in}$$

$$S_{Lg_{\text{main}}} = 1066 \text{ in}^2 = 7.4 \text{ feet}^2$$

Figure 129: Landing Gear Drag Calculations - I

$$\begin{aligned} \therefore C_{D_{LW}} &= C_{D_{lg}} \left(\frac{S_{lg1}}{S} \right) + C_{D_{lg}} \left(\frac{S_{lg2}}{S} \right) \\ &= \frac{(0.3)}{4700} [4.3 + 7 \cdot 4] \\ \therefore C_{D_{\text{landing gear}}} &= 0.00456 \end{aligned}$$

Figure 130: Landing Gear Drag Calculations-II

10.4 COMPRESSIBILITY DRAG

The compressibility effects are more pronounced when the aircraft travels at high subsonic speeds. The flow over the aircraft wing when travelling at Mach 0.3-0.4 the compressibility factor is assumed to be negligible. But VER-12XX cruises at max Mach 0.84 so the compressibility factor cannot be neglected. It is a known fact that the velocities at the top surface of the wing are usually higher than the free stream velocities but when the speed of the aircraft is greater than Mach 0.65 there can arise a condition where the velocities on the top surface of the wing may even reach Mach=1. These supersonic velocities further increase the drag with reduction in total pressure due to the generation of shock waves and the boundary layer separation also thickens. There are two components that are critical that are associated with the compressibility drag i.e. the crest

$$\begin{aligned} \therefore M_{\text{cruise}} &= 0.84 \text{ for VER-12X} \\ \therefore M_{\text{cruise}} &= M_{\text{div}} = 0.84 \\ \therefore M_{\text{div}} &= 1.02 M_{\text{cc}} \\ \Rightarrow M_{\text{cc}} &= \frac{M_{\text{div}}}{1.02} \\ \boxed{M_{\text{cc}} &= 0.82} \end{aligned}$$

Figure 131: Critical Mach Number

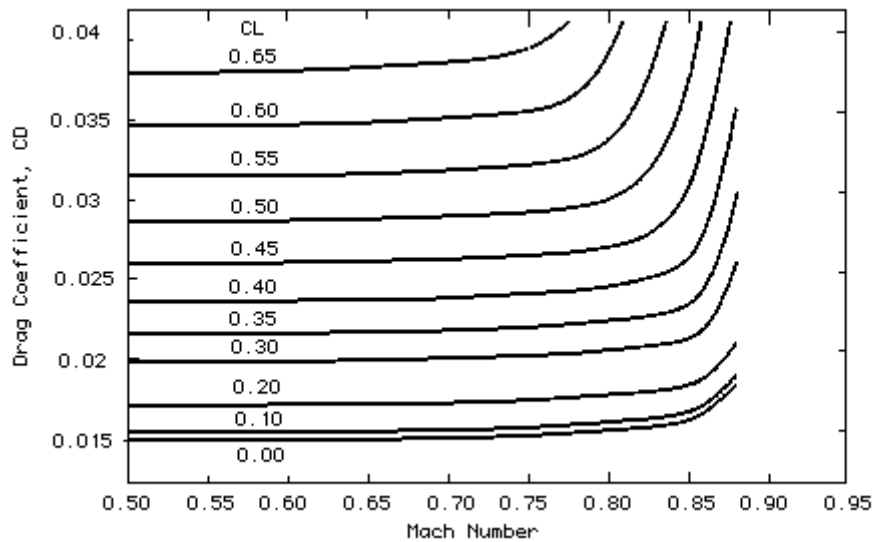


Figure 132: Drag Coefficient versus Mach Number

The figure above gives the data related to the Mach number versus the Drag Coefficient. So, from the graph the value of drag coefficient can be interpolated. The drag due to compressibility effects is 0.035

10.5 Area ruling

The Area ruling is a concept through which the drag can be minimized when the aircraft reaches high subsonic speeds. VER-12XX requires area ruling. The concepts of area ruling are not clear in Roskam and that is the reason only the Mach cone angles are determined and they are as follows

- Mach Cone Angle for $M = 1$ is 25 degrees
- Mach Cone Angle for $M = 0.84$ is 56 degrees

10.6 AIRPLANE DRAG POLARS – CALCULATED USING AAA SOFTWARE:

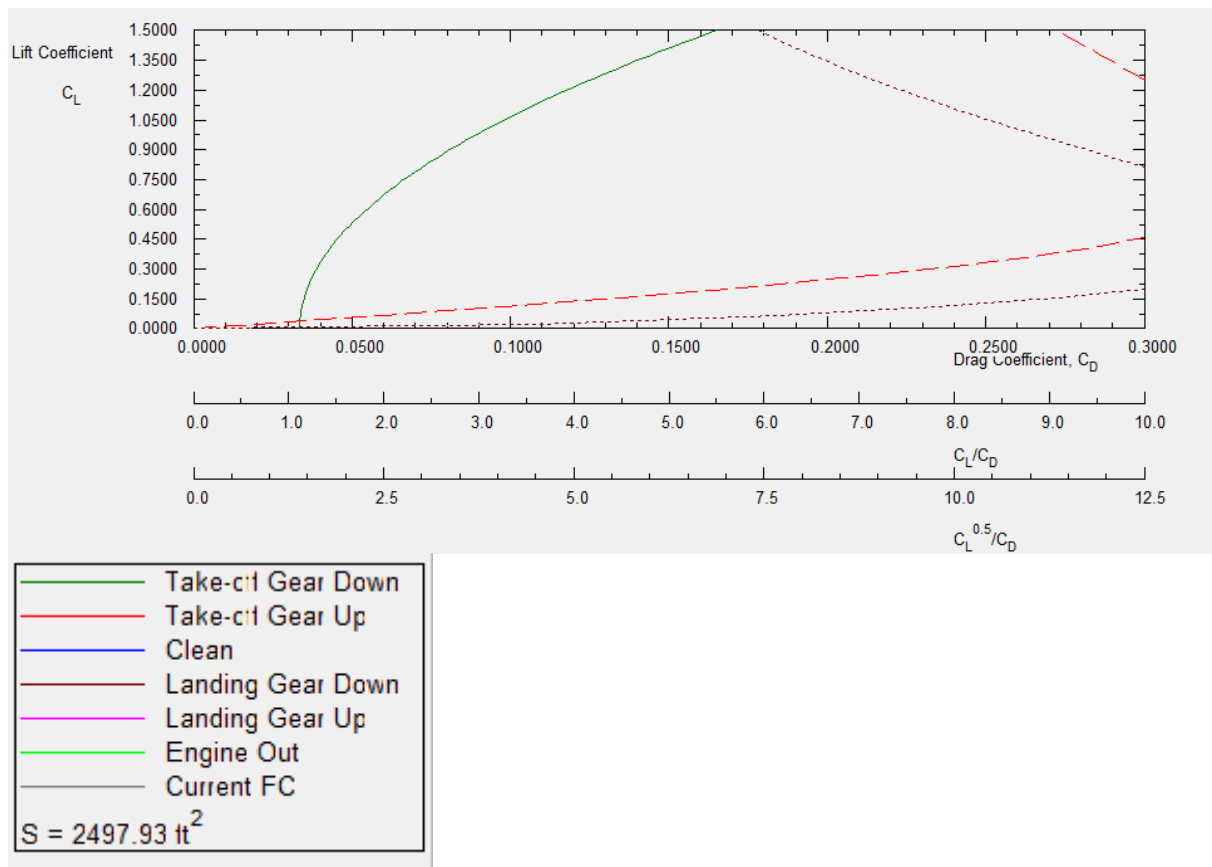


Figure 133: Take-off Gear Up Drag Polar

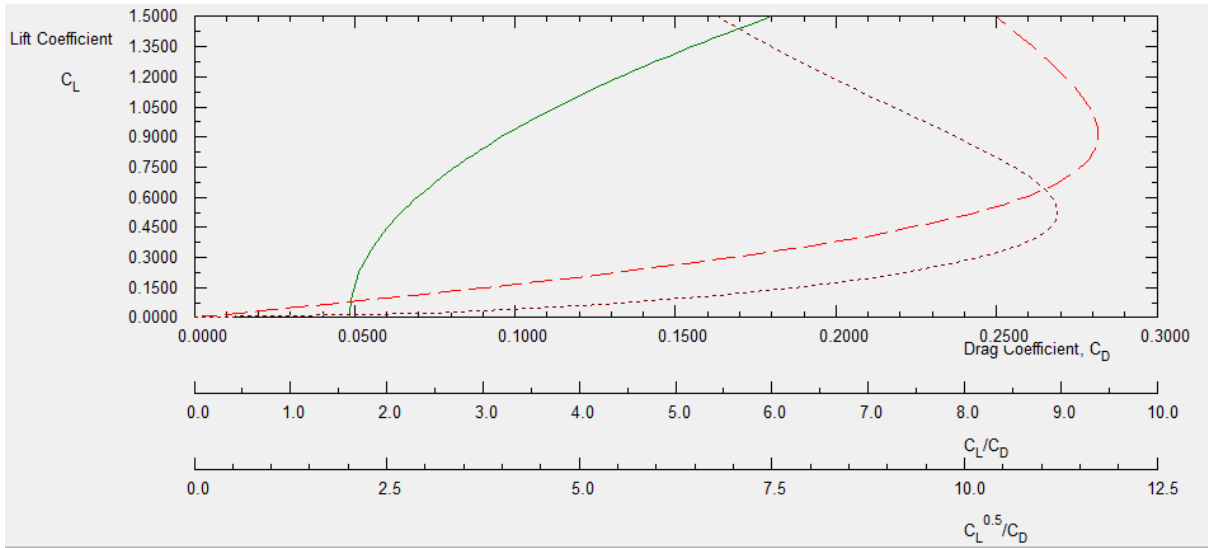


Figure 134: Take-off Gear Down Drag Polar

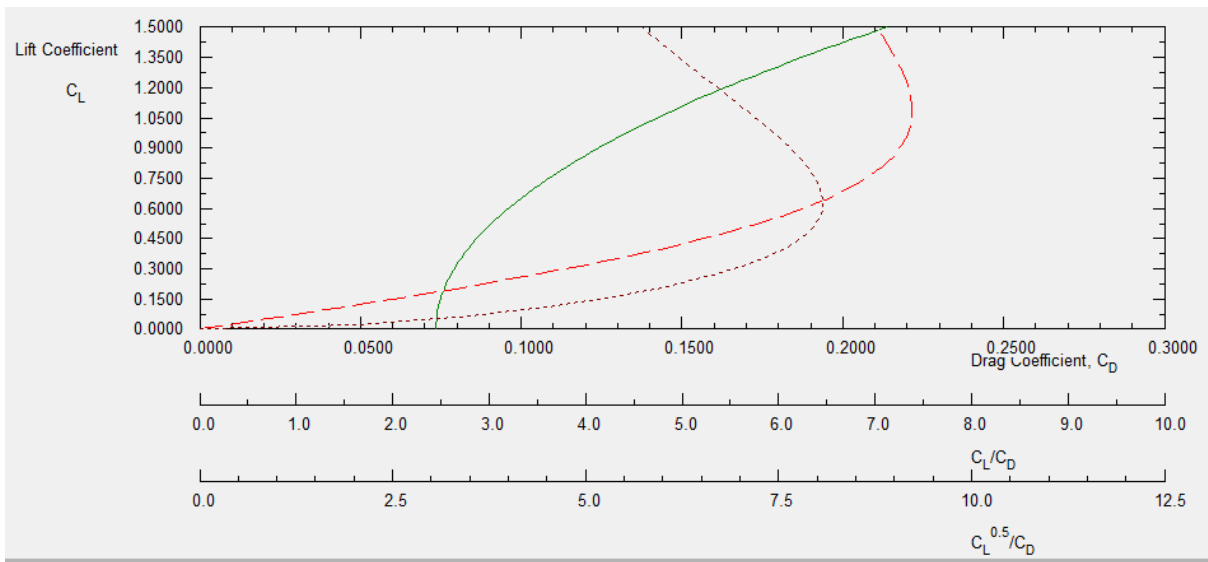


Figure 135: Drag Polar during Landing Gear 'UP'

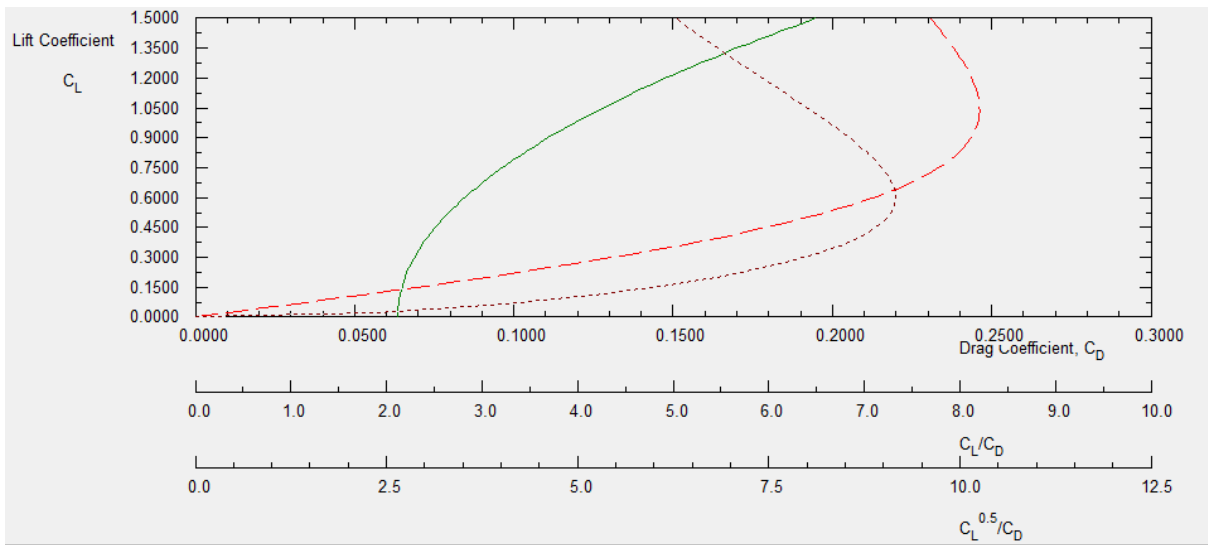


Figure 136: Drag Polar-One Engine Inoperative

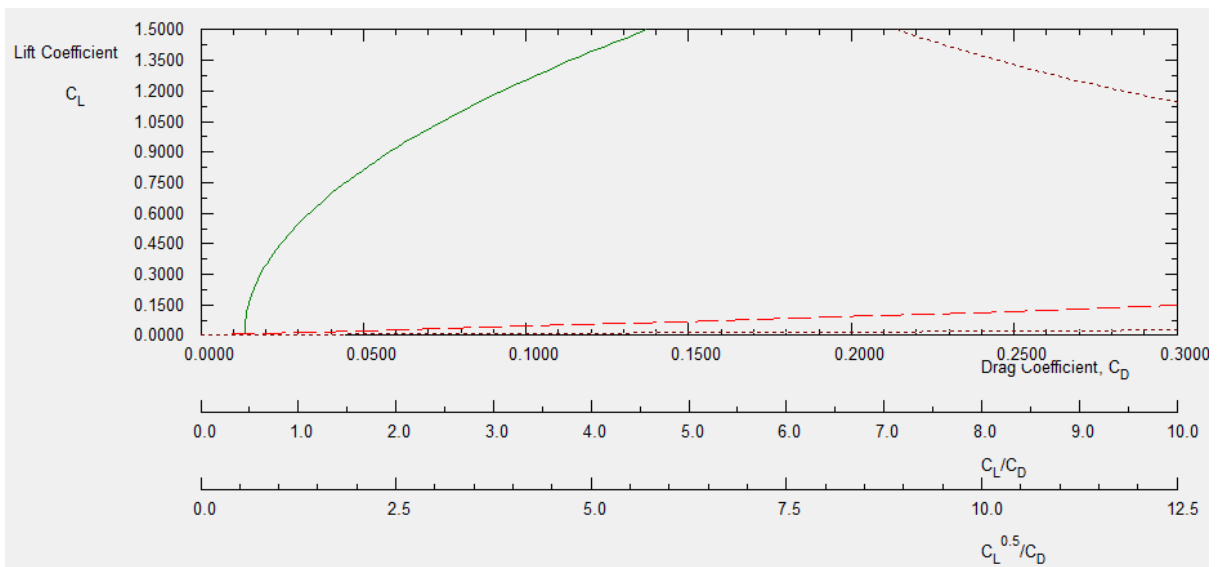


Figure 137: Clean Configuration Polar

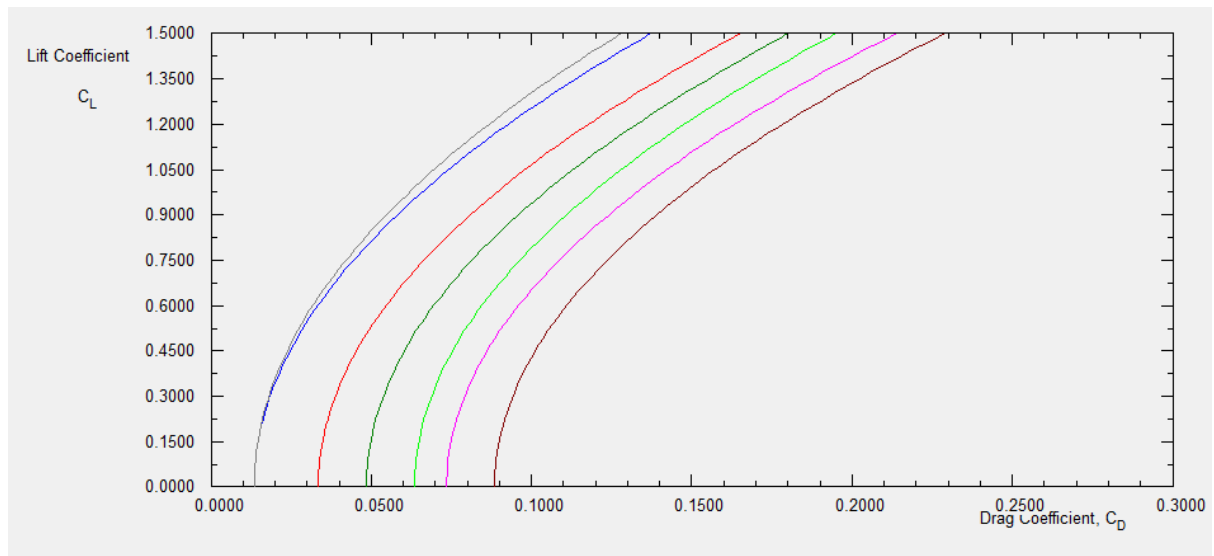


Figure 138: All Flight Conditions Drag Polar

10.7 DISCUSSION:

The drag polar gives us an understanding on the component wise drag determination. In this chapter, there are few assumptions related to the Prandtl Glauert equation are made i.e. this equation can produce the drag increment value at any point in the flight which doesn't hold when the aircraft reaches higher Mach number. Since the determination of drag polar is a class I method it does consider only few components and does not account for the realistic drag values. Also for the ease of calculations the drag increments due to the flaps are considered only those related to plain configurations but the VER-12XX uses slotted flaps. So, for this purpose the plain flap drag value is multiplied by 0.36 to get the corrected drag increments generated by the slotted flaps. The compressibility factor calculations are also limited because of their complexity in determining the crest critical Mach number of the air foil section. Drag polar is the last step in the preliminary aircraft design sequence for class I. These drag values related to aircraft components are very useful in understanding the aerodynamic behaviour of the proposed aircraft configuration. Also, the importance of area ruling during the high subsonic speeds without cutting down on the total surface area is well understood. This data is further used in the class II evaluations of VER-12XX to finish the computational and theoretical design analysis.

CHAPTER 11

CLASS-II: WING

Class-I sizing is a preliminary estimation process where few aircraft parameters were locked and there would not be a chance to revisit them as this affects the whole aircraft design. That was a crucial design phase and it requires precision in the procedures adapted for calculations as it has direct impacts on further sizing the aircraft. The key aircraft components had already been studied besides discussing their merits and demerits. For commercial aviation, safety is an important factor and it is the job of the designers to scale the functionality of each component to utmost precision as possible. In Class-I sizing, VER-12X configuration selection and primary calculations provided us with improved payload carrying capabilities and aerodynamics. Since this method involves at least 60% percent estimations from available technical data, Class-II sizing allows us to study lot more into the details of the proposed configuration which could also requires iteration process if any changes should be made.

In this design chapter, the proposed wing configuration from Chapter 6 of p.d.I will be analysed through broad range of considerations. The aerodynamics, drag contributions, structural integration to the fuselage, operational limits and mechanism of the flaps are the primary focus points in this design chapter where each component will be studied, and necessary correction will be made to produce a more robust wing design.

11.1 WING CONFIGURATION:

During Class-I sizing, key aspects of the wing (aspect ratio, incidence angle, sweep angle, taper ratio, area and air foil characteristics) have already been determined and documented. These values have been determined based on assumptions especially from current similar aircraft technical data. In this section, the proposed wing characteristics from Class-I to further evaluate the wing design. As mentioned in Class-I sizing, the configuration for VER-12X is a cantilevered low wing with dihedral and sweep back. The possibilities of using a Braced wing structure had already been discussed and for a passenger jet it is not a viable option to only consider weight as a primary factor though the Braced wing offers other advantages which on comparison the Cantilevered Wing structure do not. Wing is the primary lifting component of an aircraft, which accounts for the over-all handling capabilities, manoeuvrability and stability of the aircraft. In the following sections, a thorough analysis considering the aerodynamic effects of the proposed wing will be documented.

11.2 DESIGN ASPECTS:

11.2.1 WING LOADING:

For an aircraft, the wing size depends on the mission requirements followed by the performance criteria and it has a huge impact on various parameters. In Class-I sizing, wide range of possibilities have been determined for the selection of an optimum thrust loading for a wing loading but the study has been limited to certain assumptions and calculations leaving behind the individual effects of other factor which ultimately impacts VER-12X overall performance. **Since the critical parameters for VER-12X being take-off and stall speed, the favourable thrust loading for a for a stall speed of 125 kts is 0.25* and this gives us a wing loading of 127 lbs/ft².** These had already been determined and discussed in Class-I sizing. It is important to study the primary effects of the following characteristics individually to further understand the proposed wing design and to ensure proper wing sizing.

- Take-off
- Cruise
- Riding Qualities
- Weight

11.2.2 TAKE-OFF / LANDING FIELD LENGTH:

For shorter take-off lengths, large wings (smaller wing loading) are comparatively better than smaller wings (high wing loading). Wing size can be kept relatively small by using flaps, which provides us the possibility to attain maximum lift coefficient. It is important to study this characteristic as it determines the overall weight and is responsible for the overall performance of the aircraft.

The landing field length for a given C_{lmax} and wing loading is determined using the equation:

$$s_{TOFL} \propto \left(\frac{W}{S} \right)_{TO} \left\{ \sigma * C_{LMAX_{to}} * (T/W)_{TO} \right\} = TOP_{25} \quad (11.1)$$

$$\Rightarrow s_{TOFL} = 37.5 \left(\frac{W}{S} \right)_{TO} \left\{ \sigma * C_{LMAX_{to}} * (T/W)_{TO} \right\} = TOP_{25} \quad (11.2)$$

$$\Rightarrow s_{TOFL} = 37.5 * TOP_{25}$$

The Take-off field length for a given C_{lmax} and wing loading is determined using the equation:

$$s_L = 429 * \left(\frac{W}{S} \right)_{TO} / C_{LMAX_{LANDING}} \quad (1.3)$$

Clearly from equation 1.2 and 1.3 it can be observed that both the landing and take-off field lengths are inversely proportional to C_{lmax} which an increase in one parameter would decrease the value of other i.e. an increased C_{lmax} results in shorter take-off runs and landing. In part 1 of this project, the estimated landing and take-off field lengths are 5540 ft., 10000 ft. Table 19,20 helps in understanding the effects of C_{lmax} on the landing and take-off lengths for a given wing loading. It is observed that an increase in C_{lmax} increases the aircraft requires shorter field lengths and as the wing-loading increases it is required to carry shorter wing which would be heavier. To account for an optimum wing loading a trade study must be carried and this is clearly document in Figure 139, 140. For a conventional aircraft which requires higher wing loadings a C_{lmax} of 1.6 during take-off and a C_{lmax} of 2.6 during landing are favourable.

Note: The C_{lmax} values specified are only for clean wing configuration (no flaps or slats). The effects on further integrating the Wing with additional lift generating components will be studied in the further sections.

Table 18: Take-off field Length for a given Wing loading at respective Maximum Lift Coefficient

Wing Loading	C_{lmax}	Thrust Loading	Take-off Field Length (ft)
0	1.2	0.55	0
10	1.2	0.55	568.1818
20	1.2	0.55	1136.364
30	1.2	0.55	1704.545
40	1.2	0.55	2272.727
50	1.2	0.55	2840.909
60	1.2	0.55	3409.091
70	1.2	0.55	3977.273
0	1.4	0.73	0
10	1.4	0.73	366.9276
20	1.4	0.73	733.8552
30	1.4	0.73	1100.783
40	1.4	0.73	1467.71
50	1.4	0.73	1834.638
60	1.4	0.73	2201.566
70	1.4	0.73	2568.493

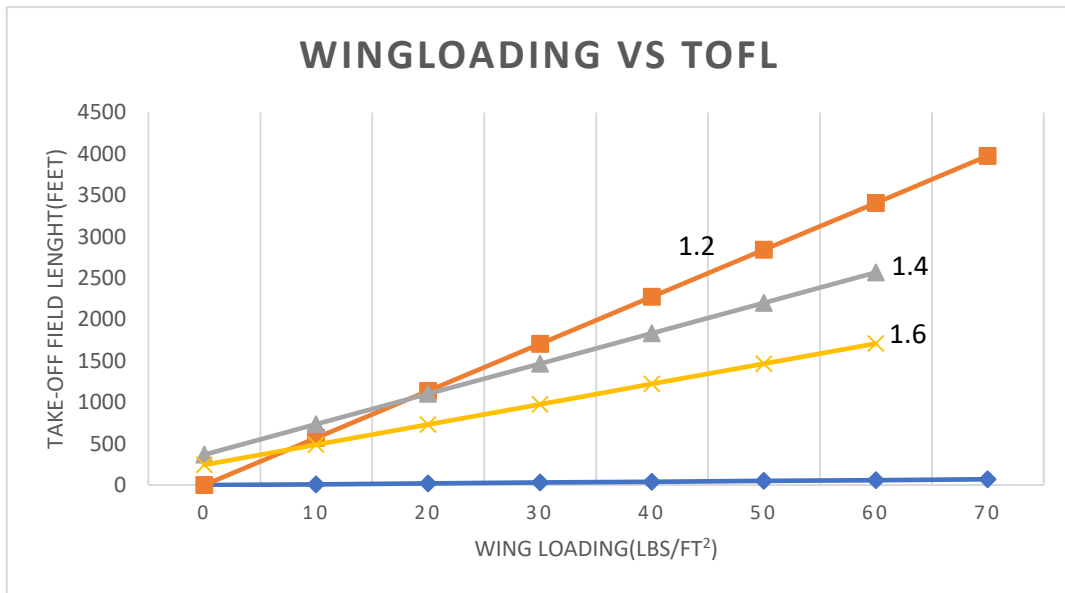


Figure 139: Take-off field Length for a given Wing loading at respective Maximum Lift Coefficient

Table 19: Landing field Length for a given Wing loading at respective Maximum Lift Coefficient

Wing Loading	C _L	Landing Field Length
0	2	0
10	2	2145
20	2	4290
30	2	6435
40	2	8580
50	2	10725
60	2	12870
70	2	15015
0	3	0
10	3	1430
20	3	2860
30	3	4290
40	3	5720
50	3	7150

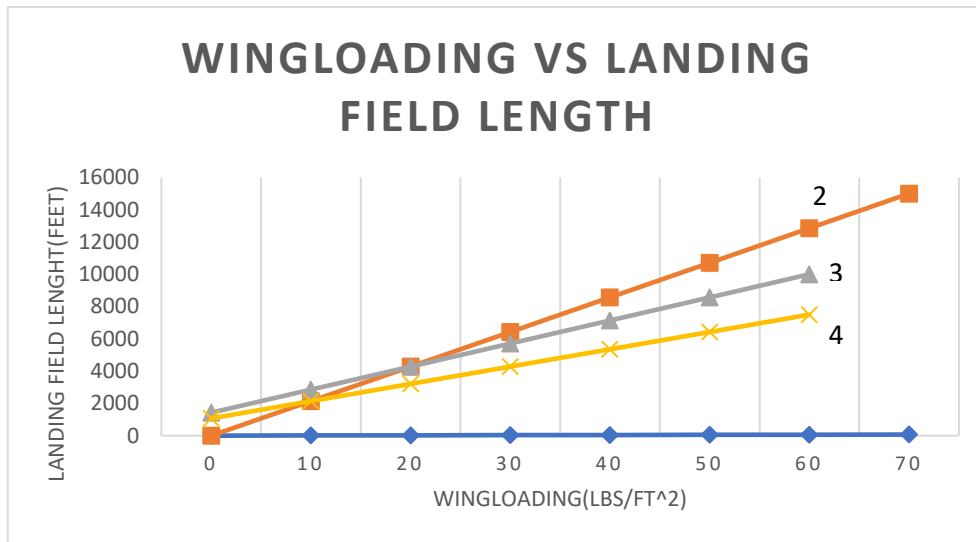


Figure 140: Landing field Length for a given Wing loading at respective Maximum Lift Coefficient

11.2.3 CRUISE

It is an advantage to maintain a cruise $C_{l_{max}}$ closer to the proposed value. To do that the proposed configuration must have higher wing loading and if the aircraft is required to cruise at higher altitudes but at moderate speeds, a larger wing area is required. The effect of wing loading on the $(L/D)_{max}$ can be studied using the equation 1.4.

$$\left(\frac{L}{D}\right)_{max} = \sqrt{\frac{\pi Ae}{4C_{D_0}}} \quad (11.4)$$

With:

$$C_{D_0} = (1/S) * \text{invlog}_{10} [a + b \log_{10} \{(\text{invlog}_{10}(c + d \log_{10} W_{TO})) + k_{ww}(S - S_{baseline})\}] \quad (11.5)$$

Table 20: Determining the Coefficient of Drag using the parameters specified in Equation 1.5 for variable Wing loading

Wing Loading	a	b	c	d	k _{ww}	W _{to}	e	Ar	S _{base}	S(feet)	C _{d_o}	(l/d) _{max}	C _l /d _{max}
80	-2.5529	1	0.0199	0.7531	1.85	160800	0.8	9.61	2010	3982	0.063	10	15
100	-2.5529	1	0.0199	0.7531	1.85	160800	0.8	9.61	1608	3982	0.007	30	5
120	-2.5529	1	0.0199	0.7531	1.85	160800	0.8	9.61	1340	3982	0.005	37	4
140	-2.5529	1	0.0199	0.7531	1.85	160800	0.8	9.61	1149	3982	0.004	40	4
160	-2.5529	1	0.0199	0.7531	1.85	160800	0.8	9.61	1005	3982	0.003	42	3
180	-2.5529	1	0.0199	0.7531	1.85	160800	0.8	9.61	893	3982	0.003	44	3

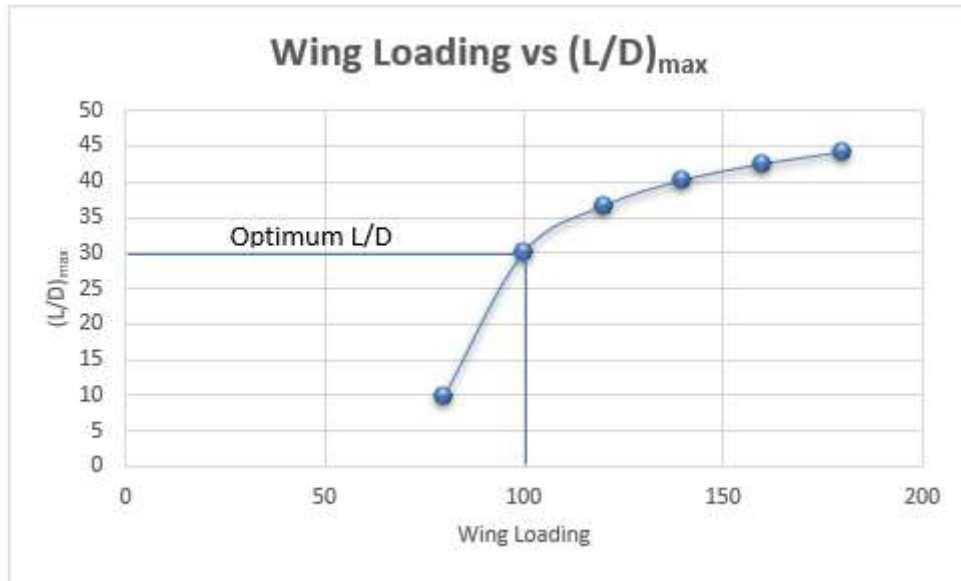


Figure 141: Wing Loading versus L/D max

11.2.4 Ride Qualities:

The ride quality of the aircraft is significantly affected as the wing loading increases. The relation between the ride quality and wing loading is given by:

$$n_{\alpha} = \frac{\bar{q} C_{L_{\alpha}}}{(W/S)} \quad (1.6)$$

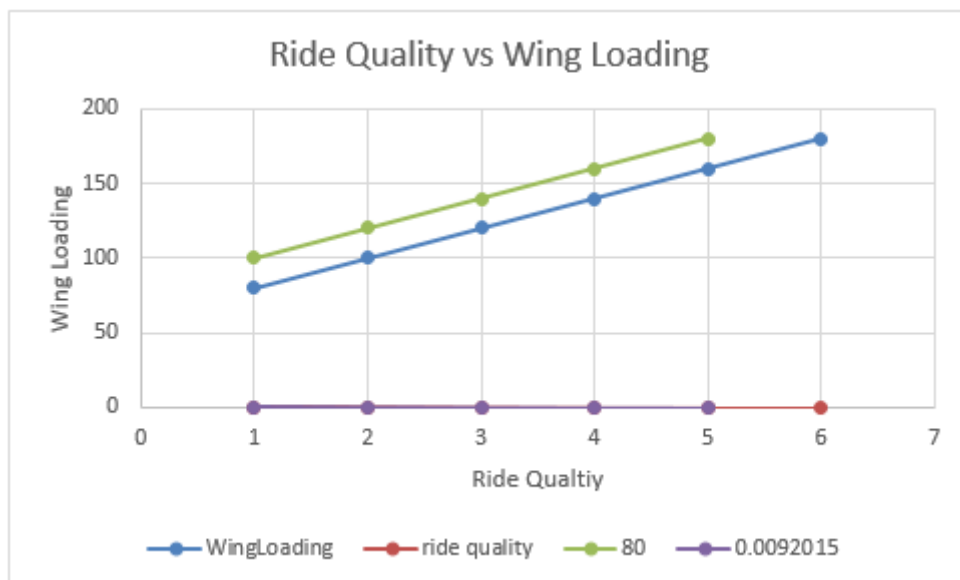


Figure 142: Ride Quality versus Wing loading

11.2 WING CONFIGURATION

Wing configuration play an important role in the overall lift for the aircraft. This is a section where the key aspects of the wing will be thoroughly analysed. Conventional aircraft has three wing placement options i.e. high, low and mid wing. Each wing configuration has its own advantage and disadvantages. In general aviation, most aircraft have high wing configuration. Few examples for high wing aircraft are Cessna 172,310.



Figure 143:High Wing Configuration - Cessna 172

High wing configuration offers effective ground clearance and better view for the pilot especially while searching for landmarks and runways. It can also be the best configuration especially for the trainers and does not become a barrier for airport equipment. In this configuration, a pilot can have a visibility of 270 degrees. An aircraft with high wing configuration will have high stability. Since the centre of gravity is below the wing and when the aircraft banks the natural tendency will make the wings level reducing the pilot' effort.

On the other hand, Low wing configuration is also the most commonly used in general aviation aircraft. Compared to the high wing the low wing configuration are not inherently stable as the centre of gravity is above the wing. For this a dihedral angle, must be used for the wings to compensate for stability. This configuration is also used for aircraft cursing at high subsonic speeds. Few examples for high wing configuration are Cessna 400 Corvails, Mooney M20.



Figure 144: Low Wing Configuration -CRJ1000

The low wing with retractable landing gear into the fuselage means a shorter gear. The result is gear easily being fitted into the wing with minimum weight of the gear structure. Since, the proposed aircraft is used for passenger travel this wing configuration will keep the aircraft afloat during an event of ‘ditching’.

Mid wing configuration is the least commonly used for the aircraft. The major problem for its rarity is that this wing configuration requires spars, which run through the fuselage. This removes the necessary space for payload and interferes with passenger seating. To avoid spars running through the fuselage additional structures must be integrated; which adds extra weight to the aircraft. In addition, the landing gear must be longer and retracted into the fuselage instead of the wing. The mid-wing configuration is better than low-wing in terms of stability as it produces less interference drag, which increase the lift to drag ratio, and hence the range. Few examples of mid-wing aircraft are Piper Aerostar, FJ 100.



Figure 145: Mid Wing Configuration -NASA Research Plane

Air foil Selection:

Wing configurations are responsible for the aircraft total lift and they vary as per the mission requirements. For VER-12X, a super critical airfoil is being for the wing configuration. A supercritical airfoil reduces the wave drag with highly cambered surface towards the aft. Figure16 shows us the supercritical airfoil section with its important graphical representation of aerodynamics forces in Figure 17,18. A symmetrical airfoil can be used but the drag rise

characteristics increases with increase Mach number and it is highly unfavorable for aircraft cruising at high subsonic speeds as the lift slope curve is higher which means the chances for attaining the required C_{lmax} are very rare. This also reduces the overall cruising altitude of the aircraft that means the aircraft must expend fuel at higher rates making it less fuel-efficient. Figure 8, 9 helps in understanding symmetrical and cambered airfoil section in terms of stability.

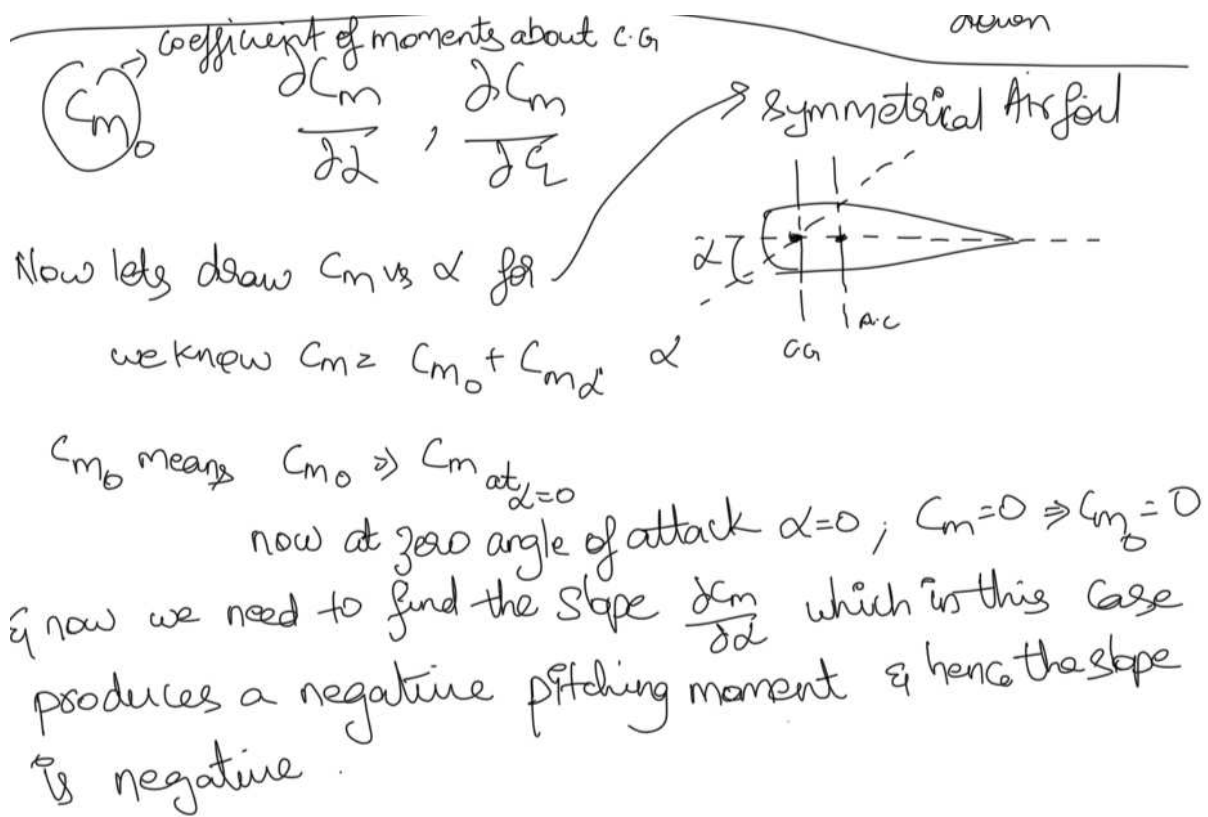
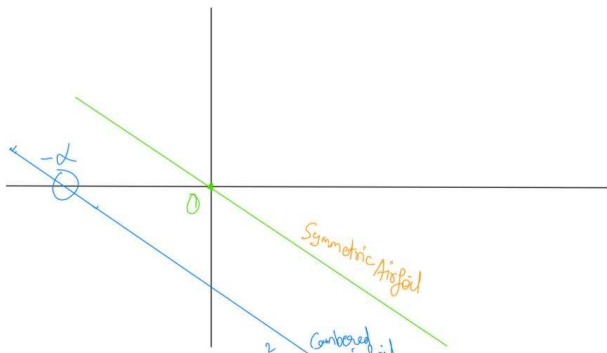


Figure 146: Symmetrical Aerofoil in Stability terms

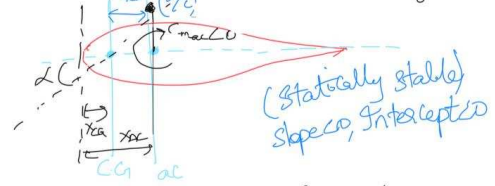
Now lets draw the C_m vs α

Wing

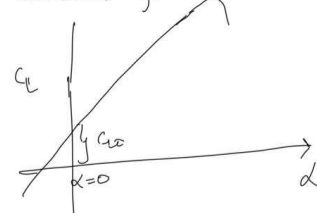


for a cambered airfoil we can trim at + angle of attack so we use reflex airfoil.

Now lets us consider a cambered airfoil



lets plot the same C_m vs α for a cambered airfoil at $\alpha=0$



$$C_{m_{total, \alpha=0}} = C_{m_{at, w}} + \underbrace{(\bar{X}_{cm} - \bar{X}_{Ac})}_{< 0} C_L$$

lets therefore C_m

Figure 147: Symmetrical, Cambered Aerofoils in stability terms

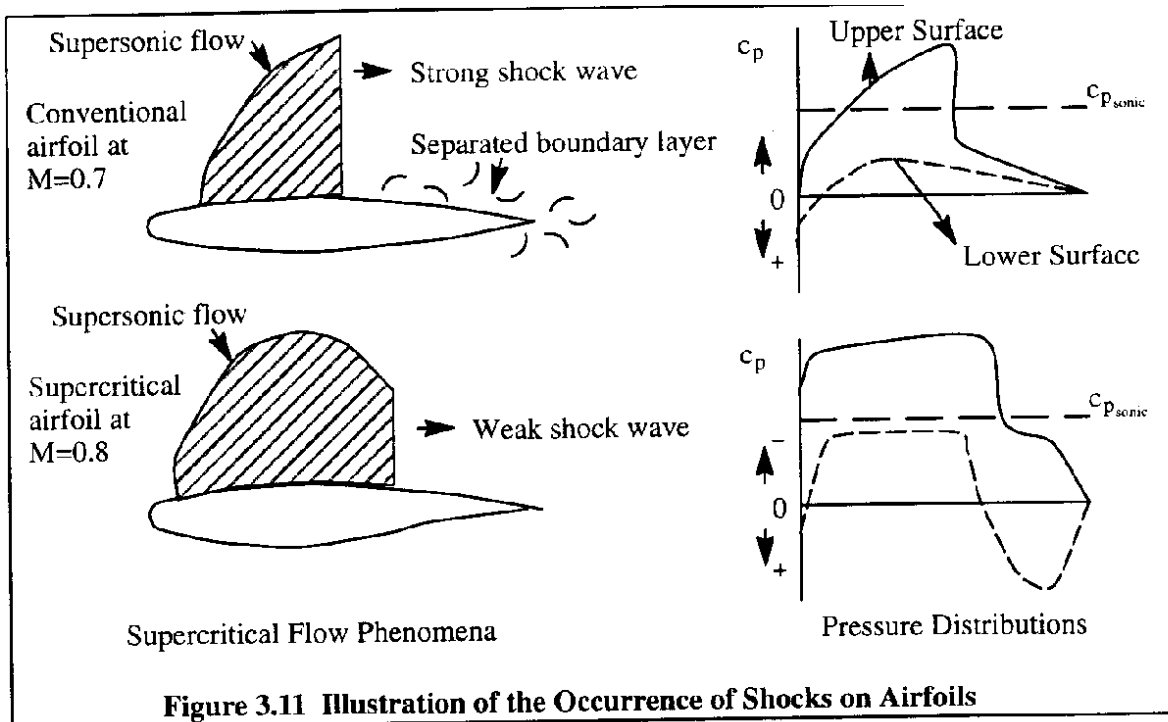


Figure 3.11 Illustration of the Occurrence of Shocks on Airfoils

Figure 148: Conventional and Supercritical Aerofoils Shock Wave separation and Pressure Distributions

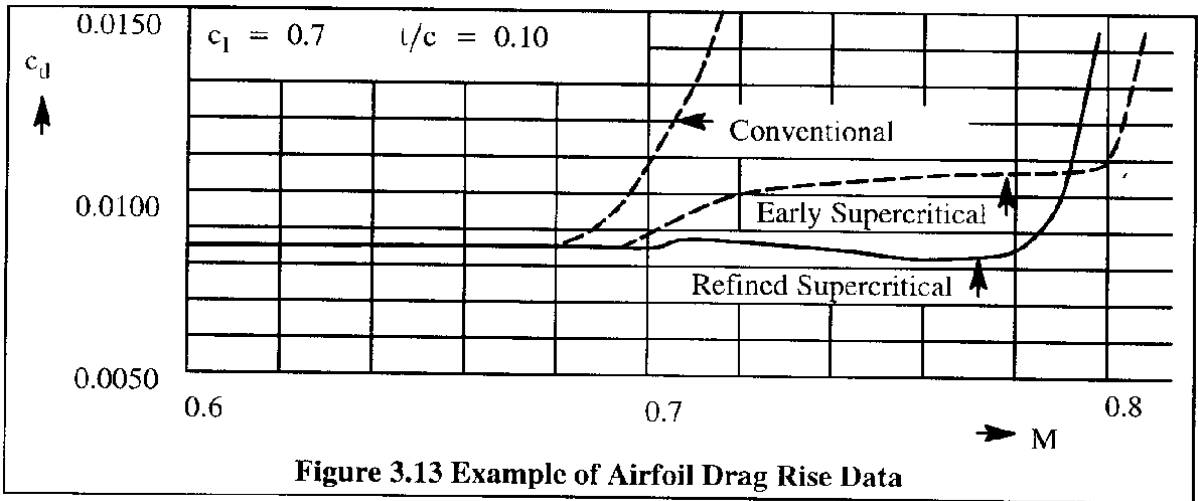


Figure 149: (Conventional, Supercritical) Aerofoil Drag Rise data as the Mach number Increases

Figure 10 helps in understanding the shock induced boundary layer separation of conventional and supercritical aerofoil. The supercritical aerofoil has a flattened upper surface and is the primary reasons for delaying the wave drag. This results in the shock wave delays when an aircraft is travelling in the transonic speed range. Unlike conventional aerofoils, from figure 11, supercritical aerofoils, helps to travel at higher mach.

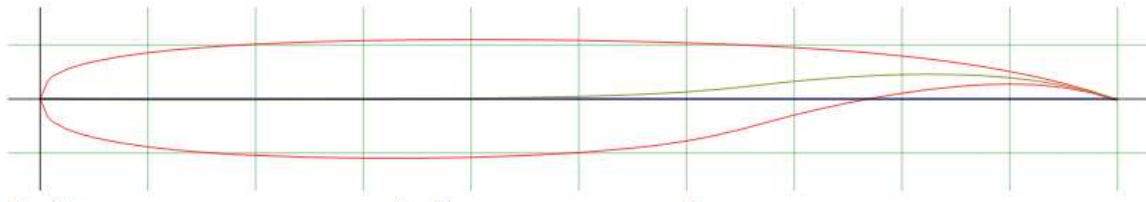


Figure 150: Super Critical Air Foil Section

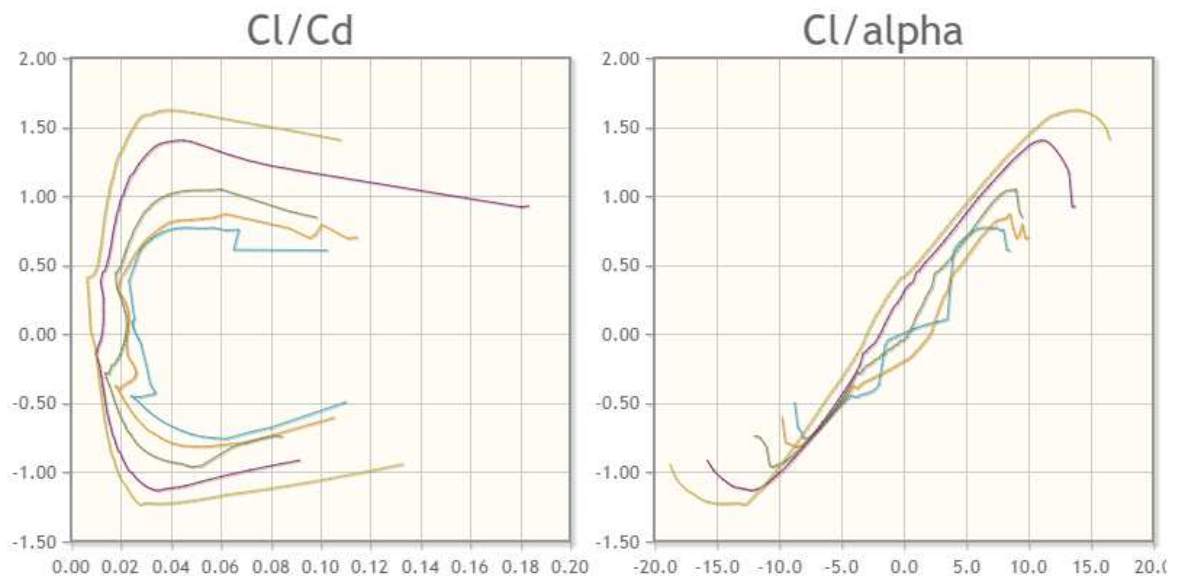


Figure 151: Coefficient of lift versus drag, Coefficient of lift versus angle of attack

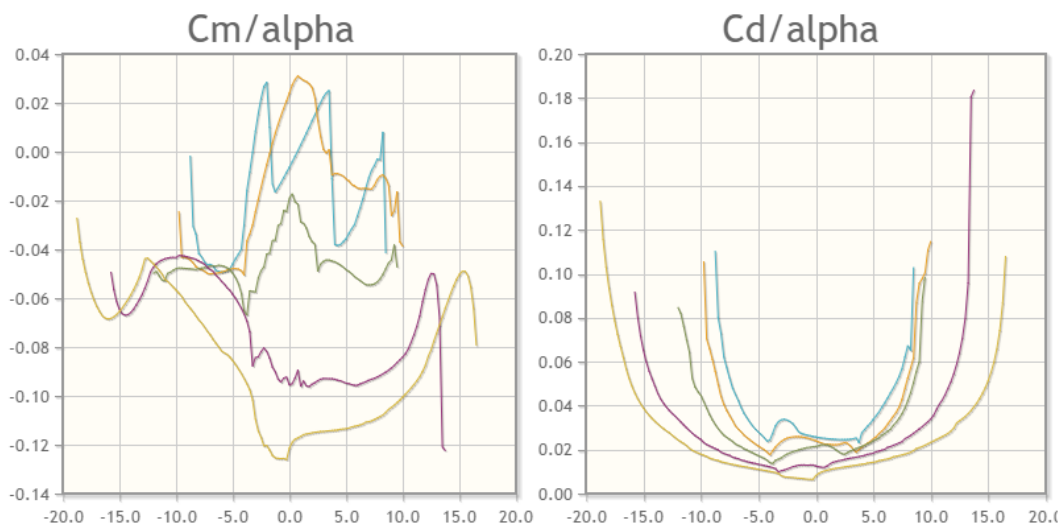


Figure 152: Coefficient of Moments versus drag, Coefficient of Drag versus angle of attack

A supercritical aerofoil cross section could be advantageous for a commercial aircraft, which are nearing speeds of Mach 1. It is a known fact that, when an aircraft is approach Mach1 with conventional wing; airflow on the top of the wing is increased reducing laminar flow, which results in shock wave generation. However, when a supercritical aerofoil is used, a delayed shock wave greatly enhances the fuel efficiency with significant drag reductions.

11.3 SWEEP ANGLE:

Swept back wings are profoundly seen in high subsonic (transport) and supersonic aircraft. The primary reasons for using sweep for aircraft wings are to improve the take-off and landing performance, lower the drag, improve the handling capabilities when flying at high speeds and to achieve an optimum L/D ratio throughout the flight performance envelope. Figure 15 is a typical swept back wing arrangement and the free stream velocity is perpendicular to the wing. Sweep introduces an angle which resolves the velocity into two components:

- Velocity component along the Chord ($V_0 \sin \Lambda$)
- Velocity component along the Span ($V_0 \cos \Lambda$)

The point of interest is the Chord wise velocity component which influences the Mach number and ultimately results shock waves. However, designers always aim to reduce this velocity component to reduce the shock waves generated due to the requirement of high subsonic and transonic speeds. This ultimately leads to drag and early boundary layer separation which results in strengthened shock waves. Sweep also influences the lift-curve slope and this is clearly shown in figure 18 which means that when an aircraft with no sweep can achieve higher C_{lmax} at relatively less angle of attacks, but opposite is the case with sweep which requires higher angle of attack to attain higher C_{lmax} .

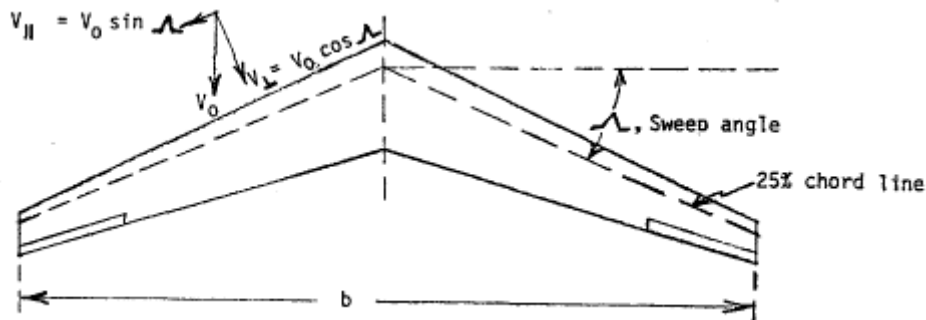


Figure 153: Sweep Angle Definition

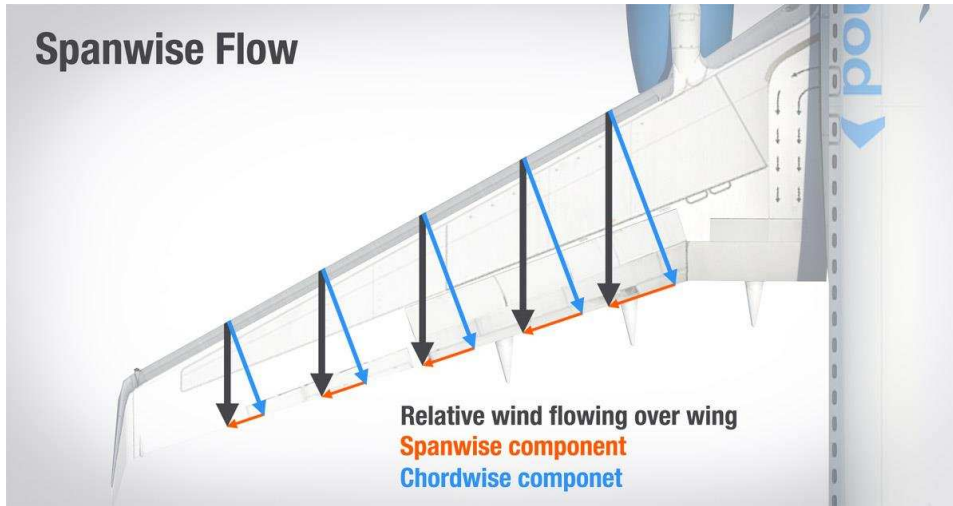


Figure 154: Airflow over a Swept Wing

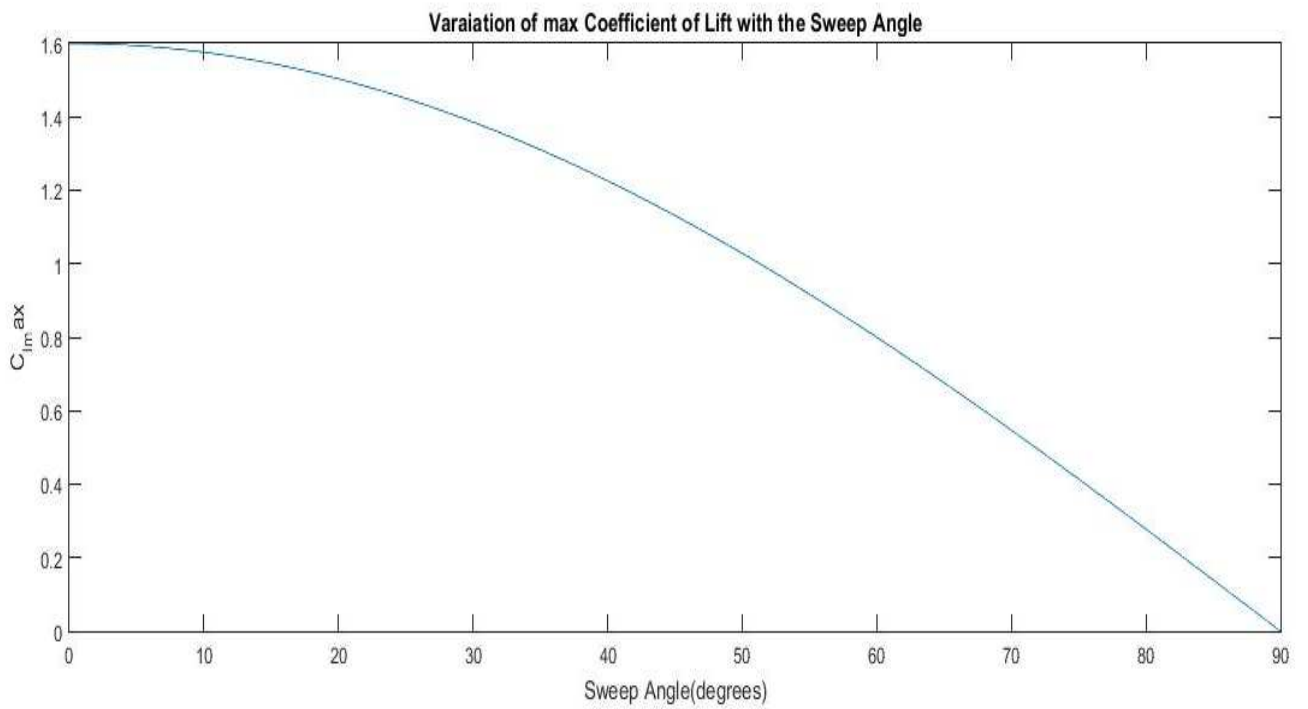


Figure 155: Variation of Max Lift Coefficient with Sweep Angle

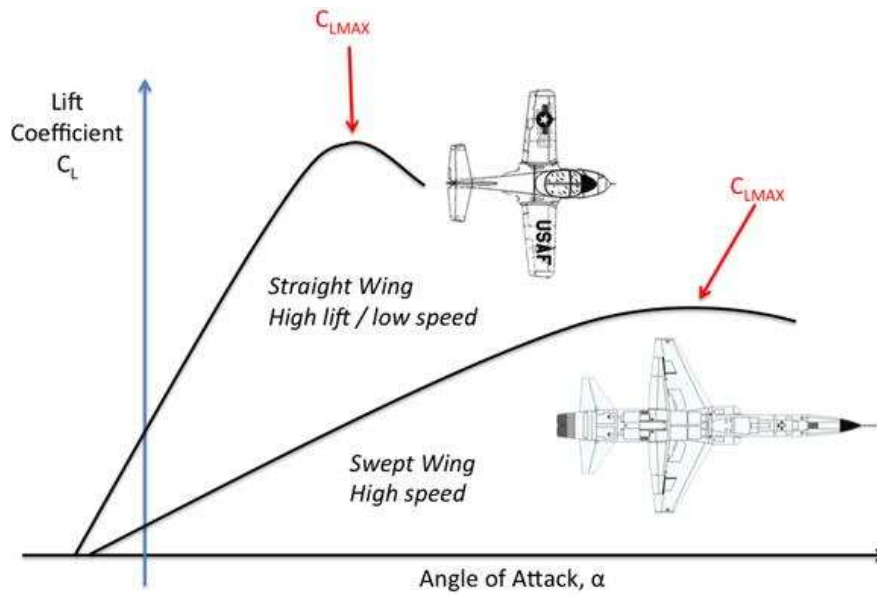


Figure 156: Straight and Swept Wing Lift-Curve Slope

The variations of max lift coefficient with the increasing sweep angle is clearly illustrated in figure 156. The $C_{L_{max}}$ decreases with an increase in sweep angle and this is because of the chord wise velocity component involving a COSINE. Through this we can conclude that a straight wing offers best $C_{L_{max}}$ than a swept back wing except for the fact that shock waves quickly appear when travelling at high subsonic speeds. For VER-12X a sweep angle of 35° is preliminarily chosen and the suppositions clearly proves that this sweep angle can be considered favourable while compromising on factors such as wing weight and stall behaviour.

11.4 WING ASPECT RATIO:

An aircraft wing aspect ratio is defined as:

$$A = \frac{b^2}{S} \quad (11.7)$$

Where b = Wing span

S = Wing Area

In p.d.I from Chapter 6, the proposed aspect ratio for VER-12X is 9.61 and this value is an estimate from the current narrow body aircraft data. For Class II, the effects of aspect ratio on some of the key aerodynamic and weight parameters of VER-12X are to be studied. This is one of the crucial areas which dictates the overall wing weight and helps in understanding whether the proposed estimate is an ideal value for the proposed wing design.

- **Induced Drag:** Wings with higher aspect ratio tend to lower induced drag but this comes with a penalty posed by C_{lmax} i.e. the aircraft either must travel at lower speeds or at higher altitude.
- **Lift Curve Slope:** Wings with highest aspect ratio tend to have high lift curve slopes which means that the aircraft can travel at high C_{lmax} at relatively lower angles of attack, but the riding quality is reduced through turbulence.

Table 21: Wing Weight comparison with and without Sweep using GD Method from 'Roskam' part V

(General Dynamics) GD METHOD	Values	Units
S (Aspect Ratio)	3982	Ft ²
A (Wing Area)	9.61	
M_H (Maximum Mach Number at Sea-Level)	0.74	
W_{to} (Take-off weight)	160800	lbs
Load factor	4	
Taper Ratio	0.15	
t/c (Max Thickness Ratio)	0.149	
Sweep Angle ($\Lambda_{1/2}$)	17.5	degrees
W_{wing(sweep)}	15478	lbs
W_{wing(no- sweep)}	14389	lbs
Spoilers and Speed Brakes (2%) (sweep)	15788	lbs
Spoilers and Speed Brakes (2%) (no sweep)	14676	lbs
Two Wings mounted reduce the weight by 5 percent(sweep)	14704	lbs
Two Wings mounted reduce the weight by 5 percent (no sweep)	13669	lbs
For fowler flaps add 2%(sweep)	15788	lbs
For fowler flaps add 2%(no sweep)	14677	lbs

- **Weight:** As the aspect ratio increases the wing weight increases and an illustration of wing weight determined using G.D. method is shown in Table2.
- **Span:** As the span increases the aspect ratio of the wing increases. Now-a-days aircraft use shark lets or winglets to increase the effective aspect ratio of the wing. Previously, designers thought of a new wing design to increase the aspect ratio but this implies increased weight which ultimately leaves them with no option rather than to retrofit the wing. To increase the L/D ratio of an aircraft it is often better to add winglets or shark lets to an existing wing which increases the aspect ratio of the aircraft.



Figure 157: United Airlines Boeing737 Winglets located at Wing tips

11.5WING THICKNESS RATIO:

The thickness ratio primarily effects the following characteristics:

- **Drag:** As the thickness ratio increases there is a profound effect on the profile drag especially in the subsonic flight regime. This is also means that increased wave drag in the transonic and supersonic flight regime. For this reason, supercritical aerofoils are used which allows us to use higher thickness ratios and aids in maintaining the required high subsonic Mach. Figure 2 is clear illustration of the wave drag versus Mach and it is to be noted that the thickness ratio² is directly proportional to wave drag through which an increase in thickness ratio the wave increases at rapid rates.
- **Weight:** Increased thickness ratio decreases the overall wing weight as the bending and torsional stiffness of the wing increases. The wing weight is computed using G.D. method from ‘Roskam’ partV, and is clearly listed in table 2.
- **Maximum Lift**
- **Fuel Volume**

11.6 WING TAPER RATIO:

Wing taper ratio is defined as the ratio of tip chord to root chord:

$$\lambda = \frac{c_t}{c_r} \quad (11.8)$$

Where c_t = tip chord

c_r = root chord

The taper ratio of aircraft wing primarily effects the following:

- **Weight:** Observing the lift curve slope clearly shows that the lift distribution tends to be not very effective at the wing tips which means a wing with taper ratio 1 will reduce the effective area and weigh more when compared with wings having a smaller taper ratio.
- **Tip Stall:** It is one of the dangerous stall condition which limits the aircraft manoeuvrability and may lead to crash. Tip stalls occur when an aircraft is moving too slow or rolls at high speeds and this again depends on wing shape. As the aircraft rolls at higher speeds the tip travels faster than the root and even a small movement of the yoke stick will result in quick movements. Wings with small taper ratios will have small tip chords which implies lower Reynolds number and lower coefficient of lift. This further exaggerates the tip stall. For this purpose, vortex generators, washout or stall fences are used. VER-12X will have Shark lets integrated at the wing tips.



Figure 158: Wing Tips with and Without Winglets

- Fuel Volume
- Cost

11.7 TWIST ANGLE:

The twist angle primarily effects wing tip stall, wing weight and induced drag. This is responsible for using 'wash-out' for VER-12X wing. If wash out is used the root is generally placed at high incidence angle relative to the tip which is an advantage in swept wing configuration. During a Stall, it is highly likely that root stalls first as it is having higher incidence angle whereas the 'tips' remain un effected which plays a crucial role in aircraft manoeuvrability. For swept wings especially during a stall, the centre of pressure moves inwards towards the root which causes span wise flow, and this results in the aircraft pitch up while pushing the aircraft further into stall and this could completely make the aircraft uncontrollable. For these reasons, a wash-out plays a crucial role to avoid tip stalls. **Induced Drag** increases with the introduction of twist. Wing twist reduces the wing weight to an extent as the aerodynamic loading towards the tip reduced which shifts the centre of pressure inboard of the wing and reduced the wing bending moments which significantly reduces the weight. The wing twist angle can be found using the equation:

$$\epsilon_{twist} = i_{tip} - i_{root} \quad (11.9)$$

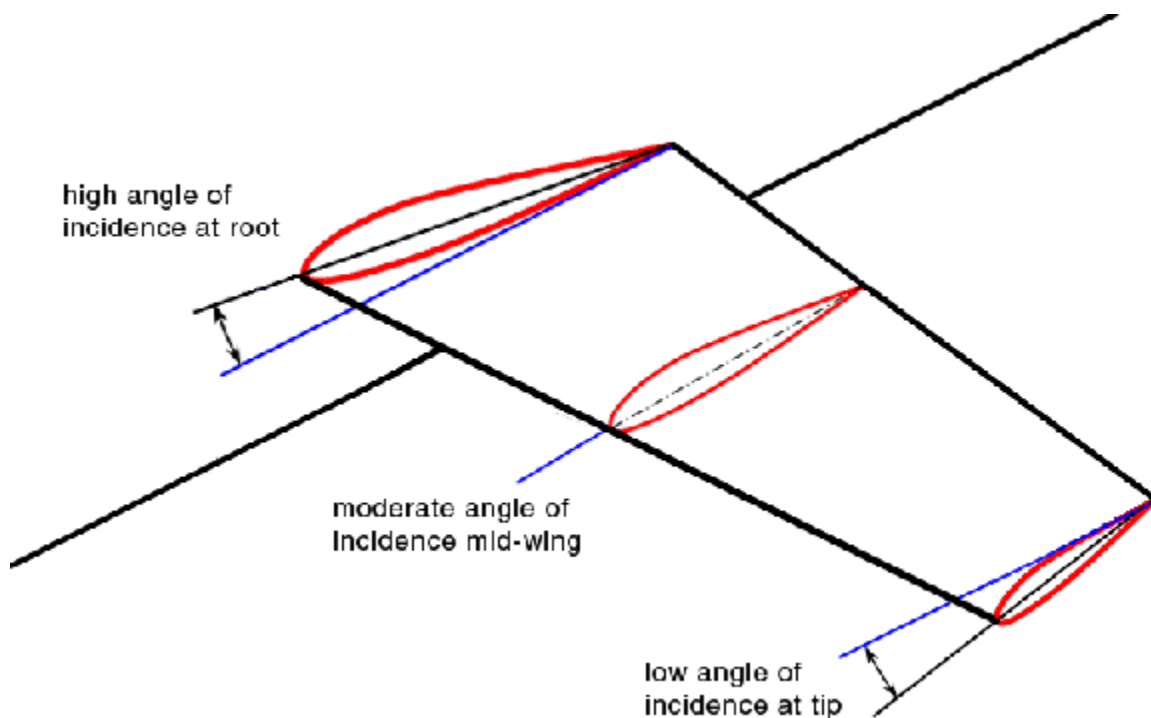


Figure 159: Incidence Angle of Wing Profile showing the Root, Mid-wing and Tip

11.8 AREA RULING:

Since VER-12X cruises at high subsonic speeds it is important to study the effects of drag rise at fuselage – wing and fuselage - empennage integration. Previously, designers faced with a challenge of reducing the wave drag whose effects are profoundly seen when an aircraft reaches Mach 1. Figure 22 shows us exactly how the drag rise characteristics comes into play without area ruling. Whitcomb came up with the concept of ‘Area Ruling’ where the effective volume of the surface remains the same but with few bulges as required. ‘Mathematically, wave drag is related to the second derivative of the volume distribution of the vehicle’ (Scott, 2002) . For a normal wing fuselage integration with no area ruling and the aircraft is required to travel at high subsonic speeds the engines must burn fuel to overcome the effects of wave drag proving a point this type of configuration must be limited to short haul travels. Reverse is the case with area ruling. Detailed study with mathematical calculations will be documented in the upcoming design chapters.

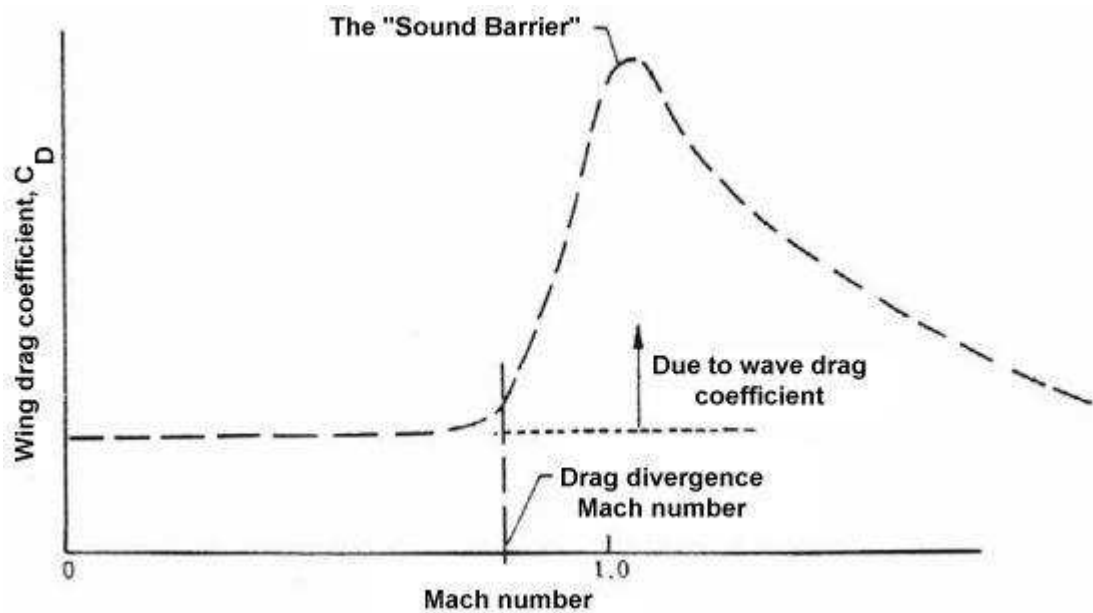


Figure 160: Wing Drag Coefficient versus Mach Number

11.9 VER-12X WING DRAWINGS:

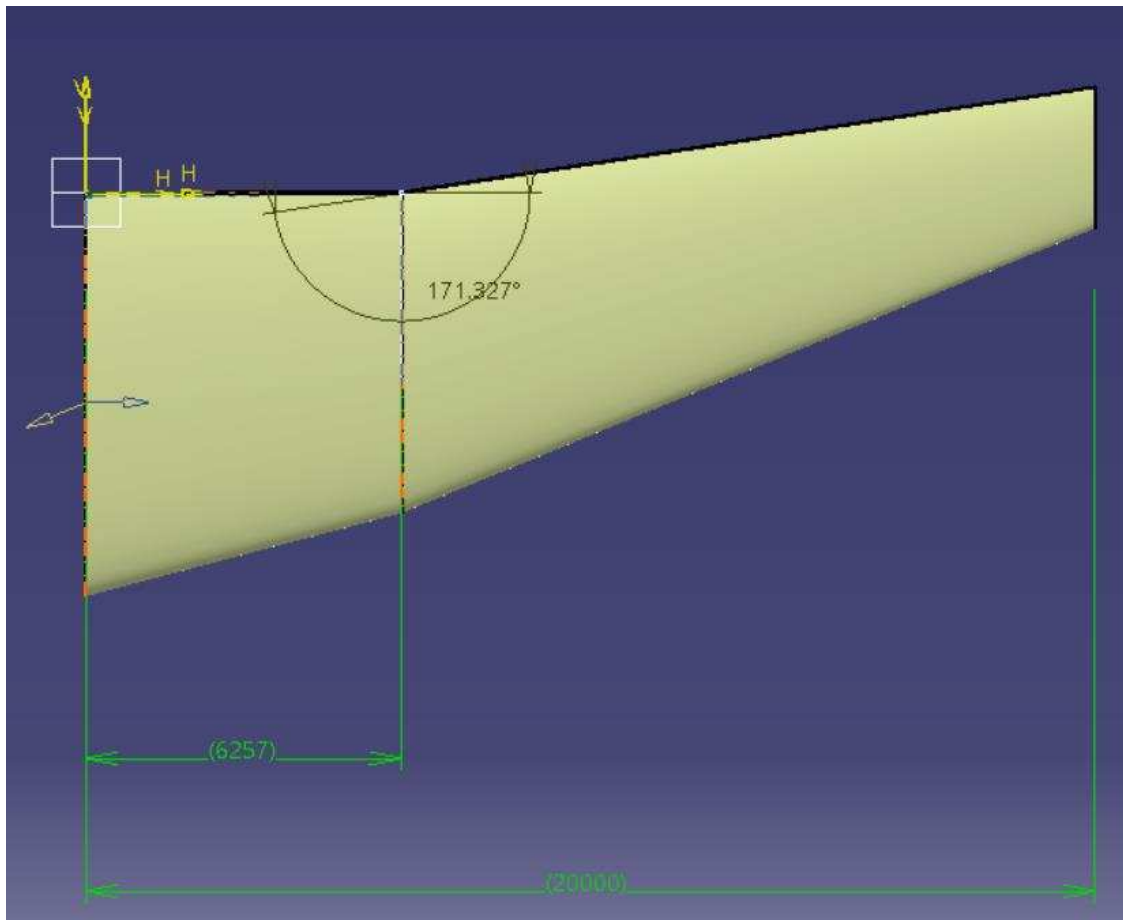


Figure 161: VER-12X with sweep

11.12 DISCUSSION:

Class II wing sizing offers a designer to dig in more into the design aspects of a configuration which may be a wing, fuselage, horizontal or a vertical tail. Through this process, any errors, assumptions made in the p.d.I can be revisited, and the design process can be re iterated so that the design evaluation is always in coherence with the proposed procedures. In p.d.I, for VER-12X wing, all the basic wing characteristics had been determined and in this design chapter firstly the wing weights are determined using G.D. method which helps in further understanding the structure weight of the aircraft and this in turn helps to make any changes to the overall structure as this is the preliminary component. Previously in p.d.I, the effects of taper ratio, thickness ratio, sweep angle and dihedral were only limited to calculations which us left with no choice than to assume them. But in this design chapter, their effects on weight, lift curve slope, max coefficient of lift, wing tips, wave drag, compressibility were clearly documented. Since VER-12X, is a passenger jet and which is required to travel at high subsonic speeds it is important to understand the aircraft wing sensitivity towards these factors and through this study few observations have been made on the wing loading effecting the handling capabilities of the aircraft, taper ratio playing a crucial role in tip stall and the thickness ratio on wave drag, maximum lift. However, after all the iterations the Wing design can now be fixed, and this design can be used in the future design chapters to analyse the stability and control of the aircraft

CHAPTER 12

EMPENNAGE

For most aircraft, Empennage is a combination of horizontal and vertical tail. It dictates the aircraft stability and control and their total area is directly proportional to the aircraft overall stability. Wing generates the necessary lift for the aircraft and other components also play their part for lift generation, however, these components can add up to generating destabilizing moments to the aircraft which requires 'Empennage' to counteract them. This makes a tailless aircraft existence in commercial aviation very rare. In p.d.I, the basic geometry of empennage had already been discussed with preliminary calculations of the horizontal and vertical tail areas, air foil selection and the lateral, longitudinal controls position. In the Class II sizing, the aerodynamic as well as operational aspects of the empennage will be considered while reviewing various types of empennage configurations and few aspects of the empennage design integrations would be discussed. The structural design considerations had been very well documented in 'Roskam – PartIII, Airplane Design' out of which only the closest matched structural configuration to VER-12X will be discussed.

12.1 EMPENNAGE CONFIGURATIONS: AERODYNAMICS AND OPERATIONAL DESIGN CONSIDERATIONS

In the p.d.I, the significance of empennage, the role it played in directional stability and control had been documented. In the further sections of this design chapter, the aerodynamic and operational design considerations will be thoroughly studied and few sections from p.d.I will be revisited as to make necessary changes in the empennage design and continue the Class-II sizing.

12.1.1 CONVENTIONAL AFT TAIL:

The selection of a conventional, three-surface or a canard configuration completely relies upon the overall aircraft design philosophy and which tells us that few important factors must be considered before arriving to a conclusion.

Achievable Trimmed Lift to Drag ratio:

In many references it is cited that, the three-surface configuration is ideal for achieving the maximum trimmed L/D ratio especially in cruise for any C.G. location than conventional or canard configuration. But the three-surface configuration can only be favourable for elliptical lift distribution and are invalid when span load distributions are considered. Nominally, a conventional configuration is the best for span load distributions and have been proved that they can generate maximum trimmed L/D which neglects the effects of propulsion installation. This is important when an aircraft is propeller driven.

To determine the achievable trimmed maximum lift coefficient with flaps up, landing/take-off there are not many adequate resources which helps in better understanding these concepts. For VER-12X, these concepts will be looked upon in the AAA (Advanced Aircraft Analysis Software) and if relevant data is found these will be documented further.

The distribution of major airplane masses (engines) play a vital role in the overall weight and balance of the aircraft. Commercial Aircraft now-a-days, have engines located forward which eventually leaves us no choice rather than to select a conventional tail. Minimum wetted area results in minimum drag which means that minimum sized empennage is always desirable. To achieve this, the empennage should be placed in locations where the product of lift curve slope and moment arm are maximized. In design chapter 2 from p.d.I, a Bombardier aircraft with engines located at the aft has been discussed and if its empennage configuration is observed

closely, the aircraft uses high swept aft tail and that was required to gain enough moment arm and ultimately to be away from ‘conventional empennage arrangement’.

12.1.2 ADDITIONAL EMPENNAGE CONFIGURATION CHOICES:

In p.d.I only the conventional tail configuration had been discussed for VER-12X, but now in this section different types of empennage configurations will be studied to compare them with the conventional empennage. This is done to completely understand and justify the selection of choosing conventional empennage configuration over various configurations. Each configuration has their own advantages and disadvantages and in aircraft design it is always a trade-off between optimum performance and mission requirements, hence, it is always good to have a better understanding before diving deep into choices.

V-Tail:

The V-tail configuration has been limited in use except for light aircraft, this design has been avoided which requires enough ground clearance. The primary advantage of using a V-tail is that the two surfaces provide the same functioning of a conventional tail which has three surfaces, and this results in reduced wetted area which means less drag. However, NASA experimental data suggests that to achieve the same amount of stability that a conventional empennage provides the surface areas should be the same. Alongside this, there is an adverse coupling effect that taunts the performance of a V-tail, especially when an aircraft perform ‘turn’ manoeuvre which forces the designers to choose an inverted V-tail configuration.



Figure 162:Waiex v-tail

T-tail:

T-tail configuration can be profoundly seen on commercial transport, fighter and freighter aircraft. Unlike conventional tail, for a T-tail the horizontal is positioned either at the top or to the bottom. 'From the viewpoint of vertical tail effectiveness per unit area, the best location for a horizontal tail is either the T-tail or the low tail configuration' (Roskam, 2011). For a propeller driven aircraft the horizontal tail is away from the prop wash and the wing wake which enhances the aerodynamic effectiveness of the horizontal tail. This in-turn reduces the size of the rudder. However, the bending and twisting loads will be imposed by the horizontal tail and this requires us to make the vertical stabilizer stronger which increases weight. In a deep stall condition, when the wing stalls the elevator will be ineffective, since, the elevator will be in wing wake which continuously pitches the aircraft nose up and this may completely reduce the controllability of the aircraft.

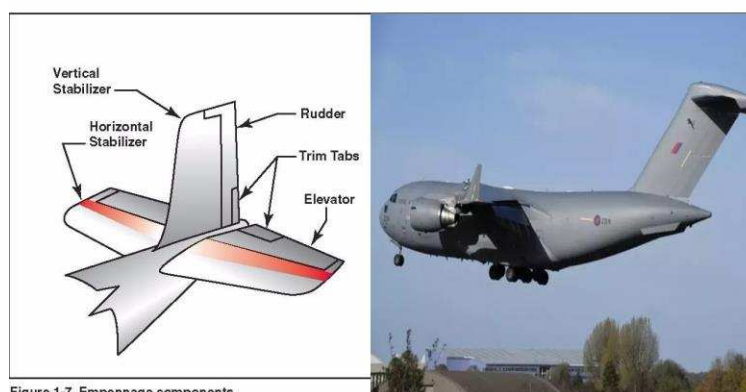
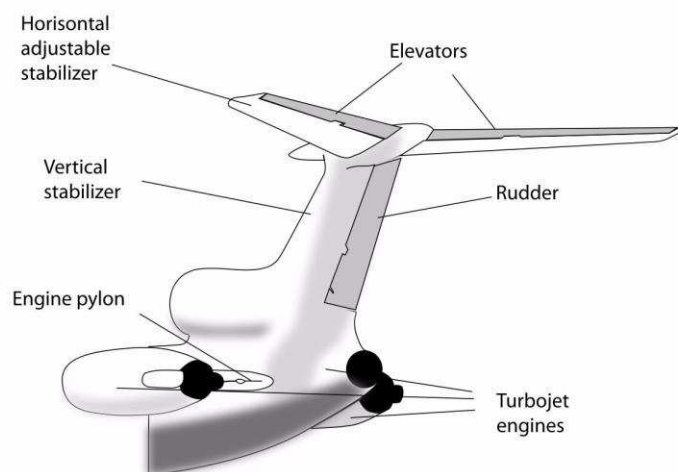


Figure 163: T-tail and Low Horizontal T-tail Configurations

12.1.3 Empennage Size: Stability, Control and Handling Considerations

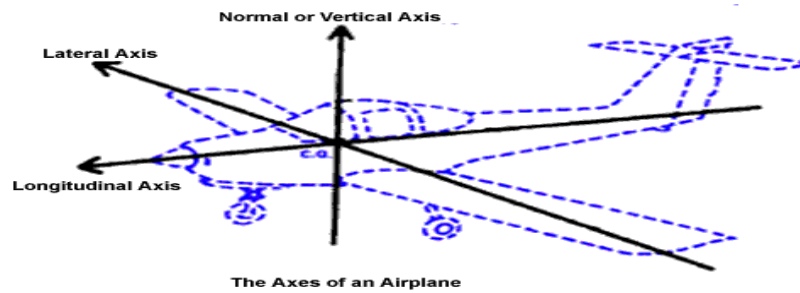


Figure 164: Aircraft Three Axes

From the longitudinal control perspective, the horizontal tail should satisfy the following conditions:

a) Longitudinal Stability Requirement:

The longitudinal stability at the forward and aft to the C.G. should always be consistent and is a requirement for static, dynamic and manoeuvring stability. Horizontal surface size is dictated by the stability requirements when once the moment arms have been decided.

b) Longitudinal Control Requirements:

The following longitudinal control requirements must be considered:

- The control power for trim must be consistent for both the forward and aft c.g. which must be within the flight envelope and airplane weight.
- The control power required for trim during rotation must be consistent for both the forward (tricycle landing gear) and aft (tail dragger) c.g. If the above condition is not satisfied the consequence is that the power required is not sufficient and this results in larger take-off lengths than predicted.
- During Cruise, the control power required must be within the limits of operational flight envelope, c.g. location and aircraft weight. This requirement plays a major role in inherently unstable aircraft.
- Control power is an important factor which must be tailored to meet the requirements for any flight condition and for artificial static or dynamic stability.

The control power requirements addressed in this section will be detailed in the stability and control design chapter.

- c) Longitudinal stick force requirements.

12.1.4 Lateral-Directional Stability requirements:

Form the lateral-directional stability perspective, the vertical tail must satisfy the following requirements:

- **Lateral Directional Stability requirements:**

The requirements for static and dynamic stability dictates that at all C.G. locations, operational flight envelope the lateral stability must be consistent which is primarily due to the inherent stability of the wing. Since Wing is designed primarily based on the performance and operational considerations it is required to fine-tune the lateral stability of the airplanes.

Directional stability often must comply for all the C.G. locations and this parameter dictates the size of the vertical tail.

- **Lateral Directional Control requirements:**

The following requirements should be considered:

- ✓ To meet the time to bank and response requirements the lateral must be sufficient.
- ✓ During an engine out condition, there should be sufficient directional power to control the aircraft
- ✓ For cross wing landings and manoeuvring, there must sufficient directional power

The control power requirements specified above will determine the sizes of the ailerons, spoilers and rudders. The second requirement above may also determine the maximum lift when a rudder is fully deflected.

- **Lateral Directional Stick and Rudder Pedal force requirements**

12.1.5 STALL AND SPIN CHARACTERISTICS:

To achieve satisfactory stall and spin characteristics, it is important to maintain the sufficient power and stability for all levels of the angles and sideslip which must comply with the operational requirements of the aircraft. The following characteristics must be addressed to understand the stall and spin behaviour of the proposed empennage configuration.

I. Stable and Unstable pitch breaks:

A pitch break condition is termed as aircraft's nose down pitching motion and it is important to study the stable and unstable pitch break points. To understand this behaviour, the coefficient of moment – coefficient of lift behaviour at the forward C.G. and the associated angle of attack- coefficient of lift must be studied. For FAR-23 certified aircraft the stable pitch breaks are acceptable, and their behaviour is shown in figure 4. However, for FAR-25 certified airplanes 'unstable' pitch breaks are acceptable, and this depends on the dynamic behaviour of the aircraft which can be a pilot induced stall or due to gusts. To combat these issues, VER-12X is fitted with stick shakers and it should also be noted that the C_{Lmax} used for certification purpose is the one that is between stick shaker and stick pusher but not the aerodynamic. This can further impose performance penalties which may increase the landing field length inadvertently.

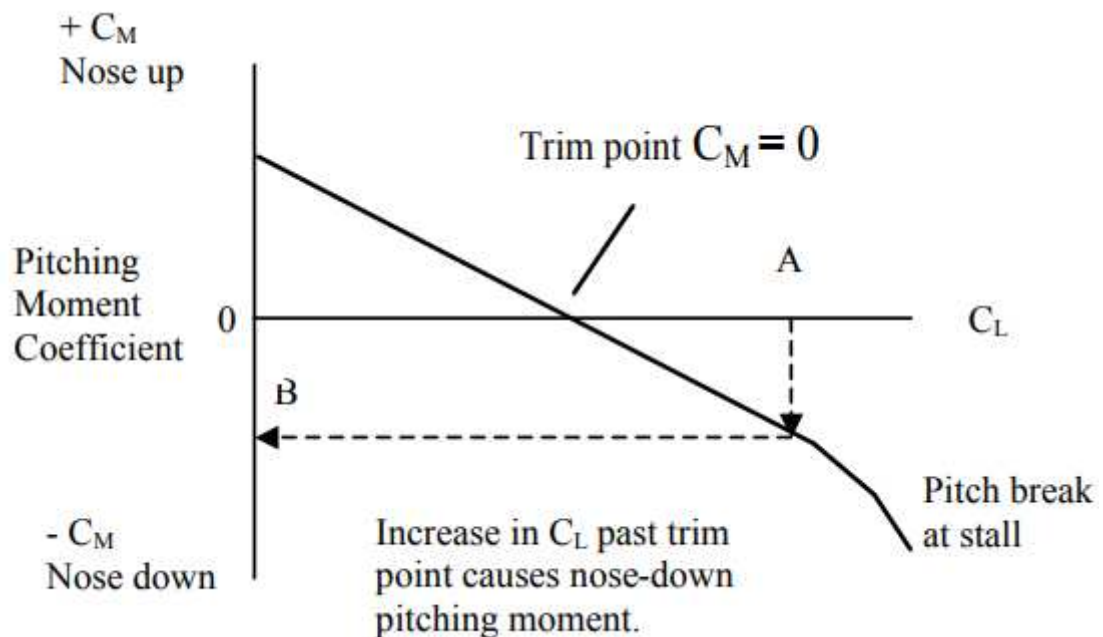


Figure 165: Pitching Moment versus Coefficient of Lift

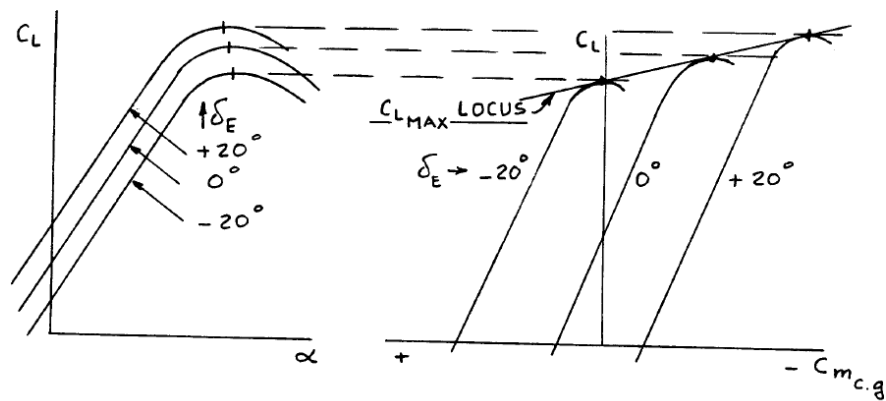


Figure 166: FAR-23 Stable Pitch Break Behaviour

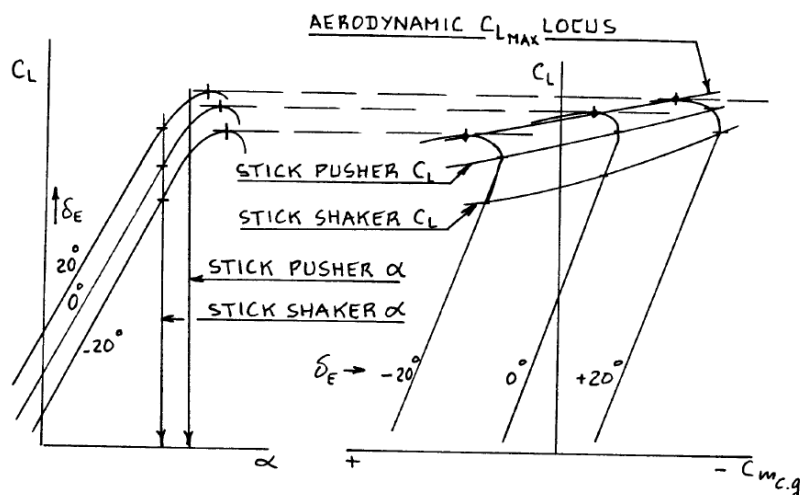


Figure 167: Unstable Pitch Breaks - FAR25

II. Stall Scenario:

To understand the stall scenario all the stall associated performance constraints will be studied for a conventional empennage configuration.

a. Conventional Configuration:

For any conventional aircraft, the wing body configuration plays a crucial role in determining the pitching moment of the aircraft especially for high angle attacks. To clearly understand this, let us consider a stall scenario in which the aircraft wing stalls along the inboard trailing edge, the downwash from the wing over the horizontal tail disappears. This results in horizontal tail perceiving positive lift and creates nose down pitching moment which is in turn perceived as stable pitch break by the pilot. Since, the airflow over the inboard part of the wing changes there are constant

changes made for the pitching moments. If wing contributes a larger positive pitching moment this ultimately results in unstable pitch breaks due to negative pitching moments imparted by the horizontal tail. It should be noted that for wings with greater aspect ratio always tend to unstable pitch breaks even for smaller sweep angles. For this the tail must be redesigned to meet the net stable pitch break requirement.

b. Deep Stall Trim Problem:

The deep stall trim problem is usually associated with the T-tail configuration with low horizontal tail. As the horizontal tail is in wing wake, especially during a stall, its performance is adversely affected and in these conditions the pilot may permanently lose the longitudinal control of the aircraft. To combat these effects and to maintain considerable power during a deep stall condition, usually the horizontal tail is swept back through which the trailing edge of the tail is kept away from the wing wake. Figure 7 clearly shows the difference as to how the location of horizontal tail effects the overall stall and spin characteristics of the aircraft. For VER-12X, conventional empennage configuration addresses these issues.

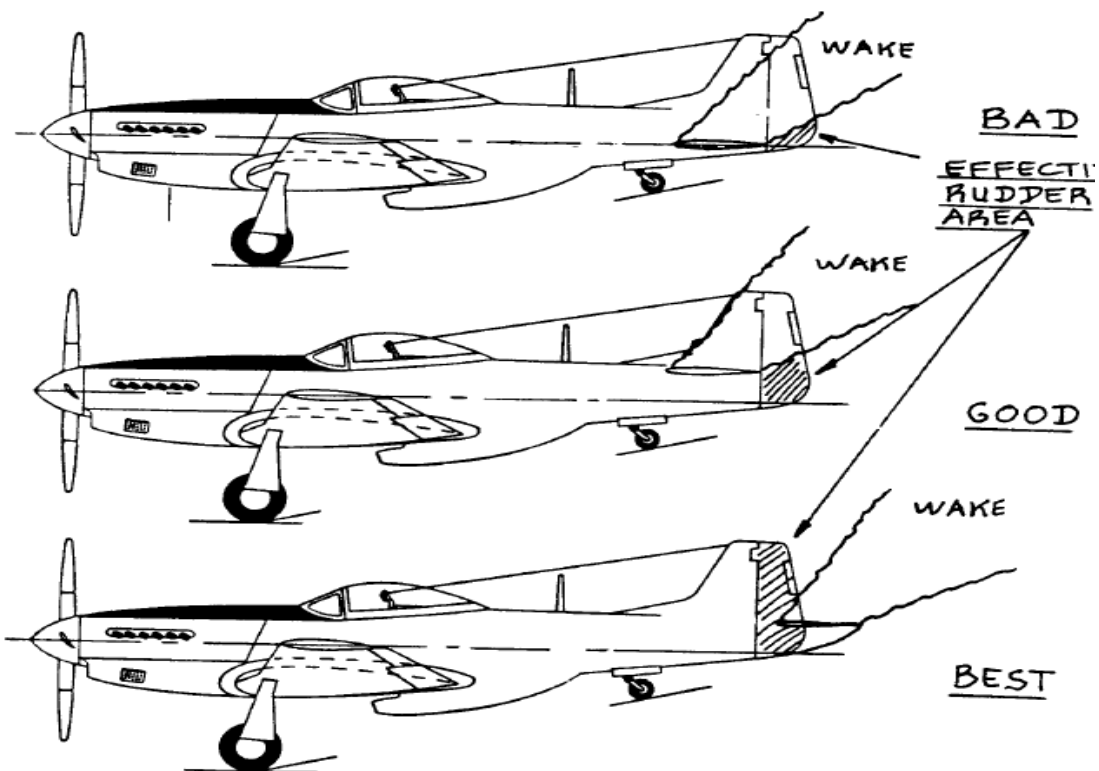


Figure 168: Empennage Configurations as related to Stall and Spin Characteristics

c. Pitch-up in high speed airplanes:

For high sub-sonic and supersonic aircraft, the inboard section is given a very high sweep angle. This results in rapid movements of centre of pressure for relatively high angle of attacks. This results in the trailing edge separation and the leading edge start to develop additional lift due to vortex generation. This in turn generates unstable pitch breaks which are hard to overcome and nearly all the aircraft today are prone to this and the only way to overcome this is to prevent separated wakes from countering the flight control surfaces. Additionally, there must be automated controls to prevent the pilot from entering an inadvertent stall condition.

d. Spin Departures and Recovery:

After an aircraft enters stall, it is essential that it is 'spin-resistant' to avoid inadvertent spin departures. 'Roskam' suggests that to avoid inherent spin departures it is required that e.q.2.1 is positive. To exactly understand this, wind tunnel tests should be done by varying the angle of attack.

$$C_{n_{\beta_{dyn}}} = \left\{ C_{n_{\beta_B}} - (I_{zz_B} / I_{xx_B}) C_{l_{\beta_B}} \tan \alpha \right\} \cos \alpha \quad (12.1)$$

The longitudinal and directional flight controls location will determine whether an aircraft can recover from spin. To make an aircraft spin resistant, the wings must be designed so that the auto rotation is delayed especially at higher angle of attacks. For commercial passenger jets, there is not any requirement that they should be recoverable from spin as the aircraft are not permitted to operate in the spin flight condition

12.1.6 EMPENNAGE PLANFORM DESIGN:

From p.d.I of VER-12X empennage design, tables 1,2 provides a detailed description of the dimensions that has already been computed.

Table 22: Horizontal Tail Geometry

Horizontal Tail Geometry	Definition
Aspect Ratio	6.1
Horizontal Tail Area	774 ft ²
Span	68 ft.
Quarter Chord Sweep	30°
Taper Ratio	0.63
Sweep Angle	28.4°
Thickness Ratio	0.3*
Air foil	NACA 009 (Symmetric)
Incidence Angle	Variable
Dihedral	11°

Table 23: Vertical Tail Geometry

Vertical Tail Geometry	Definitions
Aspect Ratio	2.0
Vertical Tail Area	760 ft ²
Span	39 ft.
Quarter Chord Sweep	30°
Taper Ratio	0.73
Sweep Angle	53°
Thickness Ratio	0.33
Air Foil	NACA 009(Symmetric)
Incidence Angle	0°
Dihedral Angle	90°

12.1.7 EMPENNAGE AIR FOIL DESIGN:

Many resources cite that the use of symmetrical air foil section is highly recommended for horizontal and vertical tail. The primary reason is that the lift generation for the empennage surface's must be same in both the direction and it cannot be achieved by using asymmetrical air foil section. For VER-12X Empennage, NACA-009 symmetrical aircraft is used and its experimental aerodynamic characteristics in terms of lift, drag, pitching moments for relative angle of attacks are shown in figure8.

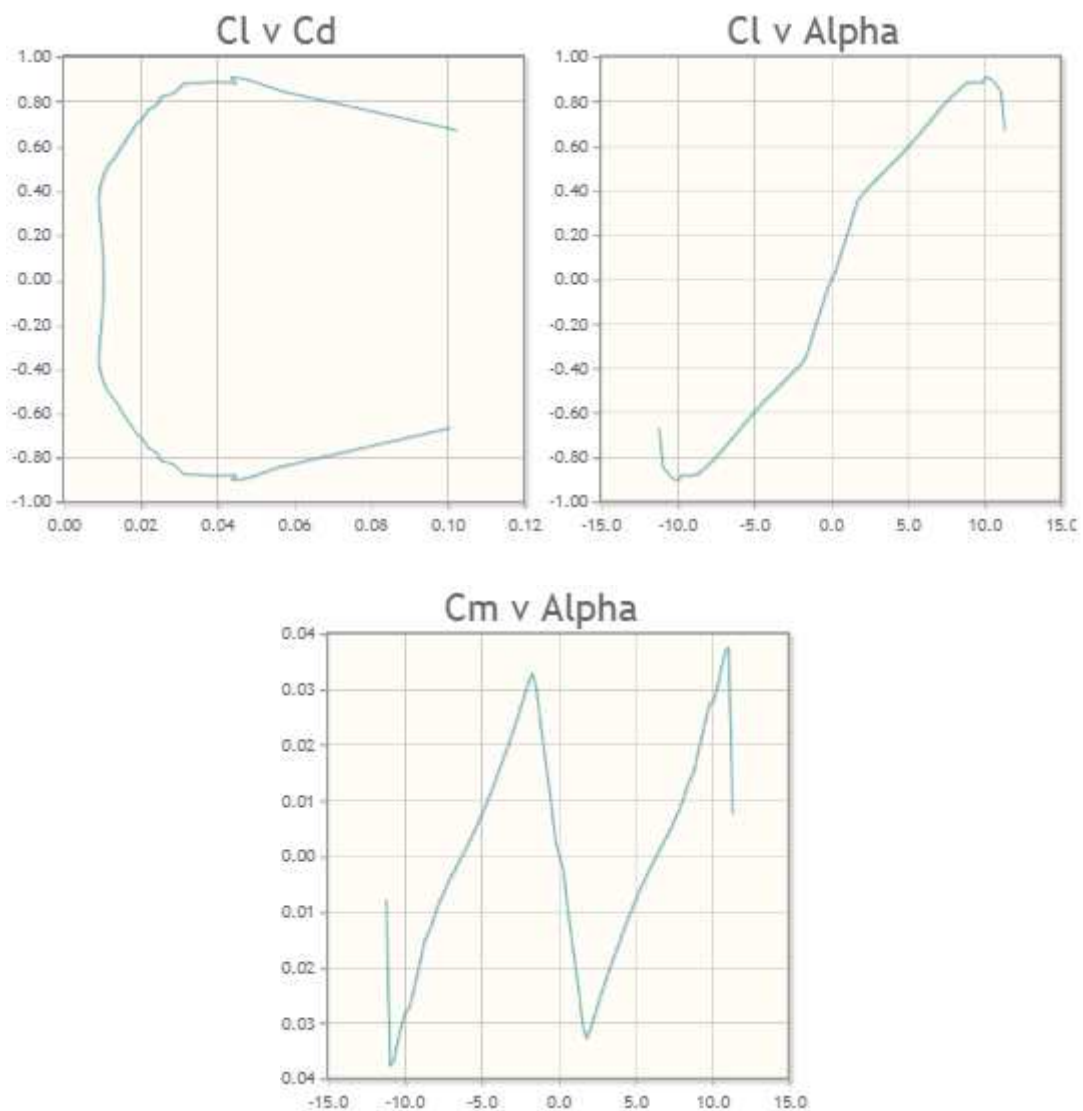


Figure 169: C_L vs C_d and C_L vs Alpha and C_m vs Alpha

12.1.8 REVIEW OF EMPENNAGE DRAG CONTRIBUTIONS:

The Empennage generates same types drag like Wing:

- Friction Drag
- Induced Drag
- Compressibility Drag
- Interference Drag
- Profile Drag

Depending on the size and disposition of the empennage the over-all airplane drag contributions varies from 10-20 percent. Since these sections has already been discussed in ‘Sub-systems Chapter-I’ only the induced drag effects will be studied in this section. Since induced drag is directly proportional to the square of the lift coefficient it must be noted that induced drag is independent of the direction of the lift. The drag produced due to Empennage will be detailed in the later design reports.

12.2 DISCUSSION:

Class II Empennage sizing offers a designer to dig in more into the design aspects of a different types of empennage configurations and then allowing to choose a configuration which is a best match. Through this process, any errors, assumptions made in the p.d.I can be revisited and the design process can be re iterated so that the design evaluation is always in coherence with the proposed procedures. In p.d.I, for VER-12X Empennage, all the basic empennage characteristics had been determined and in this design chapter firstly various kinds of empennage configuration have been studied which helps in understanding the structural, aerodynamic efficiency of the aircraft and this in turn helps to make any changes to the overall structure as this is a vital component which provides control on the aircraft. Previously in p.d.I, the effects of taper ratio, thickness ratio, sweep angle and dihedral were only limited to calculations which us left with no choice than to assume them. But in this design chapter, their effects on weight, lift curve slope, max coefficient of lift, wing tips, wave drag, compressibility were clearly documented. Since VER-12X, is a passenger jet and which is required to travel at high subsonic speeds it is important to understand the aircraft wing sensitivity towards these factors and finally on empennage. Through this study few observations have been made on the wing loading effecting the handling capabilities of the aircraft, taper ratio playing a crucial role in tip stall and the thickness ratio on wave drag, maximum lift. However, after all the iterations

for the Empennage design have been made and can now be fixed, this design can be used in the future design chapters to analyse the stability and control of the aircraft.

CHAPTER 13

V-N Diagram

The operating strength of an aircraft or aircraft performance is an important factor to study. The most widely used form for evaluating an aircraft performance within the flight envelope is through the study of the V-n or V-g diagram (V is the velocity and n or g is the load). Through this illustration a pilot can understand as to how to choose a cornering speed through which maximum performance can be obtained by being within the limits. Basically, the V-n diagrams are used to determine the design limit and design ultimate load of the proposed aircraft and corresponding speeds to which the structures remain intact within the flight envelope. For constructing the V-n diagram for VER-12X, 'Roskam Part V' is used which provides wide range of determination techniques, methods through which VER-12X's 1g stall speed(V_S), design cruising speed(V_C), design diving speed(V_D), design manoeuvring speed (V_A) can be determined.

13.1 DETERMINATION OF +1G STALL SPEED:

Wing loading, and stall speed are directly related to each other i.e. as the wing loading increases the stall speed increase by square root of wing loading. The 1g stall speed is defined as the speed at which an aircraft can generate the lift that is equal to its weight. There are no definite explanations to exactly illustrate what stall is but there have been reasons which could be primarily responsible for a stall such as sloppy controls, continuous nose pitches up. 'Roskam' presents a step wise procedure to determine the 1g stall speed and those procedures have been adopted to determine VER-12X limits. The maximum normal force coefficient is determined using e.q.13.1

$$C_{N_{\max}} = \sqrt{\{(C_{l_{\max}})^2 + (C_{D_{atC_{l_{\max}}}})^2\}} \quad (13.1)$$

The 1g stall speed for VER-12X is determined using e.q.13.2.

$$V_S = \sqrt{\{2(GW/S)/\rho C_{N_{\max}}\}} \quad (13.2)$$

13.2 DETERMINATION OF DESIGN CRUISING SPEED:

Design cruising speed or V_C or V_1 is the engine failure recognition or decision take-off speed above which the aircraft must take-off irrespective to the engine failure or tire blown off.

Depending on the aircraft type and the type of flap setting used, the V_C or V_1 will vary and the decision is left with the pilot to determine the appropriate speed for take-off.

The cruising speed for VER-12X is determined using e.q.13.3. The constant k_c is nominally considered as 33 for normal airplanes with wing loading between 20-100.

$$V_C \geq k_c \sqrt{(GW / S)} \quad (13.3)$$

13.3 DETERMINATION OF DESIGN DIVING SPEED:

The design diving speed is defined as the highest speed planned to achieve during testing. It is to be noted that design diving speed should be equal to 0.8 times the design cruising speed and if the aircraft undergo compressibility effects then the required margin should not be less than 0.05 Max Mach of the aircraft. It is always required that this margin should be greater as it is greatly affected by the atmospheric conditions (horizontal and vertical gusts) and instrument errors. The design diving speed for VER-12X is determined using e.q.13.4

$$V_D \geq 1.25 * V_C \quad (13.4)$$

13.4 DETERMINATION OF DESIGN MANOEUVRING SPEED:

The design manoeuvring speed is defined as the speed at which the aircraft stalls before exceeding the proposed g-limits so that the airframe is not damaged. The design manoeuvring speed for VER-12X is determined using the e.q.13.4

$$V_A \geq \sqrt{V_S n_{lim}} \quad (13.5)$$

13.5 DETERMINATION OF NEGATIVE STALL SPEED LINE:

The negative stall speed line for VER-12X is determined using e.q.13.6

$$V_{S_{neg}} = \sqrt{\{2 * (GW / S) / (\rho * C_{N_{MAXnegative}})\}} \quad (13.6)$$

$$C_{N_{max}} = \sqrt{\{(C_{l_{max,negative}})^2 + (C_{D_{arC_{l_{max,negative}}}})^2\}} \quad (13.7)$$

13.6 DETERMINATION OF DESIGN LIMIT LOAD FACTOR:

The maximum design load limit for VER-12X is by first calculating the positive load limit and then determining the gust load factor lines using e.q.13.8,13.9,13.10.

$$n_{lim\ positive} \geq 2.1 + \frac{24000}{GW + 10000}$$

Construction of gust load factor lines:

$$n_{lim} = 1 + \frac{(K_g U_{de} V C_{L\alpha})}{498 * (GW / S)} \quad (13.8)$$

$$K_g = \frac{0.88 \mu_g}{5.3 + \mu_g} \quad (13.9)$$

$$\mu_g = \frac{2 * (GW / S)}{\rho * c * G * C_{L\alpha}} \quad (13.10)$$

Table 24: Parameters required to construct V-n diagram for VER-12X

1-g stall speed, V_S	137 kts.
Design Cruising speed, V_C	243 kts.
Design Diving speed, V_D	304 kts
Design Manoeuvring speed, V_A	205 kts
Negative Stall speed line, $V_{S_{neg}}$	167 kts
Design positive load limit, $n_{lim\ positive}$	2.2412
Design negative load limit. $n_{lim\ negative}$	-0.8965
Gust Load Factor	For design diving speed – 1.4941 For design cruising speed – 1.7911

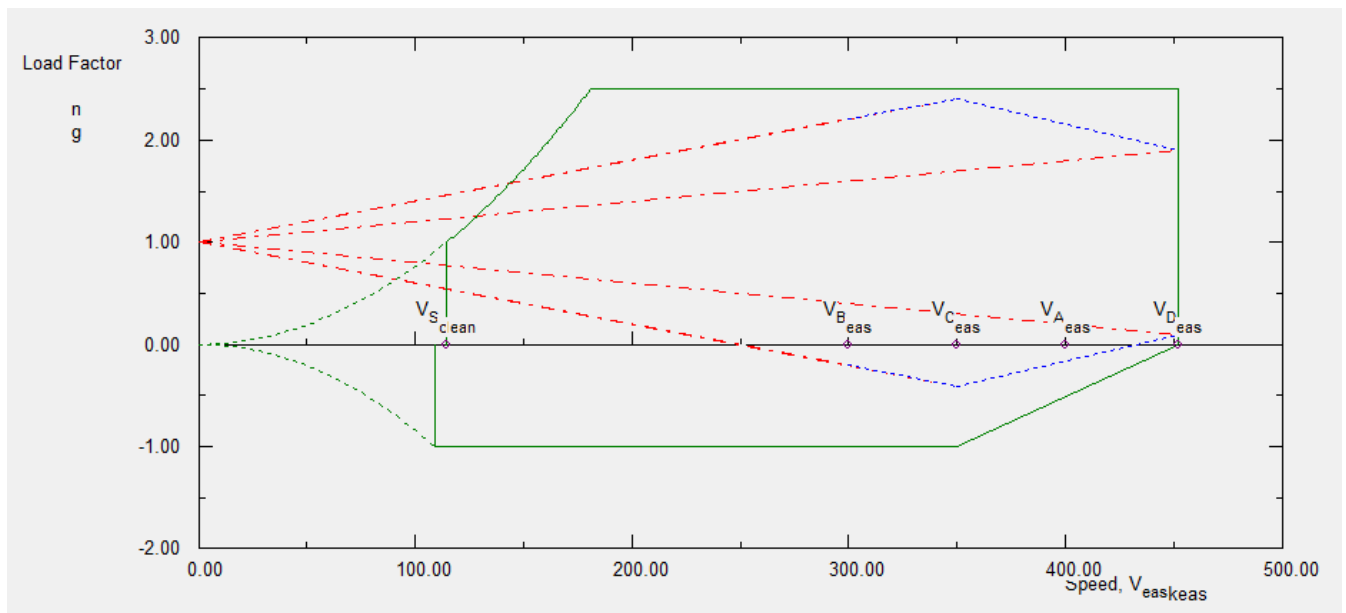


Figure 170: V-n diagram for VER-12X using AAA

CHAPTER 14

Class II - DRAG POLARS

In p.d.I, a preliminary drag polar analysis is presented for drag prediction which were calculated using the equivalent wetted area determined for fuselage, wing, empennage and landing gear. Drag is defined as the sum of zero lift drag coefficient and induced drag. In the Class II sizing, the drag due to each sub-system are analysed individually and the procedures that will be documented in this design chapter are an excerpt from 'Roskam Part VI Chapter IV'. Preliminary drag prediction methods included the study of different kinds of drag, low speed drag increments, compressibility effects and area ruling concepts. In aircraft design, to understand the primary drag effects it is sufficient to study the above factors but to gain in depth understanding on proposed configurations drag prediction it is important to consider each component individually and evaluate them for various flight sequences. The procedures laid down here can be used for straight and tapered wings. For unconventional aircraft such as flying wing, 'Roskam' refers to other books and they offer complete analysis for drag prediction. Previously, when only wetted area is considered, an in-depth analysis for which the effects of shape had not been studied and these effects will be documented in this design chapter. Alongside, primarily a drag-break down structure will be documented to understand the overall drag of the aircraft.

14.1 SUMMARY OF DRAG CAUSES:

As already discussed above, drag is defined as the sum of induced drag and zero-lift drag coefficient. This same definition will be applied to subsonic ($0 < M < 0.6$), transonic ($0.6 < M < 1.2$) and supersonic ($1.2 < M < 3.0$) speed ranges.

$$D = \text{zerolift drag} + \text{drag due to lift} \quad (14.1)$$

$$\text{zerolift drag} = \text{Skin friction drag} + \text{Pressure drag} \quad (14.2)$$

14.1.1) SKIN FRICTION DRAG:

The **Skin Friction Drag** of the zero-lift drag is caused due to the shear stresses within the thin layer of air which is called the boundary layer and they primarily arise due to the resisting forces of viscosity against a body passing through the air. The magnitude of this force is again dependent on the flow characteristics i.e. whether the flow is laminar or turbulent. Laminar or turbulent flow are again characterized by the Reynolds number, pressure distribution and on the skin or surface roughness.

14.1.2) PRESSURE DRAG:

The Pressure Drag of zero-lift drag is caused due to the displacement of the boundary layer thickness which prevents full pressure recovery at the trailing edge. In subsonic flight, if the boundary layer attached to the surface, the pressure drag remains small which is different for aircraft travelling at transonic and supersonic speeds in which it is associated with the 'Wave Drag'. As the aircraft speed increases and at the critical Mach number the wave drag causes an abrupt increase in the drag and an associated pressure drag. Pressure drag is also dependent on the surface i.e. if the surface is blunted the pressure drag increases abruptly irrelevant to the flight regime.

14.1.3) INDUCED DRAG:

The induced drag depends on the span-wise lift distribution and is directly proportional to the square of the lift coefficient. It is also called as trailing edge or vortex drag. This type of drag is discussed more in detail in 'design chapter I'

14.1.4) DRAG DUE TO LIFT:

Drag due to lift is defined as the sum of induced drag and viscous drag due to lift.

- Viscous drag is mainly generated due to change in the boundary layer because of lift. As the angle of attack increases, the boundary layer thickness increases which in turn increases the profile drag and it is the sum of skin friction and pressure drag.

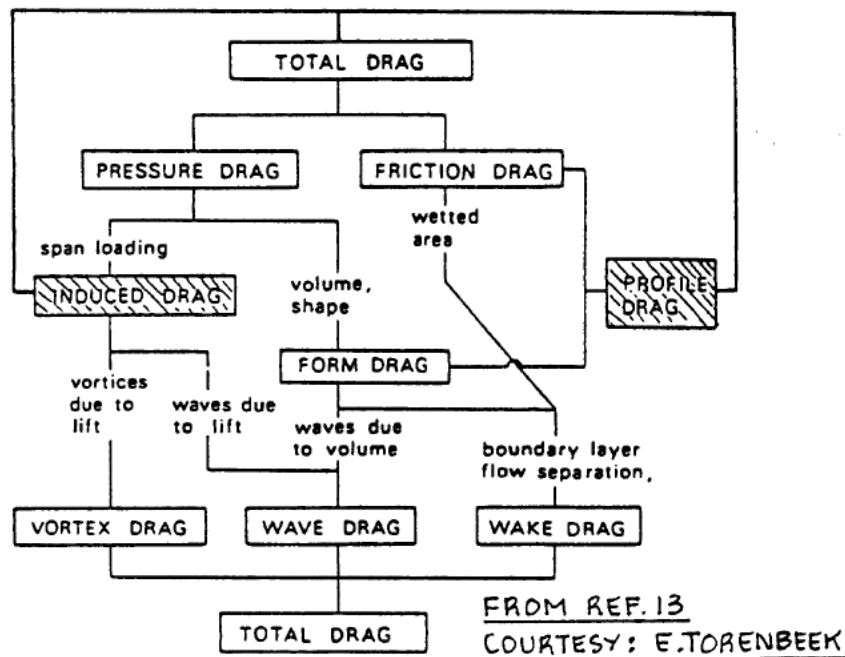


Figure 171: Drag breakdown due to physical causes

Figure 171, gives a detailed explanation on the drag break down. It can be inferred that drag prediction is based on span wise loading and total wetted area of the aircraft. Span wise loading due to lift helps us to evaluate drag due to wing tip vortices, waves due to lift and waves due to volume and on the other hand the wetted area helps us to evaluate the drag due to boundary layer separation and ultimately contributing to the overall aircraft drag.

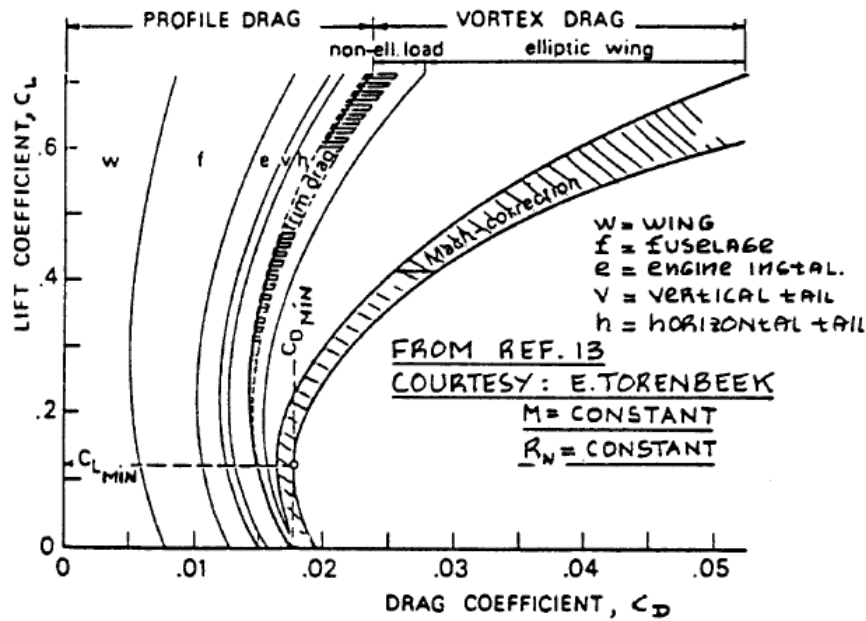


Figure 172: Typical Drag breakdown for Transport Jet

14.2) DRAG PREDICTION METHODS:

The total aircraft coefficient is usually broken down into:

$$C_D = C_{D_{wing}} + C_{D_{empennage}} + C_{D_{nacelles}} + C_{D_{flaps}} + C_{D_{landing\ gear}} + C_{D_{canopy_{wind\ shield}}} + C_{D_{stores}} + C_{D_{trim}} + C_{D_{interference\ drag}} + C_{D_{miscellaneous\ drag\ coefficients}} \quad (14.3)$$

14.2.1) SUB-SONIC WING DRAG COEFFICIENT PREDICTION:

The subsonic wing drag coefficient is found using e.q.14.4

$$C_{D_{wing}} = C_{D_{0_{wing}}} + C_{D_{LW}} \quad (14.4)$$

- $C_{D_{0_{wing}}}$ - wing zero-lift drag coefficient
- $C_{D_{LW}}$ - wing drag coefficient due to lift

14.2.1.1) Wing zero-lift drag coefficient:

The sub-sonic wing zero-lift drag coefficient is computed using e.q.14.5

$$C_{D_{0_{wing}}} = (R_{wf})(R_{LS})(C_{f_w})\{1 + L'(t/c) + 100(t/c)^4\}S_{wet_w} / S \quad (14.5)$$

To understand the drag prediction procedures, it is important to determine component wise drag manually and then compare the obtained values with computational data to check if the determined values are a close match. For this, MATLAB is used and to check these values AAA software is used alongside.

```

%% Wing Drag Prediction
% Wing- Zero lift drag coefficient
S_wet = 7000; % wetted area of the wing
S = 3982; %wing area
R_wf = 0.967; % wing fuselage interference factor
R_ls = 1.27; %lifting surface correction factor
C_f_w = 0.0033; %turbulant flat plate frictiion coefficient of the wing
L_prime =1000; % airfoil thickenss location parameter
thickness = 0.139; % thickenss ratio
C_d_o_w = (R_wf)*(R_ls)*(C_f_w)*(1+(L_prime*thickness)+100*(thickness)^4)*S_wet/S;

```

```

C_d_o_w =
    0.9977

```

14.2.1.2) Wing drag coefficient due to lift:

The wing drag coefficient due to lift is found using e.q.14.6

$$C_{D_{LW}} = (C_{L_w})^2 / \pi A e + 2\pi C_{L_w} \epsilon_t v + 4\pi^2 \epsilon_t^2 w \quad (14.6)$$

Where

- v is the induced drag factor due to linear twist found using ‘Roskam Part VI Chapter 4 page 30’
- w is the zero-lift drag factor due to linear twist found using ‘Roskam Part VI Chapter 4 page 32’

```

% Wing drag coefficient due to lift
C_l_wing = 1.5; % max lift coefficient of the wing
v = -0.0016; % induced drag factor due to linear twist
w = 0.00158; % zero-lift drag due to linear twist
epsilon_t = 0.0698132; % wing twist angle in dergrees is 4 but converted to rad
e = 0.8; % oswald efficiency
A = 9.61; % Aspect ratio
C_D_w = ((C_l_wing)^2/(pi*A*e))+(2*pi*C_l_wing*epsilon_t*v)+(4*(pi)^2*(epsilon_t)^2*w);

```

```

C_D_w =
    0.0924

```

```

% Total subsonic wing drag
C_D_wing = C_d_o_w+C_D_w;

```

```

C_D_wing =
    1.0901

```

14.2.1.3) TRANSONIC WING DRAG PREDICTION:

VER-12X cruises at high subsonic speeds and it is required to understand the drag being produced by wing at these speeds. ‘Wave drag’ which appear at the transition speed (i.e from $M = 0.75$ to 0.8) highly impacts the performance of the wing which effects the range and the cruising speed. In chapter-I, these effects had been clearly studied where a sudden increase in the drag will be clearly visible. A deep research on this effect revealed a fact that, at the wing-fuselage, wing-tail integration points the wave drag can be profoundly seen and “Mr. Witcomb” a NASA scientist came up with the idea of area ruling which greatly reduced the wave drag especially when the areas at these points are smoothed. For VER-12X, the transonic wing drag is computed using e.q.14.4

Now, the wing zero-lift drag coefficient in the transonic range is given by:

$$C_{D_{o_{wing}}} = C_{D_{0_{wing}}} + C_{D_{Wing_{wave}}} \quad (14.7)$$

For Swept wings,

```
1 %% Transonic Wing drag prediction
2 clc clear
3 thickness = 0.139;
4 C_l_max = 1.5;
5 sweep = 0.61086524; % sweep in radians
6 k = 0.95; % Constant K for super critical airfoil is 0.95
7 M_dd = k-thickness-(C_l_max/10)
8 M_C_d_wave_peak = 0.65/sqrt(cos(sweep))
9 C_d_wave_sweep = 0.00189*(cos(sweep))^2.5
10 M_dd_sweep = M_dd/sqrt(cos(sweep))
11 l = 1.2; % l = C_d_l/C_l^2 is chosen using fig.4.13
12 C_d_l_w = l*C_l_max % Wing drag coefficient due to lift
13 C_d_o_w_m = 0.9977;
14 C_d_o_w = C_d_o_w_m+C_d_wave_sweep
```

```
M_dd = 0.66100
M_C_d_wave_peak = 0.71818
C_d_wave_sweep = 0.0011478
M_dd_sweep = 0.73033
C_d_l_w = 1.8000
C_d_o_w = 0.99885
```

In the above MATLAB code, the drag divergence Mach number, the peak wave drag coefficient and the total transonic wing drag have been computed. This value when compared to normal sub-sonic wing drag resulted in reduced drag which reckons us to use the area ruling to avoid the effects of wave drag especially when the aircraft reaches the transonic region.

14.2.2) FUSELAGE DRAG COEFFICIENT PREDICTION:

Fuselage drag is the second component in the drag equation which needs to be evaluated. The drag rise characteristics are important to study as it helps in understanding the pressure drag associated with the fuselage alone because of its shape. In p.d.I, for VER-12X fuselage several cross sections have been studied out of which O-give cylindrical shape had been proposed to be the probable fuselage cross section. In Class II, the total drag due to fuselage will be determined using e.q.4.7.

$$C_{D_{fuselage}} = C_{D_{0_{fuselage}}} + C_{D_{L_{fuselage}}} \quad (14.8)$$

14.2.2.1) Fuselage zero-lift drag coefficient:

The fuselage zero-lift drag coefficient is calculated using e.q.14.9

$$C_{D_{0_{fus}}} = R_{w_{fus}} * C_{f_{fus}} \{1 + 60(l_f + d_f)^3 + 0.0025(l_f / d_f)\} S_{wet_{fus}} / S + C_{D_{b_{fus}}} \quad (14.9)$$

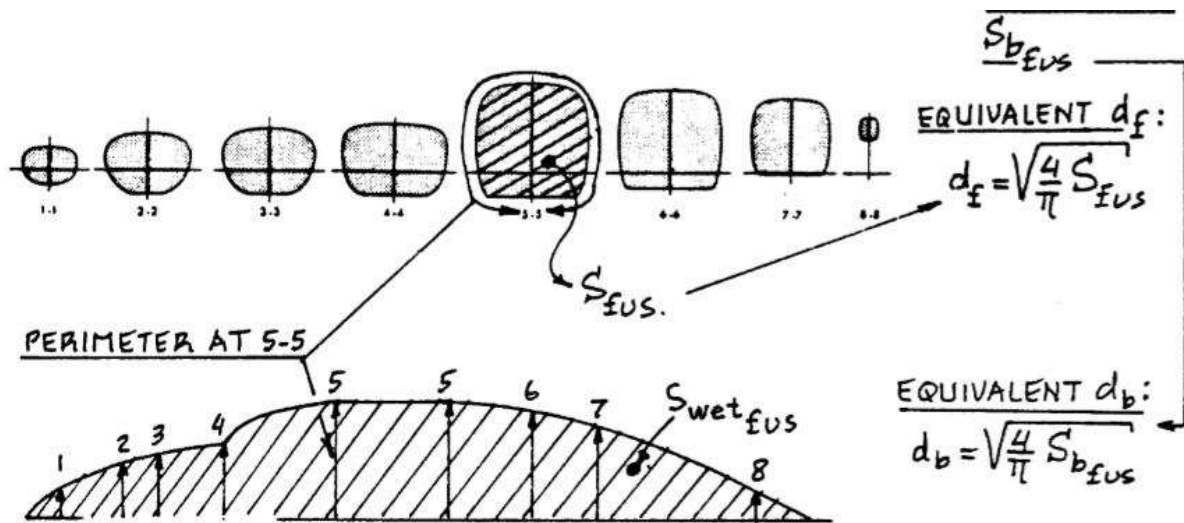


Figure 4.17 Definition of Fuselage Parameters

Figure 173: Fuselage Definitions

Figure 173, above briefly explains the fuselage definitions that were used in the code below for calculating the zero-lift drag coefficient exclusive of the base i.e. fuselage base drag coefficient.

```

%% Fuselage drag prediction
R_wfus= 0.999; % wing fuselage interference factor
S_wet_fus=4407.0314986938;% wetted area of the fuselage
C_f_fus =0.003751;%turbulant flat plate firciition coefficient of the fuselage
l_f= 143.66798; % length of the fuselage
d_f=11.58136; % max diameter of the fuselage
S_fus = (d_f^2*pi)/4;% max fuselage cross section area
d_b = 2.5; % max fuselage base diameter
S_b_fus = (d_b^2*pi)/4; % fuselage base area
C_d_b_fus = (0.029*(d_b/d_f)^3/((0.00026*(S/S_fus))^(0.5))*(S_fus/S));
C_d_o_fus = (R_wfus*C_f_fus*(1+(60/(l_f/d_f)^3)))+(0.0025*(l_f/d_f)*(S_wet_fus/S))+...
    0.00026; % fuselage zero lift drag coefficient

```

$C_{d_o_fus} =$

0.0384

14.2.2.2) Fuselage drag coefficient due to lift:

```

% Fuselage drag coefficient due to lift
eta = 0.658;
alpha = 0:0.001:0.261799; % 15 degrees
c_d_c = 1.75;
C_d_l_fus = 2*alpha.^2*(S_b_fus/S)+eta*c_d_c*alpha.^3*(pi*5.79^2)/S;

```

$$C_{d_{l_{fus}}} = 0.0007094 \quad (14.10)$$

Total fuselage drag:

```
C_d_fus = C_d_o_fus+C_d_l_fus;
```

$$C_{d_{fuselage}} = 0.0392 \quad (14.11)$$

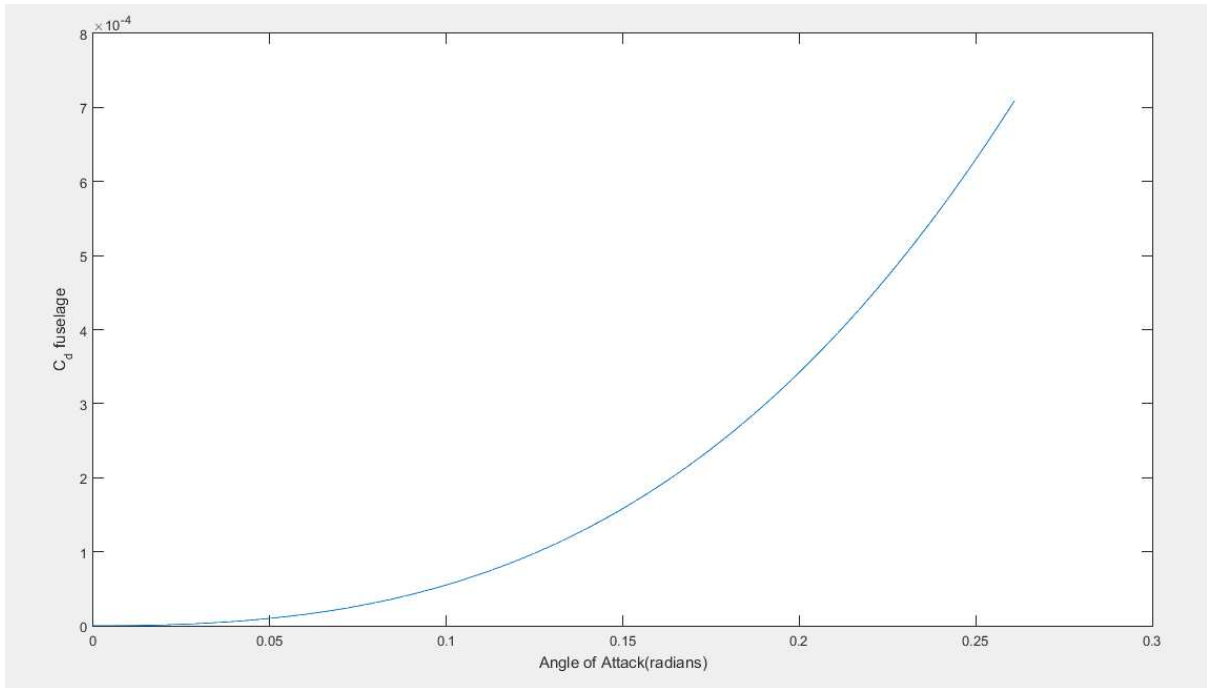


Figure 174: Aircraft angle of attack vs Fuselage Total Drag – MATLAB

Figure 174, gives us the relation between relative fuselage drag rise for a given angle of attack. As the aircraft angle of attack increases the total drag increases and in this case only the angle of attack variation from 0 to 6 degrees had been studied. E.q.14.10 dictates that the effective area of performance for VER-12X with relatively less drag penalty and it is approximately for 0.2 radians (11°).

CROSS-SECTION	DRAG COEFFICIENT (C_D)
Square	2.1
Rectangle	1.8
Triangle	1.5
Circle	1.1
Ellipse	0.6
Rhombus	2.2
Pentagon	2.5
Hexagon	2.3

Figure 175: Drag produced by various fuselage cross-section

Figure 175 above, is an excerpt from ‘Nishith Reddy Gorla thesis’ which primarily focuses on the various cross-sectional areas of the fuselage with a detailed computational analysis. These values are closely examined, and which played a prominent role in the selection of VER-12X fuselage cross section. Both the cross-sectional area and the fineness ratio of the fuselage together are responsible for generating drag. ‘Part-III, Airplane Design, Roskam’ suggest that the drag due to fuselage is greatly reduced as the fineness ratio increases. Since, the fineness for VER-12X is 7.61* the suggested value for drag is approximately 0.075 and the computed subsonic drag from 4.11 is 0.0392 which falls into the design range limits.

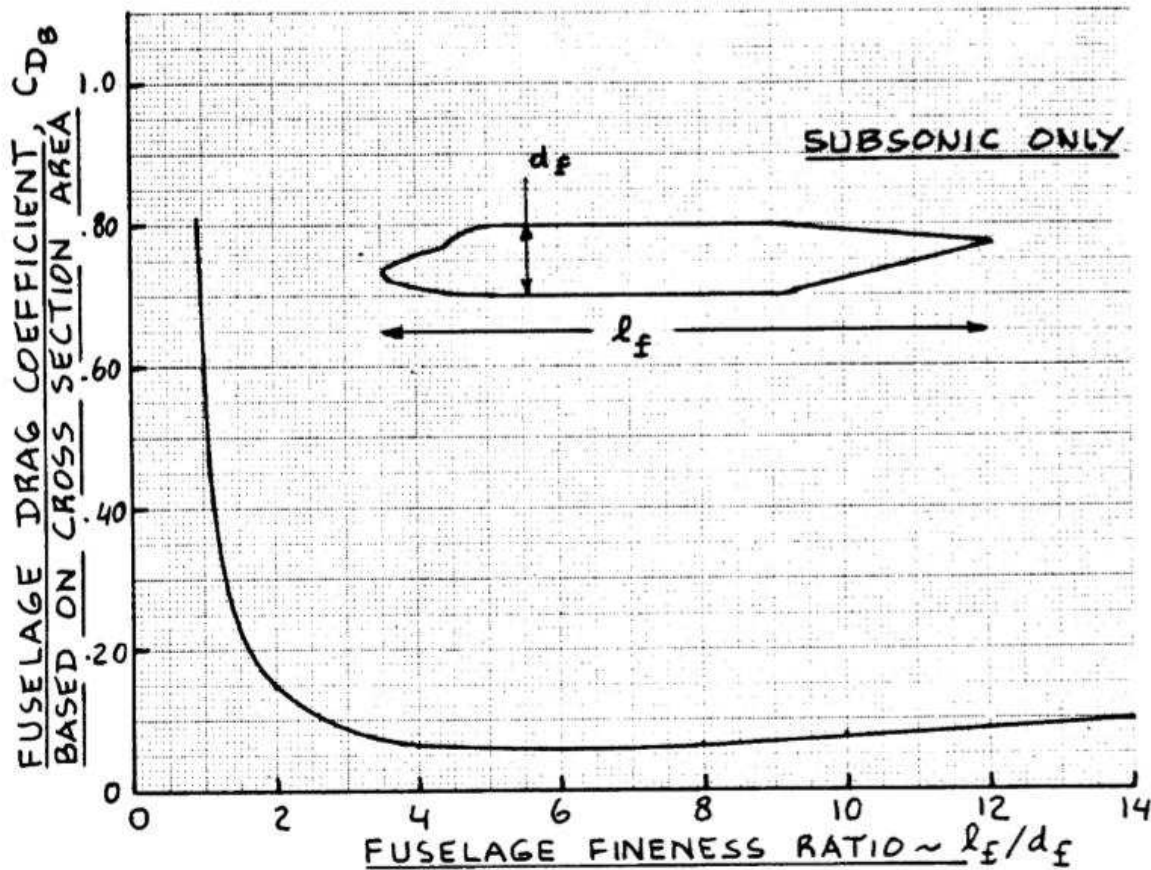


Figure 176: Fuselage fineness ratio vs fuselage drag coefficient

14.2.2.3) FUSELAGE TRANSONIC DRAG PREDICTION:

The transonic fuselage transonic drag for VER-12X can be computed using:

$$C_{D_{fus}} = C_{D_{0_{fus}}} + C_{D_{L_{fus}}} \quad (14.12)$$

Transonic fuselage zero-lift and drag due to lift can be computed using e.q.14.13, 14.16 whereas $C_{D_{fFUS}}$, $C_{D_{pFUS}}$ are the fuselage skin-friction and pressure drag.

$$C_{D_{o_{fus}}} = R_{wf} (C_{f_{D_{fus}}} + C_{D_{p_{fus}}}) + C_{D_{b_{fus}}} + (C_{D_{9_{wave_{fus}}}}) S_{fus} / S \quad (14.13)$$

$$C_{D_{f_{FUS}}} = C_{f_{fus}} (S_{wet_{fus}}) / S \quad (14.14)$$

$$C_{D_{p_{FUS}}} = (C_{f_{fus_{atM=0.6}}}) \{60 / (l_f / d_f)^3 + 0.0025 (l_f / d_f)\} (S_{wet_{fus}}) / S \quad (14.15)$$

$$C_{D_{b_{fus}}} = \alpha^2 (S_{base_{fus}}) / S \quad (14.16)$$

```
% Fuselage Transonic zero-lift drag Drag prediction
C_D_f_fus = C_f_fus*(S_wet_fus)/S; % Fuselage skin friction drag coefficient
C_D_p_fus = C_f_fus*(60/(l_f/d_f)^3+0.0025*(l_f/d_f))*(S_wet_fus)/S; % fuselage pressure drag
C_D_wave_fus = 0.06; % wave drag coefficient from Roskam part VI pg50
C_D_o_fus = R_wf*(C_D_f_fus+C_D_p_fus)+C_b_fus+(C_D_wave_fus)*S_fus/S

% Fuselage Transonic drag due to lift
C_D_b_fus = alpha.^2*(S_b_fus)/S
```

$$C_{D_{o_{fus}}} = 0.0445 \quad (14.17)$$

$$C_{D_{b_{fus}}} = 0.6352 \quad (14.18)$$

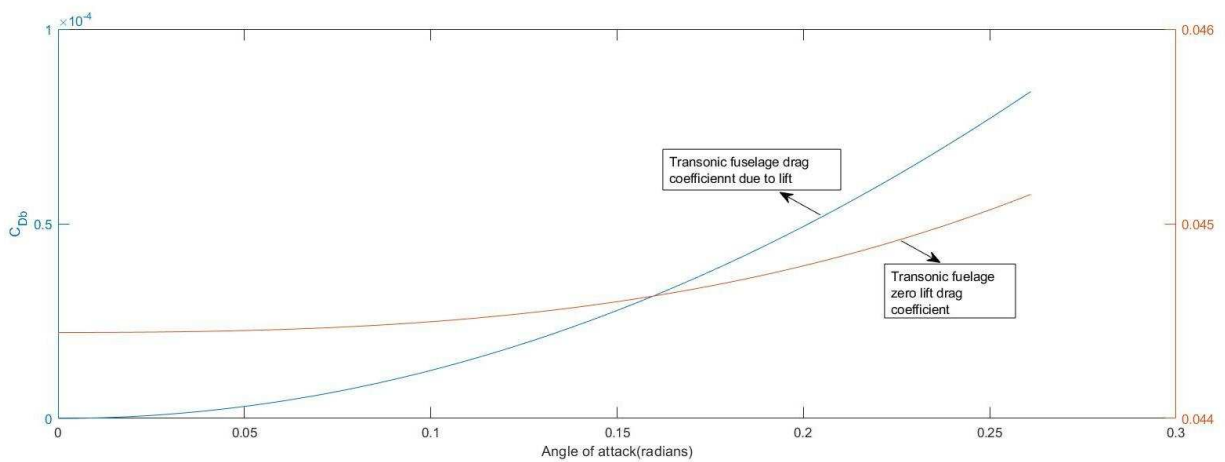


Figure 177: Angle of attack vs fuselage transonic drag

14.2.3) EMPENNAGE DRAG PREDICTION – VERTICAL TAIL:

The subsonic empennage drag for VER-12X is determined using e.q.14.11

$$C_{empennage} = C_{D_{0empennage}} + C_{D_{Lempennage}} \quad (14.11)$$

14.2.3.1) EMPENNAGE ZERO-LIFT DRAG COEFFICIENT:

The empennage zero-lift drag coefficient may be computed using the following method:

$$C_{D_{0,verticaltail}} = (R_{wf})(R_{LS})(C_{f_{verticaltail}})\{1 + L'(t/c) + 100(t/c)^4\}S_{wetvertical} / S \quad (14.12)$$

Horizontal Tail:

Almost all the horizontal tail configurations and canards can generate lift in steady flight condition which causes ‘induced drag’. The lift due to empennage is divided into sections as proposed by ‘Roskam- Airplane Design Part VI’.

- Lift due to the incidence angles of the empennage surfaces
- Lift due to the requirement for trim which is required for specific centre of gravity location. Usually, this is termed as ‘Trim Drag’.

$$C_{l_H} = C_{l_{\alpha_H}} (\alpha_H - \alpha_{o_{LH}}) \quad (14.13)$$

$$\alpha_h = \alpha(1 - d\varepsilon / d\alpha) + i_h \quad (14.14)$$

E.q. 4.13 and 4.14 had already been determined in p.d.I and those values will be used for determining the drag due to lift below.

The drag due to lift for the horizontal tail is determined using e.q.14.14

$$C_{D_{L_{EMP}}} = \{(C_{l_H})^2 / \pi A_H e_H\} S_H / S \quad (14.14)$$

Where

- Oswald efficiency for fixed horizontal tail is 0.5
- A_H is the aspect ratio of the horizontal tail.

```
%% Empennage Drag Coefficient
% Sub-sonic Vertical Tail drag coefficient
S_wet_vert = 915.46;
cbar_vert = 186.11;
R_wf_vert = 1;
R_ls_vert = 1.1456;
R_n_vert = (0.0765*482*cbar_vert)/1.20234;
L_prime_vert = 31;
thickness_vert = 0.33;
C_f_vert = 0.00275;
C_d_o_v = (R_wf_vert)*(R_ls_vert)*(C_f_vert)*(1+(L_prime_vert*thickness_vert)...
+100*(thickness_vert)^4)*S_wet_vert/S;
```

```
C_d_o_v =
```

```
0.0090
```

```
% Sub-sonic Horizontal Tail drag coefficient  
C_l_h = 6.254;  
A_h = 6.1; % Aspect ratio of the horizontal tail  
e_h = 0.5; % oswald efficiency of the horizontal tail  
S_h = 778; % Horizontal Tail area  
C_D_emp = ((C_l_h)^2/(pi*A_h*e_h))*(S_h/S) % Subsonic Horizontal tail drag due to lift
```

```
C_D_emp =
```

```
0.7975
```

The drag due to lift for horizontal tail and vertical tail computed using MATLAB are 0.8 and 0.0090 approximately. Since, VER-12X uses conventional tail configuration, all the canard parameters will be zero and hence the drag equation for horizontal tail is reduced to e.q.14.14. Therefore, the total drag produced by the entire tail is 0.8065.

Empennage transonic drag prediction:

Empennage transonic drag can be computed using e.q.14.15

$$C_{D_{\text{empennage}}} = C_{D_{\text{empennage}}} + C_{D_{\text{empennage wave}}} \quad (14.15)$$

```
%% Empennage Transonic wing drag  
C_l_max_emp = 1.3;  
sweep_vert = 0.9250245; % sweep in radians  
k = 0.87; % Constant K for conventional symmetrical airfoil is 0.87  
M_dd_emp = k-thickness_vert-(C_l_max_emp/10);  
M_C_d_wave_peak_emp = 0.65/sqrt(cos(sweep_vert));  
C_d_wave_sweep_emp = 0.00189*(cos(sweep_vert))^2.5;  
M_dd_sweep_emp = M_dd_emp/sqrt(cos(sweep_vert));  
l = 0.9; % l = C_d_l/C_l^2 is chosen using fig.4.13  
C_d_l_emp = l*C_l_max_emp; % Empennage drag coefficient due to lift  
C_d_o_emp_m = 0.9977;  
C_d_o_e = C_d_o_emp_m+C_d_wave_sweep_emp;
```

```
C_d_o_e =
```

```
0.9982
```

14.3) AAA RESULTS FOR CLASS-II DRAG ANALYSIS:

Output Parameters			
M_1	0.415	$Re_{w_{cut}}$	34.3989×10^6
$Re_{w_{tur}}$	2.7812×10^6	C_{f_w}	0.0025
$Re_{w_{lam}}$	0.0000×10^6	e_w	0.8932
		$C_{D_{gap_{hd}}}$	0.0006
		$C_{D_{o_w}}$	0.0063
		$C_{D_{L_w}}$	0.0276

Figure 178: Drag parameters of wing - Output

Output Parameters			
M_1	0.415	R_{wf}	0.98
C_{f_f}	0.0019	$C_{D_{o_{f-base}}}$	0.0035
		$C_{D_{o_f}}$	0.0037
		$C_{D_{b_f}}$	0.0000
		$C_{D_{L_f}}$	0.0009

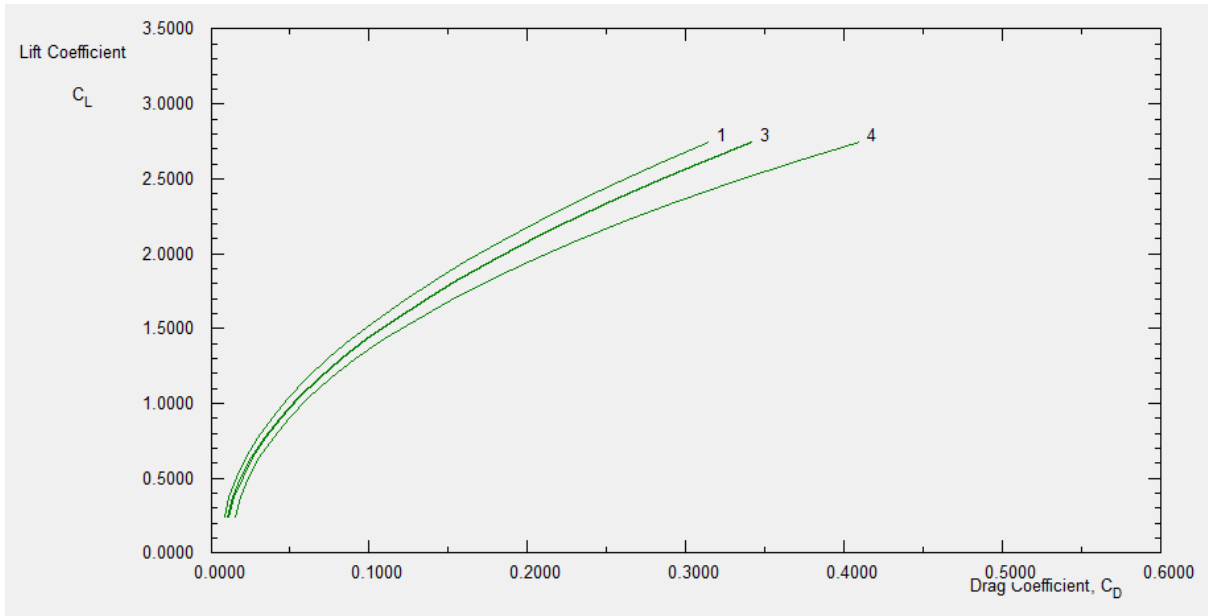
Figure 179: Drag parameters fuselage - output

Output Parameters			
M_1	0.415	e_h	0.9694
C_{f_h}	0.0027	$C_{D_{o_h}}$	0.0012
		$C_{D_{L_h}}$	0.0043

Figure 180: Drag parameters for horizontal tail - Output

Output Parameters			
M_1	0.415	e_v	1.0107
C_{f_v}	0.0026	$C_{D_{o_v}}$	0.0009
		$C_{D_{Y_v}}$	0.0000

Figure 181: Drag parameters for vertical tail - output



Drag Build-Up
 1: Wing
 2: Horizontal Tail
 3: Vertical Tail
 4: Fuselage
 M = 0.415
 $S_w = 2497.93 \text{ ft}^2$

Figure 182: Coefficient of drag versus lift – Class II AAA

Output Parameters							
S_{wet}	11357.57 ft^2	C_f	0.0043	C_{D_L}	0.0343	L/D	15.58
f	49.36 ft^2	C_{D_0}	0.0198	C_{D_1}	0.0540		

Figure 183: Overall VER-12XX drag - Class II AAA

CHAPTER 15

INSTALLED POWER

Aircraft traditionally, generate thrust/power by means of pushing air or exhaust gases backwards. Thrust power(P_t) is equal to the thrust force and aircraft velocity (e.q.15.1). The difference in the fluid velocity to which the kinetic energy is imparted by the propulsion system is given by e.q.15.2. The propulsive efficiency is defined as the ratio of thrust power and the energy expended which is shown in e.q.15.3. Maximum efficiency is obtained when there is no change in fluid velocity which renders thrust to zero. However, to maximize on propulsive efficiency, e.q.15.3 should be unity. Installed power and the power requirement plays a vital role in the aircraft mission as it decides whether the proposed configuration can meet the specified range requirements. Choosing a powerplant based on aircraft configuration validates whether the proposed powerplant is a viable option for the aircraft. In p.d.I, for VER-12XX, a turbo-jet engine is chosen in which the preliminary engine characteristics had been thoroughly studied. Whereas in Class II sizing, each of these components will be studied in detail

- Engine type and required characteristics
- Relation between engine type and flight envelope
- Installed thrust, inlet and efficiency considerations
- Stability and control considerations
- Safety and noise considerations

In this design chapter, all the above-mentioned characteristics will be studied along with the procedures those presented in ‘Part VI, Airplane Design, Roskam’ and the power requirements for VER-12X will be determined.

$$P_t = FV_o = \rho sV(V - V_o)V_o \quad (15.1)$$

$$\Delta E = \frac{\rho s}{2} V(V^2 - V_o^2) \quad (15.2)$$

$$\eta_{PE} = \frac{P_t}{\Delta E} = \frac{2}{V/V_o + 1} \quad (15.3)$$

Typically, a turbo-jet operates with an exhaust to free stream velocity of 3 and turbo-prop operates in the range of 1.5. But, this analysis is too simplistic which assumes that the fluid velocity remains constant. Since, the exhaust gases are at high pressures, these gases when they leave nozzle tend to expand and would be at high speeds compared to free stream air. On the

other hand, for propellers, the air even before entering are accelerated half way through ahead and after leaving the propeller blade. Propulsion force(thrust/power) in one way is a complicated process, as it entirely depends on the propeller flow-field, jet intake and exhaust which impacts the overall flow field of the aircraft. For a propeller driven aircraft, most of the propulsive force is exerted directly on the aircraft. Where as in turbo-jet driven aircraft; engine mounts only contribute one-thirds of the power on the aircraft. It is impossible to use simpler models to predict thrust and hence this design chapter provides a detailed analysis of the robust procedures that will be used to precisely determine thrust.

15.1 JET ENGINE THRUST CONSIDERATIONS:

Before digging in deep into the thrust produced by the jet engine, it is important to understand the basis and the underlying principles of jet engine. Primarily, air enters the engine through inlet and through a compressor which compresses the air which then it passes through the combustion chamber where the compressed air is mixed with fuel and passes through a turbine where the hot exhaust gases rushes through the nozzle providing the necessary forward force for the aircraft. The compressor should be rotated by a turbine where the energy required for this rotation is extracted from the high-pressure exhaust gases. If the aircraft should generate thrust at rapid rates, an afterburner should be used where the un-burned air is fed through the turbine back to the combustion chamber where additional fuel is mixed and thus increasing the exhaust velocity.

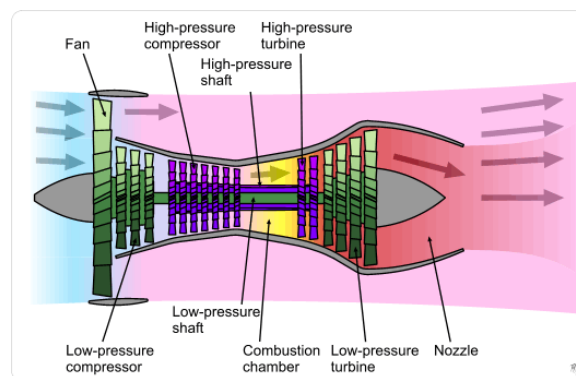


Figure 184: Jet-engine working principle

Figure 184, shows the working principle of jet engine which in simpler terms means suck (take in air), squeeze (compress air), boom (air when mixed with fuel) and blow (exhaust). One dominating that effects the performance of jet engine is that the direct proportionality relation existing between the net thrust and the mass air flow which is entering the engine. ‘Raymer in Aircraft Design’ presents a fact that an aircraft with after burning engine typically generates

126 pounds of thrust per second whereas turbo-fan engines generates 40-60 pounds of thrust per second. RAM Drag is an important factor to study and this comes into play if the air enters the engine is at supersonic speeds. Figure 185, illustrates that the RAM drag increases as the aircraft speed increases which ultimately increases the net thrust that an engine generates. To mitigate the effects of RAM drag, the inlet of an engine must be carefully selected. These effects can be favourable for supersonic jets, but for subsonic aircraft, a choked nozzle conditions appears irrespective of the aircraft speed and as the aircraft reaches transonic speed this relatively constant thrust reduces. Since, supersonic aircraft use a converging and diverging nozzle and the exhaust velocities are also supersonic therefore the ram effect will not increase thrust as the Mach number increases. The inlet losses which occur for a Mach number depends on the number of variable geometry being employed.

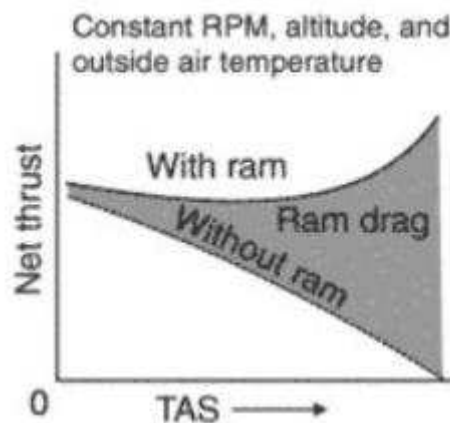


Figure 185: RAM Drag effects on turbo-jet

Thrust and propulsive efficiency are largely affected by the engine over-all pressure ratio(OPR) and is defined as the ratio of the exhaust plane to the inlet plane. OPR, generally portrays engine capability to accelerate the exhaust which generates thrust. Usually, OPR'S range from 15 to 1 and 30 to 1. Another factor that strongly influences engine performance is the 'turbine inlet temperature' (TIT). Conventional transport jets, use higher by-pass ratio engines with larger fan which helps in increased mass airflow into the engines and part of this air which does not pass through combustion is used to cool the engine.

15.2) POWER EXTRACTION REQUIREMENTS:

To operate an airplane, certain amount of electrical, mechanical and pneumatic power is required during any phase of the mission and which is provided by the engines. For these reasons, it is referred as power extraction requirements. Auxiliary power units(APU) can sometimes be used rather than conventional propulsion system. The power extraction requirements vary from aircraft to aircraft and from one mission to other. Since, VER-12X uses a turbo-jet engine all the procedures in this chapter are dedicated for determining the power extraction for a turbo-jet. The power extraction requirements for a turbo-jet engine is calculated using e.q.15.4.

$$P_{extr} = P_{el} + P_{mech} + P_{pneum} \quad (15.4)$$

The right-hand side components of e.q.15.4 are estimated using 'table 6.1, Roskam, Part VI'.

```
%% Power requirements for VER-12
% Author: Veera Venkatesh Vadaparathi
% AE-295B

%% Power extraction requirements for VER-12
P_el = 0.00070*160000; % P_el is the electrical power in shp
P_mech = 0.00060*160000; % P_mech is the mechanical power extraction in shp
for u=0:10:482
    T = 0:1000:100000
    P_pneum = 0.025*(T*u)/550; % P_pneum is the pneumatic power extraction in shp
end
P_extr = P_el+P_mech+P_pneum
```

Figure 186:Power extraction calculations - MATLAB

15.3) INLET SIZING AND INTEGRATION:

Preliminary inlet sizing is a design process through which the inlet area and the duct geometry from the inlet to the compressor face will be determined. Inlet must be sized in such a way that it matches the engine airflow requirements. The following are the important areas which play an important role in inlet sizing.

- A_∞ is the stream tube cross section at infinity and is also called as inlet capture area
- A_C is the stream tube cross section at the inlet and is also known as inlet area or cowl capture area.
- A_f is the stream tube cross section at the engine station.
- A_e is the stream tube cross section at the exit or exhaust and is also called nozzle area.
- A_∞/A_C characterizes the inlet operation.

The inlet operation is dependent on the ratio of infinite stream tube cross section to the stream tube cross section at the inlet. In this section, the sub-sonic jet engine installations are determined to identify the required inlet area, A_c .

Table 25 : GE-9X Engine characteristics

Engine make	General Electric – 9X
Engine blades	4 th generation composite fan blades, 16 total fan blades
Compressor pressure ratio	27:1
Fan diameter	134 in (340 cm)
Turbine	2-stage HP, 6-stage LP
Take-off thrust	105000 lbf (470 kN)
Pressure ratio	60:1
Bypass ratio	10:1

GE9X

Point-designed for the Boeing 777X, the GE9X will be the largest engine ever made by GE. Scheduled to enter service in 2020 with a backlog of 700 engines, it will also be the most fuel-efficient engine GE has ever produced on a per-pounds-of-thrust basis.

FIRST engine tested in March 2016

4th generation composite fan blades

ONLY 16 fan blades

The largest fan diameter in commercial aviation



8db margin to Stage 5 noise regulations

5% better specific fuel consumption (SFC) than any other twin-aisle engine in service in 2020

30% NO_x margin to CAEP 8 regulations

10% lower fuel burn than the GE90-115B

27:1 compressor pressure ratio
The highest ever in commercial aviation



Figure 187: GE-9X Engine

CHAPTER 16

CONCLUSION AND RECOMMENDATIONS

16.1. DRAWINGS & SUMMARY OF MOST IMPORTANT DESIGN PARAMETERS

The following figures represent the 3-d views of the designed aircraft

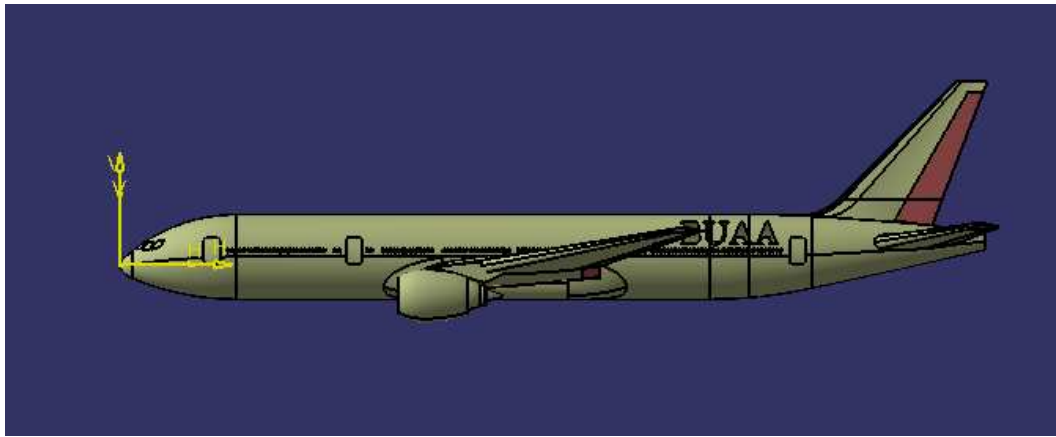


Figure 188:Side View of VER-12XX

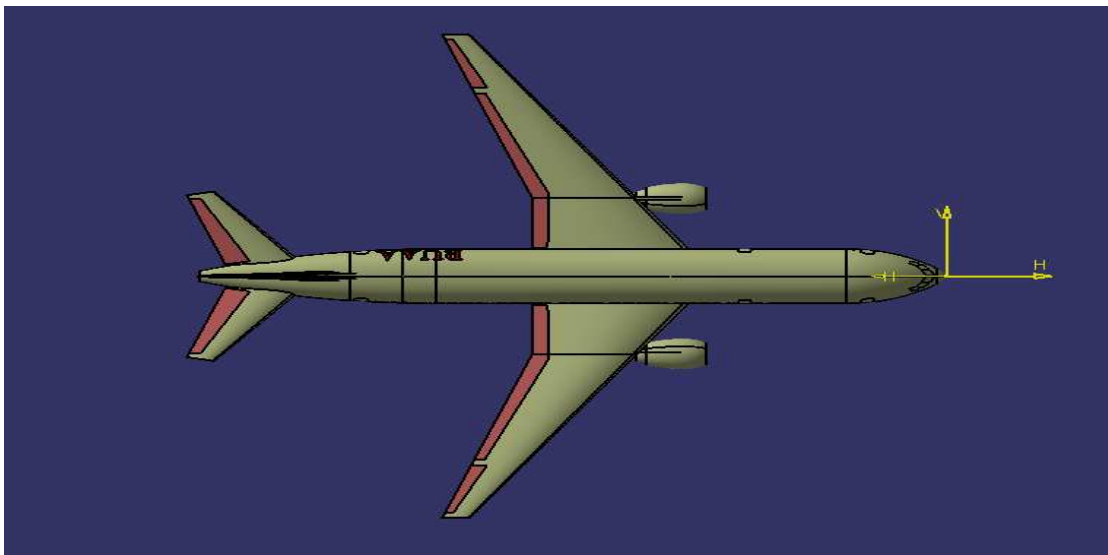


Figure 189:Top View of VER-12XX



Figure 190: Front View of VER-12XX

16.2 ENVIRONMENTAL / ECONOMIC TRADEOFFS

Aviation industry completely depend on fossil fuels and there had been concerns on the growing carbon dioxide levels globally. It is known that aviation industry alone contributes to 2.50% of the total Co2 emissions. The below figure is from the ‘road to Paris climate change summit’. It is clearly evident that by the year 2050 aviation sector is going to contribute to approximately 5 percent of the emissions.

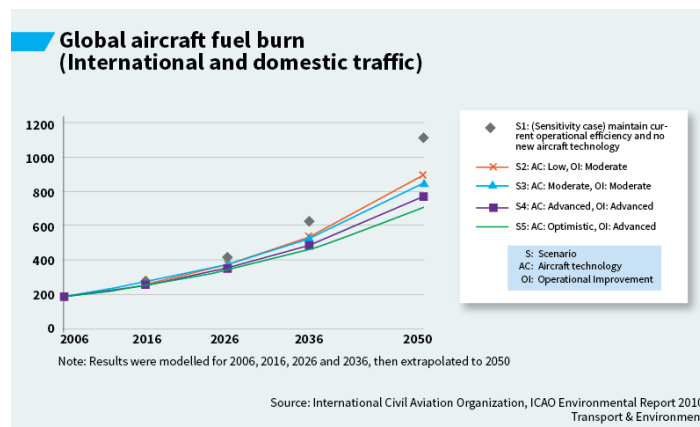


Figure 191: Global Aircraft Fuel Burn

Many reforms have taken by several other organizations around the world to cut them to below the sub minimum level but the demand for air travel is increasing tremendously which is leaving researchers no option to continue embarking on the conventional aircraft practices. The solution to this problem is to replace the existing fuels with alternate hydrogen fuel cells or solar electric panel powered propulsion technology. In the case of hydrogen fuel cells when

hydrogen is burnt the emissions will be oxygen which greatly reduces the amount of Co2 being released into the atmosphere. NASA has been successful in experimenting a new propulsion technology which cuts down the emissions to 50% by using jet-A and biofuels.

16.3 SAFETY / ECONOMIC TRADEOFFS

VER-12XX is a passenger jet and the main payload are the passengers. It is important that airlines across globe must satisfy the respective aviation rules set forth by their local certification authorities. Aircraft evacuation during emergency is an important factor and VER-12XX is safely equipped with all the necessary emergency equipment on board.

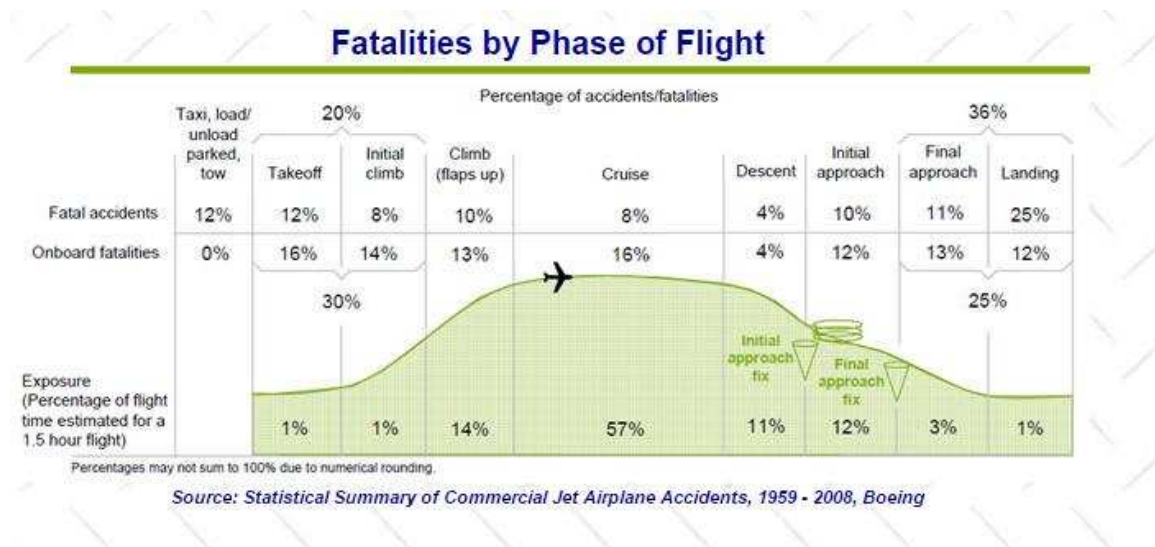


Figure 192: Fatalities by Phase of Flight

The above image gives the information about the fatalities caused during a flight phase and it can be inferred that most of the accidents/incidents happen during the final approach and landing phase of the aircraft. VER-12XX has all the state of art aural warning systems which alerts the crew timely whenever they are slipping into an unknown hazardous situation. Pilot errors are the most prevalent and timely accounts for aviation incidents which cannot be eliminated by can be reduced by promoting appropriate and intense training sessions. Also, some incidents report that some happened due to passenger’s awareness of the emergency procedures.

An extensive study on the proposed aircraft configuration have been presented from chapter 1 to chapter 15, where all the key parameters such as take-off weight, payload weight, performance constraints till the drag polar have been determined both manually and using AAA software. If we observe closely, though the payload had been increased from 150 to 200

passengers the take-off weight when compared to similar aircraft database is low and the empty weight is also relatively low which confirms us that the preliminary class I calculations proves that the proposed aircraft configurations is scalable. One reason being extensive usage of composites which significantly reduced the structure weight, the use of CFM-9X engines reduced the propulsion weight and the use of advanced computers reduced the fixed equipment weight which altogether improved the payload capacity for VER-12XX.

REFERENCES

1. 737 Detailed Technical Data. (n.d.). Retrieved from <http://www.b737.org.uk/techspecs/detailed.htm>
2. AIAA . (2010). Retrieved 09 05, 2016, from <http://enu.kz/repository/2010/AIAA-2010-9188.pdf>
3. Airlines Inform. (2012). Retrieved 09 06, 2016, from <http://www.airlines-inform.com/commercial-aircraft/Boeing-777-300.html>
4. Boeing 787 performance summary. (2011). Retrieved 08 31, 2016, from http://www.boeing.com/assets/pdf/commercial/startup/pdf/787_perf.pdf
5. Daily Mail. (n.d.). Retrieved from <http://www.dailymail.co.uk/sciencetech/article-2859920/What-Nasa-s-experimental-research-plane-doing-military-base-Africa-Claims-craft-used-create-high-resolution-3D-maps-fight-terrorism.html>
6. EASA. (2013). Retrieved 09 04, 2016, from http://www.easa.europa.eu/system/files/dfu/EASA-TCDs-E.036_Rolls--Royce_plc._Trent_1000_Series_engines-04-10092013.pdf
7. Fly Radius. (n.d.). Retrieved from <http://www.flyradius.com/bombardier-crj1000/engine-gecf34-8c5a1-cf34-8c5a2>
8. India Brand Equity Foundation. (n.d.). Retrieved 09 30, 2016, from <http://www.ibef.org/industry/indian-aviation/showcase>
9. Mavris, D. D. (1997). NASA. Retrieved 09 02, 2016, from <http://ntrs.nasa.gov/archive/nasa/casi.ntrs.nasa.gov/19970015641.pdf>
10. Stanford. (n.d.). Retrieved from http://adl.stanford.edu/aa210b/Lecture_Notes_files/AIAA-7578-329.pdf
11. Stanford. (n.d.). Retrieved 09 05, 2016, from <http://adg.stanford.edu/aa241/propulsion/engineplacement.html>
12. Stanford . (n.d.). Retrieved 09 01, 2016, from http://web.stanford.edu/~cantwell/AA283_Course_Material/GE90_Engine_Data.pdf
13. The Boeing. (2011). Retrieved 08 29, 2016, from <http://www.boeing.com/assets/pdf/commercial/airports/faqs/arcandapproachspeeds.pdf>
14. The Statistics Portal. (n.d.). Retrieved 09 03, 2016, from <http://www.statista.com/statistics/193533/growth-of-global-air-traffic-passenger-demand/>
15. The Statistics Portal. (n.d.). Retrieved 06 2016, 2016, from <https://www.statista.com/topics/3016/air-carrier-market-in-india/>
16. wikipedia. (n.d.). Retrieved 09 02, 2016, from https://en.wikipedia.org/wiki/Boeing_787_Dreamliner
17. Wikipedia. (n.d.). Retrieved from https://en.wikipedia.org/wiki/Area_rule
18. Wikipedia. (n.d.). Retrieved 09 05, 2016, from https://en.wikipedia.org/wiki/Boeing_777#777-300ER

18. Roskam. (n.d.). Aircraft Design.
19. 737 Detailed Technical Data. (n.d.). Retrieved from <http://www.b737.org.uk/techspecs/detailed.htm>
20. AIAA . (2010). Retrieved 09 05, 2016, from <http://enu.kz/repository/2010/AIAA-2010-9188.pdf>
21. Airlines Inform. (2012). Retrieved 09 06, 2016, from <http://www.airlines-inform.com/commercial-aircraft/Boeing-777-300.html>
22. Boeing 787 performance summary. (2011). Retrieved 08 31, 2016, from http://www.boeing.com/assets/pdf/commercial/startup/pdf/787_perf.pdf
23. Daily Mail. (n.d.). Retrieved from <http://www.dailymail.co.uk/sciencetech/article-2859920/What-Nasa-s-experimental-research-plane-doing-military-base-Africa-Claims-craft-used-create-high-resolution-3D-maps-fight-terrorism.html>
24. EASA. (2013). Retrieved 09 04, 2016, from http://www.easa.europa.eu/system/files/dfu/EASA-TCDSE.036_Rolls--Royce_plc._Trent_1000_Series_engines-04-10092013.pdf
25. Fly Radius. (n.d.). Retrieved from <http://www.flyradius.com/bombardier-crj1000/engine-gecf34-8c5a1-cf34-8c5a2>
26. India Brand Equity Foundation. (n.d.). Retrieved 09 30, 2016, from <http://www.ibef.org/industry/indian-aviation/showcase>
27. Mavis, D. D. (1997). NASA. Retrieved 09 02, 2016, from <http://ntrs.nasa.gov/archive/nasa/casi.ntrs.nasa.gov/19970015641.pdf>
28. Stanford. (n.d.). Retrieved from http://adl.stanford.edu/aa210b/Lecture_Notes_files/AIAA-7578-329.pdf
29. Stanford. (n.d.). Retrieved 09 05, 2016, from <http://adg.stanford.edu/aa241/propulsion/engineplacement.html>
30. Stanford . (n.d.). Retrieved 09 01, 2016, from http://web.stanford.edu/~cantwell/AA283_Course_Material/GE90_Engine_Data.pdf
31. The Boeing. (2011). Retrieved 08 29, 2016, from <http://www.boeing.com/assets/pdf/commercial/airports/faqs/arcandapproachspeeds.pdf>
32. The Statistics Portal. (n.d.). Retrieved 09 03, 2016, from <http://www.statista.com/statistics/193533/growth-of-global-air-traffic-passenger-demand/>
33. The Statistics Portal. (n.d.). Retrieved 06 2016, 2016, from <https://www.statista.com/topics/3016/air-carrier-market-in-india/>
34. wikipedia. (n.d.). Retrieved 09 02, 2016, from https://en.wikipedia.org/wiki/Boeing_787_Dreamliner
35. Wikipedia. (n.d.). Retrieved from https://en.wikipedia.org/wiki/Area_rule
36. Wikipedia. (n.d.). Retrieved 09 05, 2016, from https://en.wikipedia.org/wiki/Boeing_777#777-300ER

37. *Aviation Stack Exchange*. (n.d.). Retrieved from <https://aviation.stackexchange.com/questions/2111/what-do-winglets-do-to-increase-aircraft-performance>
38. *Quora*. (n.d.). Retrieved from What technical factors should I consider when choosing a wing sweep angle for a low-speed RC aircraft?: <https://www.quora.com/What-technical-factors-should-I-consider-when-choosing-a-wing-sweep-angle-for-a-low-speed-RC-aircraft>
39. Roskam. (n.d.). Aircraft Design.
40. Scott, J. (2002, 11 24). *AerospaceWeb.org*. Retrieved from Area Rule and Transonic Flight: <http://www.aerospaceweb.org/question/aerodynamics/q0104.shtml>
41. *American Flyers*. (n.d.). Retrieved from americanflyers.net: http://www.americanflyers.net/aviationlibrary/pilots_handbook/images/chapter_1_img_32.jpg
42. *Quora*. (n.d.). Retrieved from <https://qph.ec.quoracdn.net/main-qimg-ad53cbf492569c44885bf57c988ad98c>
43. Roskam, J. (2011). Airplane Design. In D. Roskam, *Part III: Layout of Subsystems* (p. 254). Kansas: DARC CORPORATION.
44. *What-when-how*. (n.d.). Retrieved from <http://what-when-how.com/flight/tail-designs/>
45. *Wikipedia*. (n.d.). Retrieved from https://upload.wikimedia.org/wikipedia/commons/thumb/9/90/T-tail_en.svg/1280px-T-tail_en.svg.png
46. *youshouldfly*. (n.d.). Retrieved from http://youshouldfly.com/Rhyolite_Aviation/V-Tail_info_files/Media/waiox%20v-tail/waiox%20v-tail.jpg?disposition=download
47. *NASANASA*. (n.d.). Retrieved from <https://www.nasa.gov/aero/nasa-reports-alternative-jet-fuel-research-results.html>
48. *statistics*. (n.d.). Retrieved from <http://www.planecrashinfo.com/cause.htm>